Analysis of Time Varying Systems And Its Applications

by

Susheelkumar Cherangara Subramanian

A Dissertation Presented in Partial Fulfillment
of the Requirements for the Degree
Doctor of Philosophy

Approved June 2021 by the
Graduate Supervisory Committee:

Sangram Redkar, Chair
Bradley Rogers
Thomas Sugar

ARIZONA STATE UNIVERSITY

August 2021

ABSTRACT

The inherent behavior of many real world applications tends to exhibit complex or chaotic patterns. A novel technique to reduce and analyze such complex systems is introduced in this work, and its applications to multiple perturbed systems are discussed comprehensively.

In this work, a unified approach between the Floquet theory for time periodic systems and the Poincare theory of Normal Forms is proposed to analyze time varying systems. The proposed unified approach is initially verified for linear time periodic systems with the aid of an intuitive state augmentation and the method of Time Independent Normal Forms (TINF). This approach also resulted in the closed form expressions for the State Transition Matrix (STM) and Lyapunov-Floquet (L-F) transformation for linear time periodic systems. The application of theory towards stability analysis is further demonstrated with the system of Suction Stabilized Floating (SSF) platform. Additionally, multiple control strategies are discussed and implemented to drive an unstable time periodic system to a desired stable point or orbit efficiently and optimally. The computed L-F transformation is further utilized to analyze nonlinear and externally excited systems with deterministic and stochastic time periodic coefficients.

The central theme of this work is to verify the extension of Floquet theory towards time varying systems with periodic coefficients comprising of incommensurate frequencies or quasi-periodic systems. As per Floquet theory, a Lyapunov-Perron (L-P) transformation converts a time-varying quasi-periodic system to a time-invariant form. A class of commutative quasi-periodic systems is introduced to demonstrate the proposed theory and its applications analytically. An extension of the proposed unified approach towards analyzing the linear quasi-periodic system is observed to provide good results, computationally less complex and widely applicable for strongly

excited systems. The computed L-P transformation using the unified theory is applied to analyze both commutative and non-commutative linear quasi-periodic systems with nonlinear terms and external excitation terms. For highly nonlinear quasi-periodic systems, the implementation of multiple order reduction techniques and their performance comparisons are illustrated in this work. Finally, the robustness and stability analysis of nonlinearly perturbed and stochastically excited quasi-periodic systems are performed using Lyapunov's direct method and Infante's approach.

DEDICATION

I dedicate this dissertation to my parents.

ACKNOWLEDGMENTS

I sincerely thank my advisor, Professor Sangram Redkar, for his incessant support and motivation to complete my research work successfully. Without his guidance and support, I would have never completed this work.

I would like to thank Dr. Lindy Elkins-Tanton and Interplanetary Initiative for partially funding this research work. I would also like to thank Professor Bradley Rogers and Professor Thomas Sugar for taking time from their busy schedule to be a part of my supervisory committee and providing me with all the support to complete my dissertation in a timely manner.

I would like to thank my other lab members Dr. Peter Waswa, Dr. Prudhvi Chinimilli, Dr. Sandesh Bhat, and Dr. Jason Olson, for helping me add material to this work. I would also like to thank Mr. Osama Jameel, Dr. Alvaro Vargas, Dr. Anand Makwana, Dr. Pavan Badami, and Mr. Yuchong Li for their moral support throughout my research work.

Most importantly, I would like to thank my wife Tejaswi for her endless love and support. I am also grateful for all her sacrifices and thankful for motivating me at each low point in my life. I could not have hoped for a better life partner. I would also like to thank my dog, Eddy, for the emotional support. Finally, I would like to thank all my friends and family for all their help and support.

TABLE OF CONTENTS

Page

CHAPTER Page

CHAPTER Page

CHAPTER Page

CHAPTER Page

LIST OF TABLES

LIST OF FIGURES

Figure Page

Figure Page

Figure Page

Figure Page

Figure Page

Figure Page

Figure Page

Figure Page

Chapter 1

INTRODUCTION

1.1 Motivation

Differential equations with periodic coefficients and nonlinear terms are widely observed in the field of science and engineering. They are used in modeling the dynamical behavior of ship motions by Biran and Pulido (2013), space systems by Waswa and Redkar (2020a), heart rhythms by Glass (1991), robotic systems by De La Fuente *et al.* (2020), Micro-Electromechanical Systems (MEMS), structural, thermal and fluid systems by Rega (2019). The dynamical behavior of these systems tends to exhibit linear, nonlinear, and chaotic patterns. Using dynamical systems theory, they can be modeled as time varying systems with deterministic or stochastic perturbations. Traditionally, such complex models are reduced/linearized to a time-invariant system for stability analysis and controller design. Liao *et al.* (2020); Huang *et al.* (2020) have identified the solution to few nonlinear systems as quasi-periodic in nature. Additionally, periodic coefficients could appear in either parametric excitation term, external excitation term, or both terms. Multiple approximate and numerical approaches have been developed in the past to analyze such nonlinear and chaotic systems. Some of them are constrained by computational cost and small parameter estimation. Hence there is a need to develop techniques that overcome these constraints and provide an appropriate solution representing the actual dynamics of the system.

1.2 Dissertation Scope and Overview

The system modeling for various applications in the field of science and engineering emphasizes the need for the study of time varying systems. A deep understanding of the dynamical behavior and properties of the system is enabled by the analytical techniques developed in dynamical systems theory.

The main aim of this dissertation is to investigate a novel approach that would aid in the analysis of time varying systems analytically. Though the time varying systems can be of multiple forms, this dissertation primarily concentrates on analyzing time periodic systems and quasi-periodically time varying systems. The remaining part of this dissertation is organized in the following manner

Chapter 2 provides a brief overview of various mathematical techniques used to analyze time varying systems. Furthermore, the unified theory for time periodic system is introduced and validated to identify the closed form expression for STM. The resulting solutions are compared with those from the traditional approximate and numerical techniques for validation.

Chapter 3 details the extension of the proposed unified approach towards stability analysis of auto parametrically excited systems. Initially, it is applied to identify transition curves between the stable and unstable bounds for the standard Mathieu equation. Later, using numerical simulation, the stability plots for the system of Suction Stabilized Floats are also illustrated. Additionally, the extension of the unified approach towards designing and implementing efficient and optimal controllers to guide an unstable time periodic system to a desired stable point or orbit is also detailed in this chapter.

Chapter 4 details the computation of the closed form expression for the L-F transformation using the proposed unified approach. Its application towards the analysis

of time periodic systems with multiple perturbations is also included in this chapter. The Infante's approach is employed to identify the stability bounds for stochastic parametrically excited systems. The theoretical framework is supplemented with examples of the Mathieu equation with perturbations in each category.

Chapter 5 concentrates on the investigation of the Floquet type theory for linear quasi-periodic systems. A class of commutative quasi-periodic systems is also introduced in this chapter. The analysis of a quasi-periodically time varying system is initially performed using a modified version of prior work as an indirect approach. An extension of the proposed unified approach towards the analysis of linear quasi-periodic systems is discussed and compared with the indirect approach for the temporal variations and expressions for the L-P transformation matrix.

Chapter 6 introduces the application of the computed L-P transformation, using the unified theory, towards the analysis of both commutative and non-commutative linear quasi-periodic systems with nonlinear terms and external excitation terms. For highly nonlinear quasi-periodic systems, the implementation of multiple order reduction techniques and their performance comparisons explained comprehensively in this chapter.

Chapter 7 discusses the robustness and stability analysis of nonlinearly perturbed and stochastically excited quasi-periodic systems. The computed closed form expression for the L-P transformation matrix is utilized in conjunction with Lyapunov's direct method and Infante's approach to analyzing both commutative and non-commutative quasi-periodic systems.

Chapter 8 explains the limitations of the proposed unified theory. A brief overview of techniques and strategies to overcome these constraints is also included in this chapter and clear directions for future work.

Chapter 2

MATHEMATICAL PRELIMINARIES AND THE UNIFIED THEORY

The earliest analysis of time varying systems was performed on time periodic systems. Some of the prominent research works for analyzing time periodic systems were using the Hills method by Iakubovich and Starzhinskiĭ (1975), the perturbation techniques by Nayfeh (2011a), the averaging methods by Sanders *et al.* (2007) and the Floquet theory by Floquet (1883). As explained by Sharma and Sinha (2018), the application of Hill's infinite determinants method is applicable towards the stability bounds of the system. The requirement of expressing the periodic coefficients in terms of small parameters limits the application of perturbation and averaging techniques for only weakly excited systems. As per Lyapunov (1896) and Sinha *et al.* (1996), the application of Floquet theory enabled the conversion of a linear time periodic system into a time-invariant equivalent system using the Lyapunov-Floquet (L-F) transformation. However, Sinha *et al.* (1996) explain the significance of state evolution's closed form expression (known as state transition matrix) for broad applications, from which the fundamental solution matrix is derived. So, an approximate symbolic form computation of the State Transition Matrix (STM), using Picard iteration and shifted Chebyshev polynomials, was performed by Sinha *et al.* (1993); Sinha and Juneja (1991). The design of a control system towards chaos control using this technique was described by Sinha *et al.* (2005a).

Kovacic *et al.* (2018) stated that a Mathieu equation is utilized to model many of the engineering, applied mathematics, and nonlinear vibration theory problems. Peruzzi *et al.* (2016) demonstrated the dynamical analysis and optimal controller implementation of an electronic circuit of mass Micro-electromechanical systems (MEMS)

by modeling it with uncertain time-periodic coefficients in a Mathieu equation. The stability analysis of the cracked rotor system subjected to periodic forces in machining is analyzed by Dai and Chen (2007) using the Mathieu-Hill equation. Ramakrishnan and Feeny (2012) used the method of multiple scales on a forced Mathieu equation to analyze the resonances in wind turbine blades. Kacem *et al.* (2011) studied the Euler Bernoulli beam model of the microgyroscope's sensing element described by the forced Mathieu type equation. McLachlan (1947) provides a comprehensive list of applications of the Mathieu function. In this work, multiple variants of the Mathieu equation are utilized to demonstrate the application of the theoretical framework. Some of the significant methods to analyze time varying systems are briefly explained in the following sections.

2.1 Floquet Theory

The application of Floquet theory towards stability analysis for linear time periodic systems has been demonstrated by Butcher and Sinha (1998); Sinha and Butcher (1997); Bittanti *et al.* (1984). Multiple approaches have been applied to determine the stability bounds and transition curves for time periodic systems by Kovacic *et al.* (2018). The stability analysis and response of a linear time periodic system are evaluated using the Floquet Theory. Consider a dynamical system of the form

$$\dot{\mathbf{x}} = \mathbf{A}(t)\mathbf{x} \tag{2.1}$$

where $\mathbf{x} \in \mathbb{R}^n, t \in \mathbb{R}^+, \mathbf{A}(t)$ is an $n \times n$ periodic matrix with the principal period, T. Let $\mathbf{\Phi}(t)$ be the STM that satisfies equation (2.1) and has the initial condition $\mathbf{\Phi}(0) = I$. The solution of the equation (2.1) can be written as

$$\mathbf{x}(t) = \mathbf{\Phi}(t)\mathbf{x}(0), \qquad 0 \leq t \leq T \tag{2.2}$$

For $t \geq T$, the solution can be calculated by

$$\mathbf{x}(t + mT) = \mathbf{\Phi}(t)\mathbf{\Phi}^m(T)\mathbf{x}(0), \qquad 0 \leq t \leq T, \qquad m = 1, 2, 3.... \tag{2.3}$$

where $\mathbf{\Phi}(T)$ is the Floquet transition matrix (FTM) or the Monodromy matrix. The stability criteria for periodic systems depend upon the eigenvalues of $\mathbf{\Phi}(T)$, called the Floquet multipliers, and the system is stable if all the Floquet multipliers lie on or inside the unit circle, other wise it is unstable.

According to the Lyapunov-Floquet theorem, the STM can be expressed as

$$\mathbf{\Phi}(t) = \mathbf{Q}(t)e^{\mathbf{R}t}, \qquad \mathbf{Q}(t) \in \mathbb{R}^{n\times n}, \qquad \mathbf{R} \in \mathbb{R}^{n\times n}, \qquad \forall t \geq 0 \tag{2.4}$$

where $\mathbf{Q}(t)$ is known as the L-F transformation matrix. The linear matrix transformation to a nonautonomous one is accomplished via L-F transformation, $\mathbf{x} = \mathbf{Q}(t)\mathbf{z}$. The L-F transformation matrix $\mathbf{Q}(t)$ elements contain truncated Fourier series representation, as explained by Sinha and Pandiyan (1994). Applying the L-F transformation to equation (2.1) results in equation (2.5) with a parameter-invariant linear part.

$$\dot{\mathbf{y}} = \mathbf{R}\mathbf{y} \tag{2.5}$$

where $\mathbf{R}$ is a constant $n \times n$ matrix that generally tends to be complex. The eigenvalues of the $\mathbf{R}$ are known as the Floquet Exponents, which could also be used as an indicator for the stability of the dynamical system.

2.2 State Augmentation

The application of intuitive state augmentation for reducing nonlinear systems using the Center Manifold Theory and Normal Forms technique was demonstrated by Waswa and Redkar (2019); Waswa *et al.* (2020); Waswa and Redkar (2020b). It was proved that the state augmentation method preserves the system dynamics. In

this work, a state augmentation is employed similarly to perform further analysis with time varying systems.

The intuitive state augmentation converts the time-periodic term into a state variable. This approach could be applied to periodic coefficients or periodic external forcing terms. For ease of understanding, let us consider a time periodic system given by equation (2.1), which is modified as equation (2.6)

$$\dot{\mathbf{x}} = (\mathbf{B_0} + \mathbf{B}(t))\mathbf{x} \tag{2.6}$$

where $\mathbf{B_0}(t)$ is the constant matrix, $\mathbf{x}$ is the vector containing the system states and $\mathbf{B}(t)\mathbf{x}$ is the $n \times 1$ vector containing the periodic coefficients as shown below

$$\mathbf{B}(t)\mathbf{x} = \begin{bmatrix} B_1 g_1(t) x_1 \\ B_2 g_2(t) x_2 \\ \vdots \\ B_i g_i(t) x_i \end{bmatrix}, \qquad i = 1, 2, 3, ..., n \tag{2.7}$$

where B_i is the amplitude of the forcing/periodic term and $g_i(t)$ represents a sine or cosine trigonometric function of ω_i i.e. $sin(\omega_i t)$ or $cos(\omega_i t)$. The system states are augmented as follows

$$
\left.
\begin{aligned}
p_1 &= g_1(t) \\
p_2 &= g_2(t) \\
&\vdots \\
p_n &= g_n(t) \\
\\
\dot{p}_1 &= \mp\,\omega_1 \dot{g}_1(t) = \mp\, q_1 \\
\dot{p}_2 &= \mp\,\omega_2 \dot{g}_2(t) = \mp\, q_2 \\
&\vdots \\
\dot{p}_n &= \mp\,\omega_n \dot{g}_n(t) = \mp\, q_n \\
\\
\dot{q}_1 &= \pm\,\omega_1^2 g_1(t) = \pm\,\omega_1^2 p_1 \\
\dot{q}_2 &= \pm\,\omega_2^2 g_2(t) = \pm\,\omega_2^2 p_2 \\
&\vdots \\
\dot{q}_n &= \pm\,\omega_n^2 g_n(t) = \pm\,\omega_n^2 p_n
\end{aligned}
\right\} \tag{2.8}
$$

Hence the augmented $l \times 1$ state vector is given by

$$
\tilde{\mathbf{x}} = [\mathbf{x}, p_1, p_2, \ldots, p_n, q_1, q_2, \ldots, q_n]^T \tag{2.9}
$$

The linear time periodic system gets converted to a nonlinear state augmented time-invariant system, as the periodic term expressed as states are updated to a nonlinear

vector in the form indicated in equation (2.10).

$$\tilde{\mathbf{B}}(\tilde{\mathbf{x}}) = \begin{bmatrix} B_1\breve{f}(\mathbf{x}, p_1, p_2, \ldots, p_n, q_1, q_2, \ldots, q_n) \\ B_2\breve{f}(\mathbf{x}, p_1, p_2, \ldots, p_n, q_1, q_2, \ldots, q_n) \\ \vdots \\ B_n\breve{f}(\mathbf{x}, p_1, p_2, \ldots, p_n, q_1, q_2, \ldots, q_n) \\ 0 \\ 0 \\ 0 \\ 0 \\ \vdots \\ 0 \\ 0 \end{bmatrix}, \; n = 3, 4, \ldots \tag{2.10}$$

With the state augmentation the equation (2.6) is updated as

$$\dot{\tilde{\mathbf{x}}} = \tilde{\mathbf{B}}_0\tilde{\mathbf{x}} + \tilde{\mathbf{B}}(\tilde{\mathbf{x}}) \tag{2.11}$$

where $\tilde{\mathbf{B}}_0$ is a $l \times l$ constant matrix and $\tilde{\mathbf{B}}(\tilde{\mathbf{x}})$ is a $l \times 1$ vector containing the augmented nonlinear monomial terms in $\tilde{\mathbf{x}}$. The equation (2.11) represents a nonlinear system and can be further analyzed using the traditional techniques for the analysis of such systems.

2.3 Normal Forms Technique

The Normal Forms theory originated from the works by Poincaré (1899). The theory was further developed and applied by subsequent researchers, such as Birkhoff (1927); Moser and Saari (1975); Arnold (1978); Chua and Kokubu (1988). Nayfeh (2011b) explains that it is a local transformation (known as near-identity transformation) technique used for the analysis of the nonlinear system around a fixed point

or equilibrium solution and its applications are comprehensively detailed by Murdock (2006). Though the Normal Forms technique has been predominantly used for the analysis of nonlinear equations, a mathematical framework on the application for periodic systems was detailed by Smith (1986). In Sinha *et al.* (1998), to construct a time invariant form, the L-F transformation is applied for the linear system and the Normal Forms technique for the nonlinear system. Gabale and Sinha (2009); Jezequel and Lamarque (1991) further applied this theory to nonlinear systems with periodic coefficients by incorporating a detuning parameter or a book-keeping parameter. The Normal Forms technique was majorly applied to nonlinear systems, and some researchers extended it towards stability analysis of such systems by Mond *et al.* (1993).

As explained by Nayfeh (2011b), the Normal Forms technique aids in eliminating many nonlinear terms by employing a near-identity transformation. This technique applies to both time-dependent and time-independent systems. They are detailed in the following subsections:-

2.3.1 Time Independent Normal Forms (TINF)

Consider a time-independent nonlinear dynamical system of the form.

$$\dot{\mathbf{x}} = \mathbf{A}\mathbf{x} + \mathbf{F}(\mathbf{x}) \tag{2.12}$$

where $\mathbf{A}$ is a constant $n \times n$ matrix and $\mathbf{F}(\mathbf{x})$ is a $n \times 1$ vector containing the nonlinear monomials in $\mathbf{x}$. After applying the modal transformation $\mathbf{x} = \mathbf{M}\mathbf{z}$ to equation (2.12), the Jordan canonical form is obtained as shown in equation (2.13)

$$\dot{\mathbf{z}} = \mathbf{J}\mathbf{z} + \mathbf{M}^{-1}\mathbf{F}(\mathbf{z}) \tag{2.13}$$

where $\mathbf{J}$ is the Jordan form of $\mathbf{A}$ and $\mathbf{M}$ is the modal transformation matrix. The diagonal elements of $\mathbf{J}$ matrix contain the eigenvalues of the linear matrix $\mathbf{A}$.

$$\mathbf{J} = \begin{bmatrix} \lambda_1 & & & \\ & \lambda_2 & & \\ & & \ddots & \\ & & & \lambda_n \end{bmatrix} \tag{2.14}$$

The system shown in equation (2.13) is amenable to an application of Time Independent Normal Forms, which is similar in principle to the averaging technique by Sanders *et al.* (2007). A near identity transformation (of the form equation (2.15)) is applied to equation (2.13)

$$\mathbf{z} = \mathbf{v} + \mathbf{h}_r(\mathbf{v}) \tag{2.15}$$

where $\mathbf{h}_r(\mathbf{v})$ is a homogenous vector of monomials in $\mathbf{v}$ of r degree. The general homological equation obtained by elimination of higher order nonlinearities is shown as

$$\frac{\partial \mathbf{h}_r(\mathbf{v})}{\partial \mathbf{v}} \mathbf{J}\mathbf{v} - \mathbf{J}\mathbf{h}_r - \mathbf{F}_r(\mathbf{v}) = 0 \tag{2.16}$$

where $\mathbf{F}_r(\mathbf{v})$ is expressed in terms of solutions of the homological equation of order $r-1$, for $r > 3$. An approximate solution to equation (2.16) can be expressed as

$$\left.\begin{aligned} \mathbf{h}_r(\mathbf{v}) &= \sum_{j=1}^{n} \sum_{\mathbf{m}_r} \sum_{\nu=-\infty}^{\nu=\infty} h_{j\mathbf{m}_r\nu} |\mathbf{v}|^{\mathbf{m}_r} \mathbf{e}_j, \\ \mathbf{F}_r(\mathbf{v}) &= \sum_{j=1}^{n} \sum_{\mathbf{m}_r} \sum_{\nu=-\infty}^{\nu=\infty} F_{j\mathbf{m}_r\nu} |\mathbf{v}|^{\mathbf{m}_r} \mathbf{e}_j \end{aligned}\right\} \tag{2.17}$$

where $\mathbf{m}_r = (m_1, m_2, ..., m_n)$, $\sum_{i=1}^{n} m_i = r$, $(r = 2, 3, ..., k)$, $\mathbf{e}_j$ is the j^{th} member of the natural basis and $|\mathbf{v}|^{\mathbf{m}_r} = {\mathbf{v}_1}^{m_1} {\mathbf{v}_2}^{m_2} .... {\mathbf{v}_n}^{m_n}$. After substituting equation (2.17) in

equation (2.16) and equating the coefficients of similar terms, result in

$$h_{j\mathbf{m}_r\nu} = \frac{F_{j\mathbf{m}_r\nu}}{\mathbf{m}_r.\lambda - \lambda_j} \tag{2.18}$$

where $\lambda = [\lambda_1, \lambda_2, \lambda_3 ... \lambda_n]^T$ are the eigenvalues of $\mathbf{A}$. The coefficients of r^{th} order near-identity can only be obtained if the following solvability condition is satisfied.

$$\mathbf{m}_r.\lambda - \lambda_j \neq 0 \tag{2.19}$$

The resonant nonlinear terms would remain in the near identity transformations, and equation (2.16) gets updated as

$$\dot{\mathbf{v}} = \mathbf{J}\mathbf{v} - \sum_{r=2}^{k} \mathbf{F}_r^*(\mathbf{v}) \tag{2.20}$$

where $\mathbf{F}_r^*(\mathbf{v})$ comprises of the resonant terms.

2.3.2 Time Dependent Normal Forms (TDNF)

Consider a time-dependent nonlinear dynamical system provided by equation (2.21).

$$\dot{\mathbf{x}} = \mathbf{A}\mathbf{x} + \mathbf{F}(\mathbf{x}, t) \tag{2.21}$$

where $\mathbf{A}$ is a constant $n \times n$ matrix and $\mathbf{F}(\mathbf{x}, t)$ is a $n \times 1$ vector containing the nonlinear time-dependent terms. The application of a modal transformation, $\mathbf{x} = \mathbf{M}\mathbf{z}$, converts equation (2.21) to its Jordan canonical as shown below

$$\dot{\mathbf{z}} = \mathbf{J}\mathbf{z} + \mathbf{M}^{-1}\mathbf{F}(\mathbf{z}, t) \tag{2.22}$$

where $\mathbf{J}$ is the Jordan form of $\mathbf{A}$ and $\mathbf{M}$ is the modal transformation matrix. The eigenvalues of the linear matrix $\mathbf{A}$ are populated along the diagonal elements of

Jmatrix, as indicated in equation (2.14). Further, a near-identity transformation (of the form equation (2.23)) is applied to equation (2.22).

$$\mathbf{z} = \mathbf{v} + \mathbf{h}_r(\mathbf{v}, t) \tag{2.23}$$

where $\mathbf{h}_r(\mathbf{v}, t)$ is a formal power series in $\mathbf{v}$ of degree r with T periodic coefficients.

$$\dot{\mathbf{v}} = \mathbf{J}\mathbf{v} - \left[\frac{\partial \mathbf{h}_r(\mathbf{v}, t)(\mathbf{v})}{\partial(\mathbf{v})}\mathbf{J}\mathbf{v} - \mathbf{J}\mathbf{h}_r(\mathbf{v}, t) + \frac{\partial \mathbf{h}_r(\mathbf{v}, t)}{\partial t}\right] + \mathbf{F}_r(\mathbf{v}, t) \tag{2.24}$$

The following condition eliminates the higher order nonlinear terms in equation (2.24)

$$\frac{\partial \mathbf{h}_r(\mathbf{v}, t)(\mathbf{v})}{\partial(\mathbf{v})}\mathbf{J}\mathbf{v} - \mathbf{J}\mathbf{h}_r(\mathbf{v}, t) + \frac{\partial \mathbf{h}_r(\mathbf{v}, t)}{\partial t} + \mathbf{F}_r(\mathbf{v}, t) = 0 \tag{2.25}$$

After solving equation (2.25), the solvability condition for a given degree of nonlinearity can be expressed as

$$h_{r,j,\mathbf{m}_r,l} = \frac{F_{r,j,\mathbf{m}_r,l}}{il\Omega + \mathbf{m}_r.\lambda - \lambda_j} \tag{2.26}$$

where $\lambda = [\lambda_1, \lambda_2, \lambda_3....\lambda_l]^T$ are the eigenvalues of $\mathbf{J}$ or the Floquet exponents, $\Omega = \frac{\pi}{T}$ and $-k \leq l \leq k$. All the coefficients of the near identity transformation are computed using the resonant condition indicated below.

$$il\Omega + \mathbf{m}_r.\lambda - \lambda_j \neq 0 \tag{2.27}$$

The resonant nonlinear terms would remain in the near identity transformations and equation (2.25) gets updated as

$$\dot{\mathbf{v}} = \mathbf{J}\mathbf{v} - \sum_{r=2}^{k} \mathbf{F}_r^*(\mathbf{v}, t) \tag{2.28}$$

A constant linear part of the equation (2.28) is observed in the absence of resonant terms. The system stability could be derived from this matrix. For better clarity of the concept, an application of the theory to a linear time-periodic Mathieu equation is explained in the subsequent subsection.

2.4 Unified Theory

Consider a linear time periodic system with both constant and periodic coefficients. The equation (2.1) can be updated as follows

$$\dot{\mathbf{x}}(t) = \mathbf{A}(t)\mathbf{x}(t) \tag{2.29}$$

where $\mathbf{A}(t) = \mathbf{B}_0 + \mathbf{B}(t)$. By applying the L-F transformation directly on this system, as mentioned in section 2.1 converts it into a time-invariant system, as shown below, in equation (2.30)

$$\dot{\mathbf{y}}(t) = \mathbf{R}\mathbf{y}(t) \tag{2.30}$$

The solution to equation (2.30) can be provided as

$$\mathbf{y}(t) = e^{\mathbf{R}t}\mathbf{y}(0) \tag{2.31}$$

Instead of the L-F transformation, if the periodic terms were to be augmented, the original system equation (2.29), gets updated as equation (2.11), as mentioned in 2.2. The updated system has a constant linear part ($\tilde{\mathbf{B}}_0$) and time independent nonlinear part ($\tilde{\mathbf{B}}(\tilde{\mathbf{x}})$), as shown in equation (2.11). A modal transformation on the updated system, $\tilde{\mathbf{x}}(t) = \tilde{\mathbf{M}}\tilde{\mathbf{z}}(t)$, would get the system updated as

$$\dot{\tilde{\mathbf{z}}} = \tilde{\mathbf{J}}\tilde{\mathbf{z}} + \tilde{\mathbf{M}}^{-1}\tilde{\mathbf{B}}(\tilde{\mathbf{z}}) \tag{2.32}$$

where $\tilde{\mathbf{M}}$ is the modal transformation matrix, and $\tilde{\mathbf{J}}$ is the Jordan form of $\tilde{\mathbf{B}}_0$, which contains the eigenvalues of both the original states and the augmented states, as shown below in equation (2.33).

$$\tilde{\mathbf{J}} = \left[\begin{array}{ccc|ccc} \lambda_1 & & & & & \\ & \lambda_2 & & & & \\ & & \ddots & & & \\ & & & \lambda_n & & \\ \hline & & & \lambda_{n+1} & & \\ & & & & \lambda_{n+2} & \\ & & & & & \ddots \\ & & & & & & \lambda_l \end{array}\right] \tag{2.33}$$

At this point, since equation (2.32) is in the Jordan form with semi-simple eigenvalues, a near-identity transformation (equation (2.15)) and the Time Independent Normal Forms technique could be applied as indicated in section 2.3.1. It is noted that in this particular case, one has to find higher order Normal Form than the order of the nonlinearity (i.e., two) and then replace the fictitious/augmented states with their closed form expressions. In case of no resonance, the TINF solution would result in a time-invariant system.

At this point, the near identity transformation would contain the dynamics due to both the system states and the augmented states. The near identity transformation of the reduced state can also be expressed as

$$\tilde{\mathbf{z}}(t) = \left[\mathbf{I} + \tilde{\mathbf{Q}}(t)\right] \tilde{\mathbf{v}} \approx \bar{\mathbf{Q}}(t)\tilde{\mathbf{v}}(t) \tag{2.34}$$

where $\bar{\mathbf{Q}}$ serves as the near-identity transformation matrix and contains all the higher order nonlinear terms/coefficients associated with the states, and it converts the system in equation (2.29) into a linear time-invariant system, as follows

$$\dot{\tilde{\mathbf{v}}} = \bar{\mathbf{J}}\tilde{\mathbf{v}} \tag{2.35}$$

It can be summarized that once the known temporal terms replace the augmented states, the near-identity transformation (in TINF technique), essentially serves as an L-F transformation and converts the linear time variant system to a linear time-invariant system (equation (2.35)). It is observed that it is identical to equation (2.28), considering the resonant terms are absent.

At this point, the augmented states are back substituted into the TINF solution, and it is observed that the $\bar{\mathbf{Q}}(t)$ matrix becomes a function of time. As indicated in equation (2.4), by applying L-F transformation, the STM of the TINF solution can be expressed as

$$\bar{\mathbf{\Phi}}(t) = \bar{\mathbf{Q}}(t)e^{\bar{\mathbf{J}}t} \tag{2.36}$$

As indicated in section 2.1, at t =T, the FTM of the reduced system is obtained, and the stability plots are generated based on the conditions on Floquet multipliers and Floquet exponents. Since the reduced system would preserve the dynamical characteristics of the original system, the transition curves would resemble that from the stability analysis of the original system.

It is also noted that using this technique, the closed form expression for STM is obtained for the reduced system ($\bar{\mathbf{\Phi}}(t)$) and thereby that of the original system, $\hat{\mathbf{\Phi}}(t)$, using back transformation. This would aid in predicting the state evolution of the original system over time in a closed form. The $\hat{\mathbf{\Phi}}(t)$ matrix is utilized to determine the L-F transformation matrix of the original system, $\hat{\mathbf{Q}}(t)$ analytically, using equation (2.4). Later, it is compared with the L-F transformation matrix, $\mathbf{Q}(t)$, applied directly to the original system as per Floquet theory. For clarity, a brief overview of the proposed approach is shown in Figure 2.1.

The closed form expression for the STM ($\bar{\mathbf{\Phi}}(t)$) of the TINF reduced solution is obtained from the equation (2.36). This undergoes multiple reverse transformations

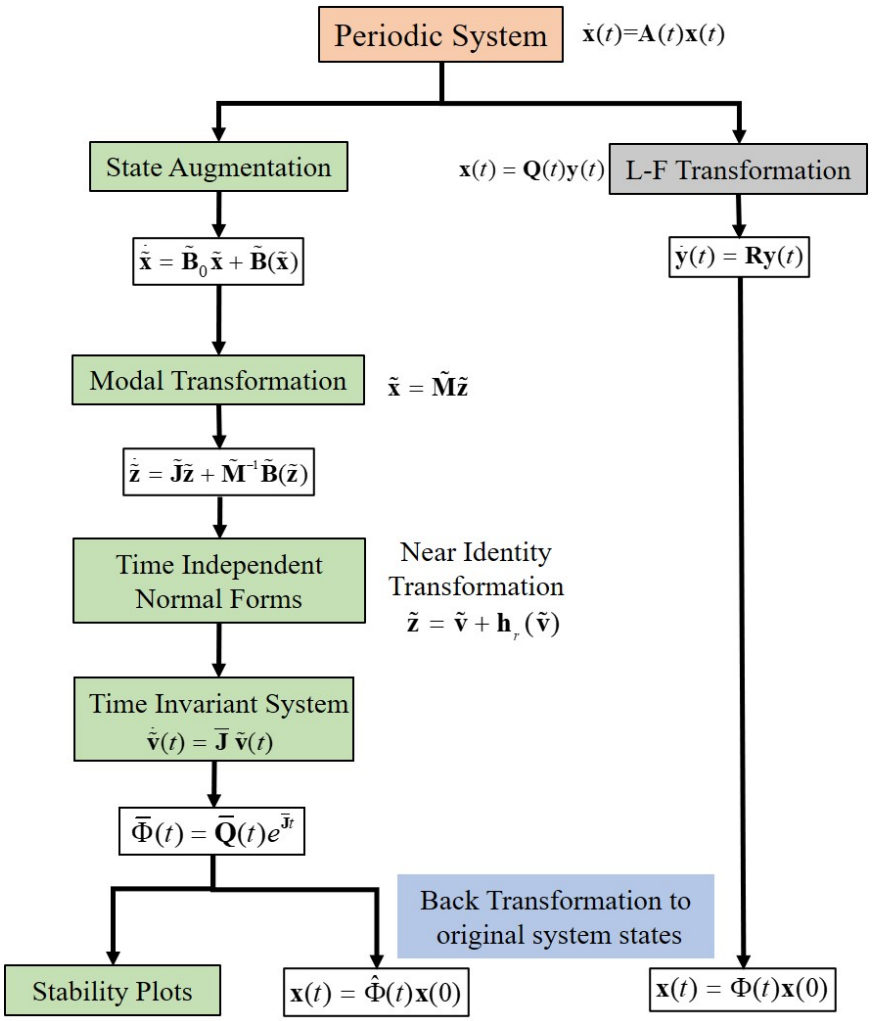

Figure 2.1: Overview of the Unified Theory

to derive the STM ($\hat{\mathbf{\Phi}}(t)$) in original coordinates, which is of the form equation (2.4). The FTM computed at $\hat{\mathbf{\Phi}}(t = T)$, is further utilized for the computation of the Exponent Matrix $\hat{\mathbf{R}}$ using the relationship

$$\hat{\mathbf{R}} = \frac{1}{T} logm(\hat{\mathbf{\Phi}}(T)) \tag{2.37}$$

The computed $\hat{\mathbf{R}}$ matrix is utilized to compute the closed form expression for the L-F transformation using the relationship

$$\hat{\mathbf{Q}}(t) = \hat{\mathbf{\Phi}}(t)e^{-\hat{\mathbf{R}}t} \tag{2.38}$$

The derived closed form expression for the L-F transformation can be verified using the equation

$$\hat{\mathbf{Q}}^{-1}(t)[\mathbf{A}(t).\hat{\mathbf{Q}}(t) - \dot{\hat{\mathbf{Q}}}(t)] = \hat{\mathbf{R}} \tag{2.39}$$

2.4.1 Application of the Unified theory

To verify the unified theory, a system with constant and time-periodic coefficients is studied. After performing the stability analysis, a case of system parameter is selected to analyze the dynamical characteristics of the system further. The application of the proposed unified approach for two systems is detailed in this section. Initially, a time periodic system with no damping is verified, and later a damping coefficient is added to the system.

System Without Damping

Consider a modified Mathieu equation as shown below.

$$\ddot{x} + (a + b\cos(\omega t))x = 0 \tag{2.40}$$

After rearrangement, it could be expressed as

$$\ddot{x} = -ax - bx\cos(\omega t) \tag{2.41}$$

By replacing the periodic coefficients with augmented states, as mentioned in section 2.2, the following is obtained

$$
\begin{aligned}
p &= \cos(\omega t) \\
\dot{p} &= -\omega \sin(\omega t) = q \\
\ddot{p} &= -\omega^2 \cos(\omega t) = -\omega^2 p = \dot{q}
\end{aligned} \tag{2.42}
$$

After substituting equation (2.42) in equation (2.41) and converting it to the state space form gives us

$$
\frac{d}{dt}\begin{Bmatrix} x \\ \dot{x} \\ p \\ \dot{q} \end{Bmatrix} = \begin{bmatrix} 0 & 1 & 0 & 0 \\ -a & 0 & 0 & 0 \\ 0 & 0 & 0 & 1 \\ 0 & 0 & -\omega^2 & 0 \end{bmatrix} \begin{Bmatrix} x \\ \dot{x} \\ p \\ \dot{q} \end{Bmatrix} + \begin{Bmatrix} 0 \\ -bxp \\ 0 \\ 0 \end{Bmatrix} \tag{2.43}
$$

By comparing equation (2.43) with equation (2.11), the following is obtained

$$
\begin{Bmatrix} x \\ \dot{x} \\ p \\ \dot{q} \end{Bmatrix} = \begin{Bmatrix} X_1 \\ X_2 \\ X_3 \\ X_4 \end{Bmatrix}, \begin{bmatrix} 0 & 1 & 0 & 0 \\ -a & 0 & 0 & 0 \\ 0 & 0 & 0 & 1 \\ 0 & 0 & -\omega^2 & 0 \end{bmatrix} = \tilde{\mathbf{B}}_0, \begin{Bmatrix} 0 \\ -bxp \\ 0 \\ 0 \end{Bmatrix} = \tilde{\mathbf{B}}(\tilde{\mathbf{x}}) \tag{2.44}
$$

As mentioned in Section 2.3.1, the unified approach is applied and performs the modal transformation. This converts the equation (2.40) to its Jordan canonical form with semi-simple eigenvalues, as shown in equation (2.32). For this section, the TINF solution of the order of three was considered to ensure that enough nonlinear terms are accounted. For more accurate results, one may have to include higher order, but it would increase the computational time. The analytical expression of the transformed system using TINF is shown in equation (2.45)

$$\frac{d}{dt}\begin{Bmatrix} V_1 \\ V_2 \\ V_3 \\ V_4 \end{Bmatrix} = \begin{pmatrix} \left(\frac{-b^2V_3V_4+a\omega^2(4a-\omega^2)}{\sqrt{-a}(4a-\omega^2)\omega^2}\right)V_1 \\ \left(\frac{1}{\sqrt{-a}}\left(-a+\frac{b^2V_3V_4}{(4a-\omega^2)\omega^2}\right)\right)V_2 \\ \left(-\sqrt{-\omega^2}\right)V_3 \\ \left(\sqrt{-\omega^2}\right)V_4 \end{pmatrix} \tag{2.45}$$

From equation (2.45), the following expressions for the augmented states could be obtained and substituted back to the expressions of the first two states

$$V_3 = e^{(-\sqrt{-\omega^2})t}V_{30}, V_4 = e^{(\sqrt{-\omega^2})t}V_{40} \tag{2.46}$$

Hence all the system dynamics are contained in the first two states and could be expressed as

$$\begin{aligned} V_1 &= e^{\left(\frac{-b^2e^{\left(-\sqrt{-\omega^2}\right)t}V_{30}e^{\left(\sqrt{-\omega^2}\right)t}V_{40}+a\omega^2(4a-\omega^2)}{\sqrt{-a}(4a-\omega^2)\omega^2}\right)t}V_{10} \\ V_2 &= e^{\left(\frac{1}{\sqrt{-a}}\left(-a+\frac{b^2e^{\left(-\sqrt{-\omega^2}\right)t}V_{30}e^{\left(\sqrt{-\omega^2}\right)t}V_{40}}{(4a-\omega^2)\omega^2}\right)\right)t}V_{20} \end{aligned} \tag{2.47}$$

By expressing the updated equation (2.45) in the matrix multiplication form, the expression for $\bar{\mathbf{J}}$ matrix can be obtained. By substituting equation (2.46) in the Near Identity Transformation matrix and expressing it in the form of matrix multiplication would resemble the expression indicated in equation (2.34). The higher the order of the TINF solution, the longer the expression would be, as it accounts for more nonlinear terms. The state evolution of the system could be computed in the TINF coordinate ($\bar{\mathbf{\Phi}}(t)$) by considering only the first two states. The initial conditions in the original system coordinates ($X_{10}, X_{20}, X_{30}, X_{40}$) are substituted and perform the subsequent transformations to obtain its corresponding values in the TINF coordinates ($V_{10}, V_{20}, V_{30}, V_{40}$). By substituting the initial conditions in the TINF coordinate, the expression for the STM, $\hat{\mathbf{\Phi}}(t)$, in the original system coordinates is obtained. The evolution of the state over the period of time is determined using

$\hat{\mathbf{\Phi}}(t)$, and the results are compared with that of the numerical integration results of the system in original coordinates.

System With Damping

Consider a modified damped Mathieu equation as shown below.

$$\ddot{x} + (a + b\cos(\omega t))x + d\dot{x} = 0 \tag{2.48}$$

The state space form of the equation with damping gets updated as follows

$$\frac{d}{dt}\begin{Bmatrix} x \\ \dot{x} \\ p \\ \dot{q} \end{Bmatrix} = \begin{bmatrix} 0 & 1 & 0 & 0 \\ -a & -d & 0 & 0 \\ 0 & 0 & 0 & 1 \\ 0 & 0 & -\omega^2 & 0 \end{bmatrix} \begin{Bmatrix} x \\ \dot{x} \\ p \\ \dot{q} \end{Bmatrix} + \begin{Bmatrix} 0 \\ -bxp \\ 0 \\ 0 \end{Bmatrix} \tag{2.49}$$

By comparing equation (2.49) to equation (2.11), the following can be deduced

$$\begin{Bmatrix} x \\ \dot{x} \\ p \\ \dot{q} \end{Bmatrix} = \begin{Bmatrix} X_1 \\ X_2 \\ X_3 \\ X_4 \end{Bmatrix}, \begin{bmatrix} 0 & 1 & 0 & 0 \\ -a & -d & 0 & 0 \\ 0 & 0 & 0 & 1 \\ 0 & 0 & -\omega^2 & 0 \end{bmatrix} = \tilde{\mathbf{B}}_0, \begin{Bmatrix} 0 \\ -bxp \\ 0 \\ 0 \end{Bmatrix} = \tilde{\mathbf{B}}(\tilde{\mathbf{x}}) \tag{2.50}$$

Since the damping coefficient (d) is added to the $\tilde{\mathbf{B}}_0$ matrix, the modal transformation matrix gets updated accordingly, and so does the Jordan canonical form of the equation. Similar to the case of '*System without damping*', the resulting transformed TINF system with damping is shown below in equation (2.51)

$$\frac{d}{dt}\begin{Bmatrix} V_1 \\ V_2 \\ V_3 \\ V_4 \end{Bmatrix} = \begin{pmatrix} \left(\frac{\sqrt{d^2-4a}(d^2-4a+\omega^2)(-4b^2V_3V_4+(-d^2+4a-d\sqrt{d^2-4a})(-d^2+4a-\omega^2)\omega^2)}{-2(\sqrt{d^2-4a}+\sqrt{-\omega^2})^2(d^2-4a-\sqrt{d^2-4a}\sqrt{-\omega^2})^2\omega^2}\right)V_1 \\ \left(\frac{\sqrt{d^2-4a}(d^2-4a+\omega^2)(4b^2V_3V_4+(d^2-4a+d\sqrt{d^2-4a})(-d^2+4a-\omega^2)\omega^2)}{-2(\sqrt{d^2-4a}+\sqrt{-\omega^2})^2(d^2-4a-\sqrt{d^2-4a}\sqrt{-\omega^2})^2\omega^2}\right)V_2 \\ \left(-\sqrt{-\omega^2}\right)V_3 \\ \left(\sqrt{-\omega^2}\right)V_4 \end{pmatrix} \tag{2.51}$$

All the steps followed for the system without damping remain the same, and proceed with finding the STM, $\hat{\Phi}(t)$, in the original system coordinates. This approach could also be extended for the system with periodic external excitation, where the excitation term could be expressed as an augmented state. The results of both the systems with/without damping and their comparison with the numerical integration methods are detailed in the following subsection.

2.4.2 Simulation Results

The proposed unified theory was tested to study the dynamical behavior of the selected stable system, for both with and without damping, as per section 2.4. The Floquet multiplier and exponent results for each case were compared with that from Chebfun. The Chebfun package in MATLAB employs the shifted Chebyshev Polynomials approach to analyze a time periodic system Driscoll *et al.* (2014). Additionally, the solution in the TINF coordinate was back transformed to the original system coordinates and compared with the corresponding numerically integrated solution for temporal variations of system states. Finally, the time evolution of individual elements of the L-F transformation matrix was evaluated and compared with the truncated Fourier series obtained from Chebfun.

Stable System Without Damping

For the selected system parameters of a=2 and b=4, the dynamical characteristics of the stable system are evaluated. From the TINF solution (equation (2.47)), the analytical expression for STM is derived as indicated in (2.36). This STM is evaluated at the principal time period to obtain the FTM, $\bar{\mathbf{\Phi}}(t = T)$. Using the unified approach detailed in section 2.4.1, the resulting time-invariant $\bar{\mathbf{J}}$ matrix is determined to be

$$\bar{\mathbf{J}} = \begin{bmatrix} 0.0 - i1.5037 & 0 \\ 0 & 0.0 + i1.5037 \end{bmatrix} \tag{2.52}$$

The subsequent STM computation in the TINF coordinates and back transformation to the original coordinates results in the $\hat{\mathbf{R}}$ matrix, using equation (2.37), as

$$\mathbf{R} = \begin{bmatrix} 0.0 & 1.3125 \\ -1.7223 & 0 \end{bmatrix}, \quad \hat{\mathbf{R}} = \begin{bmatrix} 0.0 & 1.309 \\ -1.7282 & 0 \end{bmatrix} \tag{2.53}$$

The results of the $\hat{\mathbf{R}}$ matrix match the corresponding Chebfun results ($\mathbf{R}$ matrix) and provide us with enough confidence to utilize the same towards the computation of the closed form expression for the L-F transformation matrix. Using the equation (2.38), the resulting time varying $\hat{\mathbf{Q}}(t)$ matrix is computed and verified to satisfy the property in equation (2.39). The Floquet multipliers and exponents computed using $\bar{\mathbf{\Phi}}(t = T)$ and its comparison with the Chebfun results are indicated in Table 2.1 and Figure 2.2.

It is evident from Table 2.1 that the key parameters deciding the dynamic stability of the system (Floquet multipliers and exponents) obtained using both approaches agree. Since the absolute value of the Floquet multipliers lies on the unit circle, the system is simply stable. It is also noted that the Floquet Exponents match the

Table 2.1: Comparison of Dynamical Characteristics of the System Without Damping

Parameter	From Chebfun	From TINF solution
Floquet Multipliers	$0.0673 \pm i0.9977$	$0.0662 \pm i0.9858$
Floquet Exponents	$0.0000 \pm i1.5035$	$0.0000 \pm i1.5037$

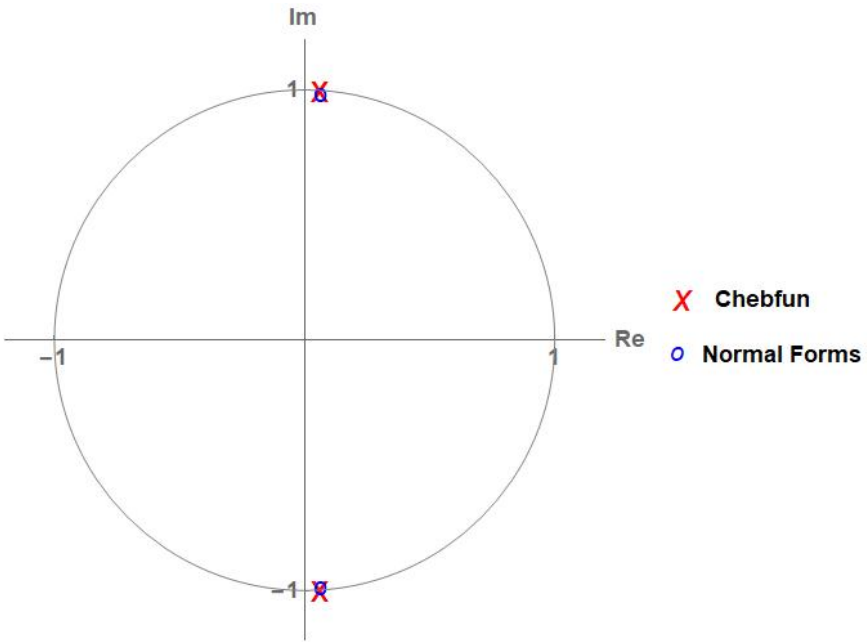

Figure 2.2: Floquet Multipliers Indicated on a Unit Circle for the System Without Damping

eigenvalues of $\bar{\mathbf{J}}$ matrix. The Floquet exponents from both approaches are observed to be majorly on the imaginary axis and hence confirming the system is stable.

As mentioned in section 2.4, the STM of the reduced TINF solution is back transformed to the original coordinates to obtain $\hat{\mathbf{\Phi}}(t)$ matrix. This matrix is then multiplied with the initial conditions of the original system variables, as per equation (2.2), to determine the system state variation. Simultaneously, equation (2.40) was numerically integrated with the same value of constants and initial conditions. The comparison of the variation of the system states is plotted in Figure 2.3 and the phase plot comparisons in Figure 2.4.

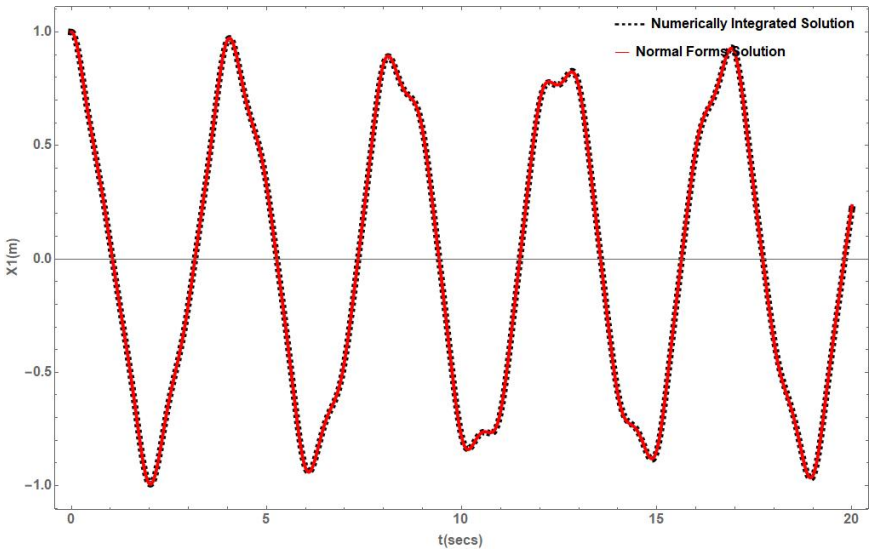

(**a**)

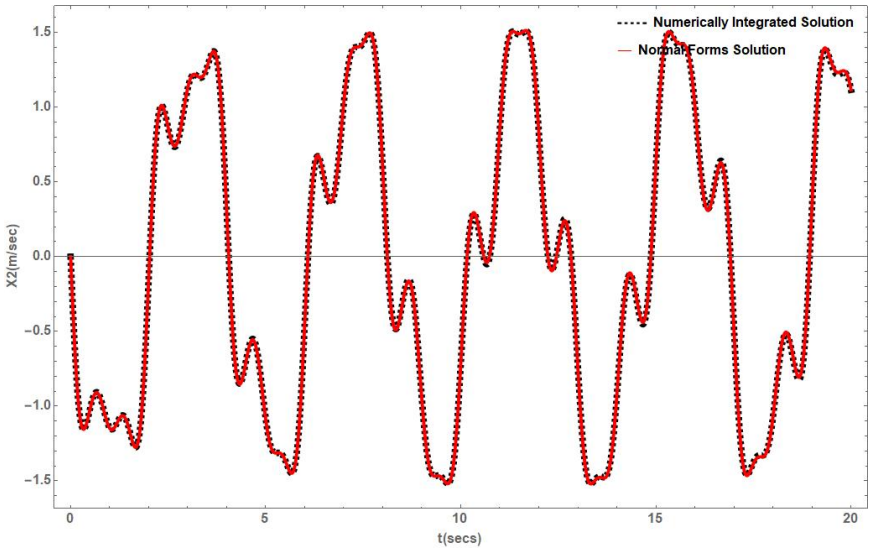

(**b**)

Figure 2.3: Comparison of Temporal Variation of System States for the System Without Damping. The System Parameters Are $a = 2, b = 4$ and $\omega = 2\pi$ for the Variation of (**a**) x_1 System State, (**b**) x_2 System State.

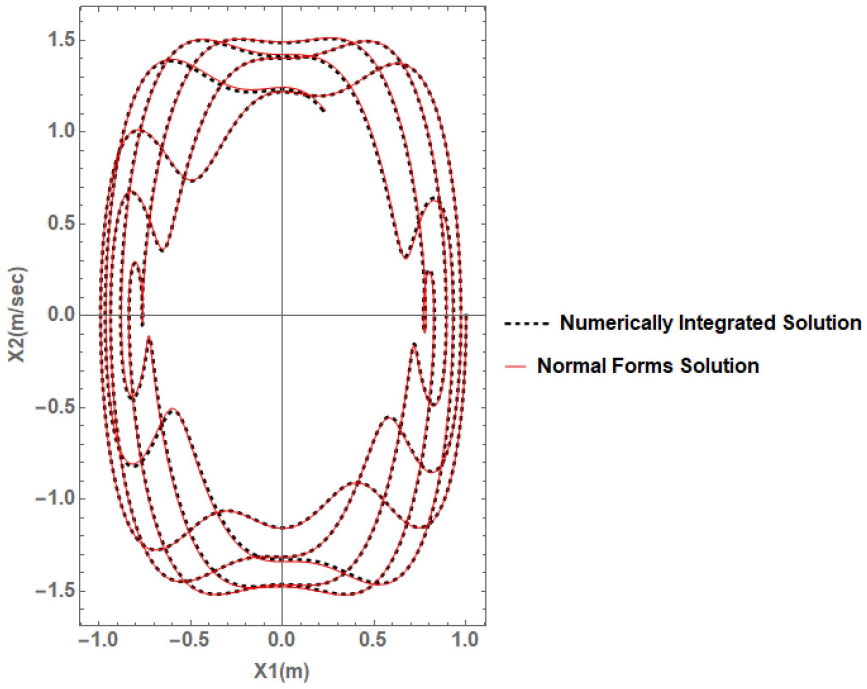

Figure 2.4: Phase Plot Comparison of the Stable System Without Damping

In Figures 2.3 and 2.4, the solid red line indicates the temporal variation based on the STM, $\hat{\mathbf{\Phi}}(t)$, determined from the TINF technique, and the black dashed line represents the numerically integrated solution of equation (2.40). In all these plots, the system is observed to follow a stable periodic behavior and does not deviate away from the initial conditions ($X_{10} = 1, X_{20} = 0$). The temporal variations and the phase plot from the proposed approach follow the numerical integration results closely. This validates the proposed approach of the TINF technique for the case of the stable system without damping. The elements of the $\hat{\mathbf{Q}}(t)$ matrix are plotted against time and compared with the truncated Fourier series obtained from Chebfun, as shown in Figure 2.5, for the duration of the principal time period.

In Figure 2.5, the black dashed line indicates the truncated Fourier series obtained from Chebfun, and the solid blue line indicates the elements of $\hat{\mathbf{Q}}(t)$ matrix, computed from closed form via the unified approach presented here. It can be observed that all the elements of $\hat{\mathbf{Q}}(t)$ matrix match perfectly with the Chebfun results for a stable sys-

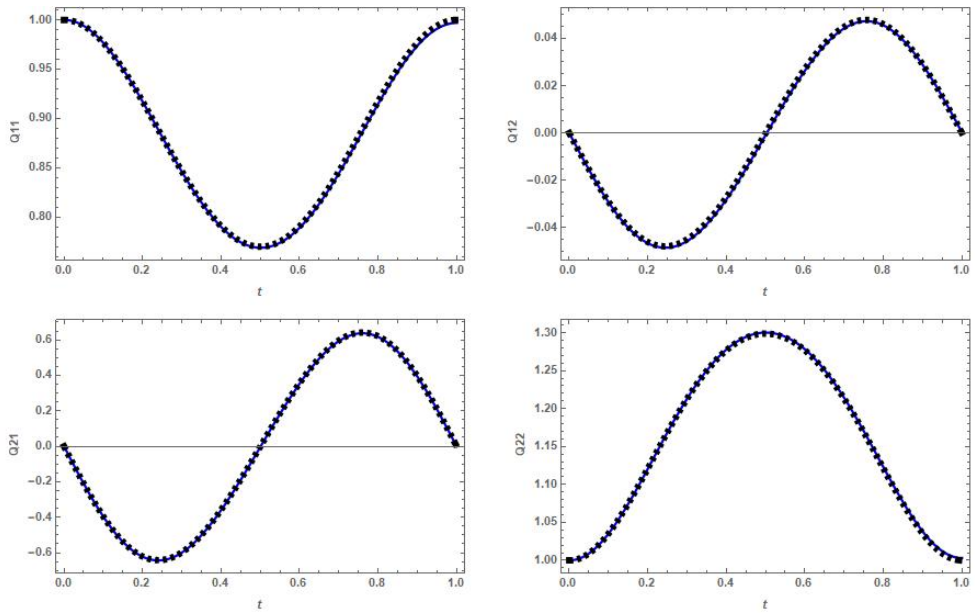

Figure 2.5: L-F Transformation Matrix Element-wise Comparisons of the Stable System Without Damping for the Duration of Principal Period. The Dashed Black Line Indicates the Chebfun Result and the Solid Blue Line Indicates the Unified Approach Results

tem without damping. Hence the analytical expression for $\hat{\mathbf{Q}}(t)$ matrix derived from the TINF solution is indeed the closed form expression for the L-F transformation matrix for a linear time periodic system.

Stable System With Damping

In addition to the selected system parameters of a=2 and b=4, a damping coefficient of d=0.30 is considered to evaluate the dynamical characteristics of the damped stable system. The system equation used in this case is equation (2.45), and the procedure mentioned in section 2.4.1 is followed. Though the equations look slightly different, the principal time period and process remain the same as the case of '*stable system without damping*'. From the TINF solution (equation (2.48)), the STM and further FTM, $\bar{\mathbf{\Phi}}(t = T)$ are evaluated. In this case, the resulting time-invariant $\bar{\mathbf{J}}$ matrix is determined to be

Table 2.2: Comparison of Dynamical Characteristics of the System With Damping

Parameter	From Chebfun	From TINF solution
Floquet Multipliers	$0.0646 \pm i0.8583$	$0.0638 \pm i0.8512$
Floquet Exponents	$-0.150 \pm i1.4957$	$-0.158 \pm i1.4959$

$$\bar{\mathbf{J}} = \begin{bmatrix} -0.158 - i1.4959 & 0 \\ 0 & -0.158 + i1.4959 \end{bmatrix} \tag{2.54}$$

The subsequent STM computation in the TINF coordinates are back transformed to the original coordinates results in the $\hat{\mathbf{R}}$ matrix, using equation (2.37), as

$$\mathbf{R} = \begin{bmatrix} 0.0467 & 1.3114 \\ -1.7355 & -0.3467 \end{bmatrix}, \quad \hat{\mathbf{R}} = \begin{bmatrix} 0.0451 & 1.3007 \\ -1.7506 & -0.3451 \end{bmatrix} \tag{2.55}$$

In this case too, the $\hat{\mathbf{R}}$ matrix matches the corresponding results from Chebfun ($\mathbf{R}$ matrix) and is utilized towards the computation of the closed form expression for the L-F transformation matrix. Again, the resulting time varying $\hat{\mathbf{Q}}(t)$ matrix is computed and verified to satisfy the property in equation (2.39). Table 2.2 displays the Floquet multipliers and exponents computed using $\bar{\mathbf{\Phi}}(t = T)$ and that from the Chebfun results.

It is evident from Table 2.2 and Figure 2.6 that the key parameters deciding the dynamic stability of the system (Floquet multipliers and exponents) are in agreement using both approaches. Since the absolute value of the Floquet multipliers lies inside the unit circle, the system is deduced to be stable. Furthermore, the Floquet exponents appear to be on the left side of the imaginary axis because of a prominent negative real part. Hence, it could be inferred that the system is asymptotically stable.

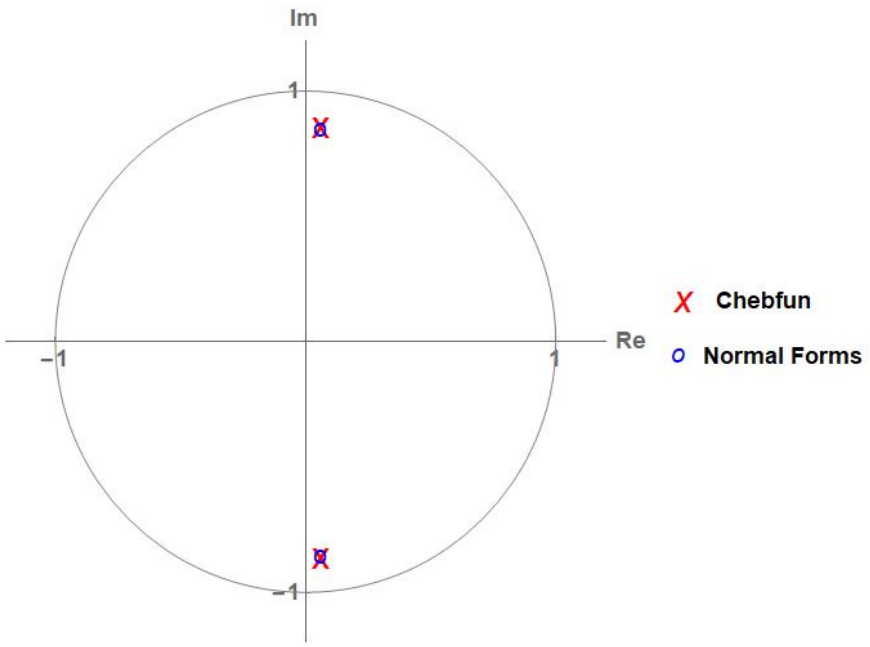

Figure 2.6: Floquet Multipliers Indicated on a Unit Circle for the System with Damping

Similar to the case of '*Stable System Without Damping*', the temporal variation of the system states are computed from the STM ($\hat{\mathbf{\Phi}}(t)$) and compared with the numerically integrated solution for the exact value of constants and initial conditions. The comparison of the temporal variation of the system is plotted in Figure 2.7, and the phase plot comparisons are displayed in Figure 2.8.

In Figures 2.7 and 2.8, the solid red line indicates the temporal variation based on the STM ($\hat{\mathbf{\Phi}}(t)$) determined from the TINF technique, and the black dashed line represents the numerically integrated solution of equation (2.45). From Figure 2.7, it is noted that the temporal variations of the system states are decaying over time due to the presence of damping. From the phase plot in Figure 2.8, it is observed that system is spiraling in from the initial conditions ($X_{10} = 1, X_{20} = 0$). In all three plots, the TINF solution is following the numerically integrated solution closely. Hence the TINF technique is capable of preserving the dynamical behavior of the original even in the presence of a damping element. The proposed unified approach is validated for

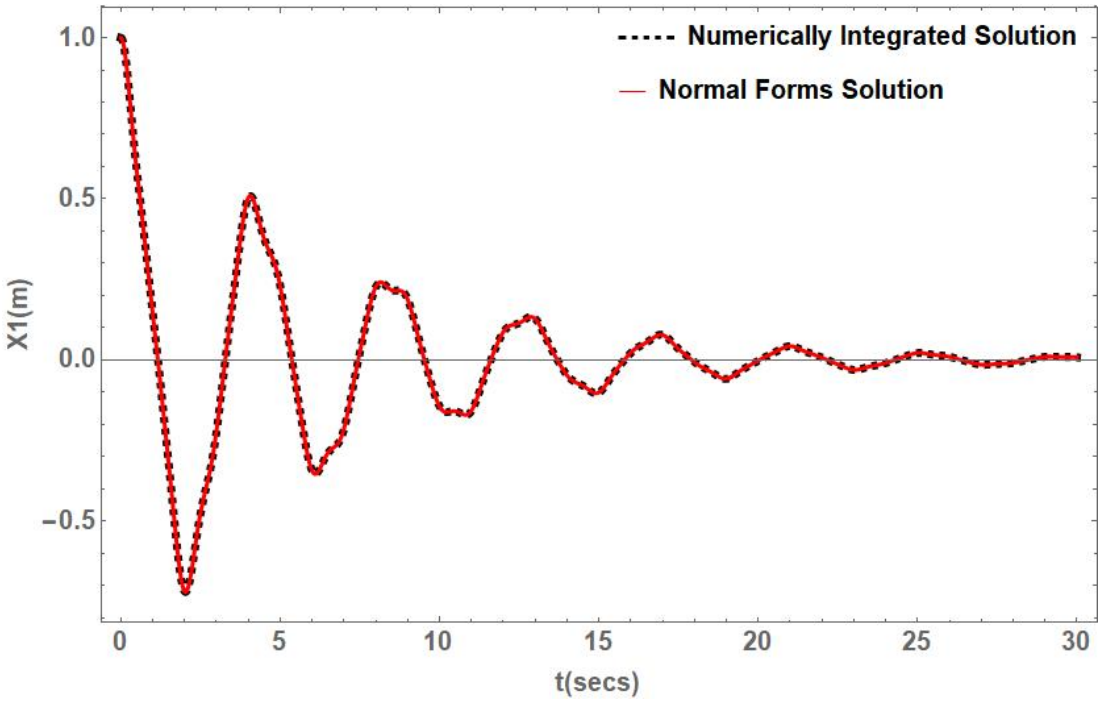

(**a**)

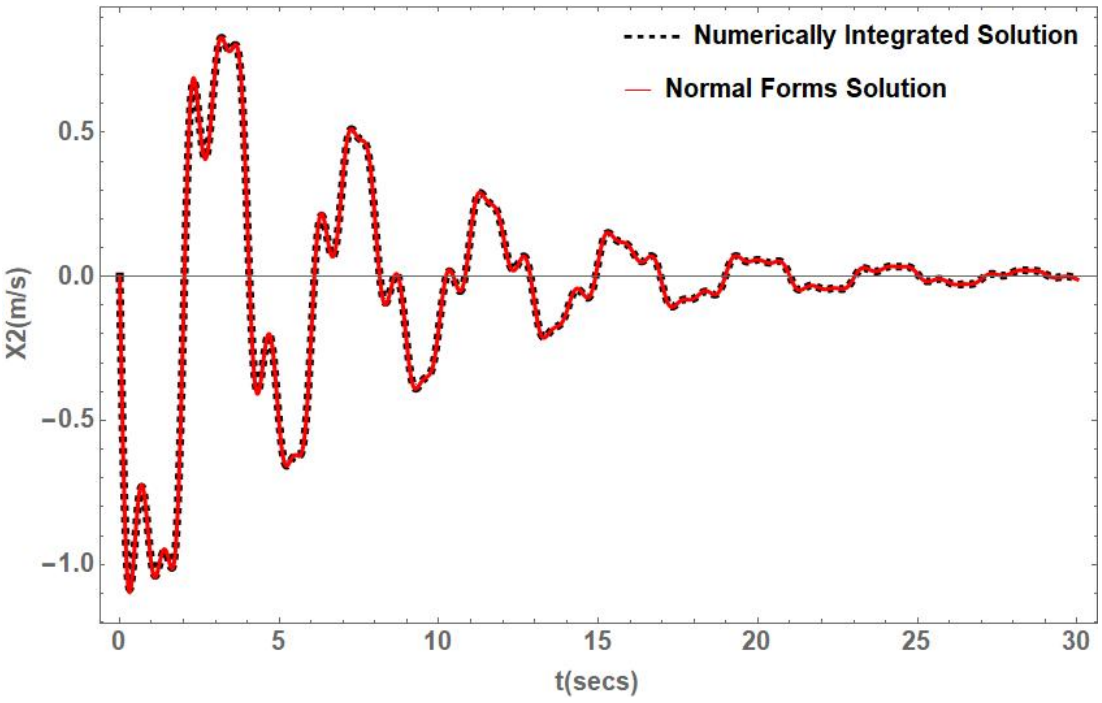

(**b**)

Figure 2.7: Comparison of Temporal Variation of System States for the System with Damping. The System Parameters Are $a = 2, b = 4, d = 0.3$ and $\omega = 2\pi$ for the Variation of (**a**) x_1 System State, (**b**) x_2 System State.

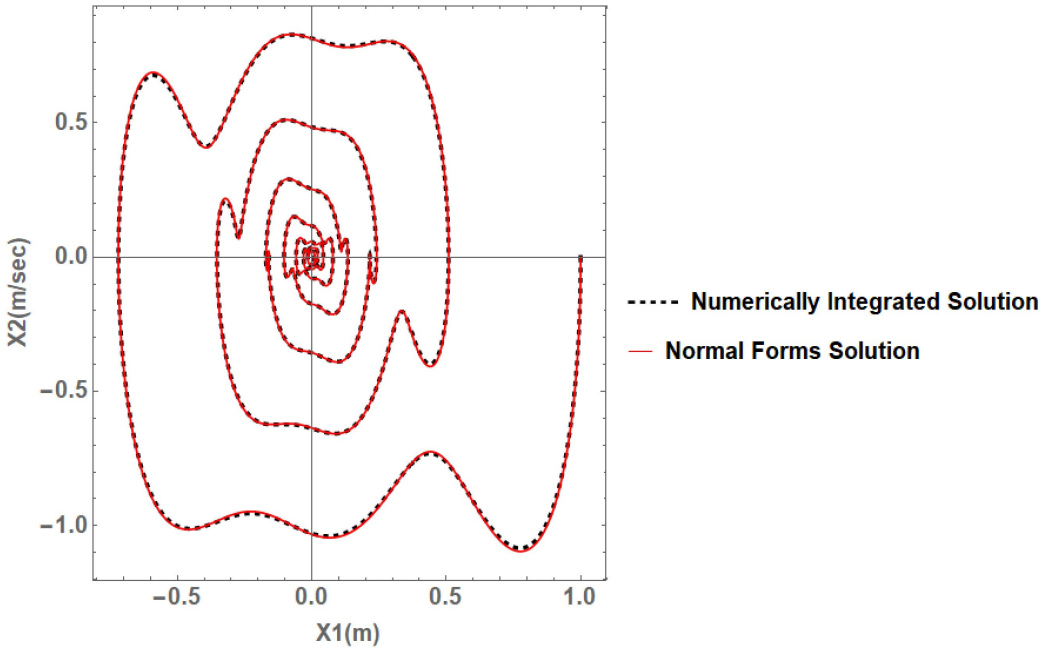

Figure 2.8: Phase Plot Comparison of the Stable System with Damping

a linear time periodic system with damping too.

Similar to the '*Stable System Without Damping*', the expression for the L-F transformation matrix of the original system, $\mathbf{Q}(t)$, was determined numerically via Chebfun and analytically using the unified approach presented here. The elements of the $\hat{\mathbf{Q}}(t))$ matrix, are plotted against time and compared with the Chebfun results for the duration of the principal period, as shown in Figure 2.9.

In Figure 2.9, the black dashed line indicates the truncated Fourier series obtained from Chebfun, and the solid blue line indicates the elements of $\hat{\mathbf{Q}}(t)$ matrix computed from the TINF solution. It is observed that all the elements of $\hat{\mathbf{Q}}(t)$ matrix match closely with the Chebfun results. Hence, the proposed unified approach is capable of providing a closed form analytical expression for the L-F transformation matrix for a linear time periodic system with and without damping.

The reduced form using the proposed unified approach successfully replicated the dynamical properties of undamped and damped cases of a time periodic dynamical

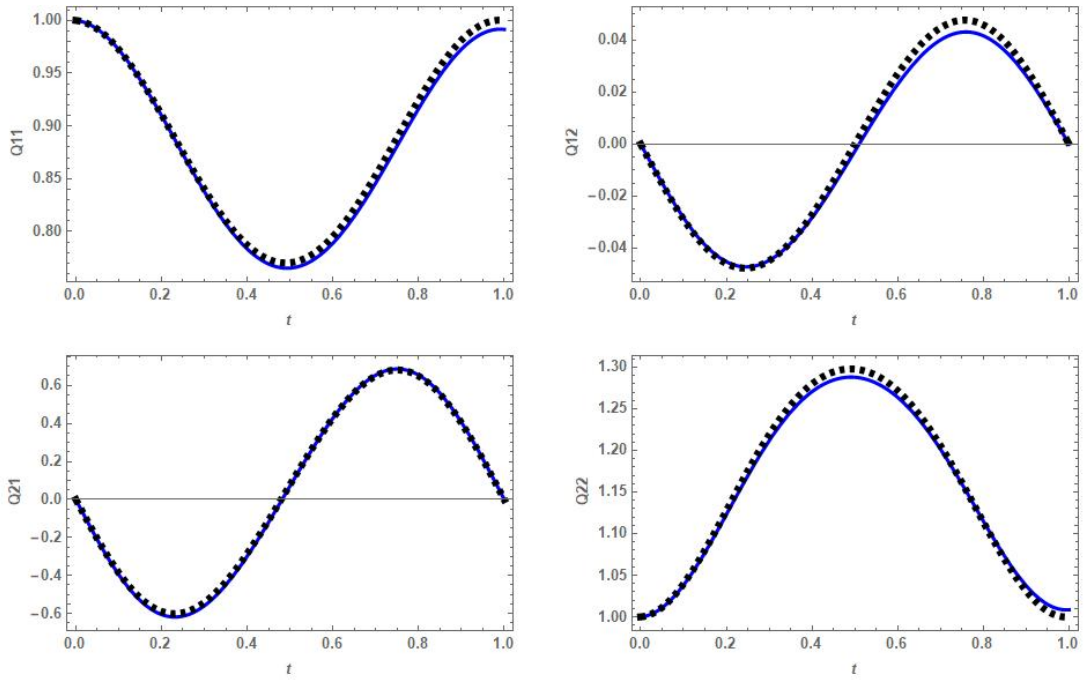

Figure 2.9: L-F Transformation Matrix Element-wise Comparisons of the Stable System with Damping ($d = 0.3$) for the Duration of Principal Period. The Dashed Black Line Indicates the Chebfun Result and the Solid Blue Line Indicates the Unified Approach Results

system. In both the cases of the modified Mathieu equation, it was observed that both the dynamical stability characteristics (Floquet Multipliers and Exponents) and the temporal variations match impeccably with the numerical techniques. The near identity transformation matrix ($\hat{\mathbf{Q}}(t)$) did not just aid in the normal form solution, but also served as an effective L-F transformation matrix. The back transformed STM, using the TINF approach ($\hat{\mathbf{\Phi}}(t)$), replicates the time evolution of the original coordinates. This could possibly replace the STM ($\mathbf{\Phi}(t)$) obtained using the Floquet theory for linear time periodic system cases with and without damping. This validates the theory that the Poincare theory of TINF could provide the same results as using the Floquet theory and could be used interchangeably. Moreover, the analytical solution from TINF theory could be used to determine the closed form solution of the L-F transformation matrix, $\mathbf{Q}(t)$. Since this method is based on the direct application

of TINF, without additional approximation, it is widely applicable.

2.4.3 Conclusions

In this chapter, multiple techniques for the analysis of time varying systems were introduced. A brief mathematical background on both Poincare theory of TINF and Floquet theory was provided. A unified theory relating both the techniques towards the analysis of time periodic systems was introduced and verified with example of dynamical study of two cases of Mathieu equation. It was observed that the results for the temporal variations from the numerical techniques matched perfectly with that from the TINF technique. This proves that the TINF technique could provide analytical solutions similar to the numerical/approximate symbolic ones obtained from Floquet Theory, with the help of state augmentation, modal and near-identity transformations. Moreover, the proposed approach provides a closed form analytical expression for the L-F transformation matrix. To the best of the author's knowledge, state augmentation in conjunction with TINF is one technique that yields the L-F transformation in closed-form.

As the STM obtained via the unified approach generates comparable results for the temporal variations and the dynamical characteristics, it can be further applied towards generating stability plots. From the stability plots, the transition curves between the stable and unstable regions can be deduced and utilized for controller implementation. In the next chapter, the application of the unified approach towards stability analysis of practical auto-parametrically excited systems and controller implementation on time periodic systems are detailed.

Chapter 3

STABILITY AND CONTROL OF PERIODIC SYSTEMS

Though many real-world dynamical systems tend to exhibit nonlinear and chaotic behavior, in many scenarios, the system equations are linearized to evaluate the stability bounds based on the attributes of the fundamental solution matrix Sinha and Butcher (1997). The knowledge of the evolution of the system states and their stability characteristics aid in designing appropriate feedback controllers. Some of the numerical and analytical techniques developed in the past were constrained by computational cost and limited application. Hence there is a need to identify methods to determine the stability bounds and design efficient controllers.

The unified theory discussed in chapter 2 has proven to provide comparable results with other numerical and approximate methods. In this chapter, the same is initially extended towards the stability analysis of a practical auto-parametrically excited system of Suction Stabilized Floats. Later, applying the same unified theory towards controller design for unstable time-periodic systems is analyzed and detailed in this chapter.

3.1 Application of Stability Analysis: Suction Stabilized Floats

The application of offshore structures in the oil and gas industry, wind turbines, solar plants is very common. Currently, in most of these applications, the offshore structures are fixed to the seabed with a solid structure that can resist the hydrodynamic forces exerted by the sea waves. However, these fixed bottom structures are economically not feasible for water depth greater than 20 m Castro-Santos *et al.* (2020). However, wind resources for more than 1TW power generation are estimated

in the far off coast of United States, at water depth greater than 30 m Wayman *et al.* (2006). Hence, there is a need to deploy economically feasible floating platforms that could withstand the hydrodynamic forces due to sea waves and aerodynamic forces due to wind loads at greater water depth. A Suction Stabilized Floating (SSF) platform is an option that would meet these requirements.

Many dynamical analysis and control techniques for various offshore structures have been demonstrated in the past. A hydrodynamic analysis of a vertical slender pile under the influence of wave action was performed, and the relationship between the scour process and bed shear stresses were studied analytically and experimentally by Corvaro *et al.* (2019). A hydrodynamic analysis and coupled dynamics study of Catenary Anchor Leg Moorings buoys and attached submarine hoses were performed by Amaechi *et al.* (2019). The dynamic response of the platform, bending moment at the base and mooring line tensions were all simultaneously analyzed by Li *et al.* (2019) to validate the significance of mooring configuration on the stability of a submerged offshore wind turbine. A probabilistic approach, including different loading conditions, damage cases and accounting for their occurrences and its effects on offshore structures' stability was implemented by Konovessis *et al.* (2014). In some applications, multiple individual units are required to function cohesively to serve as a large floating offshore structure. The dynamical analysis of such a structure comprising of multiple semi-submersible modules towards a floating airport was performed using network theory by Zhang *et al.* (2017). The stability characteristics of a hybrid spar design were evaluated analytically and experimentally using a scaled model by Utsunomiya *et al.* (2013). The nonlinear forcing effects and coupling between modes of motion are also required to be modeled to simulate the offshore environment Wang *et al.* (2020). A comprehensive study of various nonlinear hydrodynamic models applicable towards designing efficient wave energy converters is detailed by Davidson

and Costello (2020). A nonlinear kinematic and hydrodynamic model was utilized for the dynamical analysis of roll, pitch, and yaw instabilities and the occurrence of parametric resonance for an axisymmetric spar-buoy structure by Giorgi *et al.* (2020). The application of an active control system in a bottle shaped spar to control pitch disturbances is discussed by Sultania and Manuel (2010).

The heave motion due to sea waves has been considered as a simple harmonic oscillation in many ship dynamical models and aided in analyzing the phenomenon of heave-roll-pitch coupling and parametric resonance Paulling (1959); Oh *et al.* (2000); Nayfeh *et al.* (1973); Oh *et al.* (1994). A Lyapunov direct approach in conjunction with fuzzy logic was employed to determine the stability criteria for a Tension Leg Platform (TLP) by Chen *et al.* (2010). In this section, the prior work by Susheelkumar *et al.* (2017) is extended towards evaluating the dynamical characteristics of SSF and applying the unified theory towards the generation of stability plots.

3.1.1 Suction Stabilized Floating Platform

A SSF platform or Suction-Stabilized Float comprises an internal chamber maintaining a pressure lower than the atmospheric pressure. This pressure differential results in a suction effect that increases the restoring torque on the float/platform and resists perturbations in roll and pitch motions. This behavior qualifies SSF as an ideal addition for offshore structures.

The stability analysis of offshore structures is majorly derived from ship hydrostatics and hydrodynamics by Biran and Pulido (2013). The metacentric height and righting lever are the key parameters that guide the stability of ship models. For small heel angles, the metacenter being vertically above the center of gravity ensures stability Biran and Pulido (2013). For large heel angles, the righting moment generated due to the coupling forces of weight of the ship and buoyant force on the ship is

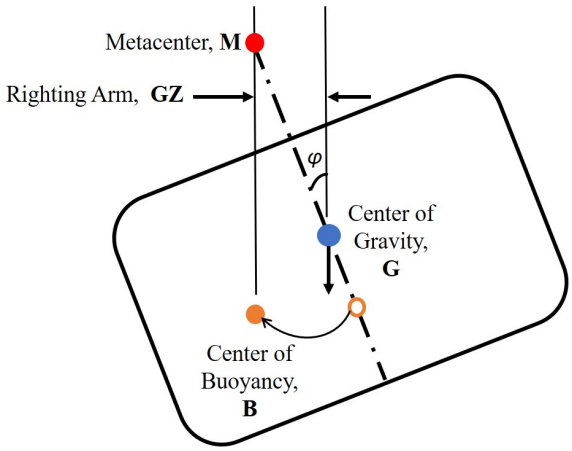

Figure 3.1: Righting Arm.

used as the criteria of stability, as explained by Modi and Seth (1980). The righting moment of a ship can be expressed as,

$$M_R = W_{ship} \times \overline{GZ} \tag{3.1}$$

where W_{ship} is the weight of the ship, M_R is the righting moment, and $\overline{GZ}$ is the horizontal distance between the center of buoyancy and center of gravity of the ship, as shown in Figure 3.1. As explained by Modi and Seth (1980), the value of righting moment majorly depends on $\overline{GZ}$, and for small heel angles, the righting lever is calculated using the metacentric height, as shown in equation (3.2).

$$\overline{GZ} = \overline{GM} \sin \phi \tag{3.2}$$

Consider a circular shaped SSF platform, as shown in Figure 3.2, with an internal chamber of radius R. Using a vacuum pump connected to the internal chamber via a check valve, the vacuum is created in the internal chamber. The pressure inside the internal chamber is less than the atmospheric pressure ($P < Pa$). Due to the pressure differential, the water level inside the internal chamber rises by $h = \frac{Pa-P}{\rho g}$(where g is the acceleration due to gravity and ρ is the density of the water). In the equilibrium

position, the resolution of forces in the vertical direction is given by

$$(P_a - P)A_b + V_b g\rho = Mg \tag{3.3}$$

where M is the total mass of the float and V_b is the displaced volume. Since the surface effect of air cushion is present, a direct application of Archimedes law is not feasible. However, equation (3.3) is similar to the weight balance equation of a surface effect ship, such as hovercraft, riding on an air cushion, as explained by Faltinsen (2005). However, the internal chamber of the surface effect ships contain positive pressure (above atmospheric pressure), and that of SSF platforms have negative pressure (below atmospheric pressure). Moreover, the air cushion in the surface effect ship decreases the metacentric height and righting lever, thereby resulting in a destabilizing effect, as explained by Faltinsen (2005). Whereas, the vacuum in SSF platform increases the metacentric height and righting lever. The equation for righting lever for the SSF platform is derived using the approach presented in Faltinsen (2005).

Consider the circular SSF platform heeled by an angle ψ, with respect to the vertical, as shown in Figure 3.3. The atmospheric pressure, outside the platform, is indicated by P_a and P indicates that inside the internal chamber. As the platform heels, the area A_1 appears outside the water on the right side and an equal area (due to symmetry) disappears into the water on the left side. A differential pressure of $P_0 = P_a - P$ acts on the area A_1, resulting in a force in the negative Y' direction and is represented by

$$F_{A_1} = P_0 \times A_1 \tag{3.4}$$

The restoring moment due to this force in the clockwise direction is given by

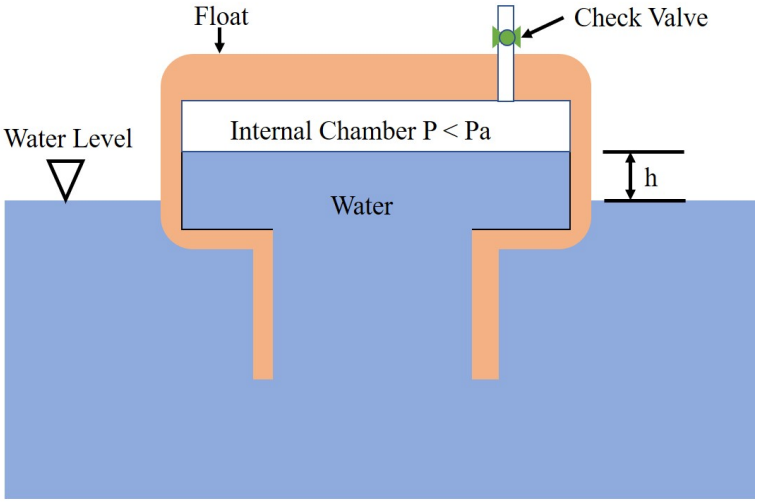

(**a**)

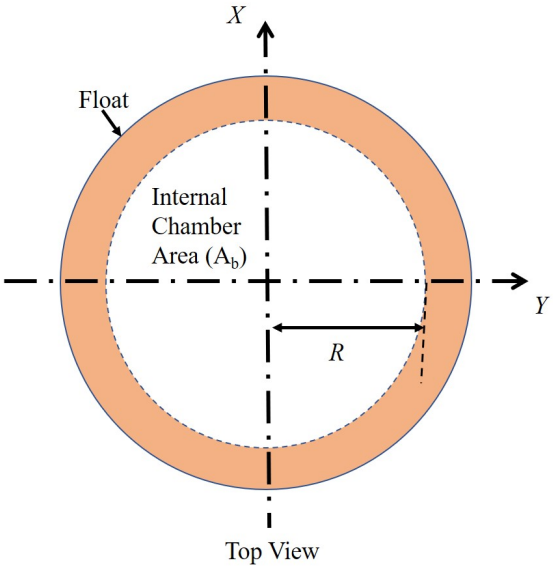

(**b**)

Figure 3.2: Suction Stabilized Floating (SSF) Platform (**a**) Front View, (**b**) Top View.

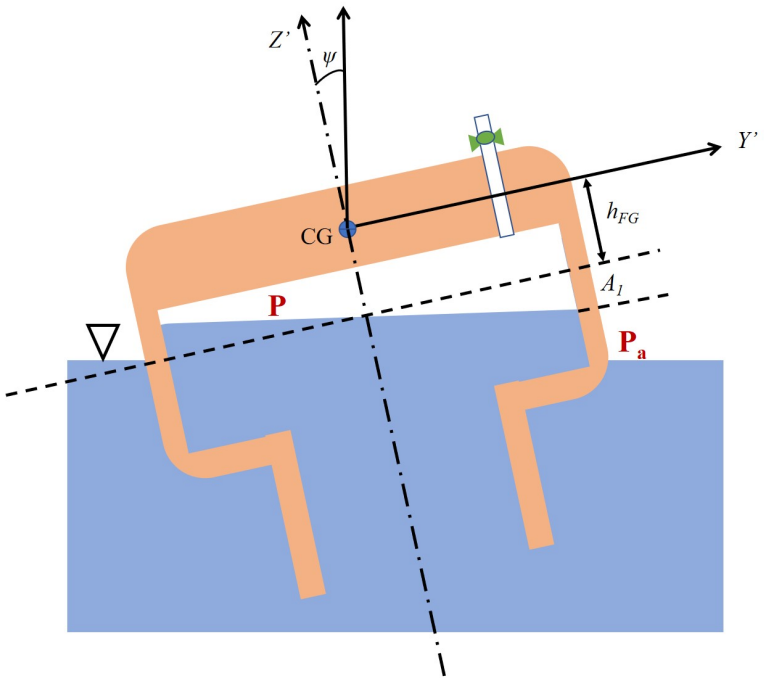

Figure 3.3: SSF Platform Heeled by an Angle θ.

$$M_{A_1} = h_{FG} \times P_0 \times A_1 \tag{3.5}$$

The cylindrical wedge section generated due to the heel angle represents a cylindrical hoof, and the lateral surface area is given by $A_1 = 2Rh_{wedge}$ Harris and Stöcker (1998). For the given tilted SSF (where $h_{wedge} = R\tan\psi$), the moment equation can be updated as

$$M_{A_1} = h_{FG} \times P_0 \times 2 \times R \times R\tan\psi \tag{3.6}$$

A similar moment is obtained when the SSF platform heels in the clockwise direction. Due to the symmetrical shape and restoring action, the total moment is represented by

$$M = 2 \times M_{A_1} = 4 \times h_{FG} \times P_0 \times R^2 \tan\psi \tag{3.7}$$

For small heel angles, $\tan\psi \approx \psi$, thereby reducing the total restoring moment due to suction stabilization effect as

$$M = 4h_{FG}P_0R^2\psi \tag{3.8}$$

It is observed from equation (3.8) that the restoring moment is opposite to the direction of the heel and is proportional to the heel angle, ψ. This effect of suction stabilization can be represented as a torsional spring of stiffness, k_t, attached to the CG and can be equated to

$$k_t = 4h_{FG}P_0R^2 \tag{3.9}$$

Considering conservatively ($4 \approx \pi$), the torsional stiffness can also be approximated to

$$k_t \approx h_{FG}P_0\pi R^2 = h_{FG}P_0A_b \tag{3.10}$$

where A_b is the cross-sectional area of the internal chamber. The effectiveness of this torsional spring in stabilizing the SSF platforms is evaluated in the subsequent subsections.

Dynamical Model for SSF

As detailed by Susheelkumar *et al.* (2017), the dynamical model of SSF was inspired by the ship dynamical models. Similar to the ship motions in the sea, the SSF also experiences heave and pitch actions directly. The periodic variation of hull geometry leading to the periodic variation of water plane area results in the periodic variation of metacentric height. A transfer of energy is observed from the heave motions into roll motions. However, due to the energy transfer and the occurrence of parametric

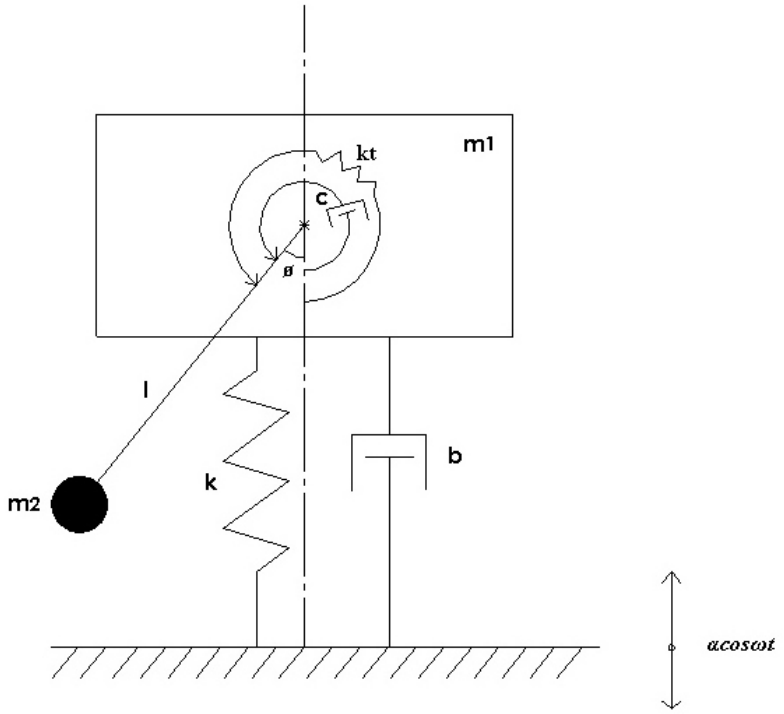

Figure 3.4: Heave-Roll Model for SSF.

resonance, the roll motions are developed and amplified in a certain range of frequencies of sea wave Nabergoj *et al.* (1994); Tondl *et al.* (2000); Cheung *et al.* (2000); Vidic-Perunovic (2011).

The dynamical behavior of ship motions is investigated using a heave-roll model Ibrahim and Grace (2010); Nabergoj *et al.* (1994); Tondl *et al.* (2000). In this model, the ships are subjected to a vertical displacement under the influence of moderate longitudinal waves, and the stability characteristics under the coupled action of heave and roll motions are studied. Since the properties of ship and SSF platforms are comparable, the heave-roll model for ships or floating platform models with cranes Ellermann *et al.* (2002) are modified to incorporate the restoring torque due to suction stabilization indicated in Figure 3.4.

As shown in Figure 3.4, the vertical motion of mass m_1 (corresponding to vertically displacing mass of ship/platform) represents the heave motion, and the pendulum ac-

tion of the rotating mass m_2 (corresponding to the rotating mass of the ship/platform) represents the roll motion. The linear and rotational damping coefficients are denoted by b and c, respectively. The length of the pendulum is represented by l, which rotates with an angular displacement ϕ. A linear spring of stiffness k is connected between the mass m_1 and the base of the system. Additionally, a rotational/torsional spring of stiffness, k_t, representing the suction stabilization effect, is added to the model. The base of the system experiences a periodic wave motion $\alpha \cos \omega t$, where ω is the frequency of the wave motion. The vertical displacement of the SSF platform is identified by z and roll angle by ϕ. The equations of motion for the SSF platform are derived using the Lagrangian method and are outlined in Appendix-A.

$$(m_1 + m_2)\{\ddot{z} - \alpha\omega^2 \cos(\omega t)\} + b\dot{z} + kz + m_2 l\{\ddot{\phi} \sin\phi + \dot{\phi}^2 \cos\phi\} = 0 \tag{3.11}$$

$$m_2 l^2 \ddot{\phi} + c\dot{\phi} + k_t\phi + m_2 gl \sin\phi + m_2 l\{\ddot{z} - \alpha\omega^2 \cos(\omega t)\} \sin\phi = 0 \tag{3.12}$$

The equations of motion are simplified for the dynamical analysis in the subsequent subsection.

Analysis of SSF Model Dynamics

The equations of motion of SSF represented in equations (3.11) and (3.12) are dependent on the geometrical properties. The equations are transformed in the dimensionless form to evaluate the effectiveness of the suction stabilization effect. The dimensionless form is indicated as follows

$$\ddot{x} + \overline{B}\dot{x} + q^2 x + \mu\{\ddot{\phi} \sin\phi + \dot{\phi}^2 \cos\phi\} = a\eta^2 \cos(\eta\tau) \tag{3.13}$$

$$\ddot{\phi} + \overline{C}\dot{\phi} + \sin\phi + q_t^2\phi + \{\ddot{x} - a\eta^2 \cos(\eta\tau)\} \sin\phi = 0 \tag{3.14}$$

The semi-trivial solution of equations (3.13) and (3.14) are represented as

$$x_0(\tau) = a(M\cos(\eta\tau) + N\sin(\eta\tau)) \tag{3.15}$$

$$\phi_0(\tau) = 0 \tag{3.16}$$

where $M = \frac{\eta^2(q^2-\eta^2)}{(q^2-\eta^2)^2+(\overline{B}\eta)^2}$ and $N = \frac{\overline{B}\eta^3}{(q^2-\eta^2)^2+(\overline{B}\eta)^2}$. By adding small perturbations to x and ϕ as

$$x = x_0 + s \tag{3.17}$$

$$\phi = \phi_0 + \theta \tag{3.18}$$

By applying first order approximations to equations (3.13) and (3.14), the following is obtained

$$\ddot{s} + \overline{B}\dot{s} + q^2 s = 0 \tag{3.19}$$

$$\ddot{\theta} + \overline{C}\dot{\theta} + (1+q_t^2)\theta - a\eta^2\{(1+M)\cos(\eta\tau) + N\sin(\eta\tau)\}\theta = 0 \tag{3.20}$$

The equation (3.19) will generate stable solutions since it is a homogeneous differential equation with constant coefficients. However, equation (3.20) is a damped Mathieu equation, and its stability bounds are based on the system parameters. It is noted that equation (3.20) preserves all the system parameters about the SSF model. The system parameters ($\overline{B}$ and q^2) of the heave motions (from equation (3.19)) are also observed to appear in equation (3.20). Hence the analysis of reduced order roll motion consolidates the dynamical behavior of the SSF system model.

For the cases with a really low linear damping term $\overline{B}$ and rotational damping term $\overline{C}$, the value of N is negligible, thereby eliminating any terms multiplied by them. Additionally, the $(1+q_t^2)$ term can be replaced with δ and the $a\eta^2(1+M)$ term with 2ϵ, thereby updating the equation (3.20) as follows

$$\ddot{\theta} + (\delta - 2\epsilon\cos(\eta\tau))\theta = 0 \tag{3.21}$$

The equation (3.21) is the standard Mathieu equation when $\eta = 2$ and could be analyzed using the Floquet theory. It is also feasible to use the direct application of the Normal Forms approach (detailed in Section 2.4), by representing the periodic term as an augmented state. However, for the cases with significant linear damping term $\overline{B}$, the value of N is significant, and equation (3.20) is updated as follows

$$\ddot{\theta} + \overline{C}\dot{\theta} + (\hat{\delta} - \hat{\epsilon}\{\frac{\cos(\eta\tau)}{N} + \frac{\sin(\eta\tau)}{(1+M)}\})\theta = 0 \tag{3.22}$$

where $\hat{\delta} = (1 + q_t^2)$ would still be the linear constant term and $\hat{\epsilon} = a\eta^2(1+M)N$ will be the coefficient of periodic forcing term. As detailed in prior work, the generic solution for the Mathieu equation can be substituted in equation (3.20) to solve for the non-trivial solutions for the constant coefficients to derive the expression for threshold amplitude. However, in this work, the system equations are analyzed using the Floquet theory and Normal Forms techniques analytically, and results are discussed in the subsequent sections.

3.1.2 Simulation Results

The reduced order expressions for the SSF dynamical model have studied analytically and evaluated for stability. The linear damping and linear stiffness are attributed to the heave motion due to the sea waves. The reduced order SSF model with negligible linear damping (equation (3.21)) can be evaluated using both the TINF technique and Floquet theory. The transition curves between the stable and unstable regions are obtained analytically and plotted. Further, for the SSF system with significant linear damping, the stability plots are generated using the Floquet theory on the system equation (3.22). In both cases, the parameter in the horizontal

coordinate is attributed to the suction stabilization effect. The temporal variations of the system states are plotted in each case to validate the stability behavior obtained.

SSF with Negligible Linear Damping ($\overline{B} \approx 0$)

As explained earlier, the SSF dynamical model was reduced by the form equation (3.21), where δ is the linear constant term, and 2ϵ is the amplitude of the parametric excitation. When $\eta = 2$, the principal period of the system is $T = \pi$ secs. The standard Mathieu equation (3.21) was numerically integrated for different sets of initial conditions ($\theta_0 = 1.0, \dot{\theta}_0 = 0.0$ and $\theta_0 = 0.0, \dot{\theta}_0 = 1.0$) and the system states were evaluated at the principal period (T). The values of system states were concatenated such that the Floquet theory was applied to identify the stability bounds numerically, as detailed by Kovacic *et al.* (2018). The condition of both the Floquet multipliers being on or inside the unit circle was used as the criteria for identifying the stability bounds. The standard template of the system parameter variation in the $(\delta - \epsilon)$ plane was adapted to generate the plots shown in Figure 3.5a.

Meanwhile, as detailed in Section 2.2, the periodic term in equation (3.21) is augmented, resulting in the updated equation as

$$\frac{d}{d\tau}\begin{Bmatrix}\theta\\ \dot{\theta}\\ p\\ \dot{q}\end{Bmatrix} = \begin{bmatrix}0 & 1 & 0 & 0\\ -\delta & 0 & 0 & 0\\ 0 & 0 & 0 & 1\\ 0 & 0 & -\eta^2 & 0\end{bmatrix}\begin{Bmatrix}\theta\\ \dot{\theta}\\ p\\ \dot{q}\end{Bmatrix} + \begin{Bmatrix}0\\ 2\epsilon\theta p\\ 0\\ 0\end{Bmatrix} \tag{3.23}$$

where $p = \cos(\eta\tau); q = -\eta\sin(\eta\tau)$. The equation (3.23) is in the form similar to equation (2.11) and undergoes modal transformation and near-identity transformation to apply the TINF technique, as explained in Section 2.3.1. The Floquet multipliers from the reduced TINF solution were computed as per equation (2.36) and utilized

to generate the stability plot indicated in Figure 3.5b.

In Figure 3.5, the shaded area indicates the unstable region, and the white area indicates the stable region for the standard Mathieu equation. It is observed that the plot generated using the Normal Forms solution (Figure 3.5b) replicates the one from the Floquet Theory application on numerically integrated results (Figure 3.5a) quite well. Both these plots agree with the results obtained in Kovacic *et al.* (2018). This validates the application of the unified theory towards stability analysis of time periodic systems.

From both the sub-figures in Figure 3.5, the system parameters $\delta = 3.0$ and $\epsilon = 1.0$ corresponds to a stable point. The STM of the reduced TINF solution is back transformed to obtain $\hat{\mathbf{\Phi}}(t)$ matrix. This matrix is then multiplied with the initial conditions of the system states in equation (3.21) to determine the system state evolution. Simultaneously, equation (3.21) was numerically integrated with the same value of system parameters and initial conditions ($\theta_0 = 1, \dot{\theta}_0 = 0$). The comparison of the variations of the system states is plotted in Figure 3.6.

As mentioned in Figure 3.6, the solid red line indicates the temporal variation based on the STM, $\hat{\mathbf{\Phi}}(t)$, determined from the TINF technique, and the black dashed line represents the numerically integrated solution of equation (3.21). In both plots, the system follows a stable bounded periodic behavior and does not deviate away from the initial conditions.

SSF with Significant Linear Damping ($\overline{B} = 1.0$)

For the case of the SSF model with significant linear damping, the dynamical behavior is represented by equation (3.22). Since this system is also considered to be a Mathieu equation, the stability plots are initially generated in the standard template of $(\hat{\delta} - \hat{\epsilon})$ plane. Though the linear constant term variation $(\hat{\delta})$ is only attributed to the rolls

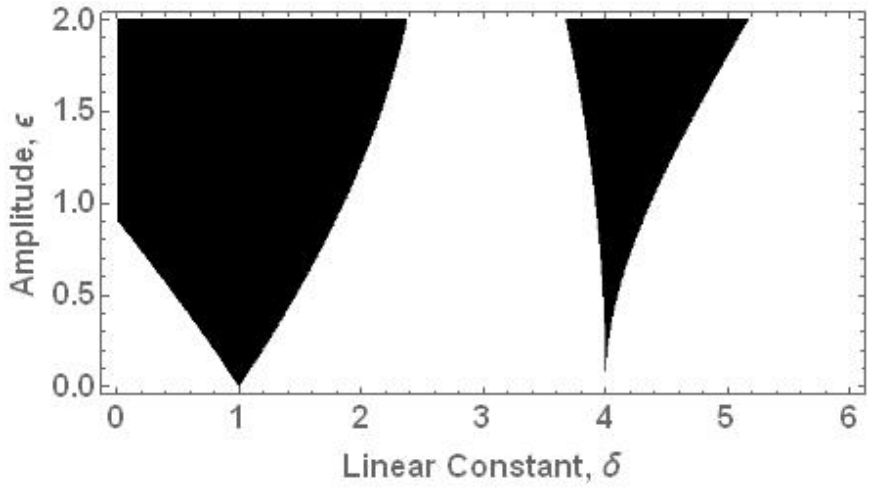

(**a**)

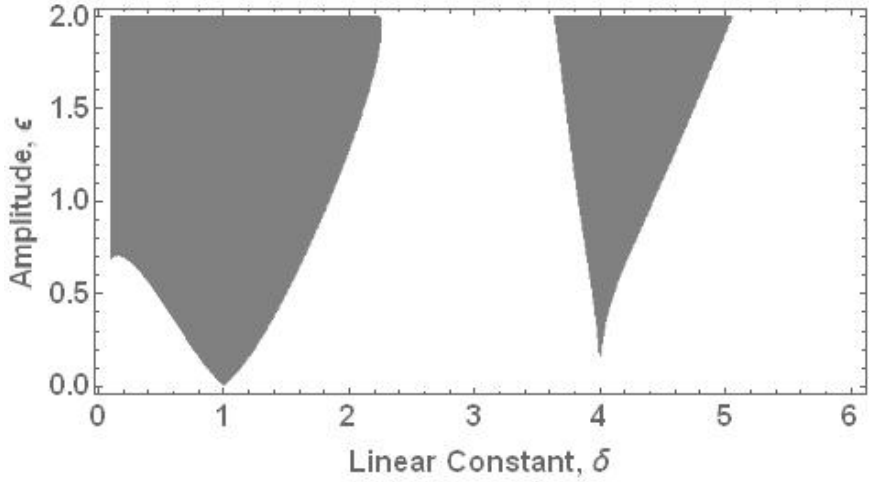

(**b**)

Figure 3.5: Comparison of Stability Plots for Standard Mathieu Equation, Where the Shaded Area Corresponds to Unstable Bounds and White Area Corresponds to Stable Bounds (**a**) Generated Using Numerical Integration and Floquet Theory, (**b**) Generated from the Normal Forms Solutions.

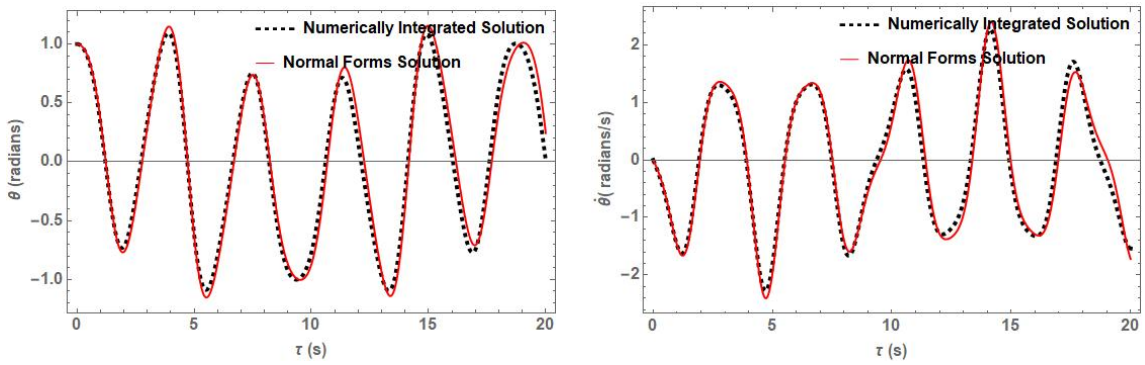

(**a**) (**b**)

Figure 3.6: Comparison of Temporal Variations of the Reduced SSF System States (**a**) Roll Angle Variation with Respect to Time, (**b**) Roll Angular Rate Variation with Respect to Time.

stiffness (q_t), the coefficient of the periodic forcing term ($\hat{\epsilon}$) comprises many variables corresponding to the wave motions. By considering the linear stiffness parameter, $q = 1$, and the frequency parameter, $\eta = 1$(thereby setting the principal time period for analysis to be $T = 2\pi$ seconds), the variation in $\hat{\epsilon}$ is solely attributed towards the variation in amplitude of wave term (a). Hence, similar stability plots can be generated in the $(a - q_t)$ plane for the equivalent range of parameters from $(\hat{\delta} - \hat{\epsilon})$ plane. For the given set of system parameters, the system equation (equation (3.22)) is numerically integrated, and both the stability plots are generated based on the Floquet multiplier condition, as displayed in Figure 3.7.

Later, for the same set of system parameters, an external rotational damper of $(\overline{C} = 0.2)$ was added and investigated for the stability characteristics. Again the stability plots were generated based on the Floquet multiplier condition, as indicated in Figure 3.8.

In both Figures 3.7 and 3.8, the white area indicates the stable region of operation, and the black/shaded region represents the unstable region of operation for the SSF platform. Though the frequency of sea waves vary, similar trends are observed for

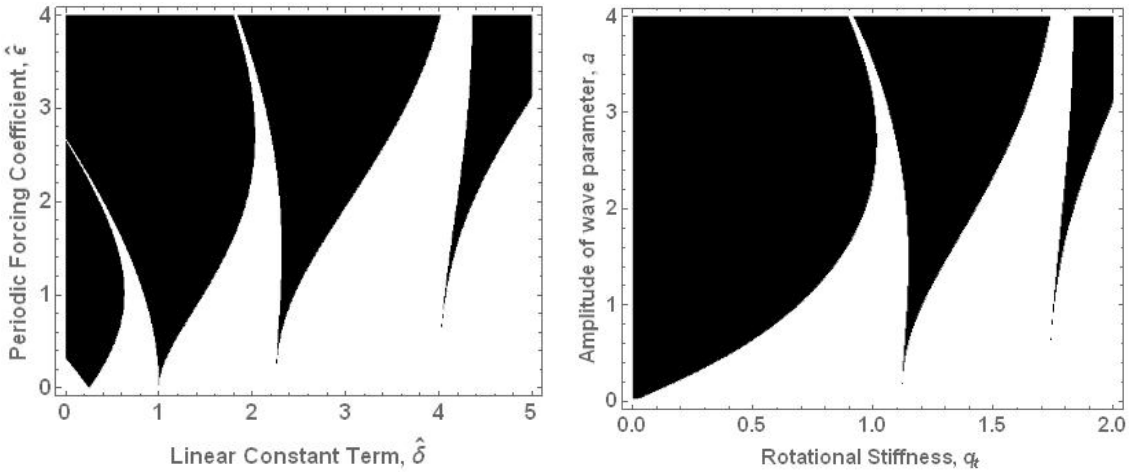

(**a**) (**b**)

Figure 3.7: Stability Plot for SSF with Significant Linear Damping and Without Rotational Damping (**a**) in $\hat{\delta} - \hat{\epsilon}$ Plane, (**b**) in $a - q_t$ Plane.

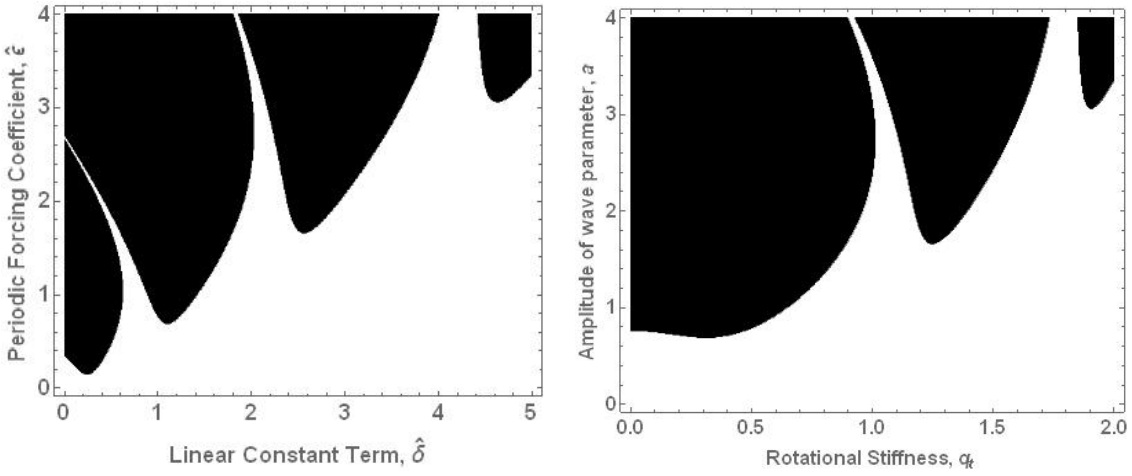

(**a**) (**b**)

Figure 3.8: Stability Plot for SSF with Significant Linear Damping and with Rotational Damping (**a**) in $\hat{\delta} - \hat{\epsilon}$ Plane, (**b**) in $a - q_t$ Plane.

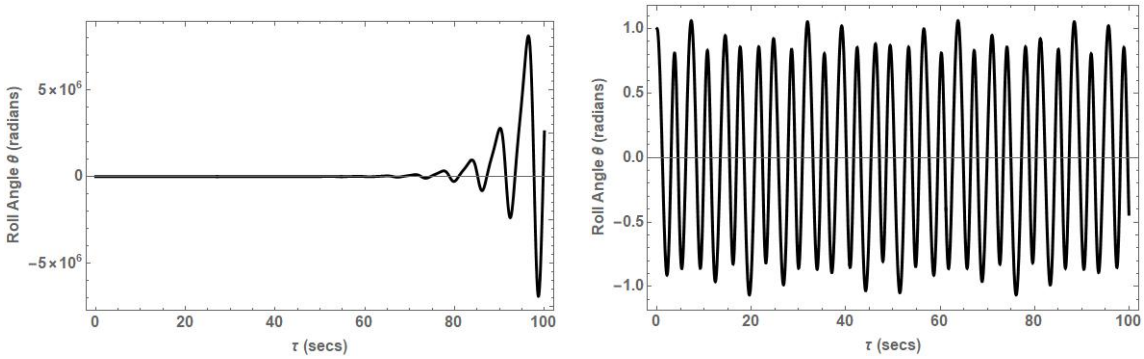

(**a**) (**b**)

Figure 3.9: Comparison of Roll Angle Variations of the SSF System with Significant Linear Damping and No Rotational Damper (**a**) when $q_t = 0.5, a = 1.0$, (**b**) when $q_t = 1.5, a = 1.0$.

the stability plots at a particular wave frequency. In both Figures 3.7b and 3.8b, the point corresponding to system parameters ($q_t = 0.5, a = 1.0$), the system is observed to be unstable. As the torsional/rotational stiffness is updated to $q_t = 1.50$, keeping the amplitude of wave parameter as $a = 1.0$, the SSF system is observed to be in the stable zone. To verify the same, the roll angle variations in equation (3.20) is numerically integrated with the initial conditions ($\theta_0 = 1.0, \dot{\theta}_0 = 0.0$). Initially, the roll angle variations for the SSF system with significant linear damping and no rotational damper are evaluated and plotted in Figure 3.9.

Similarly, the roll angle variations for the SSF system with significant linear damping and an additional rotational damper ($\overline{C} = 0.20$) is evaluated and plotted in Figure 3.10.

3.1.3 Discussion

The expression for the suction stabilization effect (equation (3.10)), indicates that torsional spring stiffness is directly proportional to the area of the base of the internal chamber. This intuitively provides an insight that the higher the base area, the higher will be the suction stabilization effect. It can also be inferred that for higher restoring

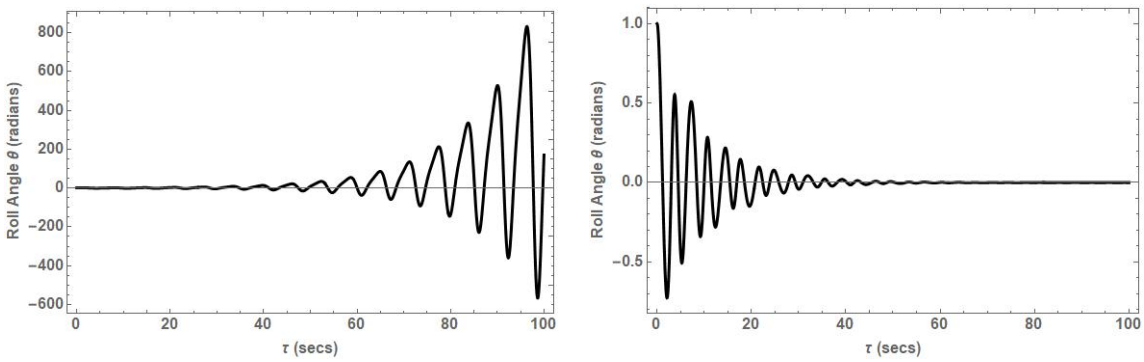

(**a**) (**b**)

Figure 3.10: Comparison of Roll Angle Variations of the SSF System with Significant Linear Damping and an Additional Rotational Damper ($\overline{C} = 0.2$) (**a**) when $q_t = 0.5, a = 1.0$, (**b**) when $q_t = 1.5, a = 1.0$.

moment, design the SSF with a larger base area at the water level. This can also be achieved by attaching multiple small units of SSF floats. As mentioned earlier, in the dynamical modeling, it was observed that the roll motion of the reduced order of the SSF model characterizes the stability features of the heave-roll coupled model. This also provides an insight into the energy transfer within the SSF model.

For the heave motions attained with negligible linear damping, the roll motion of the SSF dynamical model follows a standard Mathieu equation. The stability plot in Figure 3.5 shows that the stable region (in white) increases considerably as the linear constant (δ) increases. The δ term replaced the $(1+q_t^2)$ term in equation (3.20), which in turn was directly proportional to the suction stabilization effect. Hence it could also be concluded that in the reduced SSF model, the increase in torsional stiffness term (q_t) increases the stable bounds of the system. The temporal variations of system states from the back-transformed TINF solution follow the numerical integration results closely, as shown in Figure 3.6. This validates the direct application of the unified theory towards stability analysis of time-periodic systems.

For the heave motions attained with significant linear damping, the roll motion of the SSF dynamical model follows a modified Mathieu equation (equation (3.22)).

Though the parameters used for the stability plots are similar in this case, the effect of linear damping is evident in Figures 3.7a and 3.8a. The stability bounds have been lifted from the x-axis. However, the rotational stiffness parameter (q_t) is still observed to contribute towards improving the stability. As the value of the rotational stiffness parameter (q_t) increases, the stability bounds are observed to be more, even when the amplitude of wave parameter (a) is high. Moreover, in Figures 3.8a,b, the additional rotational damper ($\overline{C}$) is observed to smoothing the transition curves such that the stable bounds are further increased. This trend of the stability plots is observed to remain the same even with higher values of wave frequency. The additional rotational damper can be attributed to one or a combination of the add-on techniques in the float design or an active controller. To validate the stability characteristics, an unstable and stable point is selected from Figures 3.7b, 3.8b and the temporal variations are plotted with the corresponding system parameters.

Figure 3.9a corresponds to the roll motion of the SSF model with significant linear damping and no rotational damping when $q_t = 0.5, a = 1.0$. In Figure 3.7b, this corresponds to the unstable region, and it is observed that roll motion amplifies unbounded and could result in the float getting capsized. Whereas Figure 3.9b corresponds to the roll motion of the SSF model with significant linear damping and no rotational damping when $q_t = 1.5, a = 1.0$. In Figure 3.7b, this corresponds to the stable region and it is observed to exhibit a bounded roll motion over time. This validates the stability plots in Figure 3.7.

In the case of the SSF model with significant linear damping and additional rotational damper ($\overline{C} = 0.2$), the point ($q_t = 0.5, a = 1.0$) in Figure 3.8b again corresponds to the unstable region. Though it is also evident from Figure 3.10a that the roll motions grow unbounded, the range of motion has reduced drastically for the same time period. This indicates that the additional damper has some effect in

reducing the amplitude of the roll motion, but it is still not capable of stabilizing the float. However, when the rotational stiffness parameter value (q_t) is increased to $q_t = 1.5$, the system is stable, as shown in Figure 3.8b. Additionally, the roll motions corresponding to $q_t = 1.5, a = 1.0$, in Figure 3.10b almost dampen out by 50 s. Hence, the stability plots in Figure 3.8 are validated, and it can also be concluded that the higher value of the rotational stiffness (q_t) aids in stabilizing the SSF platform, which is associated with the suction stabilization effect. It can be also inferred that the additional rotational damper in conjunction with the suction stabilization can make the float attain a stable fixed point and not just a stable periodic motion. As discussed, a stable fixed point is more desirable for offshore structures in most of the applications.

3.1.4 Conclusions

In this section, a brief explanation of the SSF platforms the motivation to perform a dynamical analysis is detailed. Initially, the effect of suction stabilization was mathematically derived for the case of a symmetrically shaped float/platform. Subsequently, the dynamical behavior of SSF was compared to ship motions and derived the equations of motion using a heave-roll model. A model order reduction was performed on the resulting equations of motion to facilitate the dynamical analysis. It was demonstrated that all the major dynamical characteristics (including that of heave motions) could be represented in the reduced order roll motions. The reduced order roll motions were observed to be comparable to a parametrically excited Mathieu equation. The unified theory was employed to analytically assess the stability bounds of an SSF platform exposed to periodic sea waves. The temporal variations of the model were verified numerically to validate the dynamical characteristics of an SSF platform. In this section, the sea waves were considered to be periodic in nature. However, in reality, they could be expressed as a quasi-periodic system with incom-

mensurate frequencies. The unified theory could be extended towards a quasi-periodic system as well and is detailed in the later sections of this work.

This section provides validation of the application of the unified theory towards stability analysis of a practical auto-parametrically excited time periodic system. In the subsequent section, using this approach towards designing efficient controllers for unstable time-periodic systems is detailed.

3.2 Control of Time Periodic System

As indicated in the stability plots in the earlier section, a time-periodic system can become unstable or systems states growing unbounded in some scenarios. In such situations, a control system is essential to guide the system's behavior to the desired path. For time varying systems, the state feedback controller design using the pole placement method was introduced by Follinger *et al.* (1978). With the knowledge of closed form expression of STM, the optimal control theory is applicable towards control system design, as explained by Kwakernaak and Sivan (1972). Sinha and Joseph (1994) demonstrated the transformation of linear time periodic system to time-invariant form using the Chebyshev polynomials and designed feedback controllers using the pole-placement method and optimal control method. Deshmukh *et al.* (2000) applied L-F transformation towards order reduction and control of parametrically excited linear time periodic systems, where the control laws were determined by minimizing the error between the time-invariant auxiliary system and the transformed system. Later, by using the back-stepping technique in conjunction with Floquet theory, Deshmukh and Sinha (2004) designed a combination of linear and nonlinear controllers that guaranteed the asymptotic stability of nonlinear time periodic systems. Pandiyan and Sinha (2001) devised a linear controller design using L-F transformation and a time varying pole placement based approach for stabiliz-

ing nonlinear systems. Additionally, they also added a nonlinear controller design using the Lyapunov direct method to improve the controlled response. In the case of nonlinear dynamic systems with time-periodic coefficients, Gabale and Sinha (2011) performed an eigenvalue decomposition of the time-invariant linear part after L-F transformation to differentiate the dominant and nondominant system states. The nondominant states were expressed in terms of dominant states, and a time varying feedback controller was designed around the dominant states ensuring the system stability. Moreno-Ahedo and Diarte-Acosta (2019) recently performed stability analysis of Reid model of a mass spring system with switchable stiffness using Floquet theory. For fractional-order systems with periodic coefficients, Dabiri and Butcher (2019) detailed an optimal observer-based feedback controller design using the fractional Chebyshev collocation method.

3.2.1 Application Towards Controller Design

The transition curves for a linear time periodic system can be determined from the STM using the unified theory, as indicated in section 3.1. For the system parameters corresponding to the unstable regions, multiple control strategies can be implemented to drive the system states to the desired behavior. Since the closed form expression of the STM is computable using the unified theory, efficient controllers can be designed using multiple techniques and are detailed in this section.

Initially, a linear time periodic system (of the form equation (2.40)), without any controller is considered. The application of the unified theory on such a system to compute its STM is demonstrated in Section 2.4.1. In this subsection, multiple control strategies are discussed to control the unstable regions of the same time periodic system.

System Controlled to Stable Point

In this subsection, the aforementioned periodic dynamical system is updated to stabilize the system to a fixed point. Initially, the system equation is updated with the controller input, as indicated below

$$\dot{\mathbf{x}} = \mathbf{A}(t)\mathbf{x} + \mathbf{B}(t)\mathbf{u}(t) \tag{3.24}$$

The system can be updated as linear feedback controlled system by considering $\mathbf{u} = -\mathbf{K}\mathbf{x}$, where $\mathbf{K}$ represents the vector containing controller gains. The system equation with controller gets updated as

$$\dot{\mathbf{x}} = (\mathbf{A}(\mathbf{t}) - \mathbf{B}(t)\mathbf{K})\mathbf{x} \tag{3.25}$$

It is observed that the $(\mathbf{A}(t)-\mathbf{B}(t)\mathbf{K})$ matrix is still time periodic and the stability bounds can be determined based on the Floquet Multipliers. For this system consider $\mathbf{B} = [0\ \ 1]^T$ and $\mathbf{K} = [k_1\ \ k_2]$, the Mathieu equation, equation (2.40), gets updated as

$$\ddot{x} + (a + k_1 + b\cos(\omega t))x + k_2\dot{x} = 0 \tag{3.26}$$

The state space form of the equation (3.26) with controller terms, after the state augmentation, can be expressed as

$$\frac{d}{dt}\begin{Bmatrix} x \\ \dot{x} \\ p \\ q \end{Bmatrix} = \begin{bmatrix} 0 & 1 & 0 & 0 \\ -a-k_1 & -k_2 & 0 & 0 \\ 0 & 0 & 0 & 1 \\ 0 & 0 & -\omega^2 & 0 \end{bmatrix} \begin{Bmatrix} x \\ \dot{x} \\ p \\ q \end{Bmatrix} + \begin{Bmatrix} 0 \\ -bxp \\ 0 \\ 0 \end{Bmatrix} \tag{3.27}$$

The unified theory, detailed in section 2.4, is applied to the above time periodic equation with controller terms to compute the closed form expression of the STM.

Since the controller gains are added to the $\tilde{\mathbf{B}}_0$ matrix, the modal transformation matrix gets updated accordingly, and so does the Jordan canonical form of the equation. Similar to the case of the system without a controller, the resulting transformed TINF system with a linear controller is shown below

$$\frac{d}{dt}\begin{Bmatrix} V_1 \\ V_2 \\ V_3 \\ V_4 \end{Bmatrix} = \begin{pmatrix} \left(\frac{(4k_1+k_2^2+4(a-\omega^2))(4b^2V_3V_4-(4k_1-k_2^2-k_2\sqrt{-4k_1+k_2^2-4a}+4a)\omega^2(4k_1-k_2^2+4a-\omega^2))}{2\sqrt{-4k_1+k_2^2-4a}(\sqrt{-4k_1+k_2^2-4a}-2\sqrt{-\omega^2})(\sqrt{-4k_1+k_2^2-4a}+2\sqrt{-\omega^2})\omega^2(4k_1-k_2^2+4a-\omega^2)}\right)V_1 \\ -\left(\frac{(4k_1+k_2^2+4(a-\omega^2))(4b^2V_3V_4-(4k_1-k_2^2+k_2\sqrt{-4k_1+k_2^2-4a}+4a)\omega^2(4k_1-k_2^2+4a-\omega^2))}{2\sqrt{-4k_1+k_2^2-4a}(\sqrt{-4k_1+k_2^2-4a}-2\sqrt{-\omega^2})(\sqrt{-4k_1+k_2^2-4a}+2\sqrt{-\omega^2})\omega^2(4k_1-k_2^2+4a-\omega^2)}\right)V_2 \\ -V_3\sqrt{-\omega^2} \\ V_4\sqrt{-\omega^2} \end{pmatrix} \tag{3.28}$$

All the steps followed for the system without a controller in section 2.4.1, remain the same and computation of the state transition matrix ($\bar{\mathbf{\Phi}}(t)$), is further used for the stability analysis.

System Controlled to Desired Time Periodic Orbit

In this subsection, the control technique is applied such that an unstable system following equation (2.40) is directed towards a desired time periodic orbit. The methodology is adopted from the formulation detailed in Sinha *et al.* (2005a). Consider the system dynamical equation (equation (2.38)) updated with the controller term as indicated below

$$\ddot{x} = -ax - bx\cos(\omega t) + u \tag{3.29}$$

with $u = u_f + u_t$, where u_f is the feedforward control, and u_t is the time-varying feedback control. The feedforward control term can be expressed as

$$u_f = \ddot{s} + (a + b\cos(\omega t))s \tag{3.30}$$

Consider the unstable system be stabilized to follow the desired periodic orbit, $s = \alpha \cos(\zeta t)$, and the error vector of system states can be expressed as

$$\mathbf{e} = \begin{bmatrix} e(t) \\ \dot{e}(t) \end{bmatrix} = \begin{bmatrix} x(t) - s(t) \\ \dot{x}(t) - \dot{s}(t) \end{bmatrix} \tag{3.31}$$

The feedback control can be expressed as

$$u_t = \mathbf{Ke} = \begin{bmatrix} k_1 & k_2 \end{bmatrix} \begin{bmatrix} x - s \\ \dot{x} - \dot{s} \end{bmatrix} = k_1(x - s) + k_2(\dot{x} - \dot{s}) \tag{3.32}$$

By adding equation (3.32) to equation (3.30) and substituting back in equation (3.29), gives us

$$\ddot{x} = -ax - bx\cos(\omega t) + \ddot{s} + (a + b\cos(\omega t))s + k_1(x - s) + k_2(\dot{x} - \dot{s}) \tag{3.33}$$

By rearranging the terms and expressing the resulting equation in the state-space form in equation (3.34)

$$\frac{d}{dt} \begin{Bmatrix} e \\ \dot{e} \end{Bmatrix} = \begin{bmatrix} 0 & 1 \\ -a - b\cos(\omega t) - k_1 & -k_2 \end{bmatrix} \begin{Bmatrix} e \\ \dot{e} \end{Bmatrix} \tag{3.34}$$

It is observed that the resulting system is very similar to equation (3.26), with the variation in just the system states considered. The method of state augmentation and TINF is followed the same way, as explained earlier in section 2.4, to compute the state transition matrix.

A pole placement technique can be adopted to fix the eigenvalues of the FTM to the desired stability. The corresponding values of the controller gains can be evaluated for controlling the unstable system towards either a stable point or a stable periodic orbit.

System with Linear Optimal Controller

The Floquet Multipliers based approach can be avoided for controlling an unstable system by incorporating a time varying controller using an optimization technique detailed by Kwakernaak and Sivan (1972). For a dynamical system with the controller term expressed by the equation (3.24), is updated with a control variable $\mathbf{w}(t) = \mathbf{D}(t)\mathbf{x}(t)$ and initial condition $\mathbf{x}(t_0) = \mathbf{x}_0$, the cost function for optimization considered is

$$\mathbf{CF} = \mathbf{x}^T(t)\,\bar{\mathbf{S}}\,\mathbf{x}(t) + \int_{t_0}^{t_f} \left[\mathbf{w}^T(t)\mathbf{G}_3(t)\mathbf{w}(t) + \mathbf{u}^T(t)\mathbf{G}_2(t)\mathbf{u}(t)\right] dt \tag{3.35}$$

where $\bar{\mathbf{S}}$ is a non-negative-definite symmetric matrix, $\mathbf{G}_2(t)$ and $\mathbf{G}_3(t)$ are positive-definite symmetric matrices for $t_0 \leq t \leq t_f$. The Hamiltonian form of the state differential equation is expressed as

$$\mathbf{H} = \begin{Bmatrix} \dot{\mathbf{x}}(t) \\ \dot{\bar{\mathbf{p}}}(t) \end{Bmatrix} = \begin{bmatrix} \mathbf{A}(t) & -\mathbf{B}(t)\mathbf{G}_2^{-1}(t)\mathbf{B}^T(t) \\ -\mathbf{G}_1(t) & -\mathbf{A}^T(t) \end{bmatrix} \begin{Bmatrix} \mathbf{x}(t) \\ \bar{\mathbf{p}}(t) \end{Bmatrix} \tag{3.36}$$

where $\mathbf{G}_1(t) = \mathbf{D}^T(t)\mathbf{G}_3(t)\mathbf{D}(t)$ and $\bar{\mathbf{p}}(t)$ is the adjoint variable. The adjoint variable is related to the system state as $\bar{\mathbf{p}}(t) = \mathbf{S}(t)\,\mathbf{x}(t)$ with the boundary condition $\bar{\mathbf{p}}(t_f) = \bar{\mathbf{S}}\,\mathbf{x}(t_f)$. After incorporating the boundary conditions, the $\mathbf{S}(t)$ matrix is derived to be

$$\mathbf{S}(t) = \left[\Phi_{21}(t,t_f) + \Phi_{22}(t,t_f)\bar{\mathbf{S}}\right]\left[\Phi_{11}(t,t_f) + \Phi_{12}(t,t_f)\bar{\mathbf{S}}\right]^{-1} \tag{3.37}$$

where $\Phi_{11}(t,t_0), \Phi_{12}(t,t_0), \Phi_{21}(t,t_0), \Phi_{22}(t,t_0)$ are obtained from partitioning the state transition matrix of Hamiltonian equation expressed in equation (3.36). Using these properties and the cost function (equation (3.35)), the optimal control input $\bar{\mathbf{u}}(t)$, for the time span $t_0 \leq t \leq t_f$, is found to be

$$\bar{\mathbf{u}}(t) = -\mathbf{G}_2^{-1}(t)\mathbf{B}^T(t)\mathbf{p}(t) = -\bar{\mathbf{K}}(t)\mathbf{x}(t) \tag{3.38}$$

where $\bar{\mathbf{K}}(t) = [k_1(t)\ \ k_2(t)]$ is the time varying optimal feedback control gain vector and can be expressed as

$$\bar{\mathbf{K}}(t) = \mathbf{G}_2^{-1}(t)\mathbf{B}^T(t)\mathbf{S}(t) \tag{3.39}$$

The linear control law generated from this technique provides the optimal control input for any initial condition automatically, without the use of pole placement or Floquet multipliers. The numerical simulation results for a linear time periodic Mathieu equation are detailed in the subsequent subsections.

3.2.2 Results and Discussion

The unified approach is applied to the time periodic system to evaluate the dynamical characteristics and generate stability charts again for the modified Mathieu equations. The condition of both the Floquet multipliers being on or inside the unit circle is used as the criterion for identifying the stability bounds. A case of an unstable system is selected from the stability chart to apply multiple control strategies to stabilize the system.

System Without Controller

The original linear time periodic system of the Mathieu equation without controller (equation (2.40)) is analyzed for $\omega = 2\pi$, for which the principal period is $T = 1$ sec. The system parameters (linear constant part, a and the amplitude of excitation, b) are altered to generate stability plots based on the Floquet multipliers. As explained in Kovacic *et al.* (2018), the numerical integration results of the Mathieu equation are utilized to apply the Floquet theory directly to the original system states and generate the stability plots displayed in Figure 3.11a. Simultaneously, the same system is subjected to state augmentation, modal transformation, near identity transformations, and the TINF technique. The resulting STM (as per equation (2.36)) is evaluated at

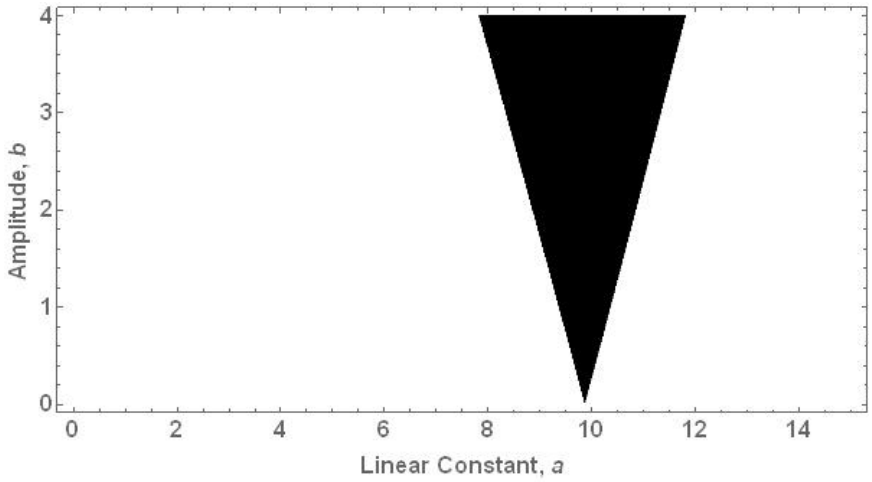

(**a**)

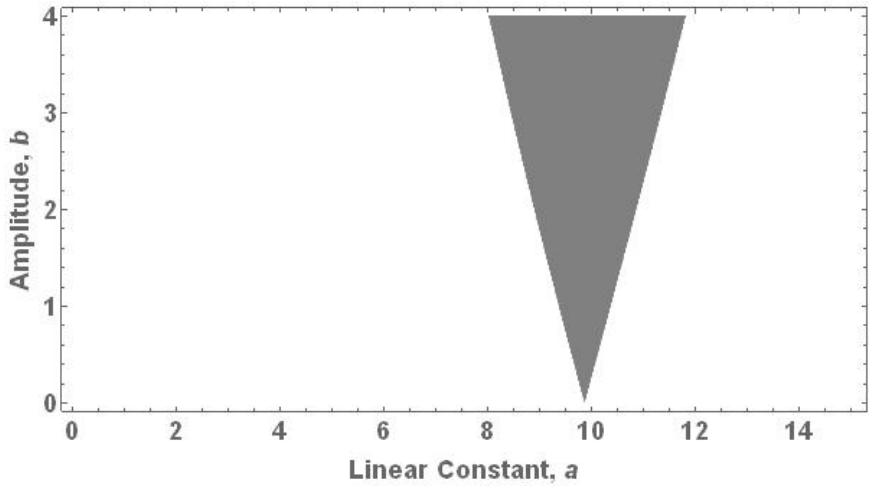

(**b**)

Figure 3.11: Comparison of Stability Plots for Mathieu Equation, Where the Shaded Area Corresponds to Unstable Bounds and White Area Corresponds to Stable Bounds (**a**) Generated Using Numerical Integration and Floquet Theory, (**b**) Generated from the TINF Solutions.

principal period ($T = 1$ sec) to obtain the FTM. Subsequently, the stability plots are created based on the Floquet multipliers condition, as indicated in Figure 3.11b.

In both Figures 3.11a and 3.11b, the shaded area represents the unstable region, and the white area indicates the stable region of the original system. The transition curves from both the figures are observed to match very well. From Figures 3.11a

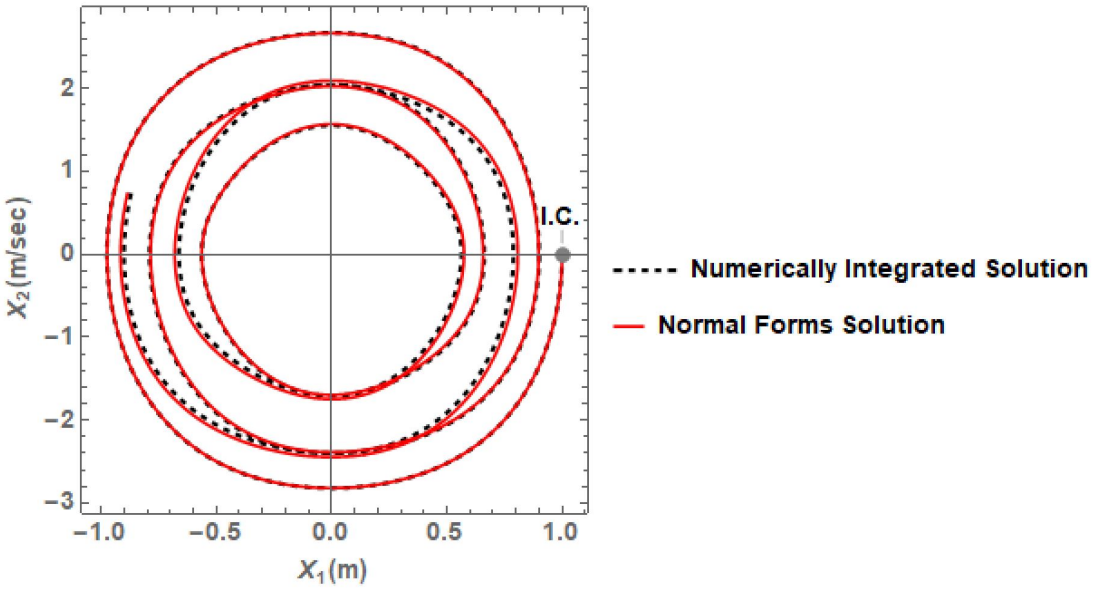

Figure 3.12: Phase Plot Comparison of a Stable System Without a Controller.

and 3.11b, a common stable point ($a = 8$, $b = 2$) is selected, and the phase plot variation of the back transformed TINF solution is compared against the numerically integrated solution of the Mathieu equation, as shown in Figure 3.12.

In Figure 3.12, the black dashed line represents the numerically integrated solution in the original coordinates, and the solid red line indicates the back transformed TINF solution. Both the methods are provided with the same set of initial conditions (I.C.), marked by a gray dot in the plot corresponding to $X_{10} = 1.0$ and $X_{20} = 0.0$. It is observed that the back transformed TINF solution follows the numerically integrated solution closely. This verifies again that the TINF solution preserves the original stable system's dynamical characteristics and maintains the temporal variations bounded. Similarly, a common unstable point ($a = 8$, $b = 4$) is selected and utilized to demonstrate the implementation of various linear feedback controllers in the subsequent subsections.

System Controlled to Stable Point

As explained in section 3.2.1, the Mathieu equation is updated with the linear controller terms (k_1, k_2), as shown in equation (3.26). The Floquet theory is still applicable to the updated system with the modified $\mathbf{A}(t)$ matrix. The updated system follows state augmentation, modal transformation, near identity transformations and application of the TINF technique to result in equation (3.28).

The evaluation of the stability bounds based on the controller gains variation for the given unstable system aids in its selection. Hence, for the given unstable case of $a = 8$ and $b = 4$, the TINF solutions are computed in symbolic form, keeping the controller gains as symbolic variables. The resulting STM matrix is evaluated at the principal period, $T = 1$ sec, and the stability plots are generated based on the Floquet multipliers for varying controller gains (k_1, k_2), as shown in Figure 3.13. The method of pole placement is also applicable towards identifying the ideal controller gains.

In Figure 3.13, the shaded gray area represents the unstable region, and the white area indicates the stable region for the system with controller. The effectiveness of the feedback controller is verified by plotting the temporal variations of the system states. A point from the unstable region (***P1***) corresponding to the controller gain values ($k_1 = 2.0$, $k_2 = 0.5$) and a point from the stable region (***P2***) corresponding to the gain values ($k_1 = 2.0$, $k_2 = 2.0$) are considered for the phase plot comparison with the uncontrolled unstable system, as displayed in Figure 3.14.

As indicated in Figure 3.14, the solid blue line represents the system without a controller, the dashed magenta line represents the system with a controller gain value of ***P1***, and the solid red line indicates the system with a controller gain value of ***P2***. It is observed that all the systems, in Figure 3.14, started off with the same set of initial conditions (I.C.), marked by a gray dot in the plot corresponding to $X_{10} = 1.0$,

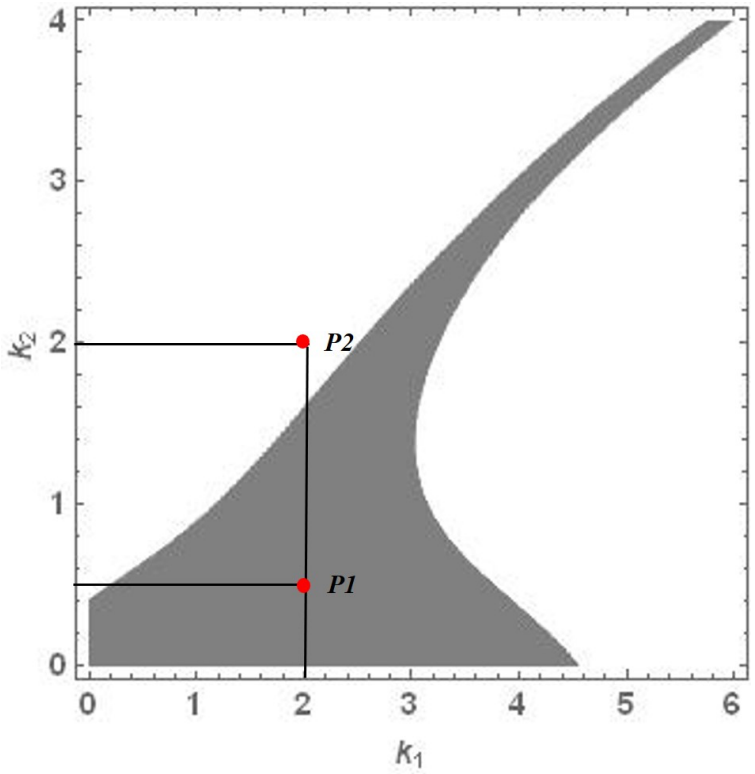

Figure 3.13: Stability Plot Based on Controller Gain Variations, Where the Gray Shaded Area Represents the Unstable Region and the White Area Corresponds to the Stable Region.

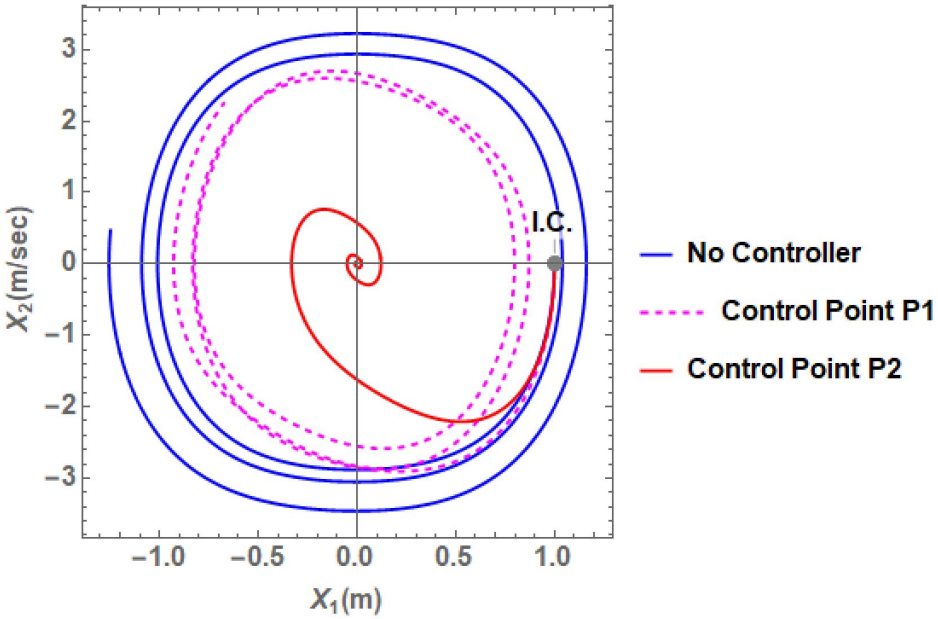

Figure 3.14: Phase Plot Comparison of System States with Controller Implementation Towards a Stable Point for an Unstable Mathieu Equation.

$X_{20} = 0.0$ and the simulations ran for 5 seconds. However, as expected from the stability plot (Figure 3.13), the controller gains corresponding to the stable region ***P2***, successfully stabilize the uncontrolled system to a stable point, whereas the one corresponding to the stable region ***P1*** remains unbounded.

System Controlled to a Desired Time Periodic Orbit

As explained in section 3.2.1, the Mathieu equation is updated with the linear controller terms (k_1, k_2) and error states $(e(t), \dot{e}(t))$, as shown in equation (3.33). The resulting $\mathbf{A}(t)$ matrix is similar to that in equation (3.26), and with the application of the unified approach, the derived TINF solution resembles equation (3.28) with the system states modified to error states. This results in the same stability plot, as indicated in Figure 3.13.

Analogous to the approach for '*System Controlled to Stable Point*', to verify the effectiveness of the feedback controller, a point from the unstable region (***P1***) and a point from the stable region (***P2***) are considered for the phase plot comparison with the uncontrolled unstable system, as shown in Figure 3.15. The desired time periodic orbit is given by $s = 0.5\cos(4t)$.

As indicated in Figure 3.15, the solid blue line represents the system without a controller, the dashed magenta line represents the system with the controller gain value of ***P1***, the solid red line indicates the system with the controller gain value of ***P2***, and the solid black line corresponds to the desired time periodic orbit. It is observed that all the systems, in Figure 3.15, started with the same set of initial conditions (I.C.), marked by a gray dot in the plot corresponding to $X_{10} = 1.0$, $X_{20} = 0.0$ and the simulations ran for 5 seconds. However, as expected from the stability plot (Figure 3.13), the controller gains corresponding to the stable region ***P2***, successfully stabilizes the uncontrolled stable system to the desired periodic orbit

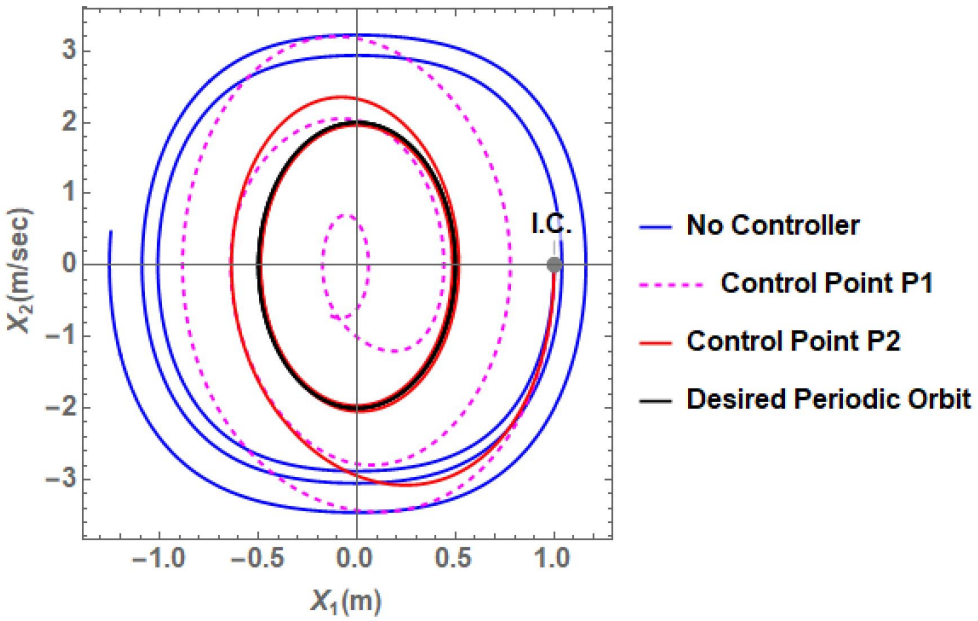

Figure 3.15: Phase Plot Comparison of System States with Controller Implementation Towards a Desired Time Periodic Orbit for an Unstable Mathieu Equation.

swiftly, whereas the one representing the unstable region ***P1*** remains unbounded and failed to reach the desired orbit.

System with Optimal Controller Gain

As mentioned in section 3.2.1, the feedback controller gain values can be considered time varying, without computing the stability characteristics of the dynamical system. However, a closed form expression for the STM of the Hamilton system is essential to compute the optimized solution. In this approach, since the selection of controller gain values is avoided, the requirement to generate a stability plot based on the controller gain variation is also eliminated.

The demonstration of the effectiveness of this controller approach is performed on the same unstable Mathieu equation with parameters $a = 8$, $b = 4$, and $\omega = 2\pi$. The boundary conditions are considered at $t_0 = 0.0$ sec and $t_f = 20.0$ secs. The matrices $\mathbf{D}, \bar{\mathbf{S}}$ are considered to be 2×2 identity matrix ($\mathbf{I}_2$), $\mathbf{G}_2 = 1.0$, $\mathbf{G}_3 = 10 * \mathbf{I}_2$ and

$\mathbf{B} = [0\ \ 1]^T$. After substituting these values in the Hamiltonian form of the dynamical system (equation (3.36)), the closed form expression of the STM is computed using the unified approach. The application of the state augmentation to the Hamiltonian form results in 6 state variables (2 original system states, 2 adjoint state variables, and 2 fictitious augmented states), as shown in the equation below

$$\frac{d}{dt}\begin{Bmatrix} x \\ \dot{x} \\ \bar{p}_1 \\ \bar{p}_2 \\ p \\ q \end{Bmatrix} = \begin{bmatrix} 0 & 1 & 0 & 0 & 0 & 0 \\ -a & 0 & 0 & -1 & 0 & 0 \\ -10 & 0 & 0 & a & 0 & 0 \\ 0 & -10 & -1 & 0 & 0 & 0 \\ 0 & 0 & 0 & 0 & 0 & 1 \\ 0 & 0 & 0 & 0 & -\omega^2 & 0 \end{bmatrix} \begin{Bmatrix} x \\ \dot{x} \\ \bar{p}_1 \\ \bar{p}_2 \\ p \\ q \end{Bmatrix} + \begin{Bmatrix} 0 \\ -bxp \\ b\bar{p}_2 p \\ 0 \\ 0 \\ 0 \end{Bmatrix} \tag{3.40}$$

The updated system in equation (3.40) undergoes modal transformation, near-identity transformation, and the TINF technique. The closed form expression for the back transformed STM in the Hamiltonian coordinates is used in equation (3.37) to compute $\mathbf{S}(t)$ matrix. The time evolution of the resulting $\mathbf{S}(t)$ matrix elements for first 10 seconds are displayed in Figure 3.16.

In Figure 3.16, though all the elements are observed to have the same periodic behavior, the magnitude of each of them are different. After the $\mathbf{S}(t)$ matrix is computed, the optimal feedback controller gain variation over the period of time, is computed using equation (3.39) and plotted for the first 10 seconds in Figure 3.17.

In Figure 3.17, each element of the optimal controller gain vector is also observed to follow a time periodic behavior. These gain variation coupled with the system state variation contributes the feedback control input to the system plant. The resulting stabilized system state variation is verified by plotting the temporal variations. For the same unstable Mathieu equation, the temporal variations of the system states

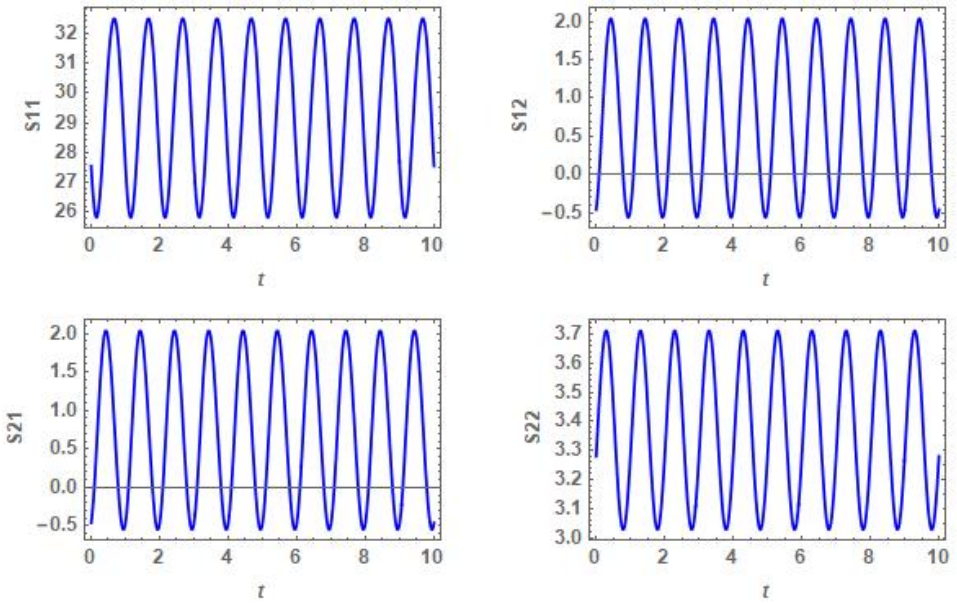

Figure 3.16: The Element-wise Variation of $\mathbf{S}(t)$ Matrix over Time.

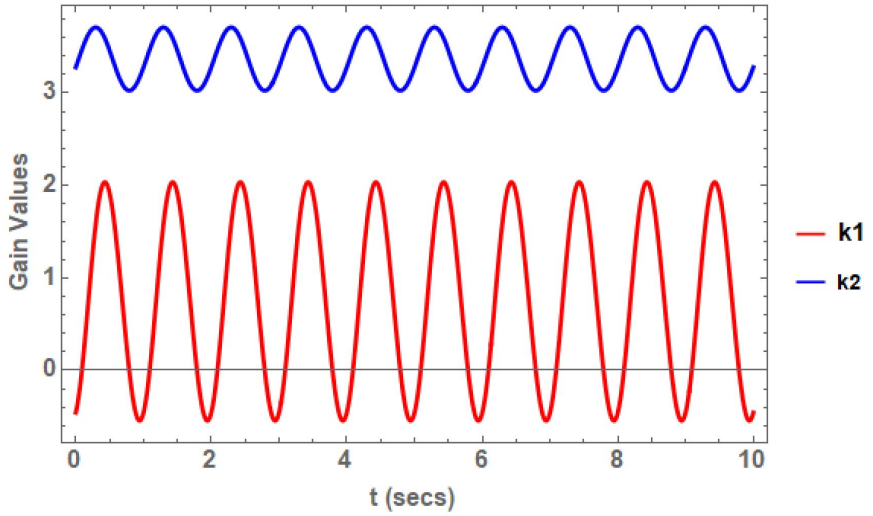

Figure 3.17: The Variation of the Optimal Feedback Controller Gain Values over Time.

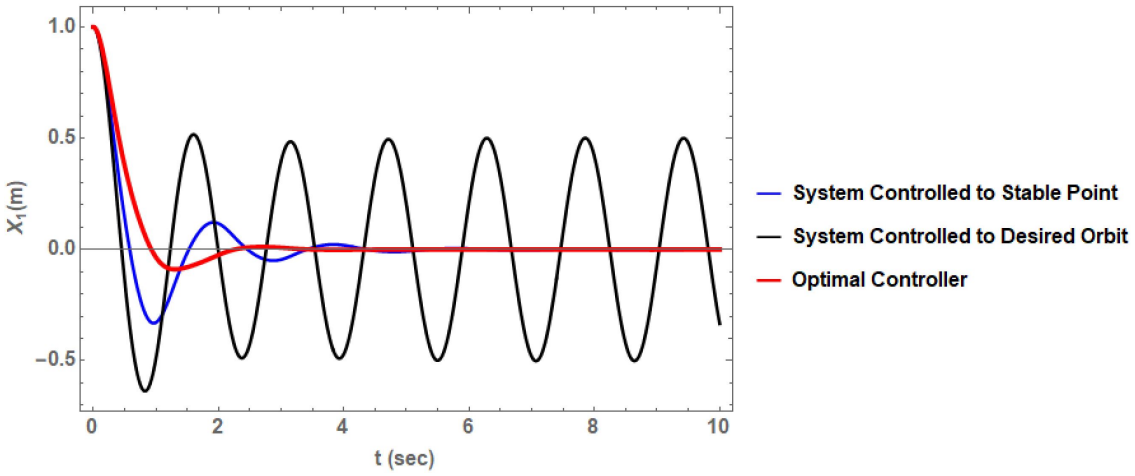

(**a**)

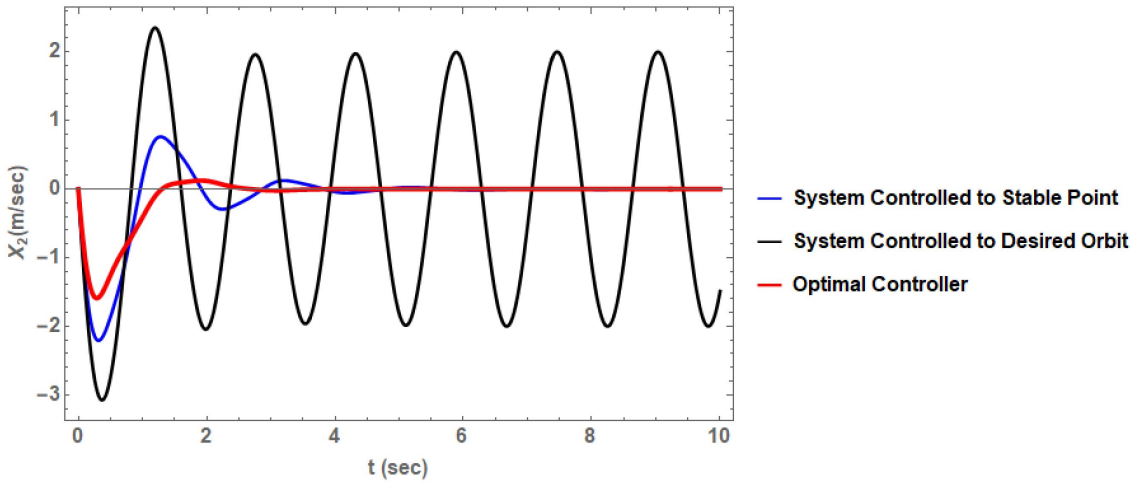

(**b**)

Figure 3.18: Comparison of Temporal Variations for All Three Linear Feedback Controller Strategies (**a**) x_1 State Variation, (**b**) x_2 State Variation.

with all three control strategies discussed in this work, are displayed in Figure 3.18.

In both Figures 3.18a and 3.18b, the solid blue line corresponds to the variation of system states controlled to stable point using a fixed controller gains ($k_1 = 2.0$, $k_2 = 2.0$), and it is observed to stabilize in about 6 seconds. In the same plots, the solid black line represents the variation of system states controlled to stable desired periodic orbit using the same fixed controller gains ($k_1 = 2.0$, $k_2 = 2.0$), and it is

observed to stabilize in about 2-3 seconds. In these plots, the solid red line attributes to the variation of system states optimally controlled to a stable point by 4 seconds. All these control strategies are provided with the same set of initial conditions ($X_{10} = 1.0, X_{20} = 0.0$). The optimal feedback controller gain behavior can be modified by changing the weights of terms in the optimization cost function. However, the optimal feedback controller is observed to be insensitive to the system state initial conditions, whereas the other two feedback controller strategies are sensitive.

In this section, the closed form expression of STM for a parametrically excited linear time periodic system was computed using the unified approach, and the stability was generated based on the Floquet multipliers at the principal period. The transition curves obtained using this method are found to be comparable to that of the numerical techniques. For stabilizing an unstable linear time periodic system, three linear feedback controller strategies have been discussed. For fixed controller strategies, as an alternative to pole placement, a stability plot is generated to identify the ideal gain values to make the system bounded. It is verified using numerical simulations that the controller gain values corresponding to the stable region successfully stabilized the system to a stable fixed point and a desired periodic orbit. However, the fixed controller strategies are susceptible to the initial conditions of the unstable system. For the case of the optimal controller approach, the controller gain values are time varying and are insensitive to the initial conditions of the unstable system. Consequently, the need for stability plots to identify the ideal gain values is eliminated. A comparison of the temporal variations of the unstable system with all three linear feedback control strategies are included. All the numerical simulations are performed on the case of a linear Mathieu equation, and the results are verified.

3.2.3 Conclusion

In this section, the unified theory was applied towards generating stability plots for a linear time periodic system of modified Mathieu equation. Applying three linear feedback controller strategies on linear time periodic systems to drive it towards a stable point or periodic trajectory was also demonstrated in this section. The theory was verified by plotting the temporal variations of all the strategies applied to an unstable case. The controllers were observed to be effective in stabilizing the unbounded system.

The unified approach is demonstrated towards the stability analysis and control of linear time periodic systems. The nonlinear systems need to be linearized to perform such analysis. However, the unified approach can also generate closed form expressions for L-F transformation, which would aid in the analysis of nonlinear and externally excited systems.

Chapter 4

APPLICATIONS OF L-F TRANSFORMATION

As per Floquet theory, a linear time periodic system can be converted to a linear time-invariant form via L-F Transformation. Initially, the closed form solution for the L-F transformation matrix was computed, by Wu (1978), only for the class of commutative periodic systems. The STM needs to be computed as an explicit function of time to determine the same for a general case. The approximate method explained by Sinha *et al.* (1996) has been the conventional approach to compute the symbolic form of L-F transformation. However, one needs to account for more terms in the Chebyshev expansion for higher accuracy. Sinha *et al.* (1996) also demonstrated the application of L-F transformation towards the identifying resonance conditions for both free and forced parametrically excited time periodic systems.

The unified theory, detailed in section 2.4, is also capable of computing the state evolution as an explicit function of time and thereby computing the closed form expression for the L-F transformation. The computed closed-form expression of L-F transformation is further applied in the analysis of perturbed time periodic systems. In this chapter, the cases of periodic systems with external excitation, nonlinear terms, and stochastic excitations are considered for analysis and compared with numerical techniques in the subsequent sections.

4.1 Symbolic Computation of L-F Transformation

In this section, the unified theory is applied to a linear time varying system, as detailed in 2.4.1, resulting in the time-invariant form with the constant matrix in the Jordan form. In this chapter, the L-F transformation ($\bar{\mathbf{Q}}(t)$) resulting in the Jordan

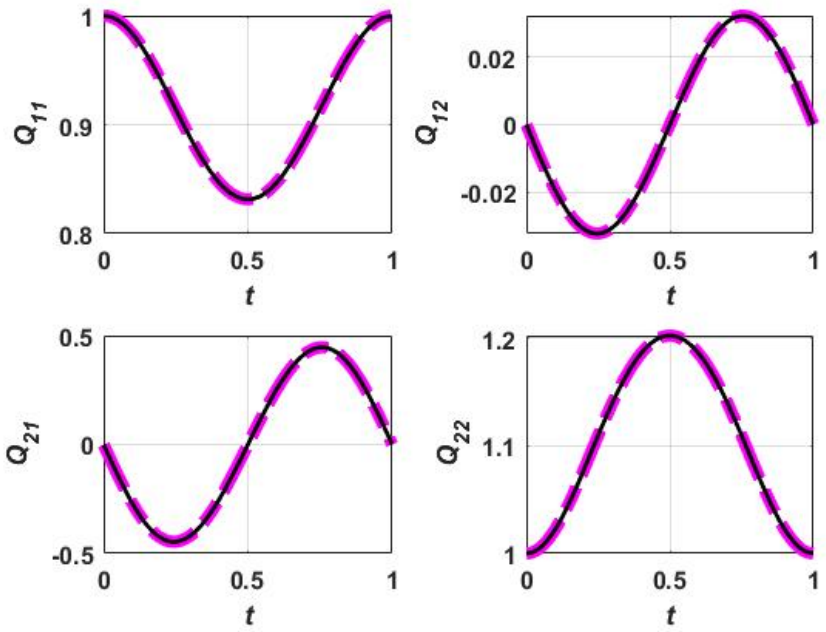

Figure 4.1: Comparison of Element-wise Variation of $\hat{\mathbf{Q}}(t)$ Matrix (Displayed in Solid Black Line) with $\mathbf{Q}(t)$ Matrix from Chefun (Displayed in Dashed Magenta Line) for the Principal Time Period ($T = 1$ Sec).

form is utilized for further analysis.

A time periodic system of the form equation (2.40) is considered. The system parameters of $a = 3, b = 2.5$ and $\omega = 2\pi$ are considered for this computation. Using the unified approach detailed in section 2.4.1, the resulting time-invariant $\bar{\mathbf{J}}$ matrix is determined to be

$$\bar{\mathbf{J}} = \begin{bmatrix} 0.0 - i1.76 & 0 \\ 0 & 0.0 + i1.76 \end{bmatrix} \tag{4.1}$$

To verify the accuracy of the the L-F transformation ($\bar{\mathbf{Q}}(t)$) for further analysis, it was back transformed to the original coordinates to obtain its corresponding matrix, $\hat{\mathbf{Q}}(t)$. The element-wise variations of $\hat{\mathbf{Q}}(t)$ matrix are compared with the Chebfun results in Figure 4.1.

In Figure 4.1, the element-wise variation of the computed L-F transformation

matrix ($\bar{\mathbf{Q}}(t)$), indicated in solid black line, is compared with that obtained from Chebfun (indicated in dashed magenta line). It is observed that the $\bar{\mathbf{Q}}(t)$ matrix is in excellent agreement with the Chebfun results for the principal time period in all four elements and is eligible to use for further analysis.

4.2 Computation of Inverse of L-F Transformation

For a parametrically excited linear periodic system of the form in equation (2.40), the L-F transformation is sufficient for performing the analysis. The inverse of the L-F transformation is needed for assessing nonlinear systems or systems with deterministic or stochastic excitations. The L-F transformation is a matrix where the matrix elements contain truncated Fourier series with parametric frequencies. Inverting a time varying matrix is not a trivial problem, and in this section, two possible approaches are presented to obtain the inverse of the L-F transformation matrix.

4.2.1 Symbolic Computation of Inverse Matrix

In minimal cases, when the L-F transformation matrix is small (2×2) and contains only a few terms, symbolic computation software, such as MATHEMATICA or MAPLE, may be able to find the inverse. However, the inverse computed with this direct approach should be checked for the following conditions.

$$\begin{aligned} \bar{\mathbf{Q}}^{-1}(0) &= \mathbf{I} \\ \bar{\mathbf{Q}}^{-1}(t) \times \bar{\mathbf{Q}}(t) &= \mathbf{I} \end{aligned} \tag{4.2}$$

The expression provided for $\bar{\mathbf{Q}}^{-1}(t)$ may need further simplification for ease in future use.

4.2.2 Adjoint Method

As detailed in Sinha *et al.* (1996); Iakubovich and Starzhinskiĭ (1975), the inverse of the L-F transformation matrix can also be determined using the adjoint system, which is given by

$$\dot{\boldsymbol{\kappa}} = -\mathbf{A}^T(t)\boldsymbol{\kappa} \tag{4.3}$$

The STM of the original system ($\boldsymbol{\Phi}(t)$) is related to that of the adjoint system ($\boldsymbol{\Psi}(t)$) as follows

$$\boldsymbol{\Phi}^{-1}(t) = \boldsymbol{\Psi}^T(t) \tag{4.4}$$

Using the properties of the adjoint system from equation (4.4) and using equation (2.36), the inverse of the L-F transformation matrix can be computed as

$$\bar{\mathbf{Q}}^{-1}(t) = \left[\bar{\boldsymbol{\Phi}}(t)e^{-\bar{\mathbf{J}}t}\right]^{-1} = e^{\bar{\mathbf{J}}t}\bar{\boldsymbol{\Phi}}^{-1}(t) = e^{\bar{\mathbf{J}}t}\boldsymbol{\Psi}^T(t) \tag{4.5}$$

This method of inverse computation is validated in Sinha *et al.* (1996) using the exponent matrix ($\mathbf{R}$), and interested readers are redirected to the same further details.

4.2.3 Recurrent Neural Network

One can also use a dynamical method using a recurrent neural network proposed for inversion of the time-varying matrix. One could use the gradient method Zhang *et al.* (2009a), Zhang dynamics Zhang *et al.* (2009b), or Chen dynamics Xiao *et al.* (2018) to find an inverse. This section briefly presents the Zhang dynamics approach that could be used for inverting the L-F transformation.

Consider a time-varying matrix $\mathbf{Y}(t)$ with inverse $\mathbf{W}(t) = \mathbf{Y}^{-1}(t)$ so that the equation (4.6) is valid

$$\begin{aligned} \mathbf{Y}(t)\mathbf{W}(t) &= \mathbf{I} \\ \mathbf{Y}(t)\mathbf{W}(t) - \mathbf{I} &= \mathbf{0} \end{aligned} \tag{4.6}$$

Assuming $\mathbf{Y}(t)$ is known and $\frac{d\mathbf{Y}(t)}{dt}$ exists. The objective is to find $\mathbf{W}(t)$ using the following equation

$$\mathbf{E}(\mathbf{W}(t), t) \equiv \mathbf{Y}(t)\mathbf{W}(t) - \mathbf{I} \tag{4.7}$$

where $\mathbf{E}(\mathbf{W}(t), t)$ is a matrix-valued error function. The derivative of the error function $\dot{\mathbf{E}}(\mathbf{W}(t), t)$ should be selected such that $\mathbf{E}(\mathbf{W}(t), t) \to 0$. Thus, $\dot{\mathbf{E}}(\mathbf{W}(t), t)$ can be chosen as

$$\frac{d\mathbf{E}(\mathbf{W}(t))}{dt} = -\Gamma\mathbf{G}(\mathbf{E}(\mathbf{W}(t), t)) \tag{4.8}$$

where Γ is a scaling factor for the convergence and $\mathbf{G}(\mathbf{E}(\mathbf{W}(t), t))$ is called an activation function or matrix mapping recurrent neural network. Differentiating equation (4.7) with respect to time and substituting it to equation (4.8) yields

$$\begin{aligned} \mathbf{Y}(t)\dot{\mathbf{W}}(t) &= -\dot{\mathbf{Y}}(t)\mathbf{W}(t) - \Gamma\mathbf{G}(\mathbf{E}(\mathbf{W}(t), t)) \\ \mathbf{Y}(t)\dot{\mathbf{W}}(t) &= -\dot{\mathbf{Y}}(t)\mathbf{W}(t) - \Gamma\mathbf{G}(\mathbf{Y}(t)\mathbf{W}(t) - \mathbf{I}) \end{aligned} \tag{4.9}$$

The equation (4.9) is a matrix differential equation that can be solved numerically for $\mathbf{W}(t)$ using an appropriate initial condition. In this work $\mathbf{Y}(t)$ is the L-F transformation matrix $\bar{\mathbf{Q}}(t)$, and $\mathbf{W}(t)$ is the inverse of L-F transformation $\bar{\mathbf{Q}}^{-1}(t)$. Thus equation (4.13) can be updated as

$$\bar{\mathbf{Q}}(t)\dot{\bar{\mathbf{Q}}}^{-1}(t) = -\dot{\bar{\mathbf{Q}}}(t)\bar{\mathbf{Q}}^{-1}(t) - \Gamma\mathbf{G}(\bar{\mathbf{Q}}(t)\bar{\mathbf{Q}}^{-1}(t) - \mathbf{I}) \tag{4.10}$$

One has to select an appropriate activation function and scaling constant $\Gamma\mathbf{G}(\bar{\mathbf{Q}}(t)\bar{\mathbf{Q}}^{-1}(t) - \mathbf{I})$ to achieve convergence. The equation (4.10) can be numerically

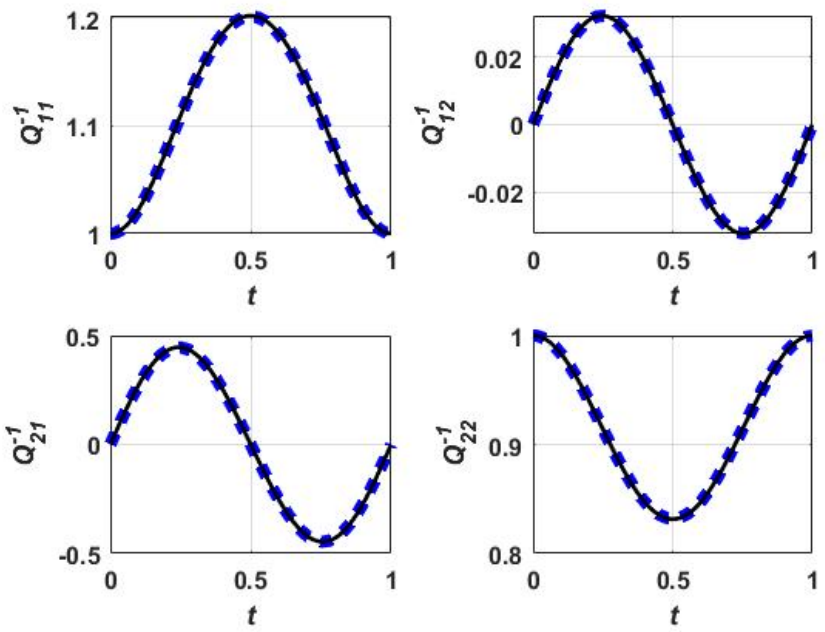

Figure 4.2: Comparison of Element-wise Variation of $\bar{\mathbf{Q}}^{-1}(t)$ Matrix from Symbolic Computation Method (Displayed in Solid Black Line) with $\bar{\mathbf{Q}}^{-1}(t)$ Matrix from ZNN Method (Displayed in Dashed Blue Line).

integrated with the initial condition $\bar{\mathbf{Q}}^{-1}(0) = \mathbf{I}$ to determine $\bar{\mathbf{Q}}^{-1}(t)$. For more details on the Zhang Neural Network, its application, and proof of convergence, the readers are directed to Guo and Zhang (2013); Guo *et al.* (2017).

The $\bar{\mathbf{Q}}(t)$ matrix computed for the Mathieu system (equation (2.40)) is inverted using two methods (symbolic computation and ZNN) and compared for the principal time period of $T = 1$ sec in Figure 4.2.

From Figure 4.2, it is observed that the $\bar{\mathbf{Q}}^{-1}(t)$ matrix computed using the ZNN approach (indicated in dashed blue line) closely follows the $\bar{\mathbf{Q}}^{-1}(t)$ matrix computed using the symbolic computation (indicated in solid blue line) in all four elements. the $\bar{\mathbf{Q}}^{-1}(t)$ matrix from either of the two approaches are eligible for the subsequent applications.

4.3 Application: Externally Excited System

Some of the parametrically excited time-periodic system may be excited by an additional external term in real-world applications. In this section, the time periodic system (expressed in equation (2.29)) is externally excited by forcing term and analyzed using the $\bar{\mathbf{Q}}(t)$ and $\bar{\mathbf{Q}}^{-1}(t)$ matrices computed earlier. Consider the system in equation (2.29) is subjected to external excitation given by

$$\dot{\mathbf{x}}(t) = \mathbf{A}(t)\mathbf{x}(t) + \mathbf{f}(t) \tag{4.11}$$

where $\mathbf{f}(t)$ is the $n \times 1$ vector containing external excitation terms. Applying the L-F transformation $\mathbf{x}(t) = \bar{\mathbf{Q}}(t)\mathbf{y}(t)$, transforms the linear time varying part to a time-invariant form. The inverse of the L-F Transformation matrix $\bar{\mathbf{Q}}^{-1}(t)$ is applied to equation (4.11) results in the following equation

$$\dot{\mathbf{y}} = \bar{\mathbf{J}}\mathbf{y} + \bar{\mathbf{Q}}^{-1}(t)\mathbf{f}(t) = \bar{\mathbf{J}}\mathbf{y} + \mathbf{F}(t) \tag{4.12}$$

Equation (4.12) needs to be solved to compute the time evolution of system states in the reduced system $\mathbf{y}(t)$, which can be further back-transformed to its corresponding system states in the original coordinates $\mathbf{x}(t)$. The system in equation (4.12) can be solved using two approaches, as illustrated in the following subsections

4.3.1 Convolution Integral Approach

The method of convolution integral can be used to solve equation (4.12). A direct application of convolution integral results in

$$\mathbf{y}(t) = \mathbf{e}^{\bar{\mathbf{J}}t}\mathbf{y}(0) + \int_0^t \mathbf{e}^{\bar{\mathbf{J}}(t-s)}\mathbf{F}(s)ds \tag{4.13}$$

The $\bar{\mathbf{Q}}(t)$ matrix would contain the terms with parametric excitation frequencies (ω_p) and the $\mathbf{f}(t)$ vector with the external excitation frequencies (ω_e). As detailed in Sinha *et al.* (1996), the external resonance condition can be given by

$$\lambda_k \neq \pm in\omega_p \pm m\omega_e; \quad n, m = 0, 1, ... \quad k = 1, 2, ... \tag{4.14}$$

where λ_k are the eigenvalues of the $\mathbf{R}$ matrix (or Floquet Exponents) that appear on the diagonal elements of the $\bar{\mathbf{J}}$ matrix. In the case of l multifrequency external excitations, $\omega_e = \sum_{r=1}^{l} \omega_r$. It is noted that this external resonance is in terms of Floquet Exponents and not the eigenvalues of the unforced system (when the magnitude of parametric excitation is assumed zero). The result obtained in the $\mathbf{y}(t)$ domain can be transformed to the original coordinate $\mathbf{x}(t)$ via reversing the sequence of transformations. For clarity, it is stated that the eigenvalues of $\bar{\mathbf{B}}_0$ matrix that appear as the diagonal elements of the $\mathbf{J}$ matrix are different from the semi-simple eigenvalues (Floquet Exponents) that appear on the diagonal elements of $\bar{\mathbf{J}}$.

4.3.2 Alternate Approach

Alternatively, the equation (4.12) system can be solved using the state augmentation and TINF approach. In equation (4.12), it is noted that the elements of $\bar{\mathbf{Q}}^{-1}(t)$ matrix comprises of Fourier series with frequencies of parametric excitation ω_p. Similarly, the external excitation term can be approximated to a Fourier series of frequency ω_e. As defined earlier, the time-periodic terms in $\bar{\mathbf{Q}}^{-1}(t)$ can be expressed again in terms of fictitious states (p_1, q_1) and that in $\mathbf{f}(t)$ vector as newly augmented states (p_2, q_2). The updated equation (4.12) can be expressed as

$$\dot{\tilde{\mathbf{y}}} = \breve{\mathbf{J}}\tilde{\mathbf{y}} + \bar{\mathbf{Q}}^{-1}(p_1, q_1)\mathbf{f}(p_2, q_2) = \breve{\mathbf{J}}\tilde{\mathbf{y}} + \mathbf{F}(\tilde{\mathbf{y}}) \tag{4.15}$$

where

$$\tilde{\mathbf{y}} = \begin{Bmatrix} y \\ \dot{y} \\ p_1 \\ q_1 \\ p_2 \\ q_2 \end{Bmatrix}, \breve{\mathbf{J}} = \begin{bmatrix} \bar{J}_{11} & 0 & 0 & 0 & 0 & 0 \\ 0 & \bar{J}_{22} & 0 & 0 & 0 & 0 \\ 0 & 0 & -i\omega_p & 0 & 0 & 0 \\ 0 & 0 & 0 & +i\omega_p & 0 & 0 \\ 0 & 0 & 0 & 0 & 0 & 1 \\ 0 & 0 & 0 & 0 & -\omega_e^2 & 0 \end{bmatrix}, \mathbf{F}(\tilde{\mathbf{y}}) = \begin{Bmatrix} \bar{Q}_{11}^{-1} f_{11} + \bar{Q}_{12}^{-1} f_{21} \\ \bar{Q}_{21}^{-1} f_{11} + \bar{Q}_{22}^{-1} f_{21} \\ 0 \\ 0 \\ 0 \\ 0 \end{Bmatrix} \tag{4.16}$$

At this point, the $\mathbf{F}(\tilde{\mathbf{y}})$ needs to be verified to contain only the nonlinear terms, and the coefficient of all the linear terms needs to be moved to the $\breve{\mathbf{J}}$ matrix. The subsequent modal transformation and application of TINF yield a time invariant form similar to equation (2.35) in the absence of resonant terms. The analytical solution of system states is obtained in the $\mathbf{v}$ domain. The back-substitution of augmented states and a series of back-transformations result in the time evolution of system states in the original coordinates ($\mathbf{x}$ domain).

It is noted that in both these approaches, $\bar{\mathbf{Q}}(t)$ and its inverse are utilized to analyze the system. A comparison of the time evolution of the system states in the original coordinates obtained using both approaches are demonstrated using the following examples.

4.3.3 Example-1: Time Periodic System Externally Excited with a Periodic Term

In this example, consider the linear time periodic system in equation (2.40)) externally excited by a periodic term is given by

$$\ddot{x} + (a + b\cos(\omega t))x = c\cos(\Omega t) \tag{4.17}$$

By comparing equation (4.17) to equation (4.11) indicates $\mathbf{f}(t) = [0 \quad c\cos(\Omega t)]^T$.

The system parameters considered in this example for the linear remains the same as earlier and that for the forcing term are $c = 3, \Omega = 7$ rads/sec. The equation (4.17) can be numerically integrated for a set of initial conditions $(x_0 = 1, \dot{x}_0 = 0)$ to evaluate the numerical solution for the system states $(x(t), \dot{x}(t))$.

As the linear part of the system remains the same as discussed in equation (2.43), the earlier computed closed form expression for $\bar{\mathbf{Q}}(t)$ and $\bar{\mathbf{Q}}^{-1}(t)$ matrices are employed to reduce the system in the form of equation (4.12). Similarly, the initial conditions $(x_0 = 1, \dot{x}_0 = 0)$ are also transformed to its corresponding values $\mathbf{y}(0)$ to solve the reduced system using the convolution integral approach.

As discussed earlier, invoking another round of state augmentation on the reduced system (as shown in equation (4.16)) generates a solution using the alternate approach. The time evolution of the system states in the original coordinates are obtained by back-substitutions and back-transformations from both the approaches and compared with the numerical integration solution, as illustrated in the temporal variations and phase plots in Figures 4.3a, b, and 4.4.

In Figure 4.4, the phase plot from the system states obtained by numerical integration of equation (4.17) is indicated by the thick blue line (C1), that by the convolution integral approach is indicated by the dashed orange line (C2) and that by the alternate approach of double state augmentation is shown by the solid black line (C3). It is observed that the temporal variations of the system states computed using all three methods start-off from the same initial condition (indicated by a black dot) and continue to be in excellent agreement with each other for 35 seconds.

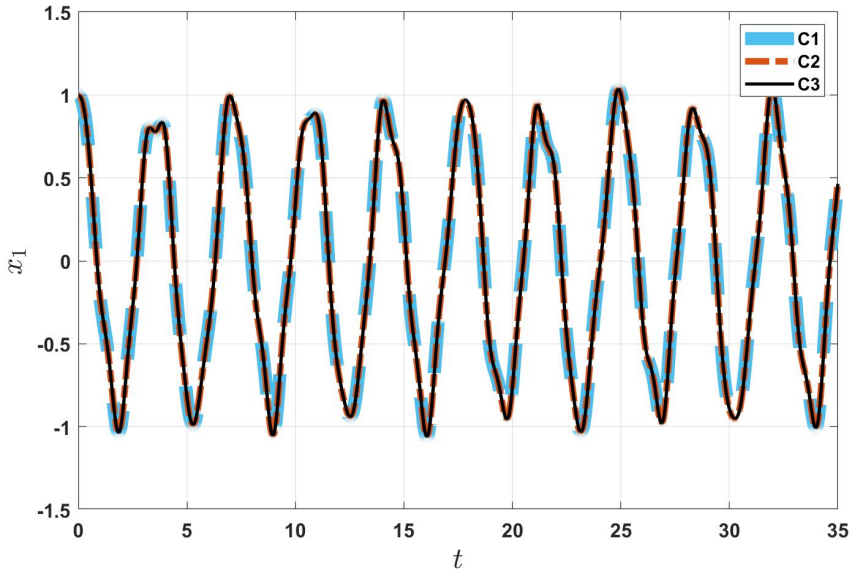

(**a**)

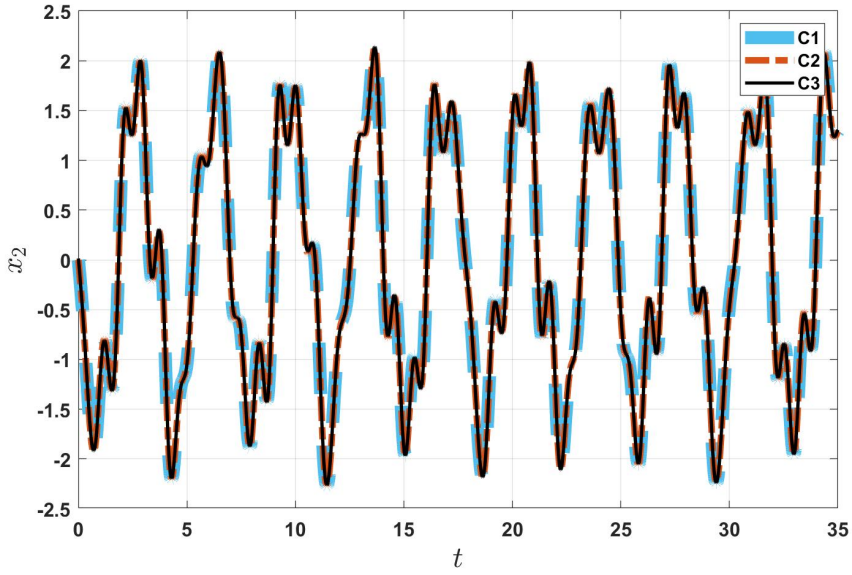

(**b**)

Figure 4.3: Comparison of the Temporal Variations of the System States of Time Periodic System Externally Excited with a Periodic Term (Example-1), Where the Thick Dashed Blue Line (C1) Represents the Numerically Integrated Solution, the Dashed Orange Line (C2) Corresponds to the Solution from Convolution Integral Approach and the Black Solid Line (C3) Represents the Solution from Alternate Approach For (**a**) x_1 State Variation, (**b**) x_2 State Variation.

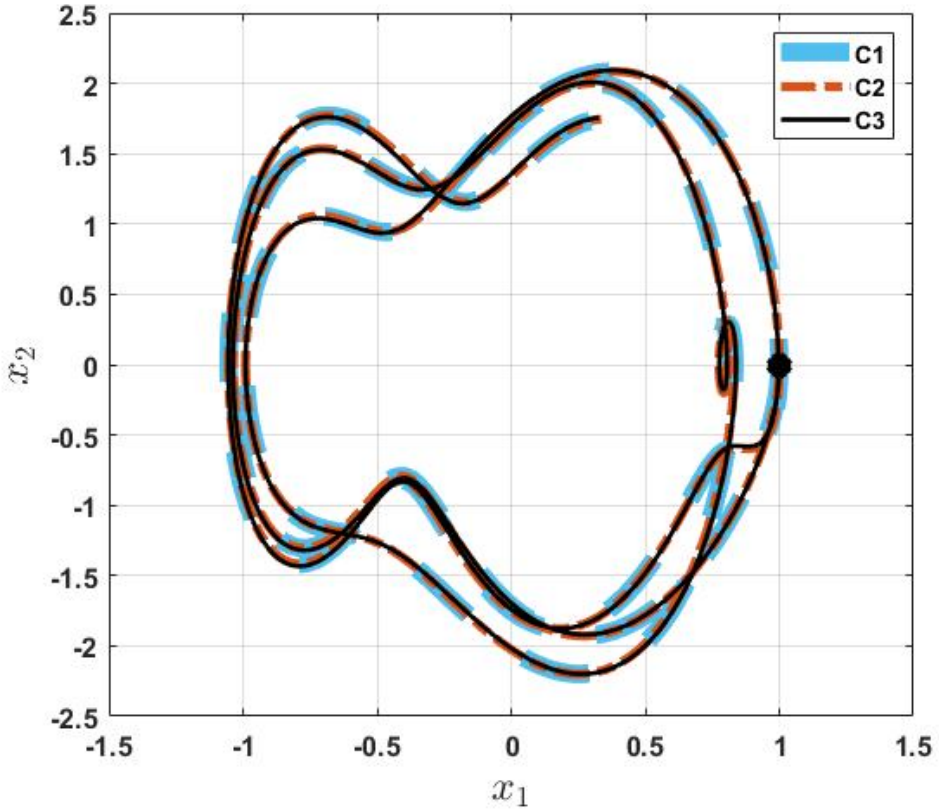

Figure 4.4: Comparison of the Phase Plot Variations of the System States of Time Periodic System Externally Excited with a Periodic Term (Example-1), Where the Thick Dashed Blue Line (C1) Represents the Numerically Integrated Solution, the Dashed Orange Line (C2) Corresponds to the Solution from Convolution Integral Approach and the Black Solid Line (C3) Represents the Solution from Alternate Approach.

4.3.4 Example-2: Time Periodic System Externally Excited with a Square Wave Term

The above discussed approach is limited to sinusoidal excitation term and applicable to other excitation wave forms such as square or triangular. In this example, the external excitation considered is a square wave of the form

$$f(t) = sgn(\cos(t)) \tag{4.18}$$

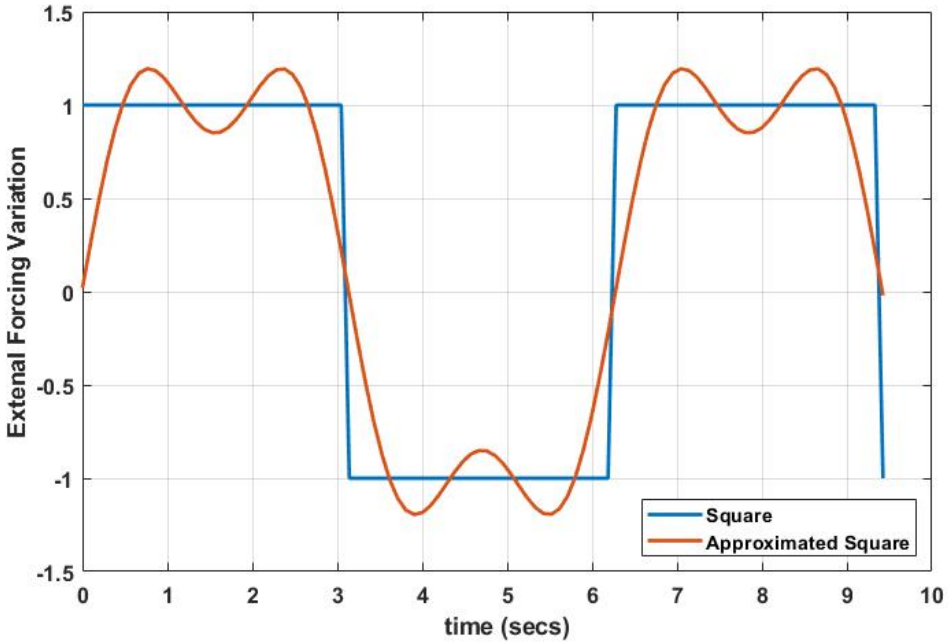

Figure 4.5: Comparison of a Square Wave (Blue Line) and Its Fourier Series Approximation (Orange Line).

The above square wave is approximated as Fourier series of the form

$$f(t) \approx 0.01\cos(t) + 1.27\sin(t) + 0.01\cos(3t) + 0.42\sin(3t) \tag{4.19}$$

The comparison of the approximated square wave to the actual square wave is indicated in Figure 4.5. By adding more terms to the Fourier series, one could get a closer approximation of the same. However, the long expression with non-prominent terms would increase the computational cost for the normal form estimates in the subsequent steps.

As discussed earlier, the closed-form expression for $\bar{\mathbf{Q}}(t)$ matrix is computed using the symbolic computation method. Subsequently, the time varying matrix is inverted using the symbolic computation method in MATHEMATICA to obtain $\bar{\mathbf{Q}}^{-1}(t)$ matrix. Further, the system in equation (4.11) is reduced to equation (4.12), with the external excitation term as equation (4.18). The $\cos(3t)$ and $\sin(3t)$ terms are ex-

panded in terms of $\cos(t)$ and $\sin(t)$ using Ptolemy's trigonometric formulae. This aids in easing the computations using the alternate approach. The comparisons of the system states' temporal variations and phase plot are indicated in Figures 4.6 and 4.7.

Similar to the case of Example-1, in Figure 4.7, the phase plot from the system states obtained by numerical integration is indicated by the thick blue line (C1), that by the convolution integral approach is indicated by the dashed orange line (C2) and that by the alternate approach of double state augmentation is represented by the solid black line (C3). It is observed even for example-2 that the temporal variations of the system states computed using all three methods start-off from the same initial condition (indicated by a black dot) and continue follow each other closely for 35 seconds.

4.4 Application: Nonlinear System

Many real world examples may not follow a truly periodic behavior and will contain inherent nonlinear behavior. In this section, the analysis of the periodic system with nonlinearity using the computed L-F transformation and other approaches is briefly explained. Consider the system in equation (2.29) is modified to contain nonlinearity as

$$\dot{\mathbf{x}}(t) = \mathbf{A}(t)\mathbf{x}(t) + \mathbf{f}(\mathbf{x}, t) \tag{4.20}$$

where $\mathbf{f}(\mathbf{x}, t)$ is the $n \times 1$ vector containing the nonlinear terms. Since equation (4.20) is nonlinear in nature, a direct application of the Normal Forms approach is feasible after the modal transformation. Due to the presence of time varying periodic terms, a Time Dependent Normal Forms (TDNF) is required to analyze the system. However, with the use of state augmentation technique, a TINF approach is also

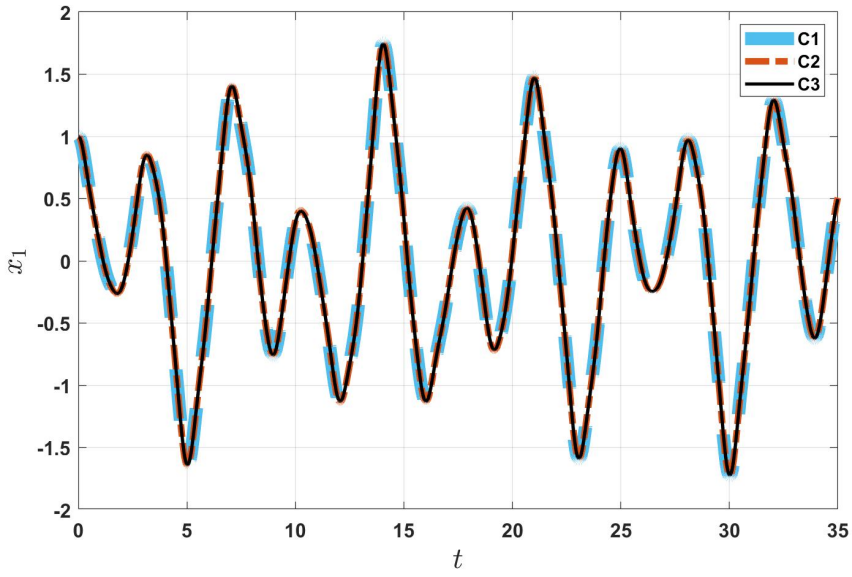

(**a**)

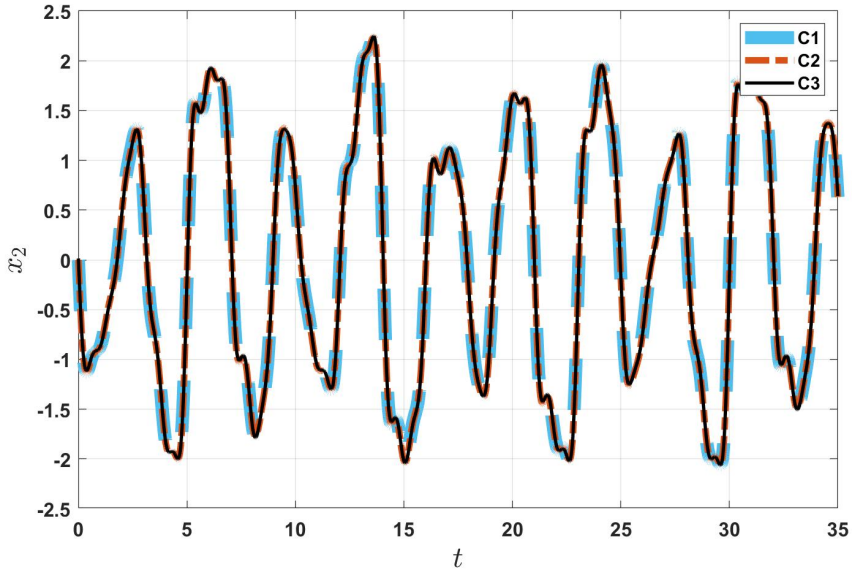

(**b**)

Figure 4.6: Comparison of the Temporal Variations of the System States of Time Periodic System Externally Excited with a Square Wave Term (Example-2), Where the Thick Dashed Blue Line (C1) Represents the Numerically Integrated Solution, the Dashed Orange Line (C2) Corresponds to the Solution from Convolution Integral Approach and the Black Solid Line (C3) Represents the Solution from Alternate Approach For (**a**) x_1 State Variation, (**b**) x_2 State Variation.

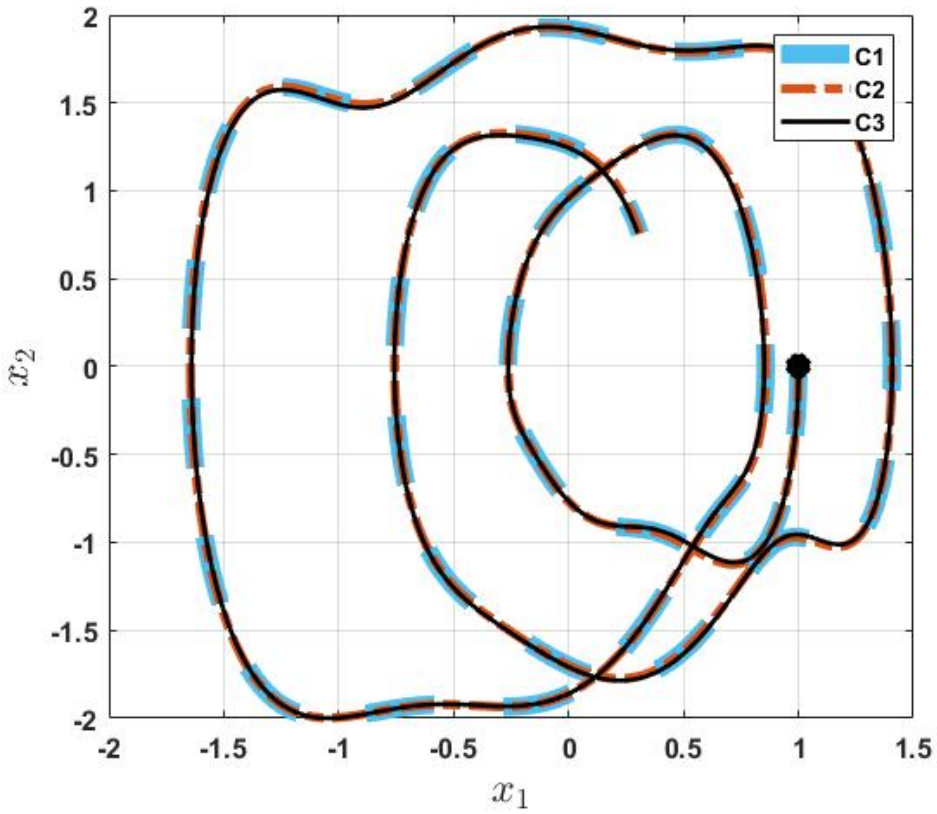

Figure 4.7: Comparison of the Phase Plot Variations of the System States of Time Periodic System Externally Excited with a Square Wave Term (Example-2), Where the Thick Dashed Blue Line (C1) Represents the Numerically Integrated Solution, the Dashed Orange Line (C2) Corresponds to the Solution from Convolution Integral Approach and the Black Solid Line (C3) Represents the Solution from Alternate Approach.

feasible, thereby reducing the computational cost.

Alternatively, the computed L-F transformation matrix $\bar{\mathbf{Q}}(t)$, aids in applying $\mathbf{x}(t) = \bar{\mathbf{Q}}(t)\mathbf{y}(t)$, that results in

$$\dot{\mathbf{y}} = \bar{\mathbf{J}}\mathbf{y} + \bar{\mathbf{Q}}^{-1}(t)\mathbf{f}(\mathbf{y}, t) = \bar{\mathbf{J}}\mathbf{y} + \mathbf{F}(\mathbf{y}, t) \tag{4.21}$$

The reduced system in equation (4.21) can be solved using the direct method of convolution integral discussed earlier to determine the time evolution of system states $\mathbf{y}(t)$. The following sub-section using an example of a nonlinear Mathieu equation is

considered and evaluated using these approaches and compared.

4.4.1 Example-3: Time Periodic System with Nonlinear Excitations

In this example, the periodic Mathieu system (equation (2.40)) is updated with a cubic nonlinearity term as follows

$$\ddot{x} + (a + b\cos(\omega t))x + x^3 = 0 \tag{4.22}$$

The comparison of equation (4.22) to equation (4.20) yields $\mathbf{f}(\mathbf{x}, t) = [0 \quad x^3]^T$. The same system parameters of $a = 3, b = 2.5$ and $\omega = 2\pi$ are considered with the initial conditions $(x_0 = 1, \dot{x}_0 = 0)$ to compute the numerically integrated solution of system states $(x(t), \dot{x}(t))$ for equation (4.22).

Analytical Solution Using TINF

As mentioned earlier, the application of state augmentation on equation (4.22) results in

$$\frac{d}{dt}\begin{Bmatrix} x \\ \dot{x} \\ p_1 \\ q_1 \end{Bmatrix} = \begin{bmatrix} 0 & 1 & 0 & 0 \\ -3 & 0 & 0 & 0 \\ 0 & 0 & 0 & 1 \\ 0 & 0 & -4\pi^2 & 0 \end{bmatrix}\begin{Bmatrix} x \\ \dot{x} \\ p_1 \\ q_1 \end{Bmatrix} + \begin{Bmatrix} 0 \\ -2.5xp_1 - x^3 \\ 0 \\ 0 \end{Bmatrix} \tag{4.23}$$

The subsequent modal transformation and near-identity transformation aids in the application of TINF to the resulting equation. For the given system, the TINF generates the solution of the form

$$\left.\begin{aligned} \dot{v}_1 &= -i1.7648v_1 - i0.2887v_1^2v_2 \\ \dot{v}_2 &= +i1.7648v_1 + i0.2887v_1v_2^2 \end{aligned}\right\} \tag{4.24}$$

With the use of complex change of variables $v_1 = u_1 - iu_2, v_2 = u_1 + iu_2$ in equation (4.24) and the subsequent application of the polar coordinate transformation $u_1 = R\cos\theta$ and $u_2 = R\sin\theta$, results in the reduced system as

$$\left.\begin{aligned} \dot{R} &= 0 \\ \dot{\theta} &= 1.5708 - 1.9385R^2 \end{aligned}\right\} \tag{4.25}$$

The expressions in equation (4.25) can be solved analytically. The resulting solutions $(R(t), \theta(t))$ follow a series of inverse transformations to generate the analytical solution for the system states $(x(t), \dot{x}(t))$ for equation (4.22).

Convolution Integral Approach Using L-F

With the use of $\bar{\mathbf{Q}}(t)$ and $\bar{\mathbf{Q}}^{-1}(t)$ matrices computed earlier, the expression in equation (4.21) can be obtained, where $\mathbf{y}$ and $\bar{\mathbf{J}}$ remain the same as the case of a linear system. The nonlinear vector is given by

$$\mathbf{F}(\mathbf{y}, t) = \left\{\begin{array}{c} \bar{Q}_{12}^{-1}(\bar{Q}_{11}y + \bar{Q}_{12}\dot{y})^3 \\ \bar{Q}_{22}^{-1}(\bar{Q}_{11}y + \bar{Q}_{12}\dot{y})^3 \\ 0 \\ 0 \end{array}\right\} \tag{4.26}$$

As mentioned earlier, the reduced system in equation (4.21) follows the convolution integral to obtain the convolution integral approach solution for the time evolution of system states in $\mathbf{y}$ domain and back transformed to obtain the same in the original system coordinates in $\mathbf{x}$ domain. The resulting temporal variations are compared with those from the numerically integrated solution, and analytical solution using TINF, in the system states temporal variations and phase plots shown in Figures 4.8 and 4.9.

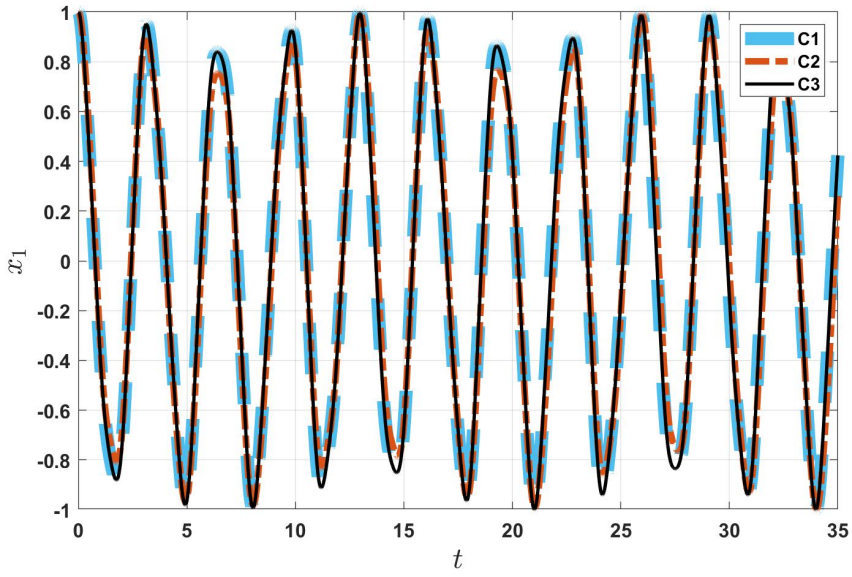

(**a**)

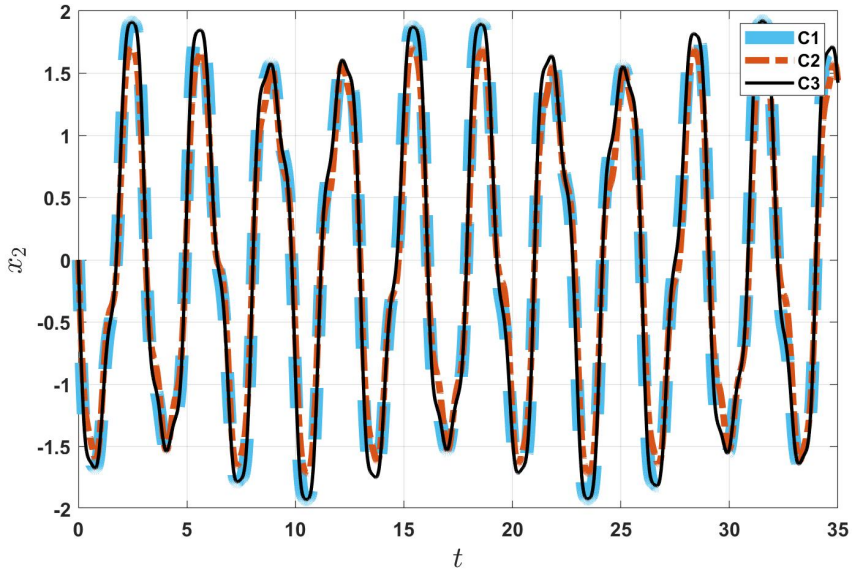

(**b**)

Figure 4.8: Comparison of the Temporal Variations of the System States of Time Periodic System with Nonlinear Terms (Example-3), Where the Thick Dashed Blue Line (C1) Represents the Numerically Integrated Solution, the Dashed Orange Line (C2) Corresponds to the Analytical Solution Using TINF and the Black Solid Line (C3) Represents the Solution from Convolution Integral Approach Using L-F For (**a**) x_1 State Variation, (**b**) x_2 State Variation.

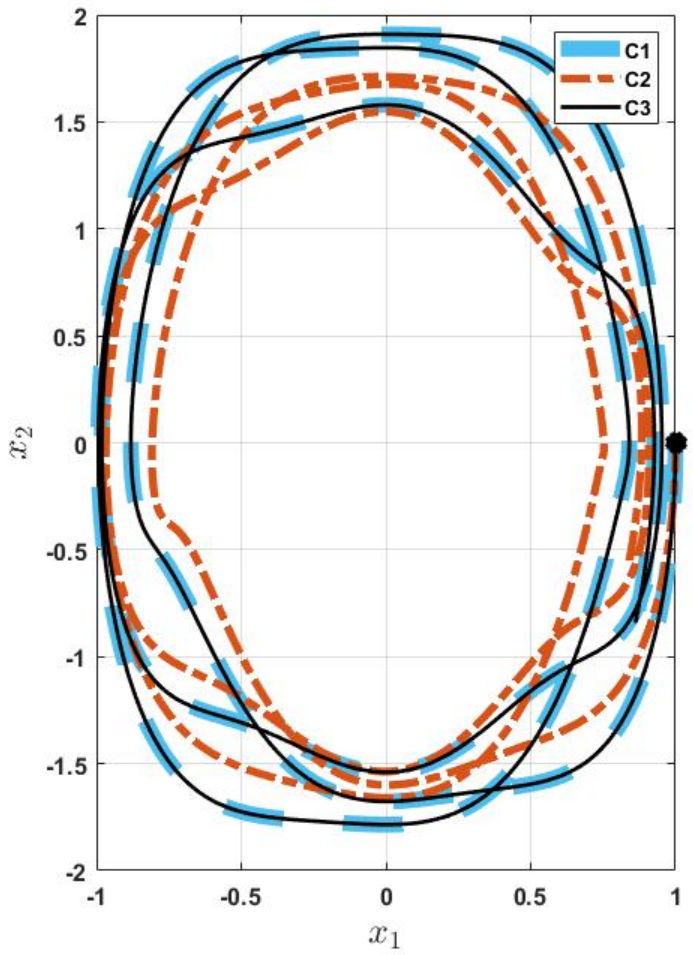

Figure 4.9: Comparison of the Phase Plot Variations of the System States of Time Periodic System with Nonlinear Terms (Example-3), Where the Thick Dashed Blue Line (C1) Represents the Numerically Integrated Solution, the Dashed Orange Line (C2) Corresponds to the Analytical Solution Using TINF and the Black Solid Line (C3) Represents the Solution from Convolution Integral Approach Using L-F.

In Figure 4.9, for example-3, the phase plot from the system states obtained by numerical integration is indicated by the thick blue line (C1), that by the analytical solution using TINF is indicated by the dashed orange line (C2) and that by the convolution integral approach using L-F transformation is represented by the solid black line (C3). The simulations are run for 35 seconds again. It is observed that the system states, for example-3 start-off at the same initial condition (indicated by a black dot) in all three approaches. However, the analytical approach using TINF is observed to drift away at the peaks of temporal variation of system states. At the same time, the convolution integral approach using the L-F transformation follows the numerical integration results closely.

4.5 Application: Stability of Stochastically Excited System

The stability analysis of an uncertain parametrically excited system is enabled using Lyapunov's direct method. The construction of an appropriate Lyapunov function enables this approach and is briefly explained in the following subsection

4.5.1 Construction of Lyapunov Functions

The Lyapunov techniques' basic idea is to utilize the time rate of energy change function $V(x,t)$ to understand system stability. As detailed by Brogan (1985), the general theorem can be stated as.

Theorem-1: *Consider a general time-varying system of the form*

$$\dot{x} = f(x,t) \tag{4.27}$$

If a sing-valued scalar function $V(x,t)$ exists, which is continuous and has continuous first partial derivatives and for which

1. $V(0,t) = 0$ *for all t;*

2. $V(x,t) \geq \gamma(||x||) > 0$ *for all* $x \neq 0$ *and for all* t*, where* $\gamma(.)$ *is a continuous, non-decreasing scalar function with* $\gamma(0) = 0$*;*

3. $\dot{V}(x,t) \geq -\alpha(||x||) < 0$ *for all* $x \neq 0$ *and for all* t*, where* $\alpha(.)$ *is a continuous, non-decreasing scalar function with* $\alpha(0) = 0$*;*

4. $V(x,t) \geq -\nu(||x||)$ *for all* x *and* t*, where* $\nu(.)$ *is a continuous, non-decreasing scalar function with* $\nu(0) = 0$*;*

5. $\gamma(||x||) \to \infty$ *as* $||x|| \to \infty$*; then* $x = 0$ *is uniformly globally asymptotically stable.*

The function γ, α, and ν are all positive constants for all t. $V(x,t)$ is said to be positive definite if $V(0,t) = 0$ and if $V(x,t)$ is always greater than or equal to a time-invariant positive function γ. Condition (1) and (2) require $V(x,t)$ to be positive definite. Similarly, condition (3) requires $\dot{V}(x,t)$ to be negative definite. Condition (5) requires $V(x,t)$ to be infinite as $||x|| \to \infty$, and condition (4) prevents $V(x,t)$ to become infinite when $||x||$ is finite.

Unfortunately, the Lyapunov theorems do not indicate how a Lyapunov function might be found. There is no unique Lyapunov function for a given system. Some are better than others. A $V_1(x)$ might be found, which indicates stability, $V_2(x)$ might predict asymptotic stability for initial states quite close to the origin, and $V_3(x)$ might show asymptotic stability for a broader region or even global asymptotic stability. If a system is stable in one of the senses mentioned, it is ensured that an appropriate Lyapunov function does exist. Consider a periodic system with stochastic perturbation given by

$$\dot{\mathbf{x}} = [\mathbf{A}(t) + \mathbf{F}(t)]\mathbf{x} \tag{4.28}$$

where $\mathbf{x}$ and periodic $\mathbf{A}(t)$ are as defined before. $\mathbf{F}(t)$ is $n \times n$ matrix whose non-zero elements $f_{ij}(t)$ are stochastic process, measurable, strictly stationary, and that they satisfy an ergodic property, as per Kushner (1967).

The linear periodic part of the equation (4.28) is assumed to be asymptotically stable, and the stability bounds on $\mathbf{F}(t)$ need to be determined. Using the L-F transformation $\mathbf{x}(t) = \bar{\mathbf{Q}}(t)\mathbf{z}(t)$, the equation (4.28) can be reduced as

$$\dot{\mathbf{z}} = [\bar{\mathbf{J}} + \mathbf{G}(t)]\mathbf{z} \tag{4.29}$$

where $\mathbf{G}(t) = \bar{\mathbf{Q}}^{-1}(t)\mathbf{F}(t)\bar{\mathbf{Q}}(t)$ and the properties of $\mathbf{G}(t)$ is the same as that of $\mathbf{F}(t)$. It is noted that the $\bar{\mathbf{J}}$ matrix is a diagonal matrix with semi-simple eigenvalues having negative real parts. The stability bounds on $\mathbf{F}(t)$ are identified using the approach presented in Infante (1968).

Theorem-2: *If, for some positive definite matrix ($\bar{\mathbf{B}}$) and some $\varepsilon > 0$*

$$E\{\lambda_{max}\left[\bar{\mathbf{J}}^T + \mathbf{G}(t)^T + \bar{\mathbf{B}}\left[\bar{\mathbf{J}} + \mathbf{G}(t)\right]\bar{\mathbf{B}}^{-1}\right]\} \leq \varepsilon \tag{4.30}$$

then equation (4.30) *is almost surely asymptotically stable in the large.*

Proof: Consider a Lyapunov function $V(\mathbf{z}) = \mathbf{z}^T\bar{\mathbf{B}}\mathbf{z}$, that is quadratic in nature. Along the trajectories of equation (4.29), define

$$\lambda(t) = \frac{\dot{V}(\mathbf{z})}{V(\mathbf{z})} = \frac{\mathbf{z}^T\left[(\bar{\mathbf{J}} + \mathbf{G}(t))^T\bar{\mathbf{B}} + \bar{\mathbf{B}}(\bar{\mathbf{J}} + \mathbf{G}(t))\right]\mathbf{z}}{\mathbf{z}^T\bar{\mathbf{B}}\mathbf{z}} \tag{4.31}$$

Using the properties of pencils of quadratic forms detailed by Gantmakher (1990), the following inequality can be obtained

$$\lambda_{min}\left[(\bar{\mathbf{J}} + \mathbf{G}(t))^T + \bar{\mathbf{B}}(\bar{\mathbf{J}} + \mathbf{G}(t))\bar{\mathbf{B}}^{-1}\right] \leq \lambda(t) \leq \lambda_{max}\left[(\bar{\mathbf{J}} + \mathbf{G}(t))^T + \bar{\mathbf{B}}(\bar{\mathbf{J}} + \mathbf{G}(t))\bar{\mathbf{B}}^{-1}\right] \tag{4.32}$$

where λ_{max} and λ_{min}, are the maximum and minimum real eigenvalues of a pencil. It follows from equation (4.31) and equation (4.32) that

$$V[\mathbf{z}(t)] = V[\mathbf{z}(t_0)]e^{(t-t_0)\left[\frac{1}{t-t_0}\int_{t_0}^{t}\lambda(\tau)\,d\tau\right]} \tag{4.33}$$

For some $\varepsilon > 0$, if $E\{\lambda(t)\} \leq -\varepsilon$, $V[\mathbf{z}(t)]$ is observed to be bounded and $V[\mathbf{z}(t)] \to 0$ as $t \to \infty$. This condition resembles the inequality in equation (4.30), which proves the results. The stability of equation (4.29) implies the stability of equation (4.28) due to the transformation $\mathbf{x} = \tilde{\mathbf{Q}}(t)\mathbf{z}$. It is noted that the eigenvalues of matrix $\bar{\mathbf{J}}$ are required to have negative real parts in order to use to inequality condition, given by equation (4.30).

Corollary-2: *If, for some positive definite matrix ($\bar{\mathbf{B}}$) and some $\varepsilon > 0$*

$$E\{\lambda_{max}\left[\mathbf{G}(t)^T + \bar{\mathbf{B}}\mathbf{G}(t)\bar{\mathbf{B}}^{-1}\right]\} \leq -\lambda_{max}\left[\bar{\mathbf{J}}^T + \bar{\mathbf{B}}\bar{\mathbf{J}}\bar{\mathbf{B}}^{-1}\right] - \varepsilon \tag{4.34}$$

then equation (4.29) *is almost surely asymptotically stable in the large.*

Proof: Following the theorem, it is noted that

$$\begin{aligned}\lambda(t) \leq \lambda_{max}\left[(\bar{\mathbf{J}} + \mathbf{G}(t))^T + \bar{\mathbf{B}}(\bar{\mathbf{J}} + \mathbf{G}(t))\bar{\mathbf{B}}^{-1}\right] \leq & \lambda_{max}\left[\bar{\mathbf{J}}^T + \bar{\mathbf{B}}\bar{\mathbf{J}}\bar{\mathbf{B}}^{-1}\right] \\ & + \lambda_{max}\left[\mathbf{G}(t)^T + \bar{\mathbf{B}}\mathbf{G}(t)\bar{\mathbf{B}}^{-1}\right]\end{aligned} \tag{4.35}$$

By splitting the term on the right hand side as a sum of two separate maximization and using the $E\{.\}$ operator

$$E\{\lambda(t)\} = \lambda_{max}\left[\bar{\mathbf{J}}^T + \bar{\mathbf{B}}\bar{\mathbf{J}}\bar{\mathbf{B}}^{-1}\right] + E\{\lambda_{max}\left[\mathbf{G}(t)^T + \bar{\mathbf{B}}\mathbf{G}(t)\bar{\mathbf{B}}^{-1}\right]\} \leq \varepsilon \tag{4.36}$$

generates the desired output. It is noted that when the second inequality in equation (4.35) becomes equality, the stability results become comparable to that provided by

the theorem. In the following subsection, the stability theorem is demonstrated on a damped periodic Mathieu system with stochastic parametric excitation.

4.5.2 Example-4: Time Periodic System with Uncertain Parametric Excitations

Consider a damped Mathieu equation of the form

$$\ddot{x} + 2\zeta\dot{x} + [a + b\cos(\omega t) + f(t)]\, x = 0 \tag{4.37}$$

where $f(t)$ represents the uncertain parametric excitation term. The same equation can be expressed in the state space form as

$$\frac{d}{dt}\begin{Bmatrix} x \\ \dot{x} \end{Bmatrix} = \begin{bmatrix} 0 & 1 \\ -(a + b\cos(\omega t)) & -2\zeta \end{bmatrix}\begin{Bmatrix} x \\ \dot{x} \end{Bmatrix} + \begin{bmatrix} 0 & 0 \\ -f(t) & 0 \end{bmatrix}\begin{Bmatrix} x \\ \dot{x} \end{Bmatrix} \tag{4.38}$$

The second part of right hand side of equation (4.38) consists of the stochastic parametric excitation ($\mathbf{F}(t)$). Considering just the linear time periodic system with damping, the L-F transformation ($\bar{\mathbf{Q}}(t)$) is computed using the state augmentation and Normal Forms approach along with the Jordan matrix, $\bar{\mathbf{J}}$.

The system parameters for this example are considered to be the same as $a = 3, b = 2.5, \omega = 2\pi$, along with the damping coefficient, $\zeta = 0.15$. Considering the positive definite matrix ($\bar{\mathbf{B}}$) to be identity matrix ($\mathbf{I}_{2\times 2}$), the expression for the theorem $\left[\bar{\mathbf{J}}^T + \mathbf{G}(t)^T + \bar{\mathbf{B}}\left[\bar{\mathbf{J}} + \mathbf{G}(t)\right]\bar{\mathbf{B}}^{-1}\right]$ can be computed. Using Schwarz's inequality and considering $E\{\sin(nt)\} = 0, E\{\cos(nt)\} = 0$, the stability condition for the given system is derived from the Infante's theorem as

$$-102.0145 + 139.33E\{f(t)^2\} - 0.783E\{f(t)\} \leq 12.4813 \tag{4.39}$$

Assuming $E\{f(t)\} = 0$, the stability condition is computed to be

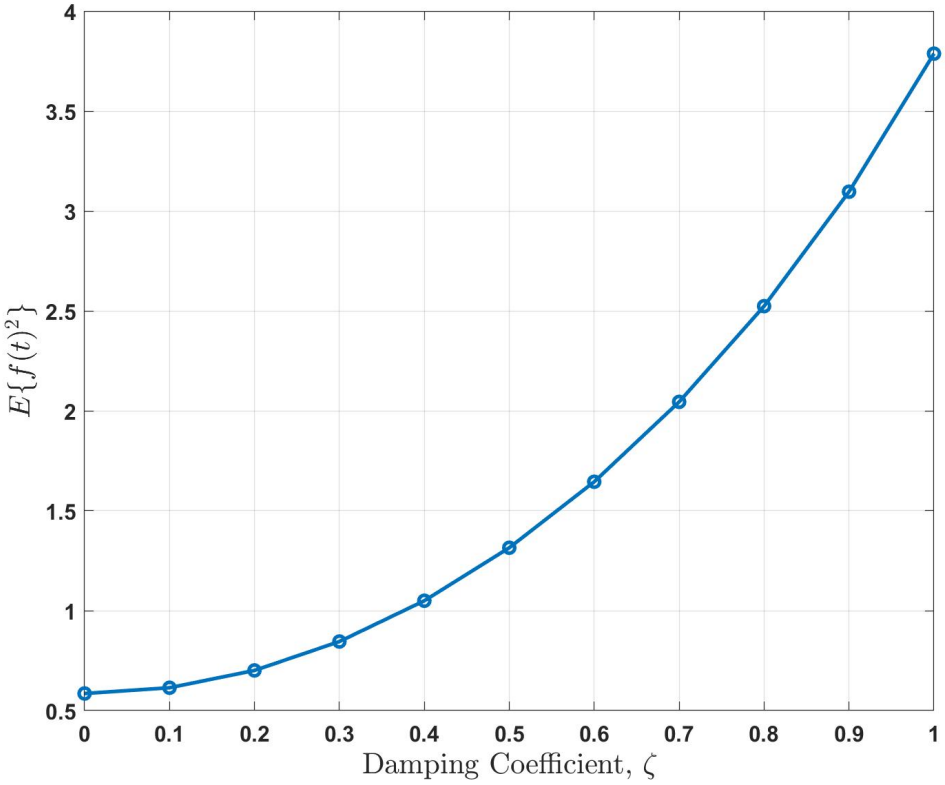

Figure 4.10: Variation of $E\{f(t)^2\}$ with Respect to Change in Damping Coefficient (ζ) .

$$E\{f(t)^2\} \leq 0.6503 \tag{4.40}$$

The variation of the threshold of the uncertainty the system can withstand with the increase in damping ζ, is depicted in Figure 4.10.

From Figure 4.10, it is observed that as the damping coefficient of the system is increased, it can keep the system stable with higher amplitudes of stochastic parametric excitations.

4.6 Conclusion

In this chapter, the application of the unified approach towards the computation of the closed form expression of the L-F transformation for a linear time periodic system

is briefly explained. Multiple techniques to invert the time varying L-F transformation matrix are also included, along with comparisons. Furthermore, the Mathieu equation with time periodic coefficients is considered with multiple perturbations for illustrative examples.

The utilization of the computed L-F transformation and its inverse towards the analysis of a time-periodic system with deterministic external and stochastic parametric excitation is demonstrated in this chapter. Both the approaches utilized the computed L-F transformation and are observed to generate results very close to the numerical integrated solution for both examples of deterministic external excitation. In the case of a system with stochastic parametric excitation, the use of computed L-F transformation, and Infante's approach to analyzing the condition of robust stability is demonstrated. In this chapter, the authors also analyzed the time periodic system with nonlinear perturbations using the computed L-F transformation and its results are observed to be better than the traditional Normal Forms approach. This provides confidence in extending the unified theory towards the analysis of quasi-periodic systems and is discussed comprehensively in the following chapters.

Chapter 5

ANALYSIS OF QUASI-PERIODIC SYSTEM

The dynamical system with periodic coefficients comprising of multiples of the same frequency represents a time periodic system. However, in some real-world applications such as sea waves and heart rhythms, the frequencies of the periodic coefficients could be incommensurate, resulting in quasi-periodic or chaotic systems, as explained by Sharma and Sinha (2018). The presence of quasi-periodic behaviors in various dynamical systems and bifurcation theory is detailed by Broer *et al.* (2009).

Davis and Rosenblat (1980) used the technique of multiple scales to determine the stability boundaries of a quasi-periodic system. Belhaq *et al.* (2002); Guennoun *et al.* (2002) applied twice to reduce a weakly damped nonlinear quasi-periodic oscillator to an autonomous system. A nonlinear quasi-periodic Mathieu equation was transformed to an approximate time-invariant form by Belhaq and Houssni (1999). The application of rotation number towards the identification of stability bounds, for the spectral theory of an almost periodic Schrödinger operator, was introduced by Johnson and Moser (1982). Zounes and Rand (1998) further analyzed the results based on rotation number for a Hills quasi-periodic systems numerically and analytically using Lyapunov exponents. Though the application of rotation number and Lyapunov exponents successfully generated the stability plots, they were observed to be computationally expensive. Furthermore, the stability plots were generated using Hill's method of infinite determinants and perturbation techniques by Zounes and Rand (1998) and Kovacic *et al.* (2018). However, Hill's method of infinite determinants was observed to fail to converge in all cases (Waters (2010)). A survey of multiple reducibility techniques for linear quasi-periodic systems was detailed by Puig (2002);

Puig and Simó (2006). These works also included a mathematical framework for the extension of Floquet theory towards quasi-periodic systems based on the L-P transformation. Redkar (2012) explained the feasibility of a Lyapunov based approach for stability analysis of a linear quasi-periodic system, in the case of a bounded nonlinearity. Wooden and Sinha (2007) used the Normal Forms technique to analyze periodic quasi-periodic systems, with the aid of a detuning parameter or book-keeping parameter and local near-identity transformations near the stable points. The method of Chebyshev polynomials and Picard iteration derived by Sinha *et al.* (1993); Sinha and Juneja (1991) was extended to quasi-periodic systems too, where the system was approximated as a periodic system. Sharma and Sinha (2020) demonstrated the control of a chaotic behavior to a periodic orbit using the same approach. Though the researchers successfully analyzed and built controllers for multiple time varying systems using these techniques, their application was limited by the requirement of higher order polynomials for better accuracy.

A dynamical equation of a linear quasi-periodic system can also be expressed as equation (2.1). However, $\mathbf{A}(t)$ will be a $n \times n$ matrix containing finite number (k) of incommensurable frequencies ($k \geq 2$). The same could be expressed as

$$\mathbf{A}(t) = (\omega_1 t, ...\omega_k t) \qquad \forall k \geq 2 \tag{5.1}$$

where $(\omega_1 t, ...\omega_k t)$ is continuous and 2π periodic in each argument, and the ratio of any two frequencies is irrational.

As per Floquet type theory, stated in Murdock (1978), the quasiperiodic system following the linear differential equation (2.1) is reducible, if there is a differentiable quasi-periodic matrix, $\mathbf{P}(t)$ (with the same frequencies), such that a linear transfor-

mation, $\mathbf{x} = \mathbf{P}(t)\mathbf{y}$ would result in

$$\dot{\mathbf{y}} = \mathbf{C}\mathbf{y} \tag{5.2}$$

where $\mathbf{C}$ is a constant complex matrix. The matrix, $\mathbf{P}(t)$, facilitates such a transformation called a Lyapunov-Perron (L-P) transformation matrix. Similar expressions are utilized by Puig (2002); Puig and Simó (2006). Since the unified theory for time-periodic system was capable of transforming it to a time-invariant form. The prospects of the extension of this theory towards a quasi-periodic system is investigated similarly in this chapter. Before applying the unified theory, a class of quasi-periodic systems known as the '*Commutative Quasi-Periodic*' system is introduced in the following section.

5.1 Commutative Quasi-Periodic System

As explained by Lukes (1982), for a general time varying system, expressed in equation (2.1), the system matrix $\mathbf{A}(t)$ is called commutative, if there exists a matrix $\mathbf{D}(t)$ such that

$$\frac{d\mathbf{D}(t)}{dt} = \mathbf{A}(t) \tag{5.3}$$

satisfying the relation $\mathbf{A}(t)\mathbf{D}(t) - \mathbf{D}(t)\mathbf{A}(t) = 0$. The $\mathbf{D}(t)$ matrix satisfying this condition is called the antiderivative of $\mathbf{A}(t)$. The analytical expression for the $\mathbf{D}(t)$ matrix can be computed using the following expression

$$\mathbf{D}(t) = \mathbf{D}(0) + \int_0^t \mathbf{A}(\zeta)d\zeta \tag{5.4}$$

The equation (2.1) is called a commutative system if the $\mathbf{A}(t)$ matrix is commutative. This condition was slightly modified for deriving the closed form expression for STM and is detailed in Wu and Sherif (1976) and Rao and Ganapathy (1979). They claim that for a time varying system, expressed in equation (2.1) if the $\mathbf{A}(t)$ matrix

can be decomposed as the following sum:

$$\mathbf{A}(t) = \sum_{i=1}^{k} C_i f_i(t) \tag{5.5}$$

where C_i is a commutative constant matrix, such that $C_i C_j = C_j C_i$ and f_i is a scalar valued function, then the STM could be expressed as:

$$\Phi(t,\tau) = \prod_{i=1}^{k} e^{C_i \int_\tau^t f_i(\theta)d\theta} \tag{5.6}$$

However, in this section, a quasi-periodic system is considered, which is initially verified for its commutative property, and L-P transformation is computed analytically. The decomposition rule, as per equation (5.5), is verified. Consider a quasi-periodic system of the form shown below

$$\begin{aligned} &\ddot{x} - 2(b_1 \sin(\omega_1 t) + b_2 \sin(\omega_2 t))\dot{x} + (a + (b_1\omega_1 \cos(\omega_1 t) + b_2\omega_2 \cos(\omega_2 t)) \\ &+ (b_1 \sin(\omega_1 t) + b_2 \sin(\omega_2 t))^2)x = 0 \end{aligned} \tag{5.7}$$

where ω_1 and ω_2 are incommensurate frequencies. The constants a, b_1, b_2 are real positive integers considered as the system parameters. Let us consider the system states as $x_1 = x$ and $x_2 = \dot{x}_1 - (b_1 \sin(\omega_1 t) + b_2 \sin(\omega_2 t))x_1$. After converting equation (5.7) in the state space form, as per the mentioned system states, and comparing it to equation (2.1), the expression for $\mathbf{A}(t)$ is given as

$$\mathbf{A}(t) = \begin{bmatrix} b_1 \sin(\omega_1 t) + b_2 \sin(\omega_2 t) & 1 \\ -a & b_1 \sin(\omega_1 t) + b_2 \sin(\omega_2 t) \end{bmatrix} \tag{5.8}$$

Initially, the antiderivative matrix, $\mathbf{D}(t)$, is computed using equation (5.4) for the system matrix expressed in equation (5.8). For the given system, the antiderivative matrix is computed as

$$\mathbf{D}(t) = \int_0^t \mathbf{A}(\tau)d\tau = \begin{bmatrix} \frac{b_1(1-\cos(\omega_1 t))}{\omega_1} + \frac{b_2(1-\cos(\omega_2 t))}{\omega_2} & t \\ -at & \frac{b_1(1-\cos(\omega_1 t))}{\omega_1} + \frac{b_2(1-\cos(\omega_2 t))}{\omega_2} \end{bmatrix} \tag{5.9}$$

The computed $\mathbf{D}(t)$ matrix is verified to satisfy the relation $\mathbf{A}(t)\mathbf{D}(t)-\mathbf{D}(t)\mathbf{A}(t) = 0$. It was found that the computed $\mathbf{D}(t)$ matrix is indeed the antiderivative matrix of the given system matrix $\mathbf{A}(t)$. Hence the system expressed in equation (5.7) is proved to be commutative. Now verification of decomposition of the given $\mathbf{A}(t)$ matrix as per equation (5.5) is initiated. The given $\mathbf{A}(t)$ matrix can be rewritten as

$$\mathbf{A}(t) = b_1 sin(\omega_1 t) + b_2 sin(\omega_2 t) \times \begin{bmatrix} 1 & 0 \\ 0 & 1 \end{bmatrix} + 1 \times \begin{bmatrix} 0 & 1 \\ -a & 0 \end{bmatrix} \tag{5.10}$$

where the constant matrices and time varying functions could be expressed as

$$C_1 = \begin{bmatrix} 1 & 0 \\ 0 & 1 \end{bmatrix} = \mathbf{I}, \quad C_2 = \begin{bmatrix} 0 & 1 \\ -a & 0 \end{bmatrix}, \tag{5.11}$$

$$f_1(t) = b_1 sin(\omega_1 t) + b_2 sin(\omega_2 t), \quad f_2(t) = 1$$

The constant matrices in equation (5.11) follow the commutative rule ($C_1C_2 = C_2C_1$). By considering τ=0, substituting equation (5.11) into equation (5.6), and after solving the integrals the following is obtained

$$\begin{aligned} \Phi(t,0) &= e^{C_1 \times (\frac{b_1(1-\cos(\omega_1 t))}{\omega_1} + \frac{b_2(1-\cos(\omega_2 t))}{\omega_2})} . e^{C_2 \times t} \\ &= \begin{bmatrix} e^{(\frac{b_1(1-\cos(\omega_1 t))}{\omega_1} + \frac{b_2(1-\cos(\omega_2 t))}{\omega_2})} & 0 \\ 0 & e^{(\frac{b_1(1-\cos(\omega_1 t))}{\omega_1} + \frac{b_2(1-\cos(\omega_2 t))}{\omega_2})} \end{bmatrix} . e^{C_2 t} \end{aligned} \tag{5.12}$$

It is noted that the expression indicated in equation (5.12) is similar to that of the Floquet decomposition for a periodic system, as expressed in equation (2.4). Since this is the case of a quasi-periodic system, the resulting expression represents the L-P transformation matrix, $\mathbf{P}(t)$. It is shown that this L-P transformation converts the linear quasi-periodic system into a time invariant system. Hence the STM of the given commutative quasi-periodic system could be expressed as

$$\Phi(t) = \mathbf{P}(t) e^{\mathbf{C}t} \tag{5.13}$$

where

$$\mathbf{P}(t) = \begin{bmatrix} e^{(\frac{b_1(1-\cos(\omega_1 t))}{\omega_1} + \frac{b_2(1-\cos(\omega_2 t))}{\omega_2})} & 0 \\ 0 & e^{(\frac{b_1(1-\cos(\omega_1 t))}{\omega_1} + \frac{b_2(1-\cos(\omega_2 t))}{\omega_2})} \end{bmatrix}, \quad \mathbf{C} = C_2 = \begin{bmatrix} 0 & 1 \\ -a & 0 \end{bmatrix} \tag{5.14}$$

The decomposition is in agreement with the properties of the L-P transformation mentioned by Murdock (1978). The equation (5.14) observed that the $\mathbf{P}(t)$ matrix is quasi-periodic and $\mathbf{C}$ matrix is time-invariant. Similar properties were discussed by Puig (2002) and Puig and Simó (2006).

From equations (5.13)) and (2.2), the closed form expression for the L-P transformation can also be computed from the temporal variations of the system states, as shown below

$$\mathbf{P}(t) = \mathbf{x}(t)\mathbf{x}^{-1}(0)e^{-\mathbf{C}t} \tag{5.15}$$

One could numerically integrate the system equations and compute the L-P transformation matrix using equation (5.15). However, the knowledge of the $\mathbf{C}$ matrix is essential to employ this equation. To verify the L-P transformation matrix, the following condition is evaluated

$$\mathbf{P}^{-1}(t)[\mathbf{A}(t).\mathbf{P}(t) - \dot{\mathbf{P}}(t)] = \mathbf{C} \tag{5.16}$$

The missing terms in the above expression are computed, as indicated below.

$$\mathbf{P}^{-1}(t) = \begin{bmatrix} e^{-(\frac{b_1(1-\cos(\omega_1 t))}{\omega_1} + \frac{b_2(1-\cos(\omega_2 t))}{\omega_2})} & 0 \\ 0 & e^{-(\frac{b_1(1-\cos(\omega_1 t))}{\omega_1} + \frac{b_2(1-\cos(\omega_2 t))}{\omega_2})} \end{bmatrix}$$

$$\dot{\mathbf{P}}(t) = (b_1 \sin(\omega_1 t) + b_2 \sin(\omega_2 t)) \begin{bmatrix} e^{(\frac{b_1(1-\cos(\omega_1 t))}{\omega_1} + \frac{b_2(1-\cos(\omega_2 t))}{\omega_2})} & 0 \\ 0 & e^{(\frac{b_1(1-\cos(\omega_1 t))}{\omega_1} + \frac{b_2(1-\cos(\omega_2 t))}{\omega_2})} \end{bmatrix} \tag{5.17}$$

The expression in equation (5.16) indeed results in the time invariant matrix **C**, and hence the theory is valid for the commutative quasi-periodic system. Similar to the L-F transformation matrix, it is verified that the L-P transformation indeed converts the quasi- periodic system to a constant coefficient system. Hence the closed form analytical solution for L-P transformation is derived for a linear parametrically excited commutative quasi-periodic system. This in agreement with the approach discussed by Puig and Simó (2006). However, quasi-periodic systems that do not comply with the non-commutative property need an alternate approach for analysis. In the following sections, multiple approaches are discussed for the same.

5.2 Indirect Approach to Compute L-P Transformation

The application of the method of Normal Forms, in conjunction with the Floquet theory was introduced by Waswa and Redkar (2020b). With the aid of an intuitive state augmentation technique, the direct application of the Normal Forms technique was feasible and capable of providing comparable results. The linear quasi-periodic system was split such that the periodic term with a higher coefficient value was considered under the linear periodic system, and the corresponding L-F transformation was applied to the system equation. The remaining quasi-periodic term was augmented after the L-F transformation, and the subsequent TDNF technique was applied to the system to eliminate the nonlinear terms.

In this section, a linear quasi-periodic system is analyzed using a similar approach but with a change in the sequence of operations. The quasi-periodic system is split such that one of the periodic coefficients is considered a part of a linear periodic system and the other coefficient as the quasi-periodic term. The split system is subjected to state augmentation and further L-F transformation to convert the linear periodic part to a time-invariant form. Subsequently, the TDNF technique is applied to reduce

the system further and complete the analysis. A detailed explanation of the modified approach is provided in the subsequent subsection.

5.2.1 Intuitive State Augmentation

With the aid of an intuitive state augmentation, the periodic terms are transformed into a state variable. This approach applies to both parametrically excited periodic terms and externally excited periodic forcing terms. In this section, let us consider a linear quasi-periodic system with only two incommensurate frequencies. The quasi-periodic system is split such that one of the periodic terms is considered in the linear periodic system and the periodic term of incommensurate frequency is considered a separate term. Hence the equation (2.1) is modified as

$$\dot{\mathbf{x}} = \hat{\mathbf{A}}_1(t)\mathbf{x} + \hat{\mathbf{A}}_2(t)\mathbf{x} \tag{5.18}$$

where $\hat{\mathbf{A}}_1(t)$ is an $n \times n$ periodic matrix with frequency ω_1 and T-periodicity. The $\hat{\mathbf{A}}_2(t)$ is an $n \times n$ periodic matrix with frequency ω_2. The quasi-periodic term with just a sine or cosine trigonometric function in $\hat{\mathbf{A}}_2(t)$, is considered as a separate state, as indicated below

$$\left.\begin{aligned} p &= \cos(\omega_2 t) \\ \dot{p} &= -\omega_2 \sin(\omega_2 t) = -q \\ \dot{q} &= {\omega_2}^2 \cos(\omega_2 t) = {\omega_2}^2 p = -\ddot{p} \end{aligned}\right\} \tag{5.19}$$

The updated system states vector with the augmented states is indicated using the following vector

$$\tilde{\mathbf{x}} = [\mathbf{x}, p, q]^T \tag{5.20}$$

This converts the $\hat{\mathbf{A}}_2(t)\mathbf{x}$ term to a $l \times 1$ nonlinear vector with both the original and augmented states. Similarly, the matrix $\hat{\mathbf{A}}_1(t)$ is appended with the coefficients of the augmented states. With the updated system states, the system equation (5.18)

is updated as follows

$$\dot{\tilde{\mathbf{x}}} = \tilde{\mathbf{A}}_1(t)\tilde{\mathbf{x}} + \mathbf{f}(\tilde{\mathbf{x}}) \tag{5.21}$$

where $\mathbf{f}(\tilde{\mathbf{x}})$ is the $l \times 1$ vector containing all the nonlinear monomial terms in $\tilde{\mathbf{x}}$. The term $\tilde{\mathbf{A}}_1(t)$ is now a $l \times l$ square matrix and is still T- periodic. Since the system is now updated as a linear periodic system, an L-F transformation, $\tilde{\mathbf{x}} = \mathbf{Q}(t)\tilde{\mathbf{y}}$, is viable. The updated system after undergoing a L-F transformation is expressed as

$$\dot{\tilde{\mathbf{y}}} = \tilde{\mathbf{R}}\tilde{\mathbf{y}} + \mathbf{Q}^{-1}(t)\mathbf{f}(\mathbf{Q}(t)\tilde{\mathbf{y}}) \tag{5.22}$$

where $\tilde{\mathbf{R}}$ is the $l \times l$ linear time invariant matrix. It is observed that the linear time periodic matrix ($\tilde{\mathbf{A}}_1(t)$) of equation (5.21) is transformed as the time-invariant matrix ($\tilde{\mathbf{R}}$) in equation (5.22). In addition to the linear matrix, the nonlinear vector is appended with augmented states and time varying coefficients. This updated system equation (5.22) is comparable to equation (2.21) and is amenable to the TDNF technique, as discussed in section 2.3.2. This would aid in eliminating the non-prominent nonlinear terms and further reducing the system to a form similar to equation (2.28). The indirect approach discussed so far is applied on a non-commutative linear quasi-periodic system in the subsequent subsection.

5.2.2 Application of the Indirect Approach to a Non-commutative Linear Quasi-periodic System

Consider a linear quasi-periodic Hill equation as shown below

$$\ddot{x} + d\dot{x} + (a + b_1 \cos\omega_1 t + b_2 \cos\omega_2 t)x = 0 \tag{5.23}$$

where a, b_1, b_2, and d are the system parameters, ω_1 and ω_2 are the incommensurate frequencies. Since equation (5.23) is not commutative, proceed with the technique to split the system equation and express it in the state space form

$$\frac{d}{dt}\begin{bmatrix} x_1 \\ x_2 \end{bmatrix} = \begin{bmatrix} 0 & 1 \\ -(a + b_1 \cos\omega_1 t) & -d \end{bmatrix}\begin{bmatrix} x_1 \\ x_2 \end{bmatrix} - \begin{bmatrix} 0 \\ b_2 x_1 \cos\omega_2 t \end{bmatrix} \tag{5.24}$$

where $x = x_1$ and $\dot{x} = x_2$. The periodic term with the frequency ω_1 and principal period, T, is considered in the linear part, and the one with frequency ω_2, is considered as the quasi-periodic term. The periodic term, with frequency ω_2, is augmented as a state as per equation (5.19). the system equation gets updated as

$$\frac{d}{dt}\begin{bmatrix} x_1 \\ x_2 \\ p \\ q \end{bmatrix} = \begin{bmatrix} 0 & 1 & 0 & 0 \\ -(a + b_1 \cos\omega_1 t) & -d & 0 & 0 \\ 0 & 0 & 0 & -1 \\ 0 & 0 & \omega_2^2 & 0 \end{bmatrix}\begin{bmatrix} x_1 \\ x_2 \\ p \\ q \end{bmatrix} + \begin{bmatrix} 0 \\ -b_2 x_1 p \\ 0 \\ 0 \end{bmatrix} \tag{5.25}$$

Now an L-F transformation, $\tilde{\mathbf{x}} = \mathbf{Q}(t)\tilde{\mathbf{y}}$, is applied to equation (5.25), that results in time-invariant coefficients in the linear term as shown below

$$\begin{aligned} \frac{d}{dt}\begin{bmatrix} y_1 \\ y_2 \\ y_3 \\ y_4 \end{bmatrix} &= \begin{bmatrix} R_{11} & R_{12} & 0 & 0 \\ R_{21} & R_{22} & 0 & 0 \\ 0 & 0 & R_{33} & R_{34} \\ 0 & 0 & R_{43} & R_{44} \end{bmatrix}\begin{bmatrix} y_1 \\ y_2 \\ y_3 \\ y_4 \end{bmatrix} \\ &+ \begin{bmatrix} Q_{11}^{-1} & Q_{12}^{-1} & 0 & 0 \\ Q_{21}^{-1} & Q_{22}^{-1} & 0 & 0 \\ 0 & 0 & Q_{33}^{-1} & Q_{34}^{-1} \\ 0 & 0 & Q_{43}^{-1} & Q_{44}^{-1} \end{bmatrix}\begin{bmatrix} 0 \\ -b_2(Q_{11}y_1 + Q_{12}y_2)(Q_{33}y_3 + Q_{34}y_4) \\ 0 \\ 0 \end{bmatrix} \end{aligned} \tag{5.26}$$

After performing the matrix multiplication, the equation (5.26) gets updated as

$$\begin{aligned}\frac{d}{dt}\begin{bmatrix} y_1 \\ y_2 \\ y_3 \\ y_4 \end{bmatrix} &= \begin{bmatrix} R_{11} & R_{12} & 0 & 0 \\ R_{21} & R_{22} & 0 & 0 \\ 0 & 0 & R_{33} & R_{34} \\ 0 & 0 & R_{43} & R_{44} \end{bmatrix}\begin{bmatrix} y_1 \\ y_2 \\ y_3 \\ y_4 \end{bmatrix} \\ &+ \begin{bmatrix} -b_2 Q_{12}^{-1}(Q_{11}y_1 + Q_{12}y_2)(Q_{33}y_3 + Q_{34}y_4) \\ -b_2 Q_{22}^{-1}(Q_{11}y_1 + Q_{12}y_2)(Q_{33}y_3 + Q_{34}y_4) \\ 0 \\ 0 \end{bmatrix}\end{aligned} \tag{5.27}$$

The equation (5.27) now has a time invariant linear part and a modal transformation of the form $\tilde{\mathbf{y}} = \mathbf{M}\mathbf{z}$ applied to it would update the equation as follows

$$\dot{\mathbf{z}} = \mathbf{J}\mathbf{z} - \mathbf{M}^{-1}\begin{bmatrix} -b_2 Q_{12}^{-1}(Q_{11}y_1 + Q_{12}y_2)(Q_{33}y_3 + Q_{34}y_4) \\ -b_2 Q_{22}^{-1}(Q_{11}y_1 + Q_{12}y_2)(Q_{33}y_3 + Q_{34}y_4) \\ 0 \\ 0 \end{bmatrix} \tag{5.28}$$

where $\mathbf{J}$ is the Jordan canonical form of $\tilde{\mathbf{R}}$. The equation (5.28) is analogous to equation (2.22) and is susceptible to the application of the TDNF technique to eliminate the non-prominent nonlinear terms. The back-substitution of the solutions for the augmented/fictitious states in the near-identity transformation results in closed form expression for the Lyapunov Perron Transformation. It is observed that the near identity transformation needs to be expanded to an order higher than the order of nonlinearity of the original system, which in this case is two.

The successive transformations of the original system states, using various techniques, resulted in a time invariant form. This resonates with the theory of L-P transformation, as mentioned in the subsection of '*Commutative linear quasiperiodic*

system'. The initial L-F transformation, subsequent modal transformation and later near-identity transformation for TDNF collectively contribute to reducing the system into a time-invariant form. Hence, all these transformations jointly are considered to contribute to an equivalent L-P transformation of the original linear quasi-periodic system. After substituting the augmented states with their periodic equivalent, the near-identity transformation contains both the frequency terms, the system characteristics and also transforms the system coefficient to its time invariant form, it can be considered as the closest form of the L-P transformation matrix. This approach is also applicable towards the commutative linear qausi-periodic system, and the results of such application are detailed in the subsequent section.

5.2.3 Results and Discussion

In this section, the theory of L-P transformation for a linear quasi-periodic system is validated using numerical simulation results. Initially, a linear quasi-periodic Hill equation is considered to demonstrate the application of the indirect approach. The reduced system from the indirect approach is back transformed to the original coordinates for comparisons of temporal variations. The temporal comparisons and other results are indicated for the case of a system without damping and that with damping.

Even though a mathematical expression was derived for the case of commutative linear quasi-periodic system the indirect approach using the TDNF technique was also applied on this system. The results from the TDNF technique are verified with both numerical integration and analytical techniques.

Linear Quasi-Periodic System Without Damping

The linear quasi-periodic Hills equation (5.23) was initially considered without damping (d=0) to test the indirect approach. The system parameters used were $a = 1.5, b_1 = 1.0, b_2 = 0.5$. The incommensurate frequencies considered were $\omega_1 = \pi$ rads and $\omega_2 = 7$ rads.

Initially, the given Hills quasi-periodic system was split as indicated in equation (5.24) and an intuitive state augmentation was applied, as indicated in equation (5.19). This added two fictitious states considering $\omega_2 = 7$ rads and the system equation was updated to the form of equation (5.25). Since ω_1 was considered in the linear periodic part, the principal time period for the periodic subsystem was $T = 2secs$. The FTM and the constant Floquet matrix of the periodic part evaluated at the principal period was found to be as equation (5.29)

$$\begin{aligned} \mathbf{\Phi}(T) &= \begin{bmatrix} -0.8372 & 0.7830 & 0 & 0 \\ -0.3821 & -0.8372 & 0 & 0 \\ 0 & 0 & 0.1367 & -0.1415 \\ 0 & 0 & 6.9343 & 0.1367 \end{bmatrix}, \\ \tilde{\mathbf{R}} &= \begin{bmatrix} 0.0 & 1.8344 & 0 & 0 \\ -0.8952 & 0.0 & 0 & 0 \\ 0 & 0 & 0 & -0.1024 \\ 0 & 0 & 5.0177 & 0 \end{bmatrix} \end{aligned} \tag{5.29}$$

The eigenvalues of these matrices indicate the stability characteristics of the linear periodic part as per Floquet theory. The Floquet Multipliers were computed to be $-0.8372 \pm i0.5470; 0.1367 \pm i0.9906$ for the undamped linear periodic system and are plotted on a unit circle, as shown in Figure 5.1.

From Figure 5.1, it is observed that all the multipliers lie on the unit circle.

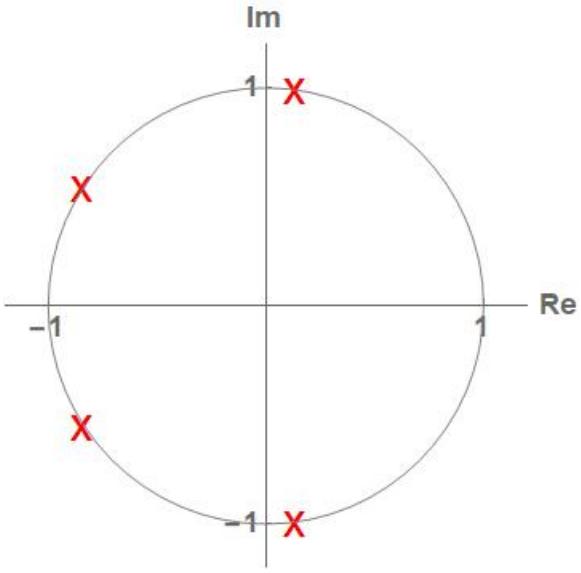

Figure 5.1: Floquet Multipliers of the Linear Part of the Undamped Quasi-periodic System

Hence, the linear part of the system can be deduced to be marginally stable. Further, the element-wise variation over time of the L-F transformation matrix, $\mathbf{Q}(t)$, was computed using Chebfun. As mentioned earlier, each element of the $\mathbf{Q}(t)$ matrix is a truncated Fourier series. The inverse of this matrix ($\mathbf{Q}^{-1}(t)$) was evaluated and used in equation (5.27), to update the system equation. The element-wise variation of both $\mathbf{Q}(t)$ and $\mathbf{Q}^{-1}(t)$ matrices for the principal time period (T=2 secs) are indicated in Figure 5.2.

Later, proceed with a modal transformation to the equation (5.27), and the near identity transformation was successively applied to facilitate the application of the TDNF technique. The time dependent terms are averaged, and the insignificant terms were discarded to reduce the system in the form of equation (5.30)

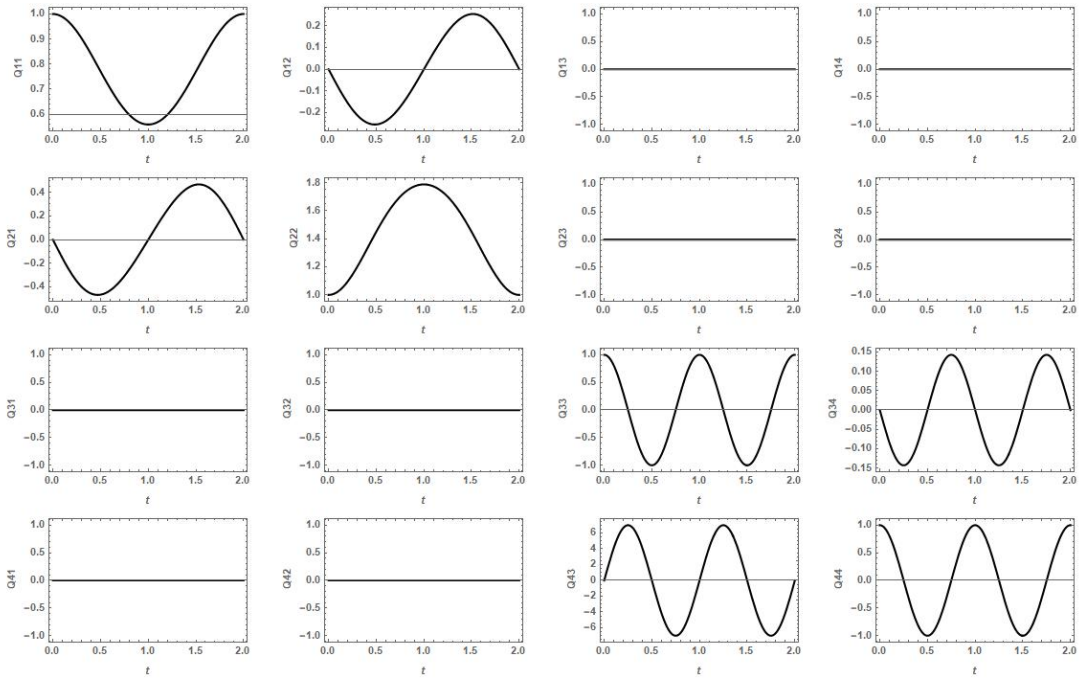

(**a**)

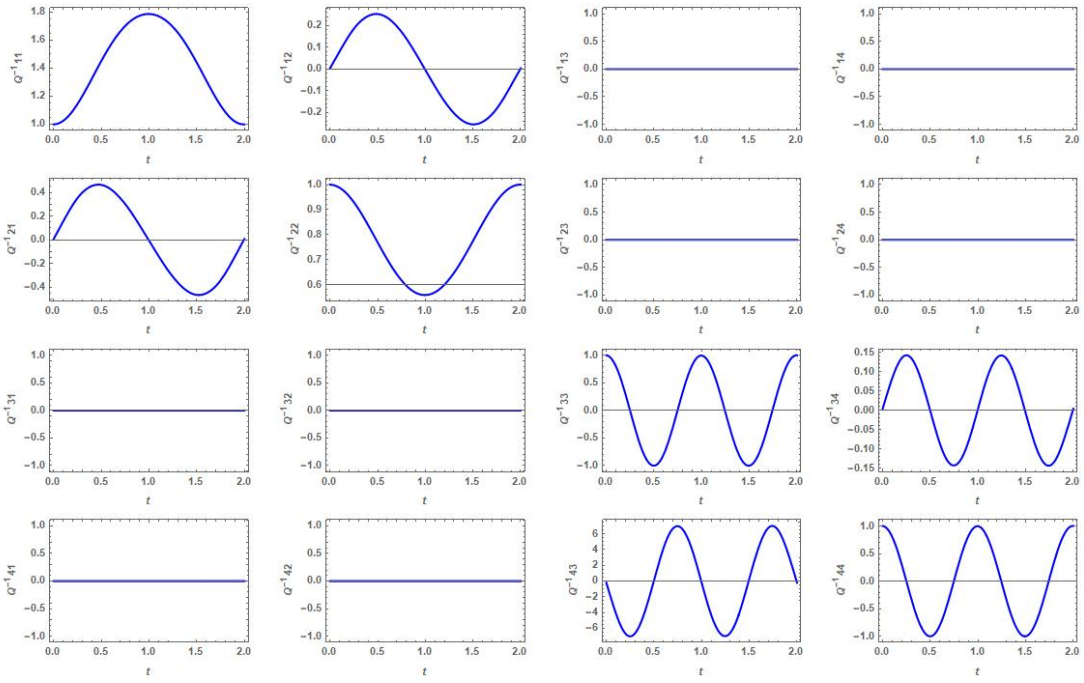

(**b**)

Figure 5.2: Element-wise Variation During the Principal Time Period for (**a**) $\mathbf{Q}_{ij}(t)$ and (**b**) $\mathbf{Q}_{ij}{}^{-1}(t)$ Matrices of the Periodic Subsystem Without Damping

$$\begin{bmatrix} \dot{v_1} \\ \dot{v_2} \\ \dot{v_3} \\ \dot{v_4} \end{bmatrix} = \begin{bmatrix} (0.0 + i1.28147)v_1 \\ (0.0 - i1.28147)v_2 \\ (0.0 + i0.71675)v_3 \\ (0.0 - i0.71675)v_4 \end{bmatrix} \tag{5.30}$$

From equation (5.30), it can be observed that the system is reduced to a time-invariant form, similar to the Floquet theory for the periodic system. However, the stability characteristics of the system are preserved in the reduced form after TDNF application. The given set of differential equations are solved to obtain the TDNF solution. This solution is back transformed to the original system coordinates to compare the results with the numerical method for the same set of initial conditions. The comparisons of the temporal variations of this system are indicated in Figures 5.3a,b and the phase plot comparisons are shown in Figure 5.4.

As indicated in these Figures 5.3a,b and 5.4, the solid red line indicates the solution obtained from the Normal Forms technique, and the black dashed line corresponds to the numerical integration method. The system was run for 50 seconds, and it is observed that the temporal variations of the back transformed Normal Forms solution follow the trend of the numerical solution. For clarity, the phase plot comparisons were run for 30 seconds, and they indicate very minimal deviation from the numerical results. It is also observed that the system is gradually growing/spiraling out from the initial condition of $x_1(0) = 0$ and $x_2(0) = 0.1$, but the phase plot is bounded. This validates that the indirect technique is applicable to a linear quasi-periodic system without damping.

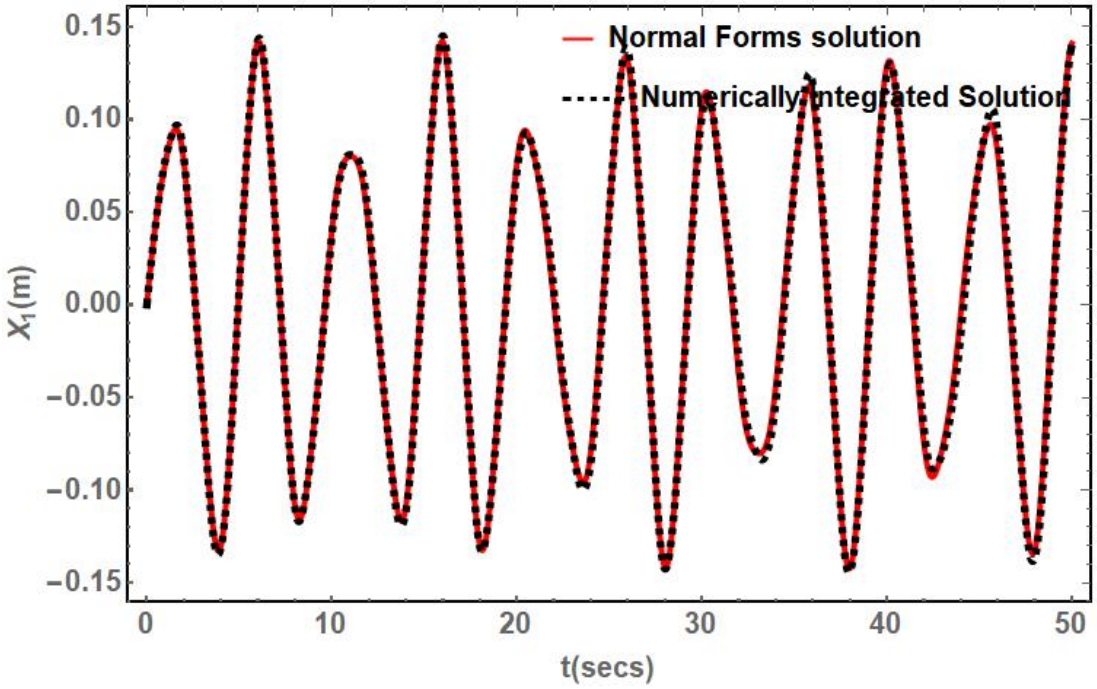

(**a**)

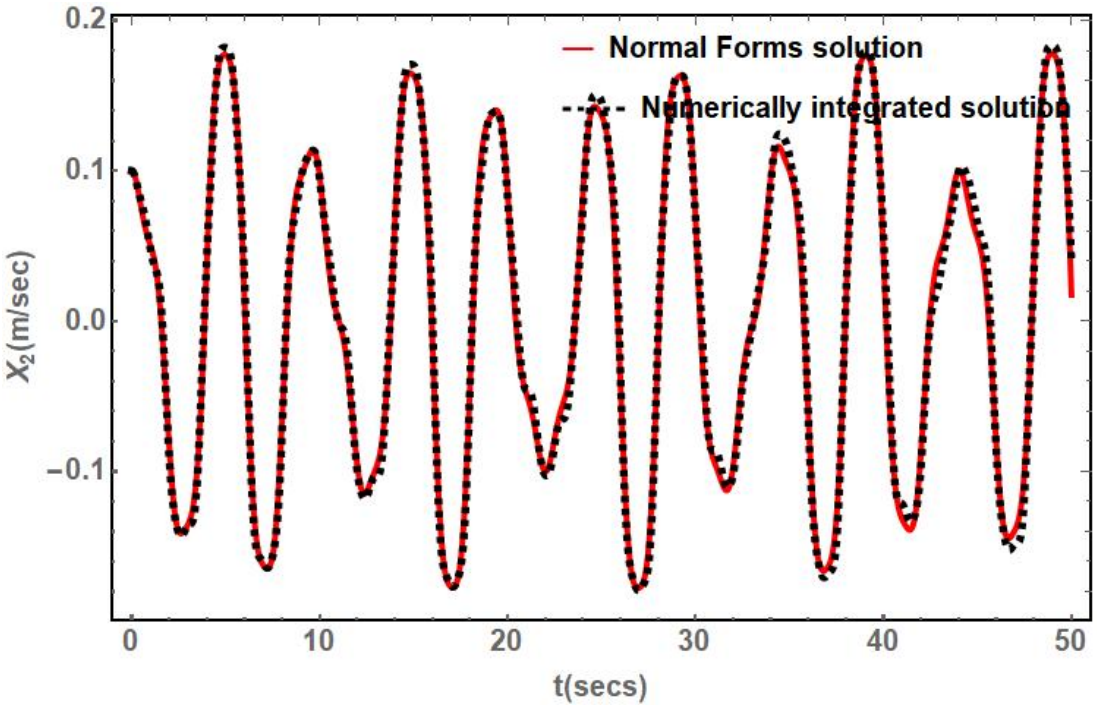

(**b**)

Figure 5.3: Comparison of System State Variation for the Quasi-periodic System Without Damping using Indirect Approach, Where (**a**) Shows x_1 State and (**b**) Shows x_2 State Variations

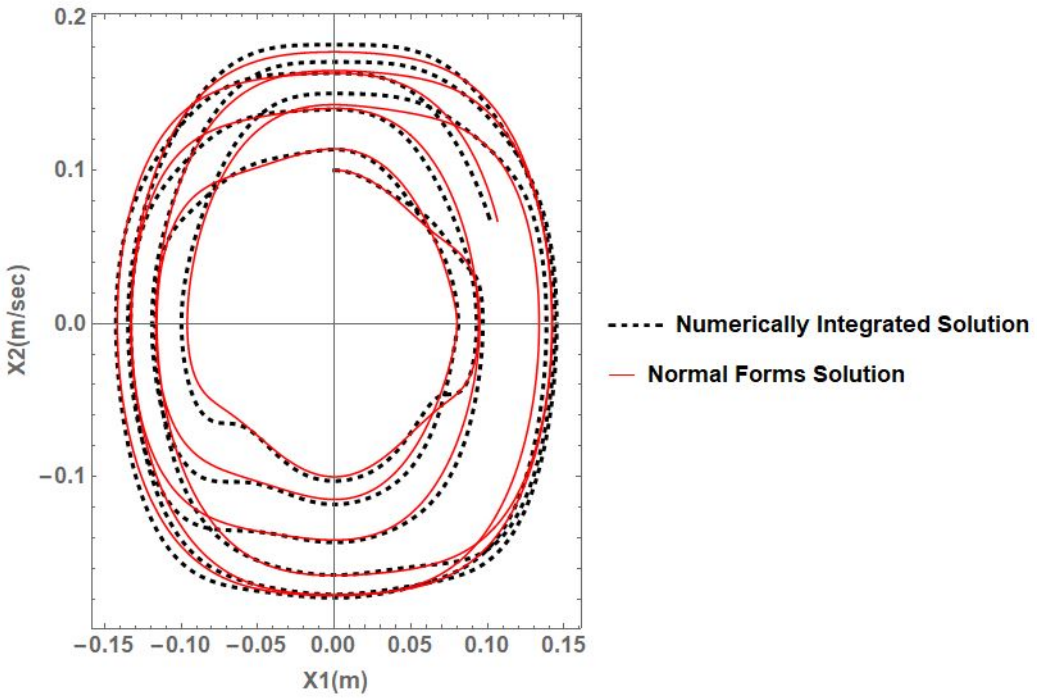

Figure 5.4: Comparison of phase plot variation for the quasi-periodic system without damping using Indirect Approach

Quasi-Periodic System With Damping

The Hills quasi-periodic system was later analyzed for the case with damping (d=0.3). The system parameters and the incommensurate frequencies remain the same as $a = 1.5, b_1 = 1.0, b_2 = 0.5, \omega_1 = \pi$ rads and $\omega_2 = 7$ rads. The process of splitting the quasi-periodic system remained the same as the case without damping. Similar to the case of *'System Without Damping'*, the periodic part with $\omega_2 = 7$ rads was considered as the quasi-periodic term and the state augmentation was applied to it. Besides, the damping coefficient was added to the linear periodic part and underwent L-F transformation with the periodic term containing $\omega_1 = \pi$ rads. The FTM and the constant Floquet matrix for the periodic part with damping was evaluated to be

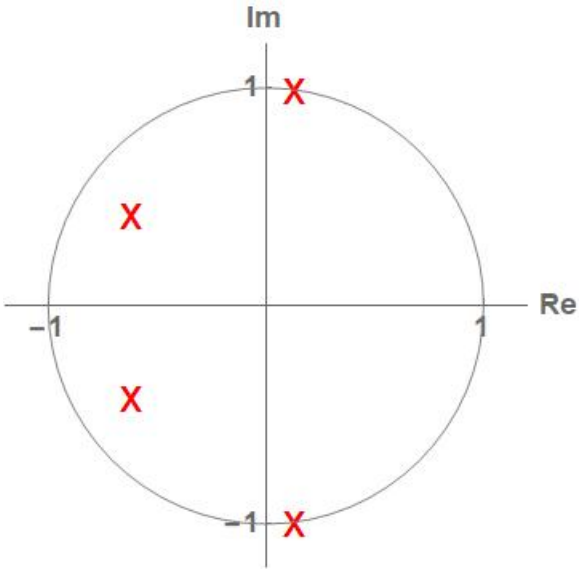

Figure 5.5: Floquet Multipliers of the Linear Part of the Damped Quasi-periodic System

$$\mathbf{\Phi}(T) = \begin{bmatrix} -0.5228 & 0.5928 & 0 & 0 \\ -0.3080 & -0.7006 & 0 & 0 \\ 0 & 0 & 0.1367 & -0.1415 \\ 0 & 0 & 6.9343 & 0.1367 \end{bmatrix},$$
$$\tilde{\mathbf{R}} = \begin{bmatrix} 0.1205 & 1.8030 & 0 & 0 \\ -0.9367 & -0.4205 & 0 & 0 \\ 0 & 0 & 0 & -0.1024 \\ 0 & 0 & 5.0177 & 0 \end{bmatrix} \tag{5.31}$$

The Floquet Multipliers were $-0.6117 \pm i0.4179; 0.1367 \pm i0.9906$ for the damped linear periodic system, and they are plotted with a unit circle in Figure 5.5.

As per Figure 5.5, since all the multipliers lie within or on the unit circle, the linear part of the system was concluded to be stable. Similar to the case without damping, both $\mathbf{Q}(t)$ and $\mathbf{Q}^{-1}(t)$ matrices were evaluated for the system with damping. The system was transformed to a form with a linear time-invariant coefficient. Subsequently,

a modal transformation and near identity transformations were applied to enable the application of the TDNF technique. The reduced Normal Forms expression for the case of a linear quasi-periodic system with damping was computed to be

$$\begin{bmatrix} \dot{v_1} \\ \dot{v_2} \\ \dot{v_3} \\ \dot{v_4} \end{bmatrix} = \begin{bmatrix} (-0.15 + i1.2711)v_1 \\ (-0.15 - i1.2711)v_2 \\ (0.0 + i0.71675)v_3 \\ (0.0 - i0.71675)v_4 \end{bmatrix} \tag{5.32}$$

The TDNF solution was computed from equation (5.32) and back transformed to the original system coordinates. The back transformed solutions were compared with the numerical integration technique for the same set of initial conditions of $x_1(0) = 0$ and $x_2(0) = 0.1$. The comparisons of the temporal variations of the system with damping are displayed in Figures 5.6a,b and the phase plot comparisons are shown in Figure 5.7.

Similar to the case without damping, the solid red line indicates the solutions obtained from the Normal Forms technique back transformed to the original coordinates, and the black dashed line corresponds to the numerical integration method in these plots. The temporal variations are simulated for 50 seconds, and the phase plot comparisons are run for 30 seconds for clarity. It is observed that the temporal variations of the reduced order Normal Forms solution follow the numerical solution closely. The phase plot comparisons indicate intermittent deviation from the numerical results and gradually decaying/spiraling in from the initial conditions.

Commutative Quasi-Periodic System

For the given commutative quasi-periodic system indicated in equation (5.7), the numerical simulation results were performed and compared with the analytical technique

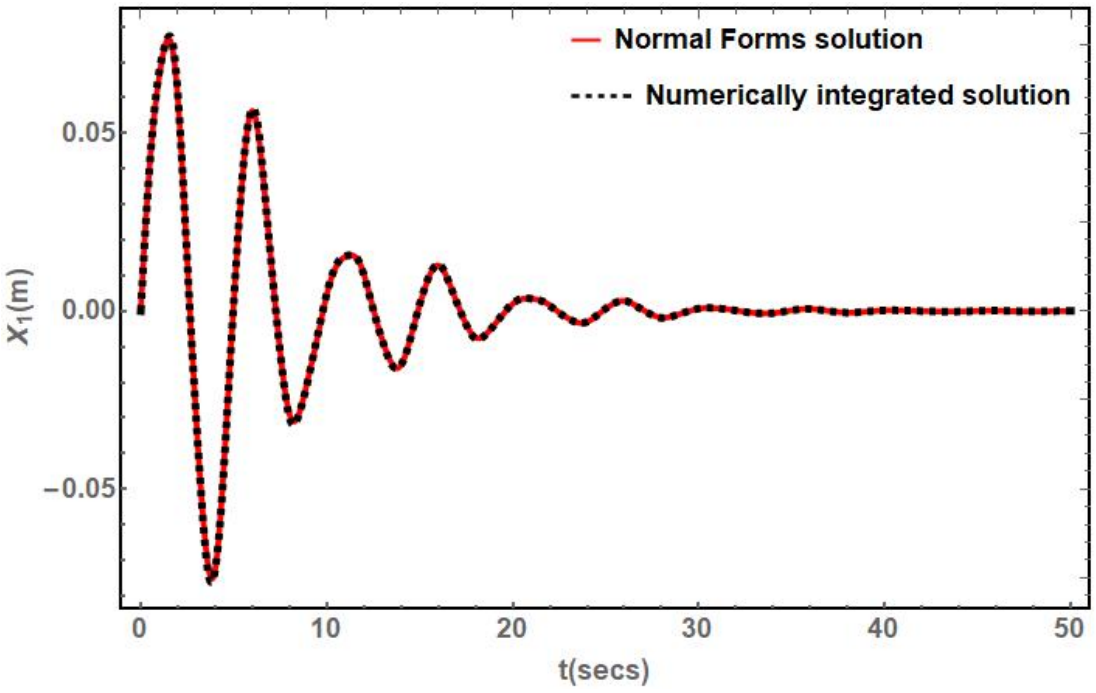

(**a**)

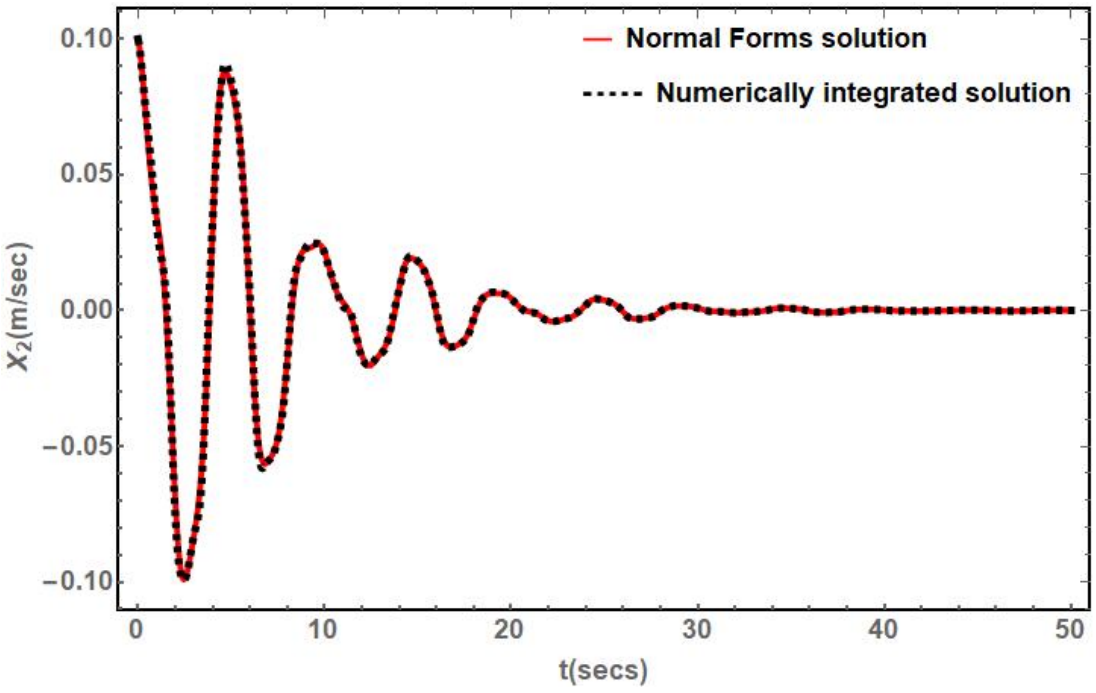

(**b**)

Figure 5.6: Comparison of System State Variation for the Hills Quasi-periodic System with Damping Using Indirect Approach, Where (**a**) Shows x_1 State and (**b**) Shows x_2 State Variations

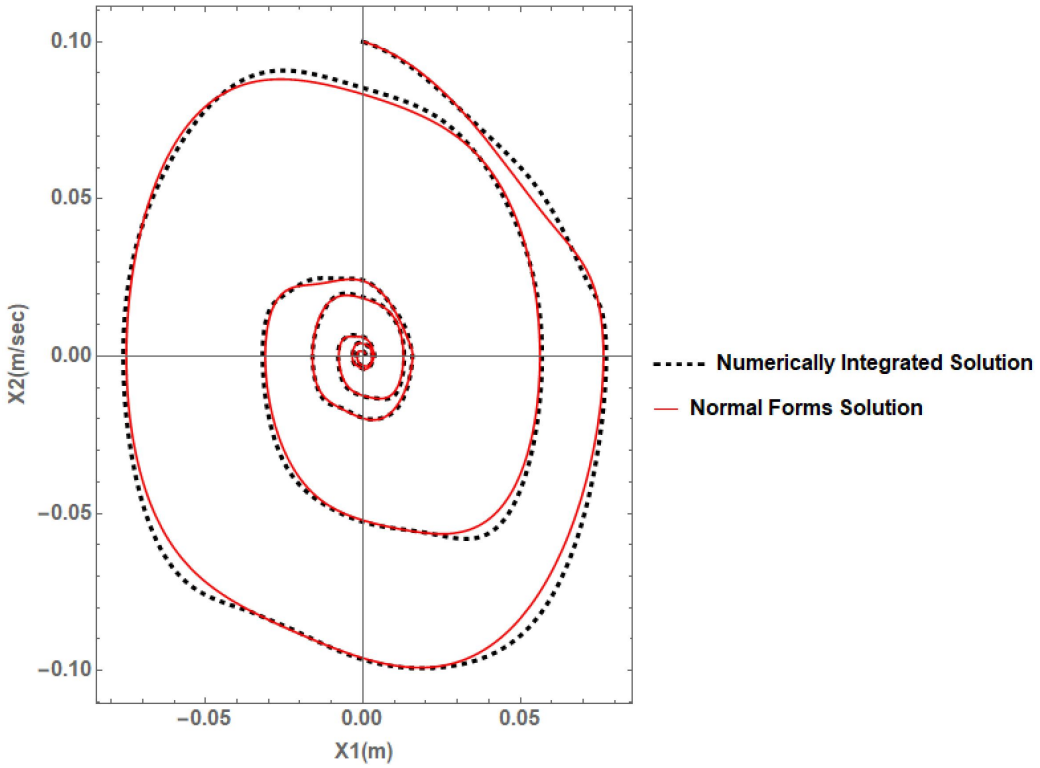

Figure 5.7: Comparison of Phase Plot Variation for the Hills Quasi-periodic System with Damping Using Indirect Approach

in this subsection. The system parameters considered were $a = 2.0, b_1 = 1, b_2 = 0.1$ and the incommensurate frequencies as $\omega_1 = 2\pi$ rads and $\omega_2 = 7$ rads. The system parameters were applied to the equation (5.14) to compute the L-P transformation ($\mathbf{P}(t)$) and $\mathbf{C}$ matrices analytically. The eigenvalues of the constant $\mathbf{C}$ matrix were observed to be $0.0 \pm i1.4142$. Similarly, the system parameters were substituted in equation (5.7) and numerically integrated to obtain the numerical solutions. In order to apply the indirect approach, the system parameters were substituted in the state space form, equation (5.8), and it was split into a form similar to equation (5.24), as indicated below

$$\frac{d}{dt}\begin{bmatrix} x_1 \\ x_2 \end{bmatrix} = \begin{bmatrix} 1\sin(2\pi t) & 1 \\ -2 & 1\sin(2\pi t) \end{bmatrix}\begin{bmatrix} x_1 \\ x_2 \end{bmatrix} + \begin{bmatrix} 0.1\sin(7t)x_1 \\ 0.1\sin(7t)x_2 \end{bmatrix} \tag{5.33}$$

The term, $\sin(7t)$, was considered as the augmented state, and the system equation was updated to a form similar to equation (5.25). Further, an L-F transformation corresponding to the linear periodic part (of the principal period, T=1 sec) was applied. The FTM and the constant Floquet matrix of the linear periodic part computed at the principal period is shown below

$$\begin{aligned} \mathbf{\Phi}(T) &= \begin{bmatrix} 0.1559 & 0.6985 & 0 & 0 \\ -1.3969 & 0.1559 & 0 & 0 \\ 0 & 0 & 0.7539 & 0.0939 \\ 0 & 0 & -4.5989 & 0.7539 \end{bmatrix}, \\ \tilde{\mathbf{R}} &= \begin{bmatrix} 0.0 & 1.00 & 0 & 0 \\ -2.0 & 0.0 & 0 & 0 \\ 0 & 0 & 0 & 0.1024 \\ 0 & 0 & -5.0177 & 0 \end{bmatrix} \end{aligned} \tag{5.34}$$

The Floquet Multipliers were computed to be $0.1559 \pm i0.9878; 0.7539 \pm i0.6570$ and are indicated in Figure 5.8.

As per Figure 5.8, all the multipliers lie on the unit circle, and hence the linear part of the system can be concluded to be marginally stable. Further, the element-wise variation of both $\mathbf{Q}(t)$ and $\mathbf{Q}^{-1}(t)$ matrices for the principal time period (T=1 sec) are indicated in Figure 5.9.

After substituting the expressions of $\mathbf{Q}(t)$ and $\mathbf{Q}^{-1}(t)$ matrices, the updated commutative system underwent a modal transformation and subsequently a series of near-identity transformations to apply the TDNF technique. The reduced system after the application of the TDNF technique is indicated below

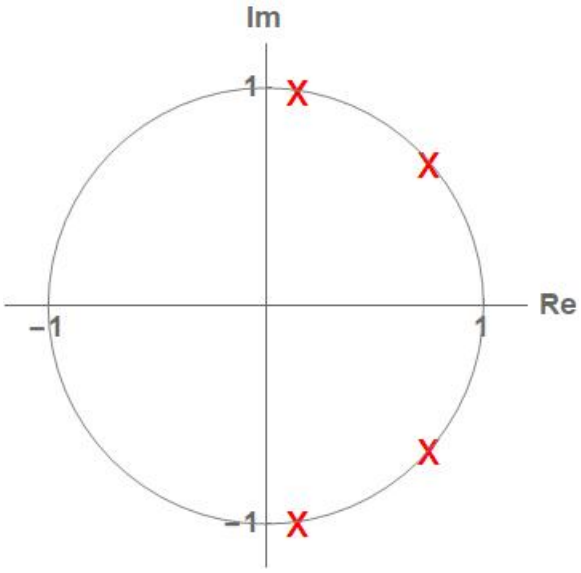

Figure 5.8: Floquet Multipliers of the Linear Part of the Commutative Quasi-periodic System

$$\begin{bmatrix} \dot{v_1} \\ \dot{v_2} \\ \dot{v_3} \\ \dot{v_4} \end{bmatrix} = \begin{bmatrix} (0.0 + i1.41421)v_1 \\ (0.0 - i1.41421)v_2 \\ (0.0 + i0.71680)v_3 \\ (0.0 - i0.71680)v_4 \end{bmatrix} \tag{5.35}$$

It is observed from equation (5.35) that the coefficients of the first two states (which are the original system states) correspond to the eigenvalues of the constant **C** matrix, computed analytically. When equation (5.35) is expressed in the matrix multiplication form, the left-top 2×2 square matrix will represent the Jordan form of the **C** matrix. Hence, the reduced form after TDNF application was observed to be time-variant and comparable to the **C** matrix. This resonates with the Floquet type theory. The computed set of differential equations, in equation (5.35), were solved to obtain the Normal Forms solution. This solution was back transformed to the original system coordinates to compare the results with the numerical and analytical method for the same set of initial conditions, $x_1(0) = 1.0$ and $x_2(0) = 0$.

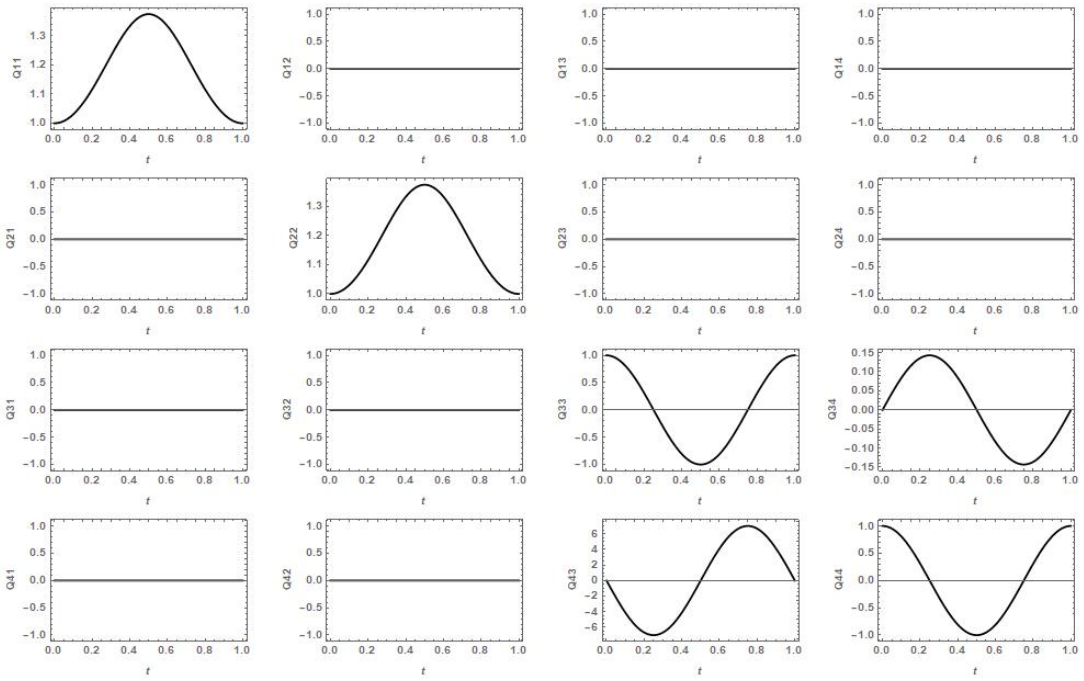

(**a**)

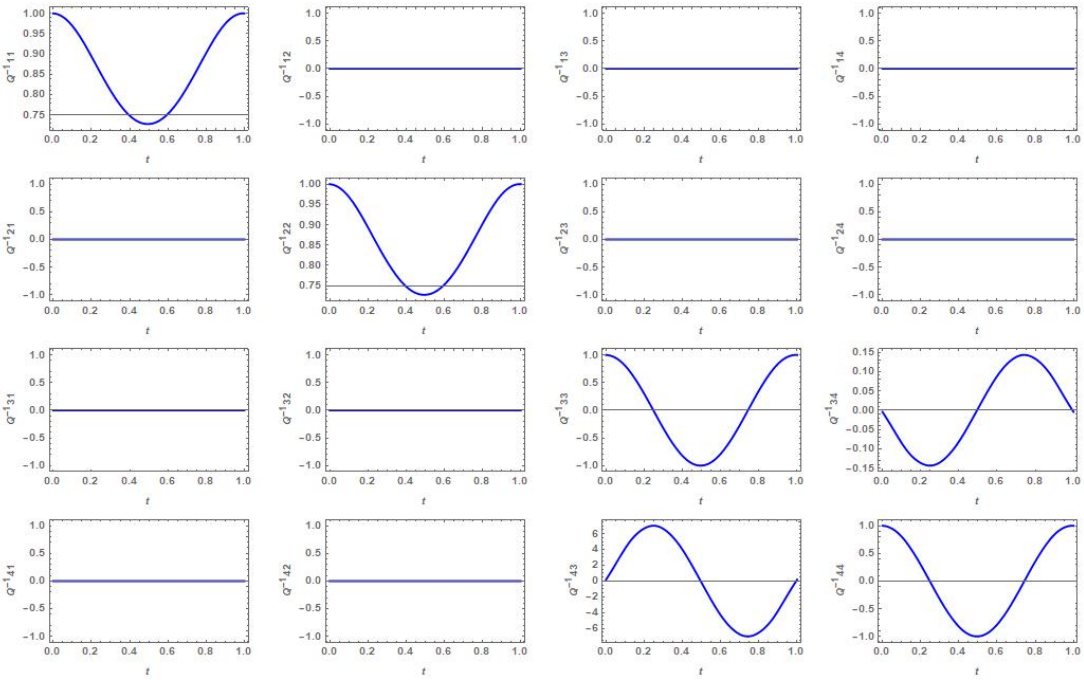

(**b**)

Figure 5.9: Element-wise Variation During the Principal Time Period for (**a**) $\mathbf{Q}_{ij}(T)$ and (**b**) $\mathbf{Q}_{ij}{}^{-1}(T)$ Matrices of the Periodic Subsystem of the Linear Commutative Quasi-periodic System

Meanwhile, the L-P transformation matrix ($\mathbf{P}(t)$) transforms the given system to a time-invariant form. The STM ($\Phi(t)$), using the analytical L-P transformation matrix ($\mathbf{P}(t)$), was computed as per equation (5.13). This STM ($\Phi(t)$) was multiplied with the same set of initial conditions to generate the system state evolution over time. The comparisons of the temporal variations of this system are displayed in Figures 5.10a,b.

As indicated in Figures 5.10a,b, the black dashed line indicates the numerically integrated solution of the original system equation (5.7), the blue dashed line indicates the state evolution variation of the analytically derived STM and the solid red line indicates the back-transformed Normal Forms solution as per the indirect approach for non-commutative systems. The simulations were run for 30 seconds, and the comparisons were observed to agree. Therefore, a given commutative quasi-periodic system can be reduced to a time invariant form analytically using an L-P transformation matrix, and the Floquet type theory can be extended towards such a system. Additionally, the indirect approach for the non-commutative system is also applicable towards the commutative system and would generate comparable results with both numerical integration and analytical approaches.

Since the temporal variations match closely and the $\mathbf{C}$ matrix was known for the given commutative system, the L-P transformation matrix was evaluated from the temporal variations of the back-transformed Normal Forms solutions. The temporal variations were evaluated for the initial conditions of $x_1(0) = 1.0; x_2(0) = 0.0$ and $x_1(0) = 0.0; x_2(0) = 1.0$. The resulting temporal variations were concatenated such that the term $\mathbf{x}(0)$, in equation (5.15), becomes an identity matrix. The fully populated $\mathbf{x}(t)$ matrix and the analytically derived $\mathbf{C}$ matrix were substituted in equation (5.15) to evaluate the L-P transformation matrix from the indirect approach. The comparisons of the element-wise variations for the L-P transformation matrix, with

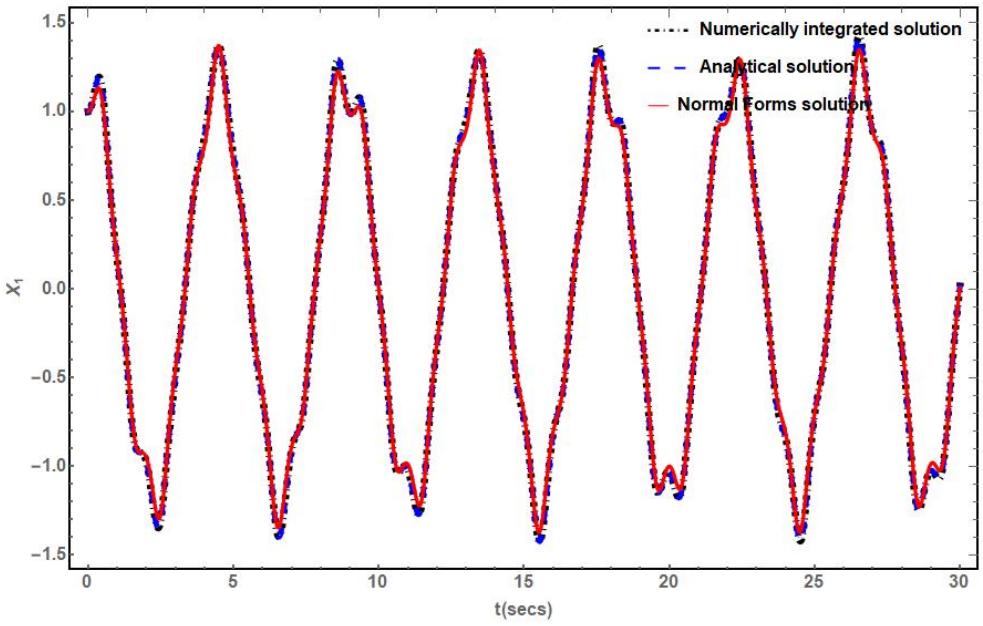

(**a**)

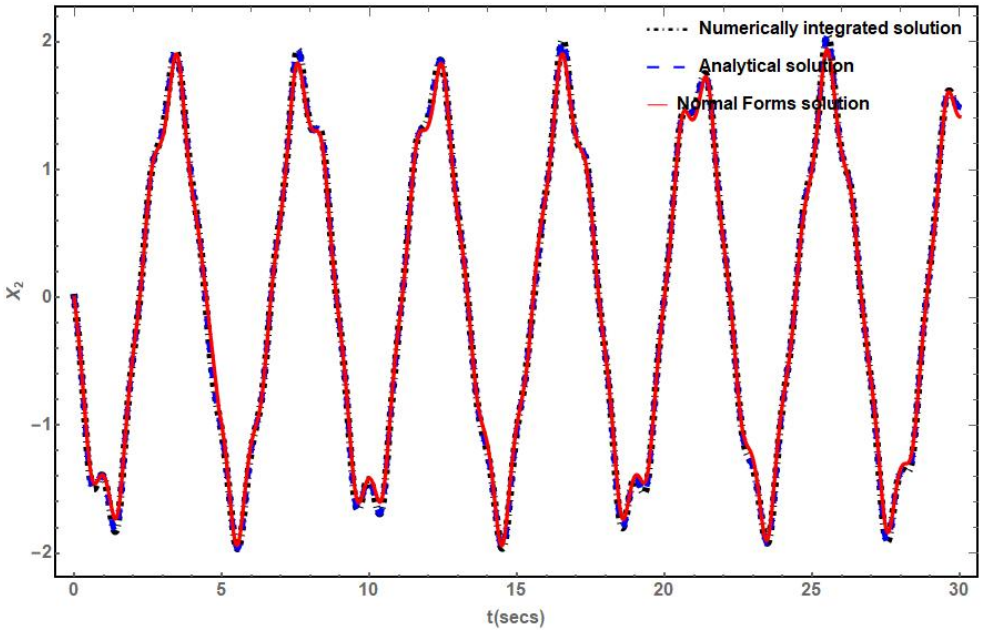

(**b**)

Figure 5.10: Comparison of System State Variation for the Commutative Quasi-periodic System Using Indirect Approach, Where (**a**) Shows x_1 State and (**b**) Shows x_2 State Variations

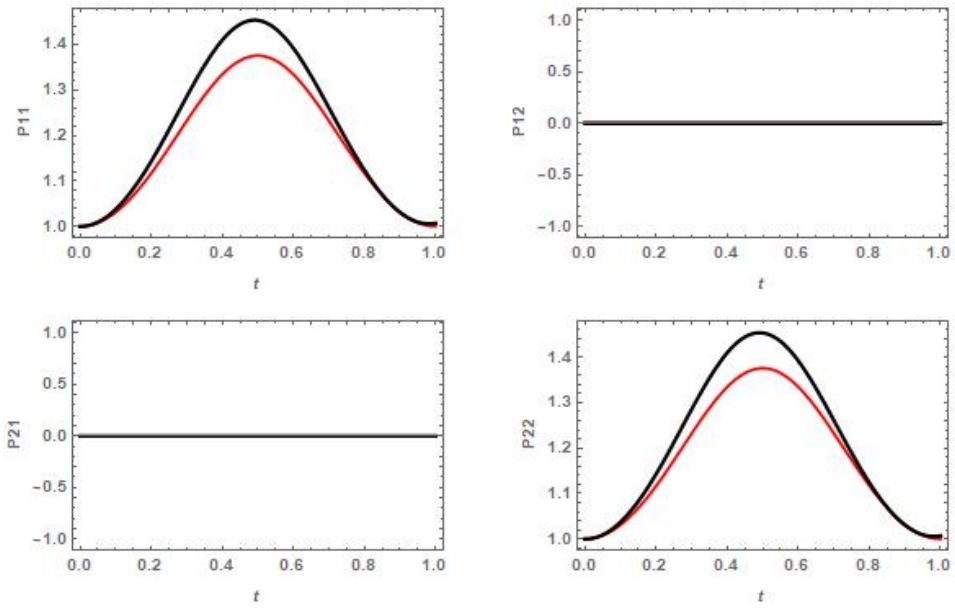

Figure 5.11: Comparison of Element-wise Variation of the L-p Transformation Matrix for the Commutative Quasi-periodic System

the analytical expression for the time period of 1 sec, are displayed in Figure 5.11.

In Figure 5.11, the black line corresponds to the analytical expression, and the solid red line corresponds to the Normal Forms derived expression. It is observed that the trend of the analytical solution is being followed by the Normal Forms derived solution for the L-P transformation matrix. This validates the indirect approach applying to both commutative and non-commutative linear quasi-periodic systems.

The extension of Floquet theory towards quasi-periodic systems was validated using the techniques discussed in this section. However, the temporal variations for the system states matched very well only when the quasi-periodic coefficients were low or insignificant. Additionally, in these cases, the L-P transformation matrix computed was not in agreement with numerical results for the commutative system. In order to facilitate the analysis of a strongly quasi-periodic and nonlinear systems, a direct approach was formulated, as discussed in the following section.

5.3 Direct Approach to Compute L-P Transformation

In this section, the unified theory (discussed in section 2.4) for the time-periodic system is extended towards quasi-periodic systems and serves as a direct approach. The direct approach overcomes the deficiencies of the indirect approach and aids in the direct computation of the closed form expression for the L-P transformation matrix.

Consider a linear parametrically excited quasi-periodic system with both constant and periodic coefficients with incommensurate frequencies expressed as equation (2.29), where $\mathbf{A}(t) = \mathbf{B}_0 + \mathbf{B}(t)$ is similar to equation (2.6) of the time-periodic system. The system initially is subjected to an intuitive state augmentation, as detailed in 2.2. The periodic and quasi-periodic terms in the $\mathbf{B}(t)$ matrix are considered separate augmented states. Similar to the case of the periodic system, the state augmentation would append the linear constant matrix ($\tilde{\mathbf{B}}_0$) with the constant coefficients of the augmented states. Additionally, the vector $\mathbf{B}(t)\mathbf{x}(t)$ is transformed to a nonlinear vector ($\tilde{\mathbf{B}}(\tilde{\mathbf{x}})$), as shown in equation (2.9). This results in the system equation being transformed to an updated system of the form indicated in equation (2.11). A modal transformation on the updated system, $\tilde{\mathbf{x}}(t) = \tilde{\mathbf{M}}\tilde{\mathbf{z}}(t)$, would transform the system to its Jordan form (similar to equation (2.12)) and is amenable to a near-identity transformation and application of Normal Forms technique. Since there is no time-dependent terms, the application of TINF is feasible, as indicated in section 2.3. Similar to the case of periodic system, the Normal Forms of order higher than the order of the nonlinearity of the equation (i.e. two for the cases indicated in this section) are required to be computed. This would result in the reduced system equation, as indicated in equation (2.20). Subsequently, the fictitious/augmented states are replaced by their closed form expressions. A time-invariant system is obtained

from the TINF solution for a linear quasi-periodic system in the absence of resonant terms.

The near-identity transformation encompasses the dynamical characteristics of both system states and augmented states. The reduced system near identity transformation can also be expressed as

$$\tilde{\mathbf{z}}(t) = \left[\mathbf{I} + \bar{\mathbf{P}}(t)\right] \tilde{\mathbf{v}} \approx \bar{\mathbf{P}}(t)\tilde{\mathbf{v}}(t) \tag{5.36}$$

where $\bar{\mathbf{P}}(t)$ serves as the near-identity transformation matrix and contains all the higher order nonlinear terms/coefficients associated with the states. This transformation converts the system equation into a linear time-invariant system, as follows

$$\dot{\tilde{\mathbf{v}}} = \bar{\mathbf{J}}\tilde{\mathbf{v}} \tag{5.37}$$

The original quasi periodic system, using the near-identity transformation, resulted in a time invariant form. It is important to note that the states in the near-identity transformation are augmented states. These augmented states are known periodic functions of incommensurate frequencies. Thus after these augmented states are replaced by the known periodic functions with incommensurate frequencies, the near-identity transformation yields a quasi-periodic transformation that converts the original quasi-periodic system into a time invariant one.

As indicated in equation (5.13), by applying L-P transformation, the STM in the Normal Forms coordinate can be decomposed as

$$\bar{\mathbf{\Phi}}(t) = \bar{\mathbf{P}}(t)e^{\bar{\mathbf{J}}t} \tag{5.38}$$

From the $\bar{\mathbf{\Phi}}(t)$ in equation (5.38), the STM of the original system, $\hat{\mathbf{\Phi}}(t)$, could be computed using back transformation. This would aid in generating the state evolution of the original system over time. Though similarities between the averaging technique

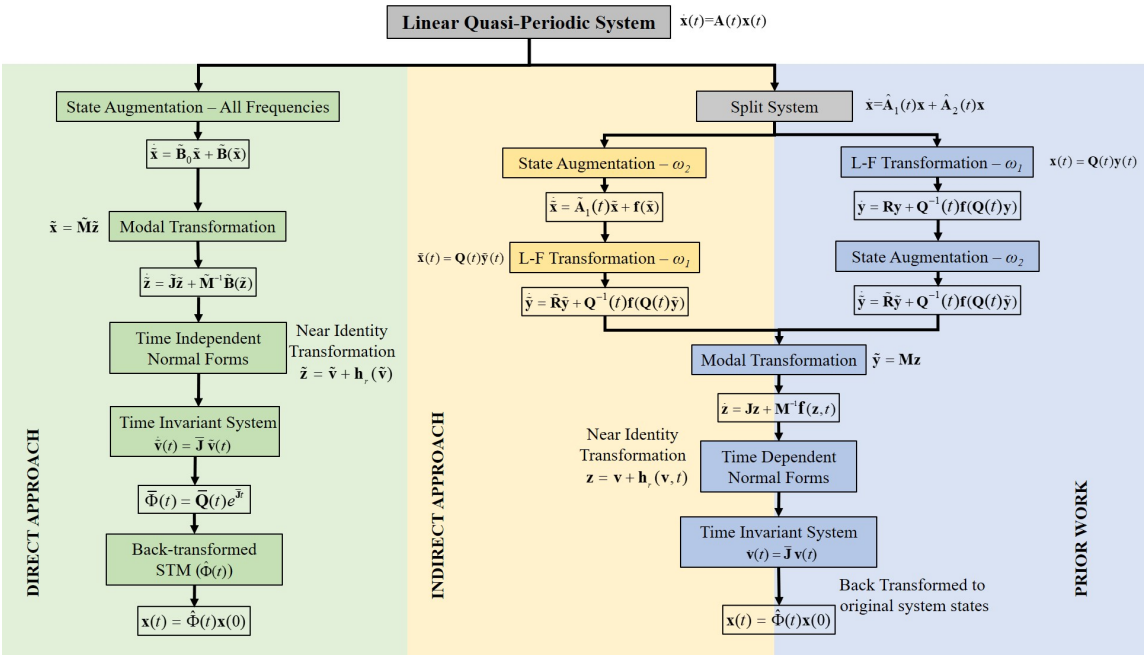

Figure 5.12: Comparison of Multiple Techniques to Analyze Linear Quasi-periodic Systems

and the Normal forms technique in the computation of monodromy matrix were also discussed by Sanders *et al.* (2007); Verhulst (1990), a practical yet straightforward technique to compute the elusive L-P transformation was not discussed explicitly.

The unified theory serves as a direct approach by augmenting all the time varying coefficients as additional fictitious states. The direct approach circumvents the requirement to split the system and perform an L-F transformation before applying the Normal Forms technique. This reduces the computational complexity. Moreover, the direct approach provides a clean expression for the L-P transformation matrix and STM. A flowchart indicating the steps involved in the direct approach, indirect approach, and prior work is indicated in Figure 5.12. The application of the direct approach towards a linear quasi-periodic system is detailed in the subsequent section.

5.3.1 Application for Non-Commutative Quasi-periodic System

Initially, the direct approach is applied on a linear quasi-periodic system without damping. Later, the original quasi-periodic system is updated with a damping term to analyze the direct approach's temporal variation.

Linear Quasi-periodic System Without Damping

Consider a Hills quasi-periodic system indicated below in equation (5.39)

$$\ddot{x} + (a + b(\cos(\omega_1 t) + \cos(\omega_2 t)))x = 0 \tag{5.39}$$

The above equation is quasi-periodic if ratio of both the frequencies, $\frac{\omega_1}{\omega_2}$, is incommensurate. After rearrangement, it could be expressed as

$$\ddot{x} = -ax - bx(\cos(\omega_1 t) + \cos(\omega_2 t)) \tag{5.40}$$

As mentioned in section 2.2, the periodic coefficients are converted to fictitious/augmented states as shown below in equation (5.41)

$$\begin{aligned}
&p_1 = \cos(\omega_1 t); \qquad p_2 = \cos(\omega_2 t) \\
&\dot{p}_1 = -\omega_1 \sin(\omega_1 t) = q_1; \qquad \dot{p}_2 = -\omega_2 \sin(\omega_2 t) = q_2 \\
&\ddot{p}_1 = -{\omega_1}^2 \cos(\omega_1 t) = -{\omega_1}^2 p_1 = \dot{q}_1; \\
&\ddot{p}_2 = -{\omega_2}^2 \cos(\omega_2 t) = -{\omega_2}^2 p_2 = \dot{q}_2
\end{aligned} \tag{5.41}$$

By substituting equation (5.41) into equation (5.40) and converting it into the

state space form results in

$$\frac{d}{dt}\begin{Bmatrix} x \\ \dot{x} \\ p_1 \\ q_1 \\ p_2 \\ q_2 \end{Bmatrix} = \begin{bmatrix} 0 & 1 & 0 & 0 & 0 & 0 \\ -a & 0 & 0 & 0 & 0 & 0 \\ 0 & 0 & 0 & 1 & 0 & 0 \\ 0 & 0 & -\omega_1^2 & 0 & 0 & 0 \\ 0 & 0 & 0 & 0 & 0 & 1 \\ 0 & 0 & 0 & 0 & -\omega_2^2 & 0 \end{bmatrix} \begin{Bmatrix} x \\ \dot{x} \\ p_1 \\ q_1 \\ p_2 \\ q_2 \end{Bmatrix} + \begin{Bmatrix} 0 \\ -bx(p_1+p_2) \\ 0 \\ 0 \\ 0 \\ 0 \end{Bmatrix} \tag{5.42}$$

By comparing equation (5.42) to equation (2.11), the following can be deduced

$$\begin{Bmatrix} x \\ \dot{x} \\ p_1 \\ q_1 \\ p_2 \\ q_2 \end{Bmatrix} = \begin{Bmatrix} x_1 \\ x_2 \\ x_3 \\ x_4 \\ x_5 \\ x_6 \end{Bmatrix}, \begin{bmatrix} 0 & 1 & 0 & 0 & 0 & 0 \\ -a & 0 & 0 & 0 & 0 & 0 \\ 0 & 0 & 0 & 1 & 0 & 0 \\ 0 & 0 & -\omega_1^2 & 0 & 0 & 0 \\ 0 & 0 & 0 & 0 & 0 & 1 \\ 0 & 0 & 0 & 0 & -\omega_2^2 & 0 \end{bmatrix} = \tilde{\mathbf{B}}_0, \begin{Bmatrix} 0 \\ -bx(p_1+p_2) \\ 0 \\ 0 \\ 0 \\ 0 \end{Bmatrix} = \tilde{\mathbf{B}}(\tilde{\mathbf{x}}) \tag{5.43}$$

The equation (5.42) is similar to equation (2.11), with a constant linear matrix and a nonlinear vector. As mentioned in section 5.3, a modal transformation (corresponding to the constant linear matrix) is applied. This results in the Jordan canonical form of the equation, similar to the form indicated in equation (2.32). The updated system is amenable to undergo near-identity transformation and application of the TINF technique. In this section, the Normal Forms solution of an order of three was considered to ensure that one account for enough nonlinear terms. For more accurate results, one may include higher order, but it would increase the computational time. The resulting reduced system after the application of the Normal Forms technique is indicated in equation (5.44).

$$\begin{bmatrix} \dot{v_1} \\ \dot{v_2} \\ \dot{v_3} \\ \dot{v_4} \\ \dot{v_5} \\ \dot{v_6} \end{bmatrix} = \begin{bmatrix} \frac{v_1}{\sqrt{-a}}\left(a + \frac{b^2(v_5 v_6 \omega_1^2(-4a+\omega_1^2)+v_3 v_4 \omega_2^2(-4a+\omega_2^2))}{(4a-\omega_1^2)\omega_1^2(4a-\omega_2^2)\omega_2^2}\right) \\ \frac{v_2}{\sqrt{-a}}\left(-a + b^2\left(\frac{v_3 v_4}{4a\omega_1^2-\omega_1^4} + \frac{v_5 v_6}{4a\omega_2^2-\omega_2^4}\right)\right) \\ -v_3\sqrt{-\omega_1^2} \\ v_4\sqrt{-\omega_1^2} \\ -v_5\sqrt{-\omega_2^2} \\ v_6\sqrt{-\omega_2^2} \end{bmatrix} \tag{5.44}$$

From equation (5.44), the closed form expressions for the augmented states could be identified as indicated below

$$v_3 = e^{(-\sqrt{-\omega_1^2})t} v_{30}, v_4 = e^{(\sqrt{-\omega_1^2})t} v_{40}, v_5 = e^{(-\sqrt{-\omega_2^2})t} v_{50}, v_6 = e^{(\sqrt{-\omega_2^2})t} v_{60} \tag{5.45}$$

The closed form expressions for the augmented states could be back substituted in the expression for the first two states. This would aid in computing the closed form expressions for the original system states. It is observed that the exponential terms for the expressions of v_3 and v_4 are complex conjugates. Hence the terms with both these states getting multiplied would result in the multiplication of their initial conditions. A similar trend is observed for v_5 and v_6 states too. With these factors accounted, the closed form expression for the first two states could be expressed as

$$\begin{aligned} v_1 &= e^{\left(\frac{1}{\sqrt{-a}}\left(a+\frac{b^2(v_{50}v_{60}\omega_1^2(-4a+\omega_1^2)+v_{30}v_{40}\omega_2^2(-4a+\omega_2^2))}{(4a-\omega_1^2)\omega_1^2(4a-\omega_2^2)\omega_2^2}\right)\right)t} v_{10} \\ v_2 &= e^{\left(\frac{1}{\sqrt{-a}}\left(-a+b^2\left(\frac{v_{30}v_{40}}{4a\omega_1^2-\omega_1^4}+\frac{v_{50}v_{60}}{4a\omega_2^2-\omega_2^4}\right)\right)\right)t} v_{20} \end{aligned} \tag{5.46}$$

By expressing the updated equation (5.46) in the matrix multiplication form, the expression for $\bar{\mathbf{J}}$ matrix is deduced. By substituting equation (5.45) in the near-identity transformation matrix and expressing it in the matrix multiplication form would resemble the expression indicated in equation (5.36). The higher the order of the TINF solution, the longer the expression would be, as it accounts for more nonlinear terms.

Since all the dynamics are observed to be expressed in the first two states, the system state evolution is evaluated in the TINF coordinate ($\bar{\mathbf{\Phi}}(t)$), using equation (5.38), for the first two states. The initial conditions in the original system coordinates($x_{10}, x_{20}, x_{30}, x_{40}, x_{50}, x_{60}$) are successively transformed to determine its corresponding values in the TINF coordinate ($v_{10}, v_{20}, v_{30}, v_{40}, v_{50}, v_{60}$). The STM in the TINF coordinate ($\bar{\mathbf{\Phi}}(t)$) is evaluated and back-transformed to its original coordinates ($\hat{\mathbf{\Phi}}(t)$). The evolution of the state over the period of time is determined using $\hat{\mathbf{\Phi}}(t)$ and the results are compared with that of the numerical integration results of the system in original coordinates.

Linear Quasi-periodic System With Damping

The Hills quasi-periodic system, equation (5.39), is updated with a damping term, as shown below

$$\ddot{x} + (a + b(\cos(\omega_1 t) + \cos(\omega_2 t)))x + d\dot{x} = 0 \tag{5.47}$$

Similar to the case without damping, the periodic coefficients are expressed as fictitious/augmented states, and the system matrix is updated, as indicated below in equation (5.48)

$$\frac{d}{dt}\begin{Bmatrix} x \\ \dot{x} \\ p_1 \\ q_1 \\ p_2 \\ q_2 \end{Bmatrix} = \begin{bmatrix} 0 & 1 & 0 & 0 & 0 & 0 \\ -a & -d & 0 & 0 & 0 & 0 \\ 0 & 0 & 0 & 1 & 0 & 0 \\ 0 & 0 & -\omega_1^2 & 0 & 0 & 0 \\ 0 & 0 & 0 & 0 & 0 & 1 \\ 0 & 0 & 0 & 0 & -\omega_2^2 & 0 \end{bmatrix} \begin{Bmatrix} x \\ \dot{x} \\ p_1 \\ q_1 \\ p_2 \\ q_2 \end{Bmatrix} + \begin{Bmatrix} 0 \\ -bx(p_1 + p_2) \\ 0 \\ 0 \\ 0 \\ 0 \end{Bmatrix} \tag{5.48}$$

The subsequent procedure to reduce the quasi-periodic system remains akin to the case without damping. A modal transformation on the updated linear constant

matrix (containing damping term) is performed to convert the updated system equation to its Jordan canonical form with semi-simple eigenvalues. Furthermore, near-identity transformations and the TINF technique reduce the system by eliminating non-prominent nonlinear terms. The STM ($\bar{\mathbf{\Phi}}(t)$) is computed from the TINF solution and back-transformed to determine $\hat{\mathbf{\Phi}}(t)$ matrix. The time evolution of the system states is determined using $\hat{\mathbf{\Phi}}(t)$ matrix and compared with numerical techniques.

The results of the temporal variation of the system states for the Hills quasi-periodic system (both with and without damping), suing the direct approach, are discussed in the subsequent section. This direct approach is also applicable towards the commutative linear quasi-periodic system, and the results of such application are detailed in the following section.

5.3.2 Results and Discussions

The direct approach is applied on a parametrically excited linear quasi-periodic system, with semi-simple eigenvalues, and compared with numerical simulations. A Hills quasi-periodic system without damping (indicated in equation (5.39)) is initially considered. The sequential application of state augmentation, modal transformation, and TINF technique reduces the system to a time-invariant form, as detailed in subsection 5.3.1. The reduced system is back-transformed to the original coordinates, and the temporal variations are compared with the numerical integration method. Later, the initial Hills quasi-periodic system is updated with a damping coefficient, and the procedure is repeated for temporal variation comparisons. Furthermore, the same direct approach is applied to the commutative quasi-periodic system. In this section, for all the quasi-periodic systems the frequencies with incommensurate ratios are $\omega_1 = 2\pi$ rads and $\omega_2 = 7$ rads.

Quasi-periodic System Without Damping

Initially, the Hills quasi-periodic system without damping is evaluated as described in subsection 5.3.1. The linear constant term is considered as $a = 3.0$, and the common coefficient of the time varying part is considered to be $b = 2.5$ for equation (5.39). The original system is subjected to state augmentation, modal transformation, and near-identity transformation to facilitate the application of the TINF technique. As indicated in equation (5.44), the reduced system after TINF application is computed as

$$\begin{bmatrix} \dot{v_1} \\ \dot{v_2} \\ \dot{v_3} \\ \dot{v_4} \\ \dot{v_5} \\ \dot{v_6} \end{bmatrix} = \begin{bmatrix} (0.0 - i1.7892)v_1 \\ (0.0 + i1.7892)v_2 \\ (0.0 - i6.2832)v_3 \\ (0.0 + i6.2832)v_4 \\ (0.0 - i7.0000)v_5 \\ (0.0 + i7.0000)v_6 \end{bmatrix} \tag{5.49}$$

As mentioned earlier, expressing equation (5.49) in the matrix multiplication form provides an expression for $\bar{\mathbf{J}}$ matrix, and it is observed to be time-invariant. Hence, the original linear parametrically excited quasi-periodic system is reduced to a time-invariant form, similar to equation (5.37).

The near-identity transformations are also expressed in the matrix multiplication form, similar to equation (5.36). The closed form expressions for the augmented states (from equation (5.49)) are substituted in the near-identity transformation matrix expression to obtain $\bar{\mathbf{P}}(t)$. The individual elements of the updated near-identity transformation matrix ($\bar{\mathbf{P}}(t)$) is indicated in the Appendix-B. The updated $\bar{\mathbf{P}}(t)$ matrix is observed to be time varying and containing both the incommensurate frequencies of the original quasi-periodic system.

As discussed in section 5.3, the STM in the TINF coordinate is computed using equation (5.38). The STM from the reduced system using the TINF technique is then back transformed to the original coordinates. The state evolution of the system using the back-transformed STM ($\hat{\mathbf{\Phi}}(t)$) for the initial conditions of $x_1(0) = 1, x_2(0) = 0$ are plotted and compared with the numerically integrated results of the original system. The comparisons of the temporal variations are indicated in Figure 5.13. The phase plot variations and their comparison with the numerical technique are indicated in Figure 5.14.

In all three plots, the numerically integrated solution is represented by the black dashed line, and the solution from the Normal Forms technique is represented by the solid red line. It is observed that the given linear quasi-periodic system is bounded and the Normal Forms solution coincides with the numerical techniques in all three plots. More cases of comparisons of temporal variations for different values of coefficients are indicated in Chapter 8.

Quasi-periodic System With Damping

The Hills quasi-periodic system updated with damping term ($d = 0.3$), as indicated in equation (5.47), is evaluated in this subsection. All the other system parameters remain the same as the case without damping ($a = 3.0, b = 2.5, \omega_1 = 2\pi$ and $\omega_2 = 7$). Similar to the system without damping, the system with damping also undergoes state augmentation, modal transformation, and application of Normal Forms technique to reduce the system as follows:-

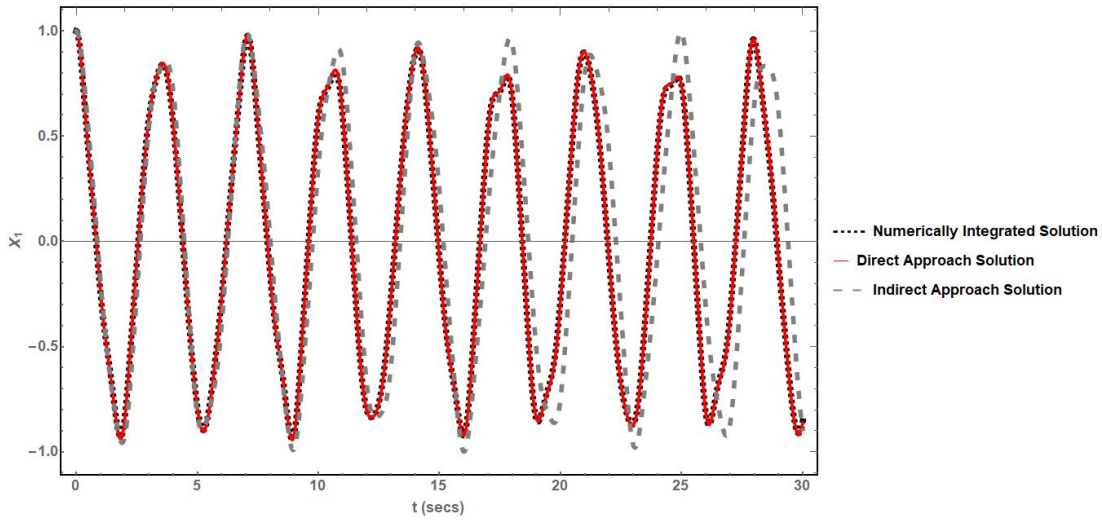

(**a**)

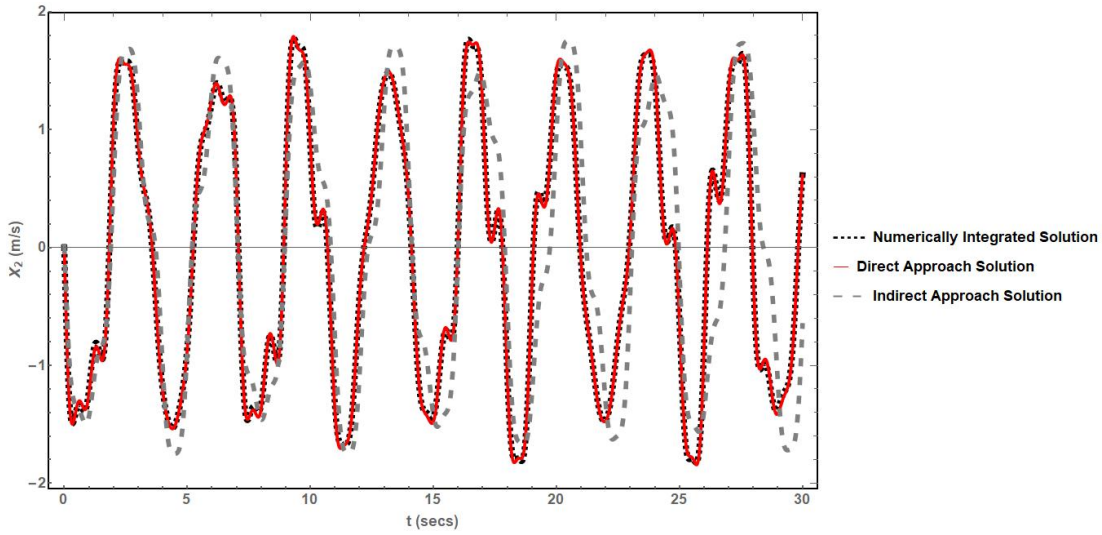

(**b**)

Figure 5.13: The System State Variation Comparisons Using Direct Approach on the Hills Quasi-periodic System Without Damping of (**a**) x_1 State, (**b**) x_2 State

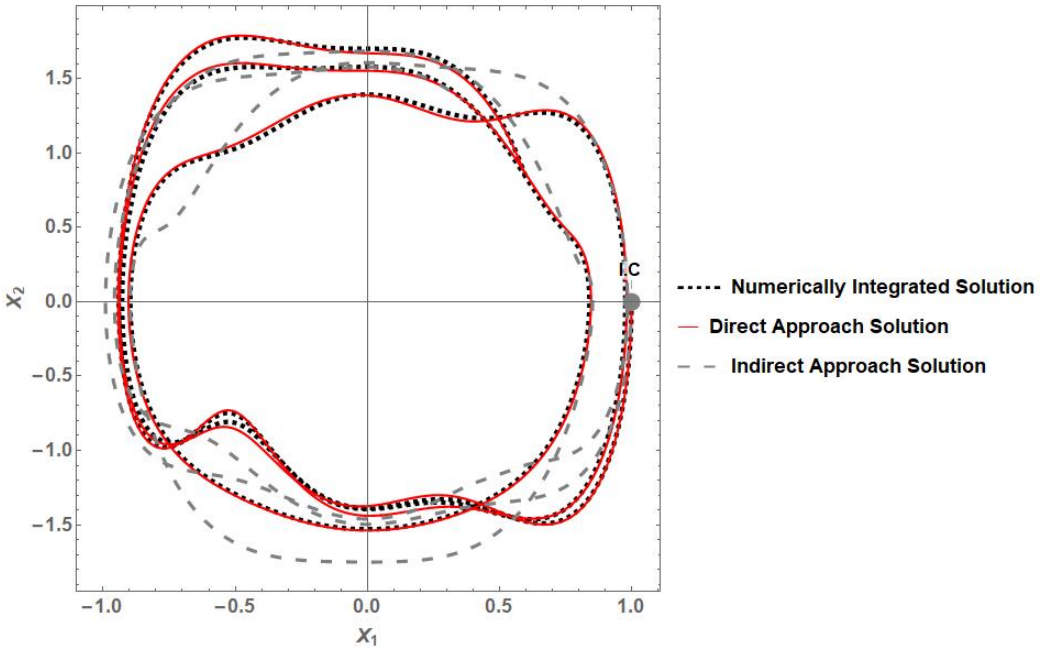

Figure 5.14: Phase Plot Comparisons of System States Using Direct Approach on the Hills Quasi-periodic System Without Damping

$$\begin{bmatrix} \dot{v_1} \\ \dot{v_2} \\ \dot{v_3} \\ \dot{v_4} \\ \dot{v_5} \\ \dot{v_6} \end{bmatrix} = \begin{bmatrix} ((-0.125 - i1.7275) - (0. + i0.0033)v_3v_4 - (0. + i0.0019)v_5v_6)v_1 \\ ((-0.125 + i1.7275) + (0. + i0.0033)v_3v_4 + (0. + i0.0019)v_5v_6)v_2 \\ (0.0 - i6.2832)v_3 \\ (0.0 + i6.2832)v_4 \\ (0.0 - i7.0000)v_5 \\ (0.0 + i7.0000)v_6 \end{bmatrix} \tag{5.50}$$

It is observed that v_3, v_4, v_5, v_6 are fictitious states, and the system dynamics are captured in the time evolution of v_1 and v_2 states. Additionally, it is observed from equation (5.50), similar to the case of a system without damping, coefficients of the augmented states (v_3, v_4) are complex conjugates, and augmented states (v_5, v_6) also follow a similar trend. The closed form expression for these augmented states are computed with the knowledge of the initial conditions. It is also noted from equation (5.50) that in the expression for the first two states(v_1, v_2), the augmented states

appear together in each term, and their multiplication results in just the product of their initial conditions at any instant. Hence, the coefficient matrix ($\bar{\mathbf{J}}$) of the reduced systems for the quasi-periodic system with damping is also found to be time-invariant.

Analogous to the system without damping, the closed-form expression for the fictitious states is substituted in the near-identity expression. Furthermore, the STM($\bar{\mathbf{\Phi}}(t)$) for the quasi-periodic system with damping is computed in the TINF coordinate, using the expression equation (5.38), and back-transformed to its original coordinates. The temporal variations of the system states are computed from the back-transformed $\bar{\mathbf{\Phi}}(t)$ and compared with the numerical integration method for the same initial conditions($x_{10} = 1.0$ and $x_{20} = 0$). The comparisons of the temporal variations are indicated in Figures 5.15a,b and the phase plot variation comparison is shown in Figure 5.16.

As indicated in Figures 5.15a,b, and 5.16, the solid red line corresponds to the back-transformed TINF solution, and the dashed black line indicates the numerical integration results. In the temporal variations, both approaches are noted to dampen dynamics over the period of time. In the phase plot, the system behavior is observed to spiral in from the initial condition. It is also observed that state evolution from the direct approach follows the numerical integration results closely in all three plots. Thus the direct expression for $\bar{\mathbf{\Phi}}(t)$ from the TINF solution, captures the state evolution characteristics, and the direct approach is validated for a linear quasi-periodic system with damping. The L-P transformation is expressed as a finite quasi-periodic Fourier series that introduces some approximation and numerical integration floating-point approximations causing a slight mismatch in Figures 5.15 and 5.16.

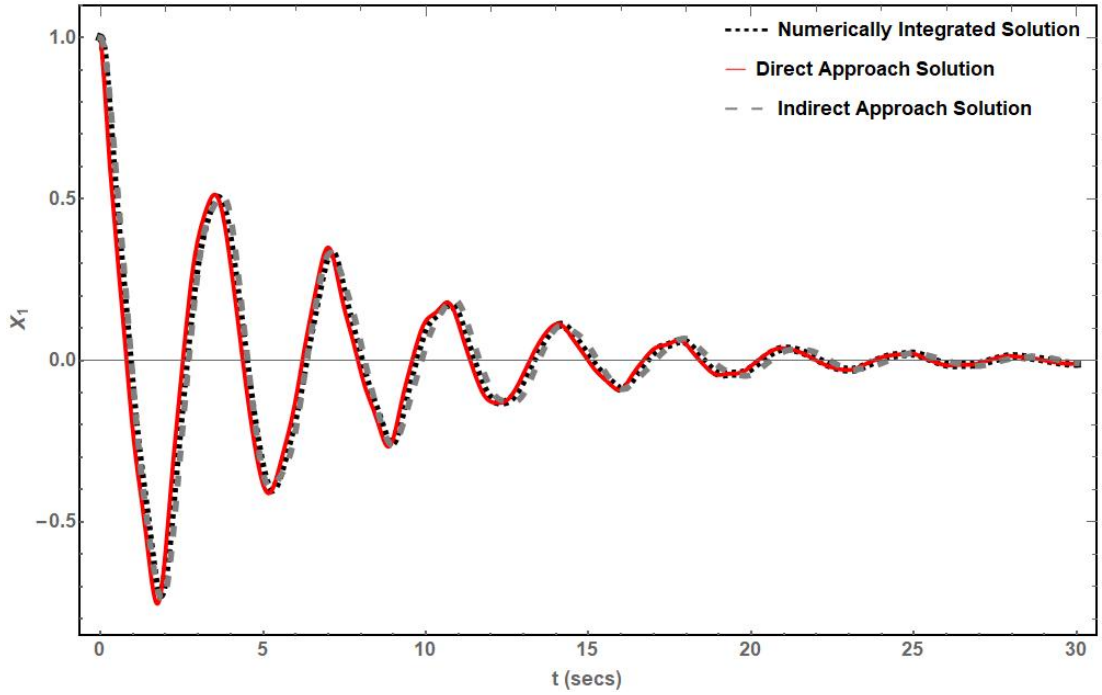

(**a**)

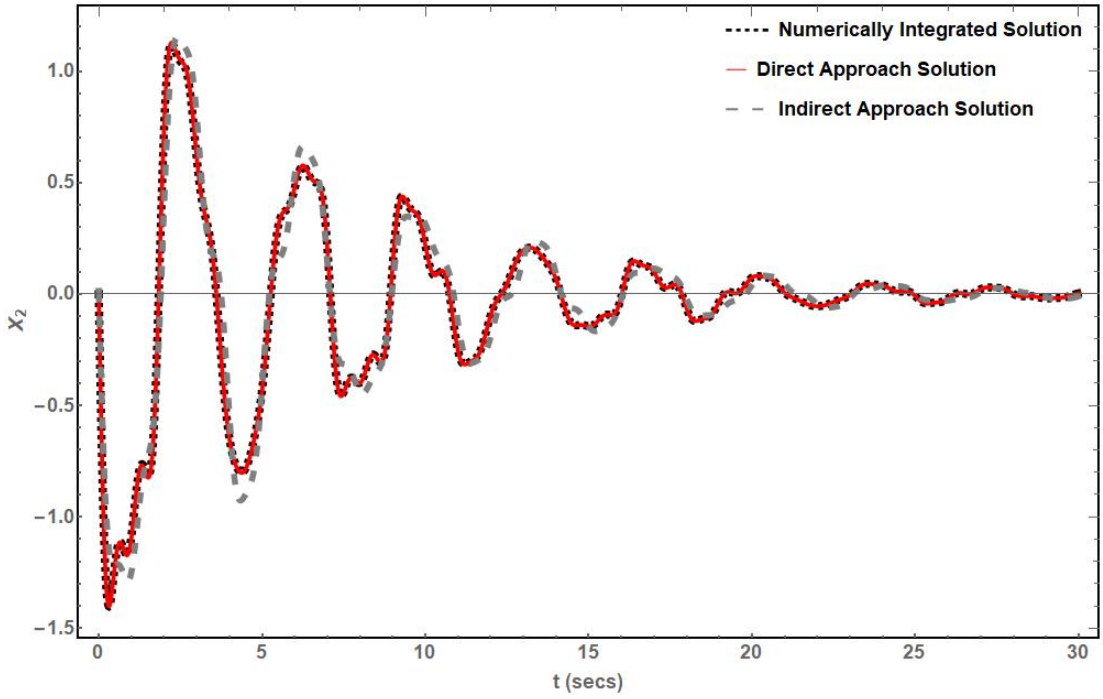

(**b**)

Figure 5.15: The System State Variation Comparisons for Direct Approach on the Hills Quasi-periodic System with Damping of (**a**) x_1 State, (**b**) x_2 State (equation 5.47)

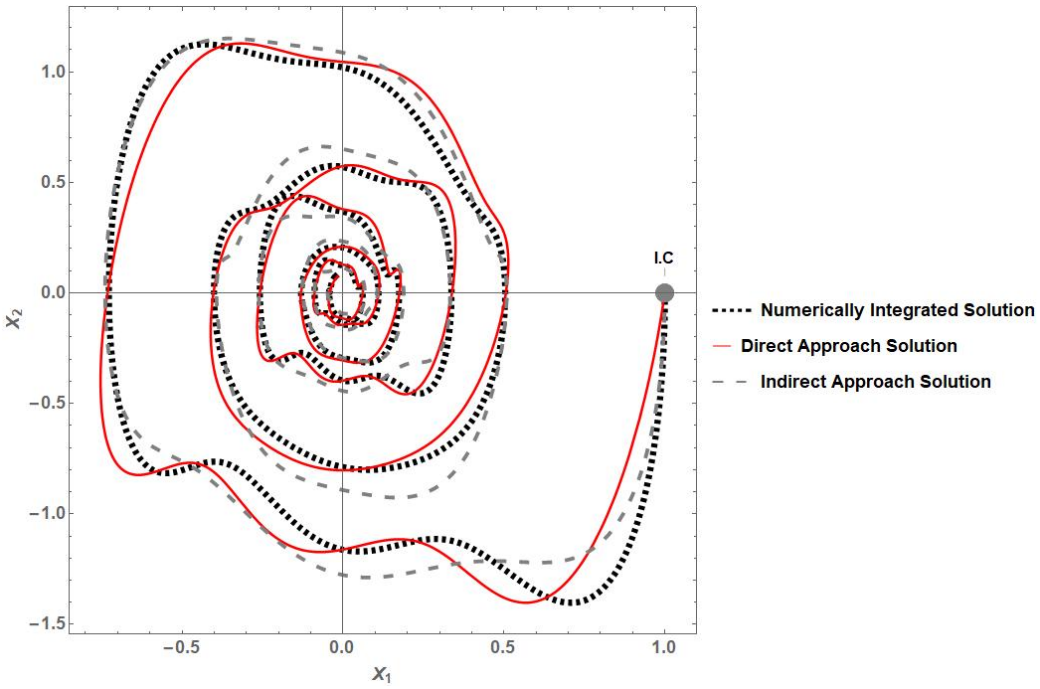

Figure 5.16: Phase Plot Comparisons of System States for Direct Approach on the Hills Quasi-periodic System with Damping (equation 5.47)

Commutative Quasi-periodic System

In this section, the analysis of was performed on a different commutative quasi-periodic system, where the trigonometric *sine* functions are replaced with *cosine* functions as indicated below

$$\begin{aligned}&\ddot{x} - 2(b_1\cos(\omega_1 t) + b_2\cos(\omega_2 t))\dot{x} + (a + (b_1\omega_1\sin(\omega_1 t) + b_2\omega_2\sin(\omega_2 t))\\&+ (b_1\cos(\omega_1 t) + b_2\cos(\omega_2 t))^2)x = 0\end{aligned} \tag{5.51}$$

Considering $x_1 = x$ and $x_2 = \dot{x}_1 - (b_1\cos(\omega_1 t) + b_2\cos(\omega_2 t))x_1$ as the system states and converting equation (5.51) to its state space form results in

$$\mathbf{A}(t) = \begin{bmatrix} b_1\cos(\omega_1 t) + b_2\cos(\omega_2 t) & 1 \\ -a & b_1\cos(\omega_1 t) + b_2\cos(\omega_2 t) \end{bmatrix} \tag{5.52}$$

Following the steps detailed in section 5.1, the system in equation (5.51) is verified

to follow the commutative property. Also, the analytical expression for the STM of the commutative quasi-periodic system in equation (5.51) was derived to be in the same form as equation (5.13), where

$$\mathbf{P}(t) = \begin{bmatrix} e^{(\frac{b_1(\sin(\omega_1 t))}{\omega_1} + \frac{b_2(\sin(\omega_2 t))}{\omega_2})} & 0 \\ 0 & e^{(\frac{b_1(\sin(\omega_1 t))}{\omega_1} + \frac{b_2(\sin(\omega_2 t))}{\omega_2})} \end{bmatrix}, \quad \mathbf{C} = C_2 = \begin{bmatrix} 0 & 1 \\ -a & 0 \end{bmatrix} \tag{5.53}$$

The expression for the L-P transformation matrix was also verified using the condition in equation (5.16). In this section, the direct approach was applied to the commutative quasi-periodic system indicated in equation (5.51). The results from the direct approach are compared with the analytical and numerical integration techniques for the temporal variations and L-P transformation matrix of the commutative quasi-periodic system.

The given commutative quasi-periodic system indicated in equation (5.51) is analyzed using the direct approach using the TINF technique and compared with the analytical and numerical techniques in this subsection. The system parameters used are $a = 1.5, b_1 = 1, b_2 = 1$ and the incommensurate frequencies as $\omega_1 = 2\pi$ rads and $\omega_2 = 7$ rads. The analytical expression for the L-P transformation ($\mathbf{P}(t)$) and $\mathbf{C}$ matrices are computed using equation (5.53). The eigenvalues of the constant $\mathbf{C}$ matrix are observed to be $0.0 \pm i1.2247$. Similarly, the numerical integration of equation (5.51) provides the numerical solution to the evolution of system states. The system parameters are substituted in the state space form (equation (5.13)) to proceed with the direct approach detailed in section 5.3.

The steps followed are in the same order as that of the Hills linear quasi-periodic system without damping. Likewise, the commutative system undergoes similar state augmentation, further a modal transformation, and subsequent near-identity trans-

formations to apply the TINF technique. The reduced system after the application of the TINF technique is indicated below in equation (5.54).

$$\begin{bmatrix} \dot{v_1} \\ \dot{v_2} \\ \dot{v_3} \\ \dot{v_4} \\ \dot{v_5} \\ \dot{v_6} \end{bmatrix} = \begin{bmatrix} (0.0 - i1.2247)v_1 \\ (0.0 + i1.2247)v_2 \\ (0.0 - i6.2832)v_3 \\ (0.0 + i6.2832)v_4 \\ (0.0 - i7.0000)v_5 \\ (0.0 + i7.0000)v_6 \end{bmatrix} \tag{5.54}$$

It is noted that the coefficients of the first two states (which are the original system states) in equation (5.54) resemble the eigenvalues of the analytically evaluated constant $\mathbf{C}$ matrix. The $\bar{\mathbf{J}}$ matrix is recognized by expressing equation (5.54) in the matrix multiplication, and its top-left 2×2 square matrix is the Jordan form of the $\mathbf{C}$ matrix. Hence, the reduced form after TINF application is also observed to be time-variant and comparable to the $\mathbf{C}$ matrix. This concurs with the Floquet type theory, explained in section 2.1.

Similar to the non-commutative system, the STM($\bar{\mathbf{\Phi}}(t)$) in the TINF coordinate is derived from the set of differential equations in equation (5.54). Consequently, $\bar{\mathbf{\Phi}}(t)$ is back-transformed to the original coordinates and multiplied with the initial conditions $x_1(0) = 1.0$ and $x_2(0) = 0$ to determine the evolution of system states over time. Meanwhile, the STM ($\mathbf{\Phi}(t)$), using the analytical L-P transformation matrix ($\mathbf{P}(t)$), is computed using equation (5.13). The STM ($\mathbf{\Phi}(t)$) is also multiplied with the same set of initial conditions to generate the variation of the system states over time analytically. The temporal variations of the system states computed using the direct approach are compared with the analytical and numerically integrated solutions in Figures 5.17a,b, and 5.18.

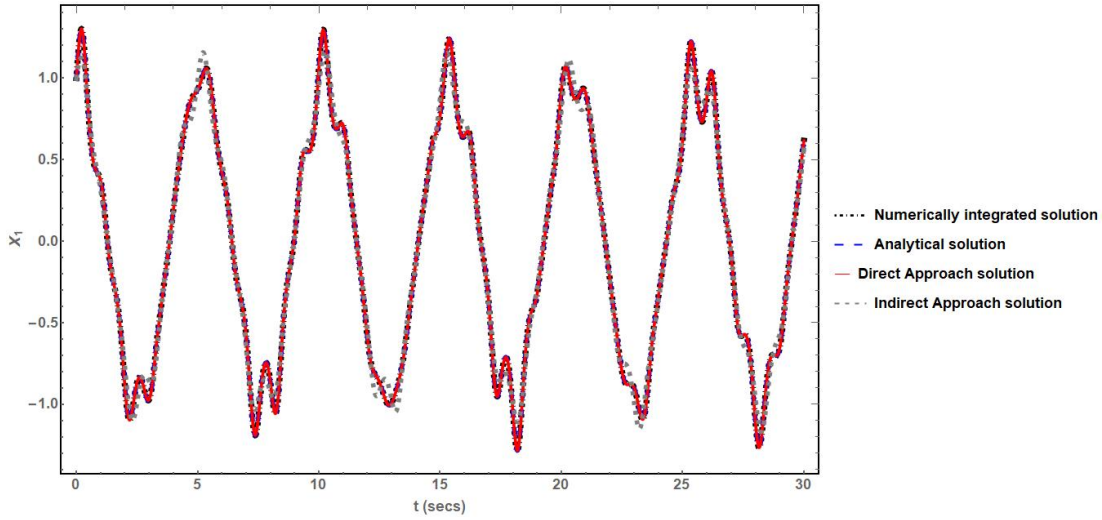

(**a**)

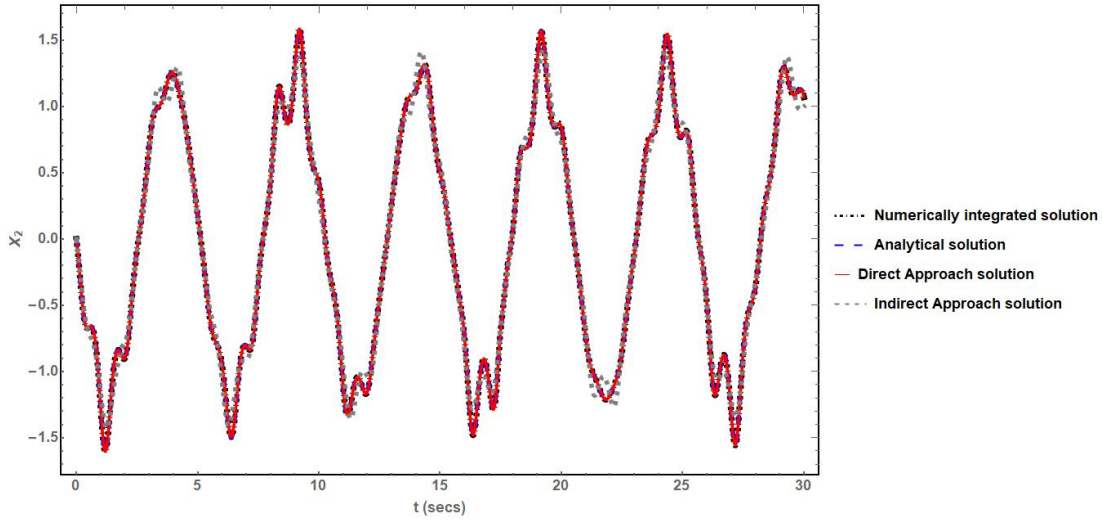

(**b**)

Figure 5.17: Comparison of System State Variation for the Commutative Quasi-periodic System Using the Direct Approach, Where (**a**) Shows x_1 State and (**b**) Shows x_2 State Variations

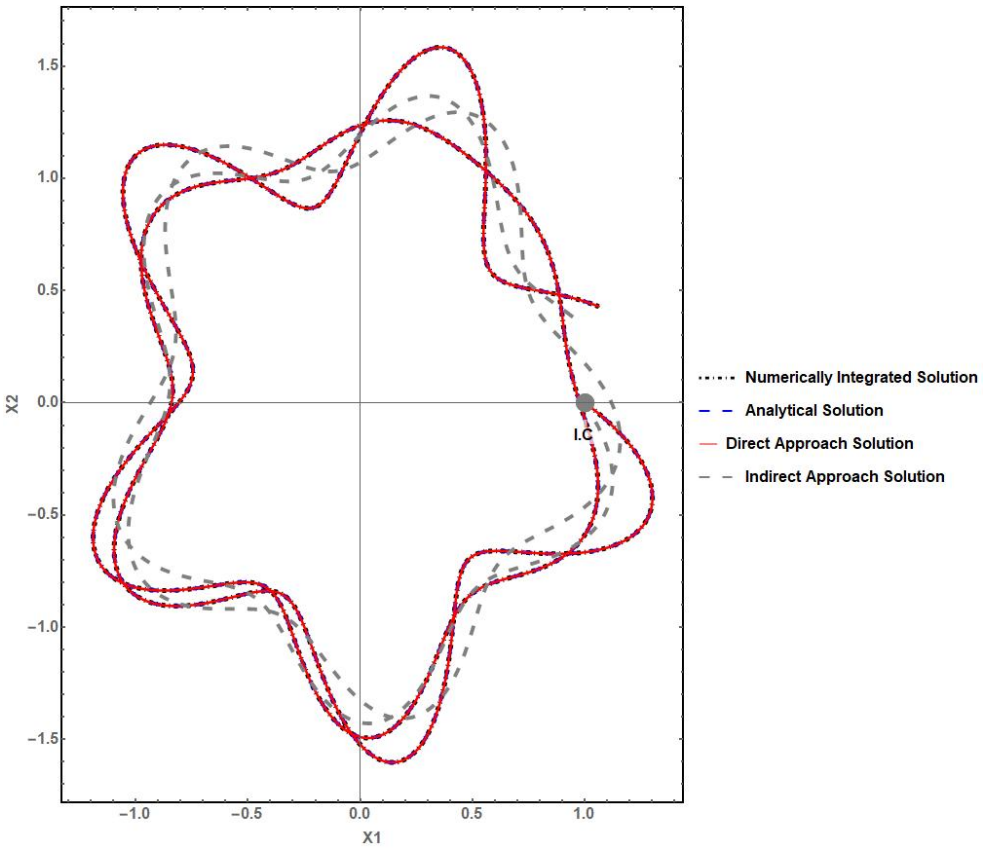

Figure 5.18: Phase Plot Comparisons of System States Using Direct Approach on the the Commutative Quasi-periodic System

As indicated in Figures 5.17a,b, the black dashed line indicates the numerically integrated solution of the original system equation (5.51), the blue dashed line indicates the state evolution variation from the analytically derived STM($\mathbf{\Phi}(t)$) and the solid red line indicates the back-transformed Normal Forms solution as per the direct approach for non-commutative systems. The simulations are run for 30 seconds, and the results are all in unison. Therefore, a given commutative quasi-periodic system can be reduced to a time invariant form analytically using an L-P transformation matrix. This validates the extension of Floquet type theory towards the commutative quasi-periodic system. Moreover, the direct approach is also applicable towards the commutative quasi-periodic system and would generate comparable results with both numerical integration and analytical approaches.

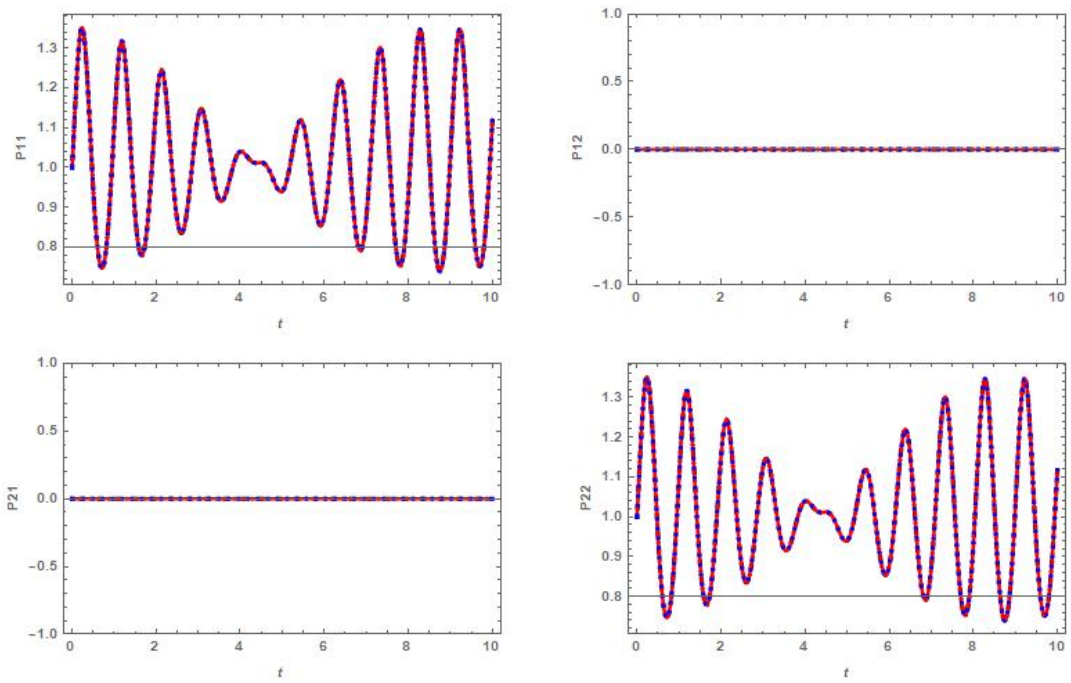

Figure 5.19: Comparison of Element-wise Variation of the L-P Transformation Matrix ($\mathbf{P}_{ij}(t)$) for the Commutative Quasi-periodic System

Since the temporal variations match closely and the $\mathbf{C}$ matrix is known for the given commutative quasi-periodic system, the L-P transformation matrix could be computed from the temporal variations of the back-transformed Normal Forms solutions. The temporal variations of the system states are evaluated for the initial conditions of $x_1(0) = 1.0; x_2(0) = 0.0$ and $x_1(0) = 0.0; x_2(0) = 1.0$. Furthermore, the resulting temporal variations are concatenated such that the term $\mathbf{x}(0)$, in equation (5.15), becomes an identity matrix. The fully populated $\mathbf{x}(t)$ matrix and the analytically derived $\mathbf{C}$ matrix are substituted in equation (5.15) to compute the L-P transformation matrix from the direct approach. Likewise, the numerically integrated solutions of the system states are also utilized to compute the L-P transformation matrix. The comparison of the element-wise variations for the L-P transformation matrix ($\mathbf{P}_{ij}(t)$), with the analytical expression and the numerically derived solutions, are evaluated for the period of 10 secs and are displayed in Figure 5.19.

In Figure 5.19, the blue dashed line represents the variations computed from analytical expression, the black dashed line represents the variations derived from the numerically integrated solutions, and the solid red line represents the variations computed from the direct approach. It is observed that all the approaches are in agreement in all four elements. It is also noted that the variation of the diagonal elements indicates the presence of two frequencies, and this in unison with the theories formulated by Murdock (1978); Puig (2002); Puig and Simó (2006). Hence the closed form expression for the L-P transformation matrix for a commutative quasi-periodic system is verified.

The $\bar{\mathbf{J}}$ matrix for both the Hills quasi-periodic systems (with and without damping) and the commutative system was proven to be time-invariant. Hence, it could be inferred that the direct approach of the Normal Forms technique was successful in reducing both the commutative and non-commutative quasi-periodic systems (with semi-simple eigenvalues) to a time-invariant form. The expression in equation (5.13) captures the dynamical characteristics from the TINF solution. The back-transformed STM ($\hat{\mathbf{\Phi}}(t)$) successfully generated the temporal variations for the system states comparable to the numerical techniques for all the cases of the quasi-periodic system discussed. Furthermore, the closed-form expression for the L-P transformation matrix was computed from these temporal variations and validated with the analytical and numerical techniques for the commutative system. Since this method is based on the direct application of Normal Forms, it is widely applicable.

The technique used in this section is based on state augmentation and the application of Normal Forms to compute the L-P transformation. The overall approach could be viewed as a variation of averaging technique by Sanders *et al.* (2007). However, this approach works quite well even though the coefficient multiplying the quasi-periodic term is not small and results comparable to both numerical and analytical techniques

are obtained. Furthermore, the frequencies close to zero and very large would also affect the approximation process. However, this approach may not yield satisfactory results for systems with very strong periodic and quasi-periodic excitation. In such cases, one has to employ the method of successive L-F transformation in conjunction with state augmentation and the Normal Forms technique. This method is briefly explained in Chapter 8.

5.4 Conclusion

In this chapter, a brief overview of quasi-periodic systems and their applications are provided. Furthermore, a new class of quasi-periodic systems, satisfying the commutative property was introduced. The extension of Floquet theory towards the analysis of commutative quasi-periodic systems was demonstrated analytically. The transformation of a linear quasi-periodic commutative system to a time-invariant form was verified and validated analytically using a toy problem.

Later, a modified version of prior work introduced an indirect approach to analyze the non-commutative linear quasi-periodic systems. The indirect approach was too successful in transforming a non-commutative linear quasi-periodic system to a time-invariant form. It was also capable of reproducing the temporal variations of the system states comparable to that of numerical methods for linear systems with weak quasi-periodic excitations. Moreover, splitting the system to perform L-F transformation becomes challenging when both periodic and quasi-periodic terms are equally excited.

A direct approach, analogous to the unified theory for a periodic system, was introduced to aid in the analysis of an equally excited non-commutative quasi-periodic systems. It was observed that the direct approach avoids the intermediate step of splitting the system and performing L-F transformation. The direct state augmen-

tation reduces the computational complexity and aids in providing a closed form expression for the L-P transformation and STM for the linear quasi-periodic systems. Both indirect and direct approaches were tested with the case of Hills quasi-periodic system with and without damping. It was observed that the results for the temporal variations from the numerical techniques matched very well with both approaches in both cases. A successive L-F transformation technique is proposed for a strong quasi-periodic system, where direct application of Normal Forms or averaging type techniques are not expected to provide good results. A generic framework to this approach is introduced in Chapter 8.

Furthermore, both indirect and direct approaches were tested on the commutative quasi-periodic system and reproduced results comparable to the analytical and numerical techniques. The results were validated using comparisons on temporal variations and element-wise variation of the L-P transformation matrix. However, the element-wise variation of the L-P transformation matrix was observed to be better using the direct approach. This validates the extension of the unified theory applicable to both commutative and non-commutative linear quasi-periodic systems. Since the L-P transformation matrix from the direct approach performs better, it is applied to analyze nonlinear systems and model order reduction in the subsequent chapter.

Chapter 6

APPLICATIONS OF L-P TRANSFORMATION

The earliest analysis on quasi-periodic systems, using the Floquet type theory, was performed by Murdock (1978). As per this theory a transformation (known as Lyapunov-Perron Transformation) converts the linear time varying coefficient of the system to a linear time invariant term. Even though the applications and properties of the Lyapunov-Perron (L-P) transformation matrix were discussed, a practical method to compute it (analytically/numerically) was not discussed.

Similar to the L-F transformation for the time-periodic system, the L-P transformation aids in the analyzing perturbed linear quasi-periodic systems. As explained in chapter 5, the unified approach can generate STM as explicit function of time, for linear quasi-periodic systems. Similarly, the closed-form expression for L-P transformation can be computed from the STM and further applied to analyze perturbed systems. The inverse of the time-varying L-P transformation matrix also can be computed using the methods detailed in section 4.2.

6.1 Application: Externally Excited Quasi-periodic System

Consider a linear quasi-periodic system subjected to external excitation given by

$$\dot{\mathbf{x}}(t) = \mathbf{A}(t)\mathbf{x}(t) + \mathbf{f}(t) \tag{6.1}$$

where $\mathbf{f}(t)$ is the external excitation term. Applying the L-P transformation $\mathbf{x}(t) = \bar{\mathbf{P}}(t)\mathbf{v}(t)$ and the inverse of the L-P Transformation $\bar{\mathbf{P}}^{-1}(t)$ results in the following equation

$$\dot{\mathbf{v}} = \bar{\mathbf{J}}\mathbf{v} + \bar{\mathbf{P}}^{-1}(t)\mathbf{f}(t) = \bar{\mathbf{J}}\mathbf{v} + \mathbf{F}(t) \tag{6.2}$$

Similar to the case of the periodic system, discussed in section 4.3, one can use convolution integral to find the system's response given by equation (6.2) or use numerical integration. The convolution integral shown in the equation (4.13) yields the resonance condition (in semi-simple case) given by equation (4.14). The result obtained in the $\mathbf{v}$ domain can be transformed to the original coordinate $\mathbf{x}(t)$ via reversing the L-P and modal transformations sequence.

6.1.1 Example-5: A Commutative Quasi-periodic System Subjected to External Excitation

In this example, the commutative quasi-periodic system, discussed in section 5.3.2, is updated with an external excitation term as shown below

$$\begin{aligned} &\ddot{x} - 2(b_1\cos(\omega_1 t) + b_2\cos(\omega_2 t))\dot{x} + (a + (b_1\omega_1\sin(\omega_1 t) + b_2\omega_2\sin(\omega_2 t)) \\ &+ (b_1\cos(\omega_1 t) + b_2\cos(\omega_2 t))^2)x = f(t) \end{aligned} \tag{6.3}$$

where ω_1 and ω_2 are incommensurate frequencies and $f(t) = c\cos(\Omega t)$ is a deterministic external excitation. The constants a, b_1, b_2 are real positive integers. It can be converted to the state space form, as indicated in equation (6.1), by considering the system states $\mathbf{x} = [x_1, x_2]^T$ as detailed in section 5.3.2. The linear part remains the same as that of equation (5.52), and hence the closed form expressions for the STM, L-P transformation matrix, and exponent matrix remains the same as indicated in section 5.3.2, which results in

$$\mathbf{P}(t) = \begin{bmatrix} e^{g(t)} & 0 \\ 0 & e^{g(t)} \end{bmatrix}, \mathbf{C} = C_2 = \begin{bmatrix} 0 & 1 \\ -a & 0 \end{bmatrix}, \quad g(t) = \frac{b_1(\sin(\omega_1 t))}{\omega_1} + \frac{b_2(\sin(\omega_2 t))}{\omega_2} \tag{6.4}$$

Since the analytical expression of $\mathbf{P}(t)$ matrix aids in reducing the linear part of the quasi-periodic system (equation (6.3)) to a time-invariant form (equation (5.2)), the application of transformation, $\mathbf{x}(t) = \mathbf{P}(t)\mathbf{z}(t)$, to equation (6.1) yields

$$\dot{\mathbf{z}} = \mathbf{C}\mathbf{z} + \mathbf{P}^{-1}(t)\mathbf{f}(t) = \mathbf{C}\mathbf{z} + \mathbf{F}(t) \tag{6.5}$$

The equation (6.5) can be solved analytically using convolution integral as

$$\mathbf{z}(t) = e^{\mathbf{C}t}\mathbf{z}(0) + \int_0^t e^{\mathbf{C}(t-s)}\mathbf{F}(s)ds \tag{6.6}$$

Once the solution of $\mathbf{z}(t)$ is obtained, the solution in $\mathbf{x}(t)$ can be obtained using the L-P transformation, $\mathbf{x}(t) = \mathbf{P}(t)\mathbf{z}(t)$. This solution is an analytical solution, as the analytical expressions in equation (6.4) are utilized to compute the solutions. Meanwhile, the L-P transformation can also be computed using the direct Normal Forms approach and back-transformed to the original coordinates. This solution is called the Normal Forms based solution. For comparison, the equation (6.3) can be numerically integrated, and the response in $\mathbf{x}(t)$ can be obtained directly, resulting in a numerically integrated solution. In Figure 6.1, the temporal variations obtained via all three methods are compared for the case of given commutative quasi-periodic system with system parameters $a = 1.5$, $b_1 = b_2 = 1$, $\omega_1 = 2\pi$ rads, $\omega_2 = 7$ rads and external excitation $c = 1$, $\Omega = 6$ rads.

In Figure 6.1, the black dashed line corresponds to the numerically integrated solution, the solid red line represents the Normal Forms based solution, and the blue

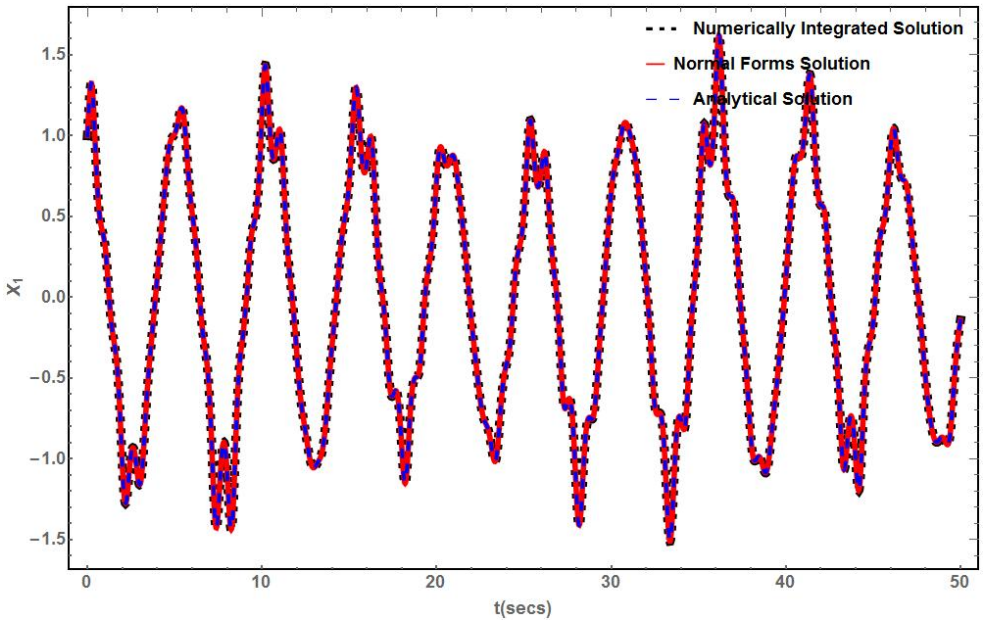

(**a**)

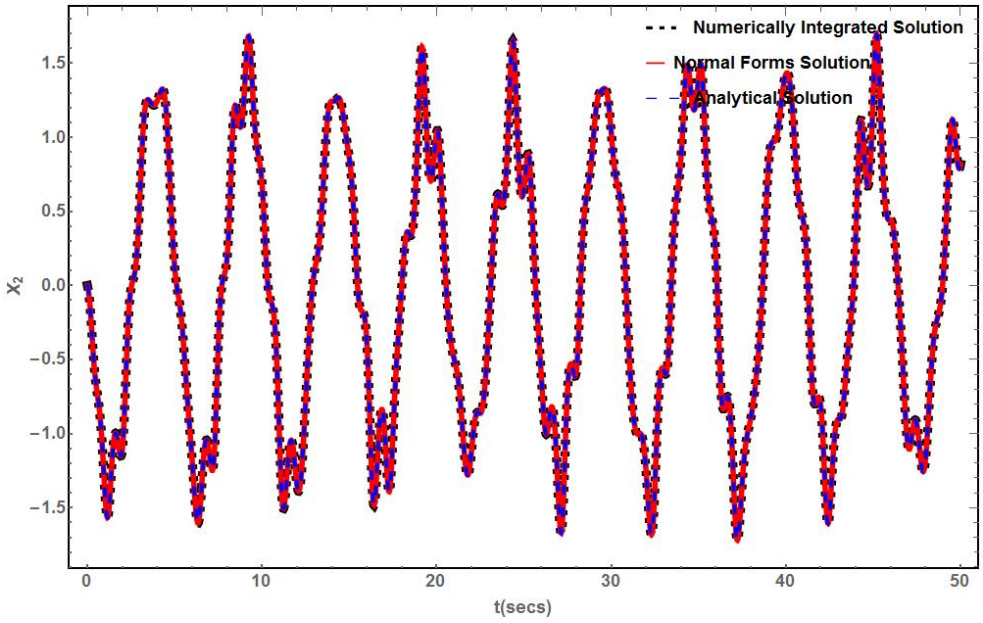

(**b**)

Figure 6.1: Comparison of System State Variation for the Commutative Quasi-periodic System with External Forcing, Where (**a**) Shows x_1 State and (**b**) Shows x_2 State Variations

long dashed line indicating the analytical solution. It can be seen that all the solutions match very well for both the system states.

6.1.2 *Example-6: A Non-commutative Mathieu-hill Type Quasi-periodic System Subjected to External Excitation*

Consider the Mathieu-Hill quasi-periodic system (from equation (5.39)) subjected to external excitation

$$\ddot{x} + (a + b\cos(\omega_1 t) + b\cos(\omega_2 t))x = c\cos(\Omega t) \tag{6.7}$$

where a and b are the system parameters, ω_1 and ω_2 are the incommensurate frequencies. By transforming the equation (6.7) into the state space form and comparing it to equation (6.1), gives us

$$\mathbf{A}(t) = \begin{bmatrix} 0 & 1 \\ -(a + b\cos(\omega_1 t) + b\cos(\omega_2 t)) & 0 \end{bmatrix}, \quad \mathbf{f}(t) = \begin{bmatrix} 0 \\ c\cos(\Omega t) \end{bmatrix} \tag{6.8}$$

The system parameters considered are $a = 3$, $b = 2.5$, the incommensurate frequencies as $\omega_1 = 2\pi$ rads, $\omega_2 = 7$ rads and external excitation $c = 1$, $\Omega = 6$ rads. One can find the L-P transformation $\bar{\mathbf{P}}(t)$ and the inverse L-P transformation $\bar{\mathbf{P}}^{-1}(t)$ for the linear system, using the direct approach using the TINF technique discussed in section 5.3. The equation (6.8) is transformed to the equation in the form of equation (6.2), where

$$\bar{\mathbf{J}} = \begin{bmatrix} 0 - i1.7893 & 0 \\ 0 & 0 + i1.7893 \end{bmatrix} \tag{6.9}$$

As before, the equation (6.2) can be solved using convolution integral to obtain solutions in the $\mathbf{v}(t)$ domain. The solution in $\mathbf{x}(t)$ can be obtained using the L-P transformation $\mathbf{x} = \bar{\mathbf{P}}(t)\mathbf{v}$. This solution is called the Normal Forms based solution.

For comparison, the equation (6.7) can be numerically integrated, and the response in $\mathbf{x}(t)$ can be obtained directly. In Figure 6.2, the temporal variations of the Normal Forms based solution and numerically integrated solutions are compared for the case of a given non-commutative quasi-periodic system.

In Figure 6.2, the black dashed line corresponds to the numerically integrated solution, and the solid red line represents the Normal Forms based solution. It can be seen that both the solutions match very well.

6.2 Application: Analysis Of Non-Linear Quasi-Periodic Systems

The L-P Transformation is computed via state augmentation, and the method of Normal Forms can be applied to quasi-periodic nonlinear systems. In the process, one obtains additional resonance conditions representing interactions between the nonlinearity and quasi-periodic excitation. Consider a quasi-periodic nonlinear system given by equation (6.10).

$$\dot{\mathbf{x}}(t) = \mathbf{A}(t)\mathbf{x}(t) + \mathbf{f}(\mathbf{x}, t) \tag{6.10}$$

After applying the L-P transformation $\mathbf{x} = \bar{\mathbf{P}}(t)\mathbf{y}$ and inverse L-P transformation $\bar{\mathbf{P}}^{-1}(t)$ computed via the methods described in section 4.2, the system can be expressed in the form

$$\dot{\mathbf{y}} = \bar{\mathbf{J}}\mathbf{y} + \bar{\mathbf{P}}^{-1}(t)\mathbf{f}(\mathbf{y}, \mathbf{t}) \tag{6.11}$$

The equation (6.11) can be solved using TDNF (detailed in section 2.3.2) where the near identity transformation of the form, similar to equation (2.23), given by

$$\mathbf{y} = \mathbf{v} + \mathbf{h}_r(\mathbf{v}, t) \tag{6.12}$$

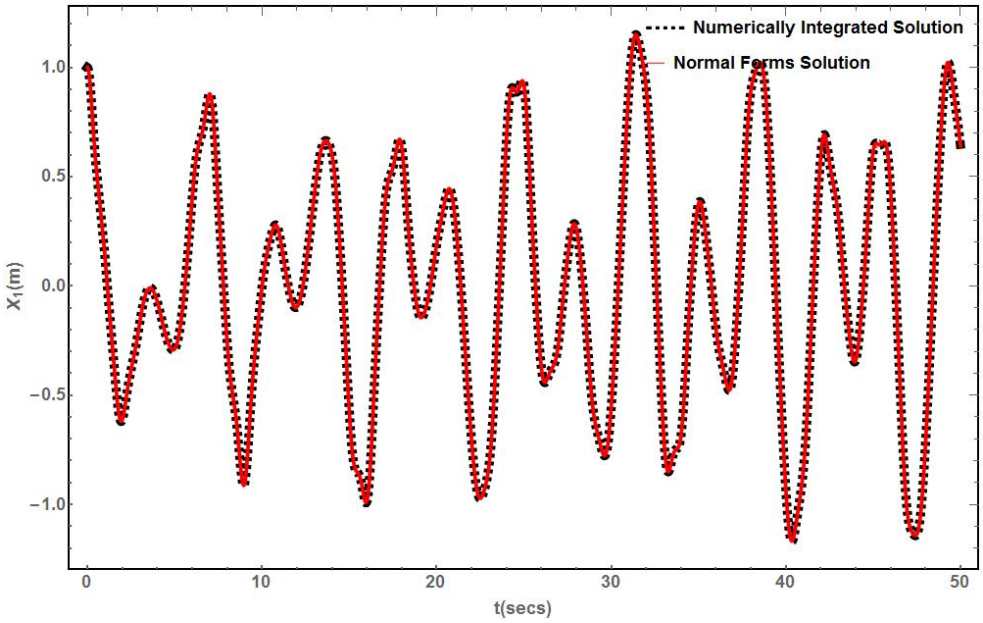

(**a**)

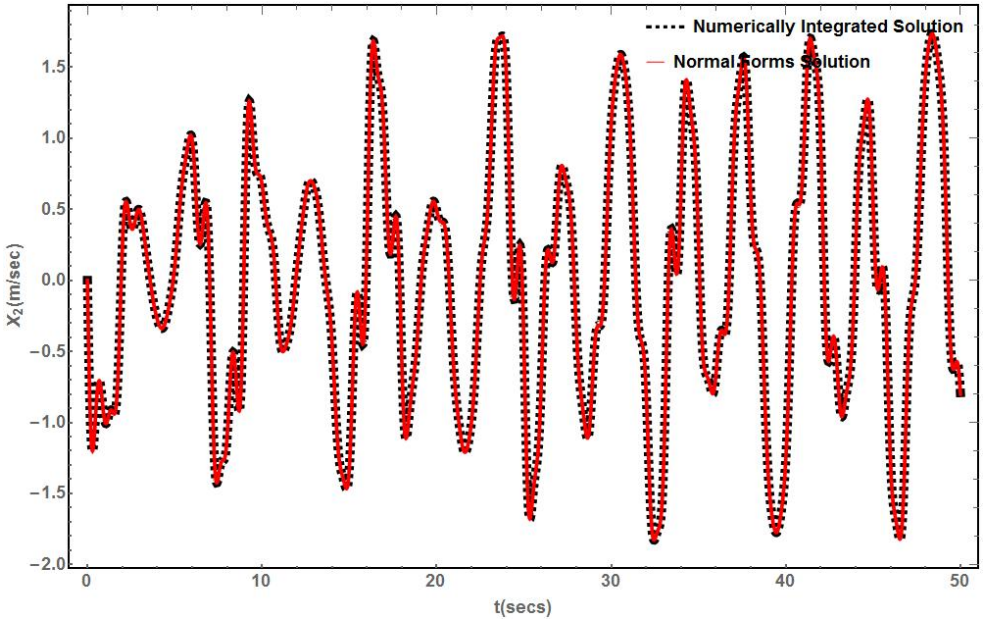

(**b**)

Figure 6.2: Comparison of System State Variation for the Non-commutative Hill's Quasi-periodic System with External Excitation, Where (**a**) Shows x_1 State and (**b**) Shows x_2 State Variations

where

$$\mathbf{h}_r(\mathbf{v},t) = \sum_{\bar{\mathbf{m}}} \bar{\mathbf{h}}_i(t)\mathbf{v}_1^{m_1}...\mathbf{v}_r^{m_r},$$
$$\bar{\mathbf{m}} = (m_1,...,m_r)^T, m_1 + ... + m_r = i,\ i = 2,3,...,k$$

and $\bar{\mathbf{h}}_i(t)$ are the unknown quasi-periodic vector coefficients. This approach yields quasi-periodic solvability conditions. For more details on this approach, interested readers are referred to Wooden and Sinha (2007). As explained in section 2.3.2, if there are no resonances, the system in equation (6.11) can be reduced to the form

$$\dot{\mathbf{v}} = \bar{\mathbf{J}}\mathbf{v} \tag{6.13}$$

After solving equation (6.13) and back-transforming it to the original coordinates, the solution in the $\mathbf{x}$ domain is obtained.

6.2.1 *Example-7: A Non-commutative Mathieu-hill Type Quasi-periodic System Subjected to Nonlinear Perturbations*

As an example, consider the Mathieu-Hill type quasi-periodic system (from equation (5.39)) subjected to nonlinear perturbation.

$$\ddot{x} + (a + b\cos(\omega_1 t) + b\cos(\omega_2 t))x + \epsilon x^3 = 0 \tag{6.14}$$

where a, b and ϵ are the system parameters, ω_1 and ω_2 are the incommensurate frequencies. By transforming the equation (6.14) into the state space form

$$\underbrace{\frac{d}{dt}\begin{bmatrix} x_1 \\ x_2 \end{bmatrix}}_{\dot{\mathbf{x}}} = \underbrace{\begin{bmatrix} 0 & 1 \\ -(a + b\cos(\omega_1 t) + b\cos(\omega_2 t)) & 0 \end{bmatrix}}_{\mathbf{A}(t)} \underbrace{\begin{bmatrix} x_1 \\ x_2 \end{bmatrix}}_{\mathbf{x}} - \underbrace{\begin{bmatrix} 0 \\ \epsilon x_1^3 \end{bmatrix}}_{\mathbf{f}(\mathbf{x})} \tag{6.15}$$

In this section, the system parameters considered are $a = 3.0$, $b = 2.5$, $\omega_1 = 2\pi$ rads, $\omega_2 = 7$ rads and $\epsilon = 0.3$. Similar to the case with external excitation (section 6.1) the L-P transformation $\bar{\mathbf{P}}(t)$ is computed for the linear part using the direct approach of the TINF technique. As mentioned earlier, by applying the L-P transformation $\mathbf{x} = \bar{\mathbf{P}}(t)\mathbf{y}$ and using the inverse L-P transformation $\bar{\mathbf{P}}^{-1}(t)$, the system in equation (6.15) can be expressed in a form similar to equation (6.11). It is noted that $\mathbf{f}(\mathbf{y}, \mathbf{t})$ has third-order monomials in $\mathbf{y}$. The equation (6.11) could be numerically integrated, and the solutions can be back transformed to obtain the temporal variations in the original coordinates, using L-P transformed solution.

However, since the Normal Forms technique is directly applicable to the nonlinear system. The TDNF of the form indicated in section 2.3.2 is applied. The TDNF solution of the equation (6.15) is given by

$$\left.\begin{aligned} \dot{v}_1 &= -i\ 1.78926 v_1 - i\ 0.0866 v_1^2 v_2 \\ \dot{v}_2 &= +i\ 1.78926 v_2 + i\ 0.0866 v_1 v_2^2 \end{aligned}\right\} \tag{6.16}$$

The given form can be solved analytically,using the complex change of variables $v_1(t) = u_1 - iu_2$, $v_2(t) = u_1 + iu_2$ and subsequently applying the polar coordinate transformation $u_1 = R\cos\theta$ and $u_2 = R\sin\theta$ one obtains

$$\left.\begin{aligned} \dot{R} &= 0 \\ \dot{\theta} &= -1.78926 - 0.08660 R^2 \end{aligned}\right\} \tag{6.17}$$

It can be observed that the equation (6.17) can be solved in the closed-form, and inverting the sequence of transformations state evolution in $x(t)$ and $\dot{x}(t)$ can be obtained. This solution is called the "Analytical Normal Forms Solution". The temporal variations of both the solutions are compared with the numerically integrated solution of equation (6.14) in Figures 6.3a,b.

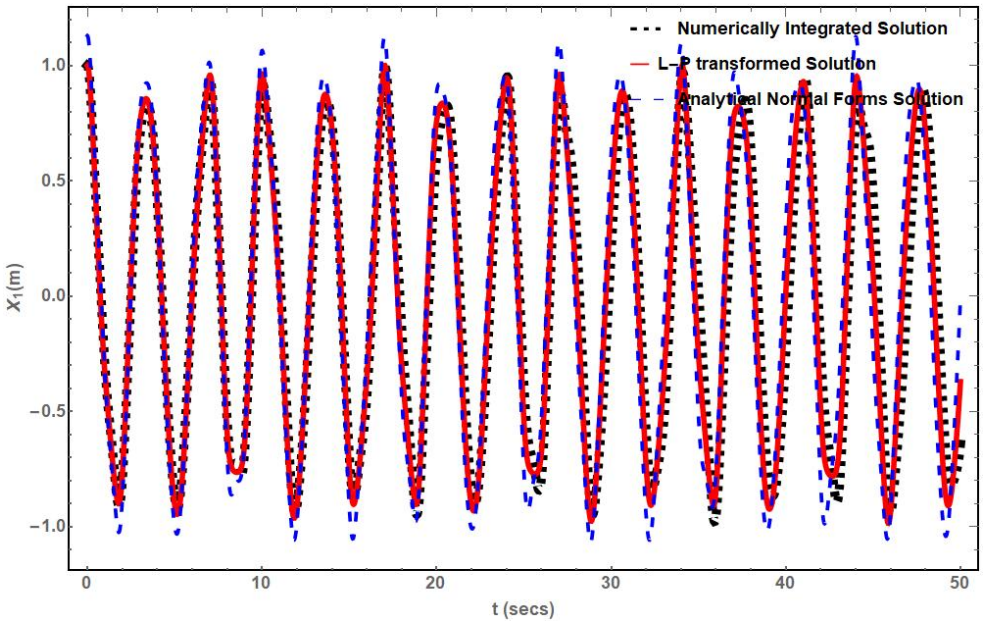

(**a**)

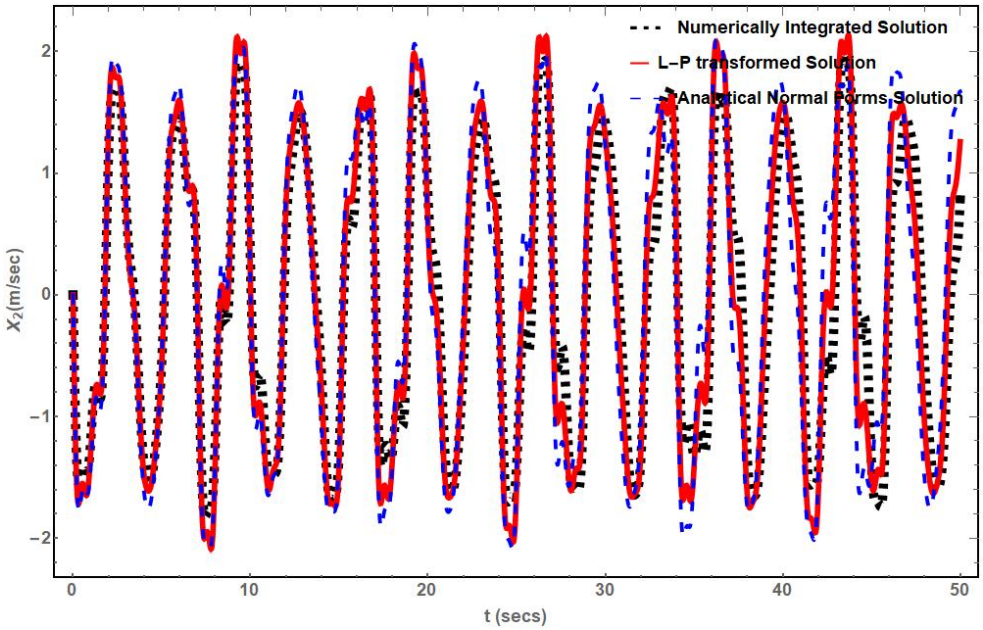

(**b**)

Figure 6.3: Comparison of System State Variation for the Non-commutative Hill's Quasi-periodic System with Nonlinear Terms, Where (**a**) Shows x_1 State and (**b**) Shows x_2 State Variations

In Figure 6.3, the black dashed line indicates the numerically integrated solution, the solid red line corresponds to the L-P transformed solution, and the blue long dashed line represents the analytical Normal Forms solution. It can be seen that all the solutions match very well for both the system states. The L-P transformed system response is in close agreement with the numerically integrated solution.

6.2.2 Conclusions

In this chapter, the applications of L-P transformation, computed using the direct approach, towards the analysis of linear quasi-periodic systems subjected to external excitations and nonlinear quasi-periodic systems are explained comprehensively. One also obtains the solvability conditions that indicate potential resonances between the quasi-periodicity and frequency of external excitation or quasi-periodicity and nonlinearity.

One could use this technique for symbolic order reduction and controller design for linear and nonlinear quasi-periodic systems. One could also use this approach to study stochastic parametric excitation on the stability of a quasi-periodic system. This approach is based on applying Normal Forms theory (that can be viewed as an extension of the higher-order averaging technique); it has the same limitations. For the nonlinear systems with higher dimensions, a model order reduction approach (similar to Sinha *et al.* (2005b)) is proposed using the L-P transformation matrix of the linear part and is presented in the next section.

6.3 Application: Model Order Reduction Techniques for Higher Order Nonlinearity

Some of the well-known model order reduction techniques include the method of Proper Orthogonal Decomposition (POD) by Kerschen *et al.* (2005), Nonlinear Normal Modes (NNM) by Apiwattanalunggarn *et al.* (2005), Slow-Fast Decomposi-

tion (SFD) by Haller and Ponsioen (2017), method of multiple scales by Luongo and Di Egidio (2005) and projection method by Sinha *et al.* (2005b); Broomhead and Kirby (2005). The application of the reduced order dynamical model towards MEMS devices is detailed by Nayfeh *et al.* (2005). The nonlinear behavior of the continuous rotor system is reduced using the standard and nonlinear Galerkin methods by Ding and Zhang (2012). Nayfeh (2008) compared the method of multiple scales with a combination of Normal Forms and center manifold reduction method for identifying Hopf bifurcations by order reduction in retarded nonlinear dynamical systems. Harrington and Van Gorder (2017) demonstrate the dimension reduction of high dimensional chaotic systems using the method of differential elimination. For the cases in which reduction is not possible in terms of differential operators, Harrington and Van Gorder (2017) also showcase a method to find the Lyapunov functions and contraction maps. Further detailed explanations on various MOR techniques and their application towards dynamical systems are provided by Rega and Troger (2005).

Generally, the order reduction procedure comprises of the following steps:-

1. Study the large-scale system and identify the dominant states contributing to the dominant dynamics.

2. Neglect or replace the non-dominant states by appropriate functions of dominant states

3. Formulate an equivalent reduced order system comprising of only the dominant states.

In this section, the 'automatic' order reduction of nonlinear ordinary differential equations with quasi-periodic coefficients is emphasized and expressed in state-space form as

$$\dot{\mathbf{x}} = \mathbf{A}(t)\mathbf{x} + \mathbf{f}(\mathbf{x}, t) \tag{6.18}$$

where $\mathbf{A}(t)$ is an $n \times n$ matrix with quasi-periodic coefficients and $\mathbf{f}(\mathbf{x}, t)$ is a nonlinear function with monomials of $\mathbf{x}$ and $\mathbf{x}$ is an n vector of appropriate dimensions. The objective of order reduction is to construct a reduced r^{th} order system

$$\dot{\mathbf{x}}_r = \mathbf{A}_r(t)\mathbf{x}_r + \mathbf{f}_r(\mathbf{x}_r, t) \tag{6.19}$$

that captures the intrinsic behavior of the large-scale system. The $\mathbf{A}(t)$ matrix is considered to be quasi-periodic and contains terms with incommensurate frequencies. To the best of the author's knowledge no techniques are available that would allow direct reduced order from equation (6.18) to equation (6.19). In this section, three order reduction techniques are presented that would facilitate such a transformation.

6.3.1 Order Reduction Using Linear Projection

Let us consider a nonlinear quasi-periodic system of the form

$$\dot{\mathbf{x}}(t) = \mathbf{A}(t)\mathbf{x}(t) + \mathbf{f}(\mathbf{x}, t) \tag{6.20}$$

where $\mathbf{x}$ is a $(n \times 1)$ vector of system states, $\mathbf{A}(t)$ is an $(n \times n)$ matrix with quasi-periodic frequencies (ω_1, ω_2) and $\mathbf{f}(\mathbf{x}, t)$ contain monomials of vector, $\mathbf{x}$. Applying the L-P transformation $\mathbf{x}(t) = \bar{\mathbf{P}}(t)\mathbf{z}(t)$ results in

$$\dot{\mathbf{z}}(t) = \bar{\mathbf{J}}\mathbf{z}(t) + \bar{\mathbf{P}}^{-1}(t)\mathbf{f}(\mathbf{z}, t) \equiv \bar{\mathbf{J}}\mathbf{z}(t) + \mathbf{u}(\mathbf{z}, t) \tag{6.21}$$

where $\bar{\mathbf{J}}$ corresponds to the constant matrix and $\mathbf{u}(\mathbf{z}, t)$ represents the nonlinear vector comprising of monomials of $\mathbf{z}$ and terms with quasi-periodic frequencies. The key objective of order reduction is to identify a reduced system (equation (6.22) that is equivalent to the nonlinear quasi-periodic system, given by equation (6.21).

$$\dot{\mathbf{z}}_r(t) = \bar{\mathbf{J}}_r \mathbf{z}_r(t) + \mathbf{u}_r(\mathbf{z}_r, t) \tag{6.22}$$

So the equation (6.21) is partitioned in the following manner

$$\begin{Bmatrix} \dot{\mathbf{z}}_r \\ \dot{\mathbf{z}}_s \end{Bmatrix} = \begin{bmatrix} \bar{\mathbf{J}}_r & 0 \\ 0 & \bar{\mathbf{J}}_s \end{bmatrix} \begin{Bmatrix} \mathbf{z}_r \\ \mathbf{z}_s \end{Bmatrix} + \begin{Bmatrix} \mathbf{u}_r(\mathbf{z}_r, \mathbf{z}_s, t) \\ \mathbf{u}_s(\mathbf{z}_r, \mathbf{z}_s, t) \end{Bmatrix} \tag{6.23}$$

where $\mathbf{z}_s$ is a $(n-r)$ vector of non-dominant states, $\bar{\mathbf{J}}_s$ is the $(n-r) \times (n-r)$ matrix corresponding to the non-dominant states and $\mathbf{u}_r(\mathbf{z}_r, \mathbf{z}_s, t)$, $\mathbf{u}_s(\mathbf{z}_r, \mathbf{z}_s, t)$ are the monomials of $\mathbf{z}$ with quasi-periodic terms. In the well-known Guyan linear projection method, the contribution of the non-dominant states is neglected since they are considered to be minimal. The resulting reduced order model can be expressed as

$$\dot{\mathbf{z}}_r(t) = \bar{\mathbf{J}}_r \mathbf{z}_r(t) + \mathbf{u}_r(\mathbf{z}_r, 0, t) \tag{6.24}$$

Equation (6.24) represents the reduced order model of the actual large-scale system (equation (6.20), as per the linear projection method. The system states in $\mathbf{x}$ can be recovered by numerically integrating equation (6.24) and employing the transformation $\mathbf{x}(t) = \bar{\mathbf{P}}(t)\mathbf{T}\mathbf{z}(t)$, where $\mathbf{T} = [\mathbf{I}_{r\times r} \quad \mathbf{0}_{r\times(n-r)}]^T$. Though the linear projection method is simple and straightforward, the selection of dominant states rests on the judgment and experience of the analyst. Moreover, for a complex system that involves internal and/or parametric resonance, this method lacks a thorough understanding of the system dynamics.

6.3.2 Order Reduction Using Nonlinear Projection

Once again, the nonlinear quasi-periodic system expressed in equation (6.20) is considered and transformed to the system in equation (6.21) using L-P transforma-

tion. It is aimed to reduce the order of the given system to an equivalent system, expressed as

$$\dot{\mathbf{z}}_r(t) = \bar{\mathbf{J}}_r \mathbf{z}_r(t) + \mathbf{u}_r(\mathbf{z}_r, \psi(\mathbf{z}_r, t), t) \tag{6.25}$$

where $\mathbf{z}_r(t), \bar{\mathbf{J}}_r, \mathbf{u}_r(\mathbf{z}_r, t)$ are as defined before in Section 6.3.1 and $\psi(\mathbf{z}_r, t)$ defines the nonlinear relationship between non-dominant states and dominant states as

$$\mathbf{z}_s(t) = \psi(\mathbf{z}_r, t) \tag{6.26}$$

The system in equation (6.21) is transformed to the reduced system (equation (6.25) via a nonlinear projection, expressed by equation (6.26). The system equation (6.25) can be integrated numerically and compared with the numerical integration results of equation (6.21) to verify the effectiveness of the order reduction using this approach.

The method to derive nonlinear projection $\psi(\mathbf{z}_r, t)$ is selected based on the system complexity, computational power availability, and the required accuracy of reduced system Redkar *et al.* (2003). A 'non-flat' sub-manifold is identified using the nonlinear projection method, and it is expected to perform better than the linear projection method. The computation of the nonlinear projection using the Singular Perturbation method is detailed in the section of applications.

6.3.3 Order Reduction Using Invariant Manifold

This order reduction approach is based on the *'Invariant Manifold Theory'*, which postulates a relationship between the dominant "master" and the non-dominant "slave" system states. Under certain conditions, the non-dominant states can be replaced by the expression in terms of the dominant states, thereby reducing the system order, as per Waswa *et al.* (2020); Sinha *et al.* (2003).

Again, consider the nonlinear quasi-periodic system given in equation (6.20), which after successive L-P and modal transformation results in equation (6.21) and can be partitioned as equation (6.23). The nonlinear relationship between the dominant ($\mathbf{z}_r$) and the non-dominant ($\mathbf{z}_s$) system states is assumed to be of the form

$$\mathbf{z}_s(t) = \sum_i \mathbf{h}_i(\mathbf{z}_r, t) \equiv \mathbf{H}(\mathbf{z}_r, t) \tag{6.27}$$

where

$$\mathbf{h}_i = \sum_{\bar{\mathbf{m}}} \bar{\mathbf{h}}_i(t)\mathbf{z}_1^{m_1}...\mathbf{z}_r^{m_r};$$
$$\bar{\mathbf{m}} = (m_1, ..., m_r)^T; m_1 + ... + m_r = i; i = 2, 3, ...k$$

where $\mathbf{h}_i(t)$ represents the unknown vector coefficients that are quasi-periodic. By substituting equation (6.27) into equation (6.23) results in

$$\frac{\partial \mathbf{H}}{\partial t} + \frac{\partial \mathbf{H}}{\partial \mathbf{z}_r}(\bar{\mathbf{J}}_r\mathbf{z}_r + \mathbf{u}_r) = \bar{\mathbf{J}}_s\mathbf{H} + \mathbf{u}_s \tag{6.28}$$

Neglecting the higher order terms the equation can be written as

$$\frac{\partial \mathbf{H}}{\partial t} + \frac{\partial \mathbf{H}}{\partial \mathbf{z}_r}\bar{\mathbf{J}}_r\mathbf{z}_r - \bar{\mathbf{J}}_s\mathbf{H} = \mathbf{u}_{si} \tag{6.29}$$

The approximate solution of the partial differential equation (6.29) can be computed by expanding the coefficient functions ($\bar{\mathbf{h}}_i(t)$) as double Fourier series, given by

$$\mathbf{h}_i(\mathbf{z}_r, t) = \sum_{j=1}^{s}\sum_{\bar{\mathbf{m}}}\sum_{p_1=-\infty}^{+\infty}\sum_{p_2=-\infty}^{+\infty} h_{j\bar{m}\nu}\, e^{\bar{i}(\bar{\mathbf{p}}\bullet\boldsymbol{\omega})t}|\mathbf{z}_r|^{\mathbf{m}}_{\sim} e_j \tag{6.30}$$

and

$$\mathbf{u}_{si}(\mathbf{z}_r, t) = \sum_{j=1}^{s}\sum_{\bar{\mathbf{m}}}\sum_{p_1=-\infty}^{+\infty}\sum_{p_2=-\infty}^{\infty} a_{j\bar{m}\nu}\, e^{\bar{i}(\bar{\mathbf{p}}\bullet\boldsymbol{\omega})t}|\mathbf{z}_r|^{\mathbf{m}}_{\sim} e_j \tag{6.31}$$

where $|\mathbf{z}_r|^{\mathbf{m}}_{\sim} = z_1^{m_1} z_2^{m_2} ... z_r^{m_r}, \bar{i} = \sqrt{-1}, m_1 + ... + m_r = i, i = 2, 3, ...k, \boldsymbol{\omega} = \{\omega_1 \quad \omega_2\}, \bar{\mathbf{p}} = \{p_1 \quad p_2\}$, $h_{j\bar{m}\nu}$ represents the unknown Fourier coefficients of the invariant manifold relation, $a_{j\bar{m}\nu}$ corresponds to the known Fourier coefficients of quasi-periodic functions, and e_j is j^{th} member of the natural basis. By comparing the Fourier coefficients results in

$$h_{j\bar{m}\nu} = \frac{a_{j\bar{m}\nu}}{\bar{i}(\bar{\mathbf{p}} \bullet \boldsymbol{\omega})t + \sum_{l=1}^{r}(m_l \lambda_l) - \bar{\lambda}_p} \tag{6.32}$$

where $\lambda_1, \lambda_2, ..., \lambda_r$ are the eigenvalues of the Jordan matrix, $\bar{\mathbf{J}}_r$, and $\bar{\lambda}_p = \bar{\lambda}_1, \bar{\lambda}_2, ..., \bar{\lambda}_s$ are the eigenvalues of $\bar{\mathbf{J}}_s$. Hence, the '*quasi-periodic reducibility condition*' is given as

$$\bar{i}(\bar{\mathbf{p}} \bullet \boldsymbol{\omega})t + \sum_{l=1}^{r}(m_l \lambda_l) - \bar{\lambda}_p \neq 0, \quad \forall \nu = 0, \pm 1, \pm 2, ...; \quad p = 1, 2, ..., s \tag{6.33}$$

The expression for vector $\mathbf{H}(\mathbf{z}_r, t)$ can be derived if the '*reducibility condition*' (given by equation (6.33) is satisfied. With $\mathbf{H}(\mathbf{z}_r, t)$ expression, the 'slave' states can be expressed as functions of 'master' states of the system. However, if the '*reducibility condition*' is not satisfied, 'slave' states cannot be expressed in terms of 'master' states, and the order reduction is not achievable.

6.3.4 Example-8: Commutative Quasi-Periodic System with Coupled Nonlinearity

Consider the following commutative system that is linearly uncoupled but nonlinearly coupled. The L-P transformation for the linear part of this "prototype" problem is known in closed form, as detailed in chapter 5.

$$
\begin{aligned}
&\ddot{x} - 2b_1(\cos(\omega_1 t) + \cos(\omega_2 t))\dot{x} + [a_1 + b_1\omega_1 \sin(\omega_1 t) + b_1\omega_2 \sin(\omega_2 t) \\
&+ {b_1}^2(\cos(\omega_1 t) + \cos(\omega_2 t))^2]x - \mu(x+y)^3 = 0 \\
&\ddot{y} - 2b_2(\cos(\omega_1 t) + \cos(\omega_2 t))\dot{y} - d\dot{y} + [3a_2 + b_2\omega_1 \sin(\omega_1 t) + b_2\omega_2 \sin(\omega_2 t) \\
&+ (b_2 \cos(\omega_1 t) + b_2 \cos(\omega_2 t) - d)^2]y - \mu(x+y)^3 = 0
\end{aligned}
\tag{6.34}
$$

Considering the system states as $x_1 = x, x_2 = (\dot{x} - b_1 x\cos(\omega_1 t) - b_1 x\cos(\omega_2 t)), x_3 = y, x_4 = 1/3(\dot{y} - b_2 y\cos(\omega_1 t) - b_2 y\cos(\omega_2 t))$ and μ to be positive and significant, equation (6.34) can be written in state space form as

$$
\frac{d}{dt}\begin{Bmatrix} x_1 \\ x_2 \\ x_3 \\ x_4 \end{Bmatrix} = \begin{bmatrix} \bar{\mathbf{A}}_1(t) & \mathbf{0} \\ \mathbf{0} & \bar{\mathbf{A}}_2(t) \end{bmatrix} \begin{Bmatrix} x_1 \\ x_2 \\ x_3 \\ x_4 \end{Bmatrix} + \begin{Bmatrix} 0 \\ \mu(x+y)^3 \\ 0 \\ \mu(x+y)^3 \end{Bmatrix} \tag{6.35}
$$

where

$$
\bar{\mathbf{A}}_1(t) = \begin{bmatrix} g_1(t) & 1 \\ -a_1 & g_1(t) \end{bmatrix}, \bar{\mathbf{A}}_2(t) = \begin{bmatrix} g_2(t) & 3 \\ -a_2 & g_2(t) \end{bmatrix}, \mathbf{0} = \begin{bmatrix} 0 & 0 \\ 0 & 0 \end{bmatrix},
$$
$$
g_1(t) = b_1(\cos(\omega_1 t) + \cos(\omega_2 t)), \quad g_2(t) = b_2(\cos(\omega_1 t) + \cos(\omega_2 t)) - d
$$

For this linearly uncoupled part of the commutative quasi-periodic system the L-P transformation is known analytically (discussed in chapter 5)and is given as

$$
\mathbf{P}(t) = \begin{bmatrix} \mathbf{P}_1(t) & \mathbf{0} \\ \mathbf{0} & \mathbf{P}_2(t) \end{bmatrix} \tag{6.36}
$$

where

$$\mathbf{P}_1(t) = \begin{bmatrix} e^{b_1\cos(\omega_1 t)+b_1\cos(\omega_2 t)} & 0 \\ 0 & e^{b_1\cos(\omega_1 t)+b_1\cos(\omega_2 t)} \end{bmatrix},$$

$$\mathbf{P}_2(t) = \begin{bmatrix} e^{b_2\cos(\omega_1 t)+b_2\cos(\omega_2 t)} & 0 \\ 0 & e^{b_2\cos(\omega_1 t)+b_2\cos(\omega_2 t)} \end{bmatrix}$$

By comparing equation (6.35) to equation (6.20), $\mathbf{x}(t) = \{x_1, x_2, x_3, x_4\}^T$, $\mathbf{A}(t) = \begin{bmatrix} \bar{\mathbf{A}}_1(t) & \mathbf{0} \\ \mathbf{0} & \bar{\mathbf{A}}_2(t) \end{bmatrix}$ and $\mathbf{f}(\mathbf{x}, t) = \{0, \mu(x+y)^3, 0, \mu(x+y)^3\}^T$. The application of L-P transformation, $\mathbf{x}(t) = \mathbf{P}(t)\mathbf{y}(t)$, to equation (6.35) yields

$$\dot{\mathbf{y}}(t) = \mathbf{C}\mathbf{y}(t) + \mathbf{P}^{-1}(t)\mathbf{f}(\mathbf{y}, t) \tag{6.37}$$

where $\mathbf{C} = \begin{bmatrix} 0 & 1 & 0 & 0 \\ -a_1 & 0 & 0 & 0 \\ 0 & 0 & -d & 3 \\ 0 & 0 & -a_2 & -d \end{bmatrix}$ After applying modal transformation, $\mathbf{y}(t) = \mathbf{M}\mathbf{z}(t)$, an equation in a form similar to equation (6.21) is obtained.

$$\dot{\mathbf{z}}(t) = \bar{\mathbf{J}}\mathbf{z}(t) + \mathbf{M}^{-1}\mathbf{P}^{-1}(t)\mathbf{f}(\mathbf{z}, t) \equiv \bar{\mathbf{J}}\mathbf{z}(t) + \mathbf{u}(\mathbf{z}, t) \tag{6.38}$$

The initial conditions of $x_{10} = 0.3, x_{20} = 0.3, x_{30} = 0, x_{40} = 0$ was transformed to the $\mathbf{z}$ domain. The system in equation (6.38) is numerically integrated with typical initial conditions and considered as the reference. The system parameters considered for the given commutative system are $a_1 = b_1 = 1, \omega_1 = 2\pi, a_2 = 3, b_2 = 2, d = 1, \omega_2 = 7$, and $\mu = 1$, for which the $\bar{\mathbf{J}}$ matrix is

$$\bar{\mathbf{J}} = \begin{bmatrix} -i1 & 0 & 0 & 0 \\ 0 & +i1 & 0 & 0 \\ 0 & 0 & -1-i3 & 0 \\ 0 & 0 & 0 & -1+i3 \end{bmatrix} \tag{6.39}$$

The numerically integrated solution for the dominant states is shown in Figures 6.4a,b. Equation (6.38) can be partitioned to a form similar to equation (6.23) for applying the order reduction techniques discussed in the subsequent subsections.

Method-1: Order Reduction Using the Linear Method

The system in equation (6.38) is expressed in four coordinates, $\{z_1, z_2, z_3, z_4\}^T$. The system states with a smaller magnitude of the system exponents are assumed to be the dominant states $\mathbf{z}_r = \{z_1, z_2\}^T$. As discussed in section 6.3.1, the input from the non-dominant states $\mathbf{z}_s = \{z_3, z_4\}^T$ are neglected, and the equivalent system dynamics is given by

$$\begin{Bmatrix} \dot{z}_1 \\ \dot{z}_2 \end{Bmatrix} = \begin{bmatrix} -i1 & 0 \\ 0 & +i1 \end{bmatrix} \begin{Bmatrix} z_1 \\ z_2 \end{Bmatrix} + \begin{Bmatrix} u_1(z_1, z_2, 0, 0, t) \\ u_2(z_1, z_2, 0, 0, t) \end{Bmatrix} \tag{6.40}$$

Equation (6.40) displays the reduced order model of the system, described by equation (6.38). This reduced order system is integrated numerically, with the same set of initial conditions and compared with the temporal variations of the reference system states (equation (6.38)) and corresponds to method-1 in Figures 6.4a,b. Similar comparisons can be obtained in the original system coordinates by using the L-P and modal transformations on the resulting system states.

Method-2: Order Reduction Using the Nonlinear Projection Based on Singular Perturbation Method

In this approach too, the system states $\mathbf{z}_r = \{z_1, z_2\}^T$ are considered as the dominant ones based on the exponents and follow the procedure outlined in section 6.3.2. Considering the Singular Perturbation technique, the derivatives of the non-dominant states are presumed to be small compared to that of the dominant states. With this consideration, the equation (6.38) can be rewritten as

$$\begin{Bmatrix} \dot{z}_1 \\ \dot{z}_2 \\ \varepsilon\dot{z}_3 \\ \varepsilon\dot{z}_4 \end{Bmatrix} = \begin{bmatrix} -i1 & 0 & 0 & 0 \\ 0 & +i1 & 0 & 0 \\ 0 & 0 & -1-i3 & 0 \\ 0 & 0 & 0 & -1+i3 \end{bmatrix} \begin{Bmatrix} z_1 \\ z_2 \\ z_3 \\ z_4 \end{Bmatrix} + \begin{Bmatrix} u_1(\mathbf{z},t) \\ u_2(\mathbf{z},t) \\ u_3(\mathbf{z},t) \\ u_4(\mathbf{z},t) \end{Bmatrix} \tag{6.41}$$

Assuming $\varepsilon = 0$, and resorting to one fixed point iteration, z_3 and z_4 can be approximated as

$$\begin{bmatrix} -1-i3 & 0 \\ 0 & -1+i3 \end{bmatrix} \begin{Bmatrix} z_3 \\ z_4 \end{Bmatrix} = - \begin{Bmatrix} u_3(z_1, z_2, 0, 0, t) \\ u_4(z_1, z_2, 0, 0, t) \end{Bmatrix} \tag{6.42}$$

The single fixed-point iteration solution of $\{z_3, z_4\}$ given by equations (6.42) is substituted into the top half of equation (6.41) to obtain the reduced order model as

$$\begin{Bmatrix} \dot{z}_1 \\ \dot{z}_2 \end{Bmatrix} = \begin{bmatrix} -i1 & 0 \\ 0 & +i1 \end{bmatrix} \begin{Bmatrix} z_1 \\ z_2 \end{Bmatrix} + \begin{Bmatrix} \bar{u}_1(z_1, z_2, t) \\ \bar{u}_2(z_1, z_2, t) \end{Bmatrix} \tag{6.43}$$

Equation (6.43) is integrated numerically, with the same set of initial conditions to obtain the behavior of the dominant states corresponding to method-2. Again the time trace of $\mathbf{z}_r$ computed using the nonlinear projection technique is compared with the time trace of $\mathbf{z}_r$ obtained by integrating equation (6.38), as shown in Figure 6.4.

Method-3: Order Reduction Using the Invariant Manifold Method

As discussed in section 6.3.3, identify a relationship between the non-dominant and dominant states using a quasi-periodic nonlinear transformation. The *'reducibility condition'* is satisfied, and the system order can be reduced, if there are no resonances (like the case under consideration). Start with equation (6.38) and select the same states $\mathbf{z}_r = \{z_1, z_2\}^T$ as the dominant states and try to find a nonlinear relationship of the form given in equation (6.26). In this case, the relationship between $\mathbf{z}_s$ and $\mathbf{z}_r$ is expressed as

$$\mathbf{z}_s = \sum_i \mathbf{h}_i(z_1, z_2, t) \equiv \mathbf{H}(z_1, z_2, t) \tag{6.44}$$

where

$$\mathbf{h}_i = \sum_{\bar{\mathbf{m}}} \bar{\mathbf{h}}_i(t) z_1^{m_1} ... z_2^{m_2}; \quad \bar{\mathbf{m}} = (m_1, m_2)^T; \quad m_1 + m_2 = 3; \quad s = 3, 4$$

where $\bar{\mathbf{h}}_i(t)$ is the unknown quasi-periodic vector coefficients. Substitute equation (6.44) into equation (6.38). After expanding the Fourier series for $\bar{\mathbf{h}}_i(t)$, $\mathbf{u}_s(\mathbf{z}_r, \mathbf{z}_s, t)$ and neglecting the higher order terms, the relationship between the dominant and the non-dominant states is given as

$$z_3 = \mathbf{H}_1(z_1, z_2, t), \quad z_4 = \mathbf{H}_2(z_1, z_2, t) \tag{6.45}$$

Equation (6.45) is substituted into the top half of equation (6.38) to obtain the reduced order model as

$$\begin{Bmatrix} \dot{z}_1 \\ \dot{z}_2 \end{Bmatrix} = \begin{bmatrix} -i1 & 0 \\ 0 & +i1 \end{bmatrix} \begin{Bmatrix} z_1 \\ z_2 \end{Bmatrix} + \begin{Bmatrix} \hat{u}_1(z_1, z_2, t) \\ \hat{u}_2(z_1, z_2, t) \end{Bmatrix} \tag{6.46}$$

The equation (6.46) is numerically integrated to obtain the time traces of the

dominant states of the reduced system, corresponding to method-3. The temporal variations are depicted in Figure 6.4.

In Figures 6.4 ab, the time traces of the reduced dominant states are indicated by the black dashed line corresponding to the numerically integrated solution, the solid magenta line corresponding to the linear method, the solid blue line corresponding to the nonlinear projection method, and the solid gray line corresponding to the invariant manifold method. Since all the methods follow the numerical solution closely, error plots are generated for each dominant system state to compare their performance. In Figures 6.5a,b, the time traces of the error in the reduced dominant states (for the numerical solution) are indicated by solid magenta line corresponding to the error plot for the linear method, the solid blue line corresponding to the error plot for nonlinear projection method and the solid gray line corresponding to the error plot for invariant manifold method.

6.3.5 Example-9: Non-Commutative Quasi-Periodic System with Coupled Nonlinearity

Consider a coupled Hills-Mathieu type nonlinear quasi-periodic system given by

$$\begin{aligned} &\ddot{x} + (\alpha_1 + \beta_1 \cos(\omega_1 t) + \gamma_1 \cos(\omega_2 t))x - \mu(x+y)^3 = 0 \\ &\ddot{y} + \delta\dot{y} + (\alpha_2 + \beta_2 \cos(\omega_1 t) + \gamma_2 \cos(\omega_2 t))y - \mu(x+y)^3 = 0 \end{aligned} \tag{6.47}$$

Considering the system states as $x_1 = x, x_2 = \dot{x}, x_3 = y, x_4 = \dot{y}$ and μ to be positive and significant, equation (6.47) can be written in state space form as

$$\frac{d}{dt}\begin{Bmatrix} x_1 \\ x_2 \\ x_3 \\ x_4 \end{Bmatrix} = \begin{bmatrix} \tilde{\mathbf{A}}_1(t) & \mathbf{0} \\ \mathbf{0} & \tilde{\mathbf{A}}_2(t) \end{bmatrix} \begin{Bmatrix} x_1 \\ x_2 \\ x_3 \\ x_4 \end{Bmatrix} + \begin{Bmatrix} 0 \\ \mu(x+y)^3 \\ 0 \\ \mu(x+y)^3 \end{Bmatrix} \tag{6.48}$$

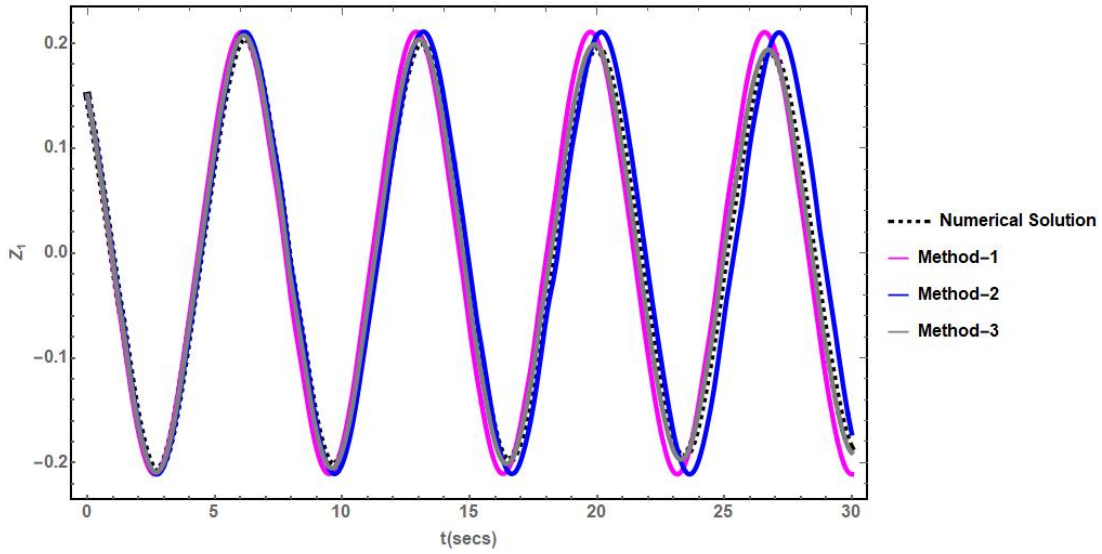

(**a**)

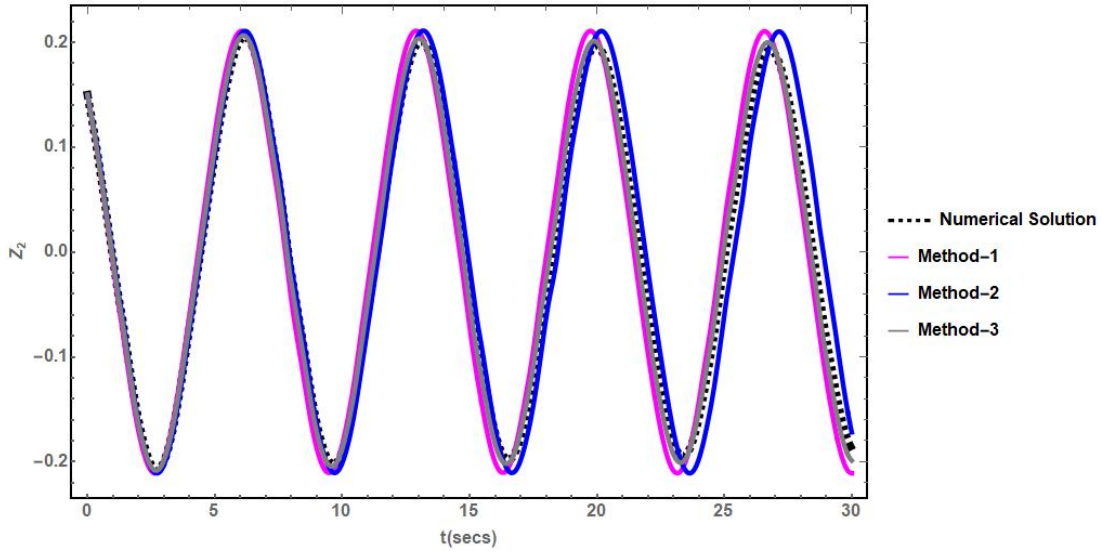

(**b**)

Figure 6.4: Comparison of System State Variation Commutative Quasi-periodic System with Coupled Nonlinear Terms, Where (**a**) Shows z_1 State and (**b**) Shows z_2 State Variations

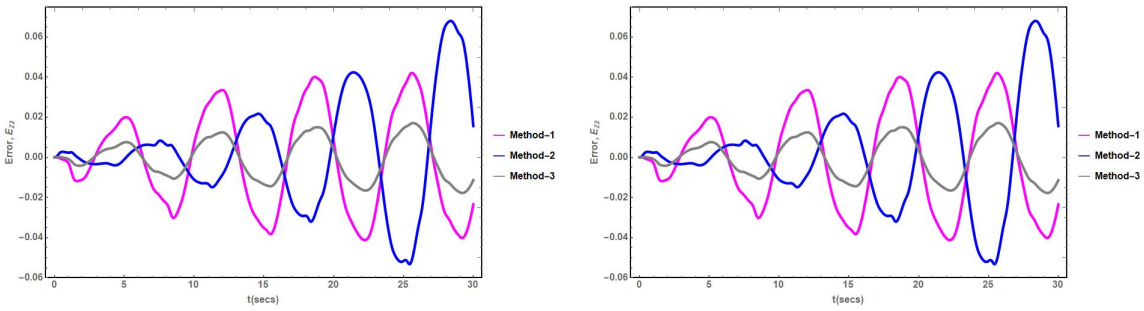

(**a**) (**b**)

Figure 6.5: Error in the System State Variation Comparison of Commutative Quasi-periodic System with Coupled Nonlinear Terms, Where (**a**) E_{z1} Is That of z_1 State, (**b**) E_{z2} Is That of z_2 State

where

$$\tilde{\mathbf{A}}_1(t) = \begin{bmatrix} 0 & 1 \\ -(\alpha_1 + \beta_1 \cos(\omega_1 t) + \gamma_1 \cos(\omega_2 t)) & 0 \end{bmatrix},$$

$$\tilde{\mathbf{A}}_2(t) = \begin{bmatrix} 0 & 1 \\ -(\alpha_2 + \beta_2 \cos(\omega_1 t) + \gamma_2 \cos(\omega_2 t)) & -\delta \end{bmatrix}$$

As detailed in section 5.3, the linear part of the equation (6.48) undergoes the state augmentation and Normal Forms technique to form the time invariant form (equation (5.37)). As explained in chapter 5, this approach yields the closed-form expression for the L-P transformation, and it contains terms with both the incommensurate frequencies. For this work, the inverse of the time varying L-P transformation matrix is computed symbolically using MATHEMATICA software. The L-P transformation and its inverse computed aids in transforming the coupled nonlinear non-commutative quasi-periodic system (equation (6.48)) to the form indicated in equation (6.38). The initial conditions of $x_{10} = 0.2, x_{20} = 0.2, x_{30} = 0, x_{40} = 0$ is also transformed to the **z**-domain. The system parameters considered for the given non-commutative nonlinear quasi-periodic system are $\alpha_1 = 9, \beta_1 = \gamma_1 = 1, \omega_1 = 2\pi, \alpha_2 = 20, \beta_2 = \gamma_2 = 2, \delta = 4, \omega_2 = 7$, and $\mu = 1$, for which the equation (6.38) is obtained as

$$\begin{Bmatrix} \dot{z}_1 \\ \dot{z}_2 \\ \dot{z}_3 \\ \dot{z}_4 \end{Bmatrix} = \begin{bmatrix} -i3 & 0 & 0 & 0 \\ 0 & +i3 & 0 & 0 \\ 0 & 0 & -2-i4 & 0 \\ 0 & 0 & 0 & -2+i4 \end{bmatrix} \begin{Bmatrix} z_1 \\ z_2 \\ z_3 \\ z_4 \end{Bmatrix} + \begin{Bmatrix} u_1(\mathbf{z},t) \\ u_2(\mathbf{z},t) \\ u_3(\mathbf{z},t) \\ u_4(\mathbf{z},t) \end{Bmatrix} \tag{6.49}$$

Method-1: Order Reduction Using the Linear Method

The transformed non-commutative system also comprises of four states $\{z_1, z_2, z_3, z_4\}^T$. Again, the system states corresponding to the smaller system exponent are assumed to be the dominant states, $\mathbf{z}_r = \{z_1, z_2\}^T$. Similar to the case of the commutative system, the contribution from the non-dominant states $\mathbf{z}_s = \{z_3, z_4\}^T$ are neglected, resulting in the system dynamics as

$$\begin{Bmatrix} \dot{z}_1 \\ \dot{z}_2 \end{Bmatrix} = \begin{bmatrix} -i3.0 & 0 \\ 0 & +i3.0 \end{bmatrix} \begin{Bmatrix} z_1 \\ z_2 \end{Bmatrix} + \begin{Bmatrix} u_1(z_1, z_2, 0, 0, t) \\ u_2(z_1, z_2, 0, 0, t) \end{Bmatrix} \tag{6.50}$$

For the non-commutative system, the equation (6.50) represents the reduced order model using the linear method (method-1). Again, the reduced order system is integrated numerically, with the same set of initial conditions and compared with the temporal variations of the reference system states (equation (6.49)), as shown in Figure 6.6.

Method-2: Order Reduction Using the Nonlinear Projection Based on Singular Perturbation Method

Based on the exponents, consider $\mathbf{z}_r = \{z_1, z_2\}^T$ as the dominant states to be retained. As the case of commutative system, based on the perturbation technique, consider the non-dominant states' derivatives to be small compared to the derivatives of the

dominant states. This updates the equation (6.48) as

$$\begin{Bmatrix} \dot{z}_1 \\ \dot{z}_2 \\ \varepsilon\dot{z}_3 \\ \varepsilon\dot{z}_4 \end{Bmatrix} = \begin{bmatrix} -i3 & 0 & 0 & 0 \\ 0 & +i3 & 0 & 0 \\ 0 & 0 & -2-i4 & 0 \\ 0 & 0 & 0 & -2+i4 \end{bmatrix} \begin{Bmatrix} z_1 \\ z_2 \\ z_3 \\ z_4 \end{Bmatrix} + \begin{Bmatrix} u_1(\mathbf{z},t) \\ u_2(\mathbf{z},t) \\ u_3(\mathbf{z},t) \\ u_4(\mathbf{z},t) \end{Bmatrix} \tag{6.51}$$

Consider $\varepsilon = 0$, and resorting to one fixed point iteration, z_3 and z_4 are approximated as

$$\begin{bmatrix} -2-i4 & 0 \\ 0 & -2+i4 \end{bmatrix} \begin{Bmatrix} z_3 \\ z_4 \end{Bmatrix} = - \begin{Bmatrix} u_3(z_1,z_2,0,0,t) \\ u_4(z_1,z_2,0,0,t) \end{Bmatrix} \tag{6.52}$$

The single fixed-point iteration solution of $\{z_3, z_4\}$ given by equations (6.52) is substituted into the top half of equation (6.51) to obtain the reduced order model as

$$\begin{Bmatrix} \dot{z}_1 \\ \dot{z}_2 \end{Bmatrix} = \begin{bmatrix} -i3 & 0 \\ 0 & +i3 \end{bmatrix} \begin{Bmatrix} z_1 \\ z_2 \end{Bmatrix} + \begin{Bmatrix} \bar{u}_1(z_1,z_2,t) \\ \bar{u}_2(z_1,z_2,t) \end{Bmatrix} \tag{6.53}$$

Similar to the case of commutative systems, the numerical integration of equation (6.53), with the same set of initial conditions, yields the time traces of the dominant states corresponding to method-2. The system state behavior of $\mathbf{z}_r$ obtained using the nonlinear projection technique is compared with the time trace of $\mathbf{z}_r$ obtained by numerically integrating equation (6.49), as shown in Figure 6.6.

Method-3: Order Reduction Using the Invariant Manifold Method

Similar to the case of the commutative system, find a nonlinear relationship between the dominant ($\mathbf{z}_r = \{z_1, z_2\}^T$) and non-dominant $\mathbf{z}_s = \{z_3, z_4\}^T$ states of the form

given in equation (6.27). As detailed in section 6.3.3, after expanding the Fourier series and neglecting the higher order terms the relationship between the dominant and non-dominant states, as indicated in equation (6.46). This relationship is substituted in the top half of equation (6.49) to obtain the reduced order model as

$$\begin{Bmatrix} \dot{z}_1 \\ \dot{z}_2 \end{Bmatrix} = \begin{bmatrix} -i3.0 & 0 \\ 0 & +i3.0 \end{bmatrix} \begin{Bmatrix} z_1 \\ z_2 \end{Bmatrix} + \begin{Bmatrix} \hat{u}_1(z_1, z_2, t) \\ \hat{u}_2(z_1, z_2, t) \end{Bmatrix} \tag{6.54}$$

The behavior of the dominant system states of the reduced system, corresponding to method-3, are obtained by numerically integrating equation (6.54), as shown in Figure 6.6.

In Figures 6.6a,b, the time traces of the reduced dominant states are indicated by the black dashed line corresponding to the numerically integrated solution, the solid magenta line corresponding to the linear method, the solid blue line corresponding to the nonlinear projection method, and the solid gray line corresponding to the invariant manifold method. Again, all the methods are observed to follow the numerical solution closely. In Figures 6.7a,b, the time traces of the error in the reduced dominant states (for the numerical solution) are indicated by solid magenta line for the linear method, solid blue line for the nonlinear projection method and solid gray line for invariant manifold method.

6.3.6 Discussion

The L-P transformation matrices and their inverse were observed to contain time varying terms with incommensurate frequencies. The reduced order system was observed to follow the numerical solution of the original system quite well for all the cases in both the dominant system states. Hence, all the order reduction methods follow the trend of the dominant system states and preserve the dynamics of the

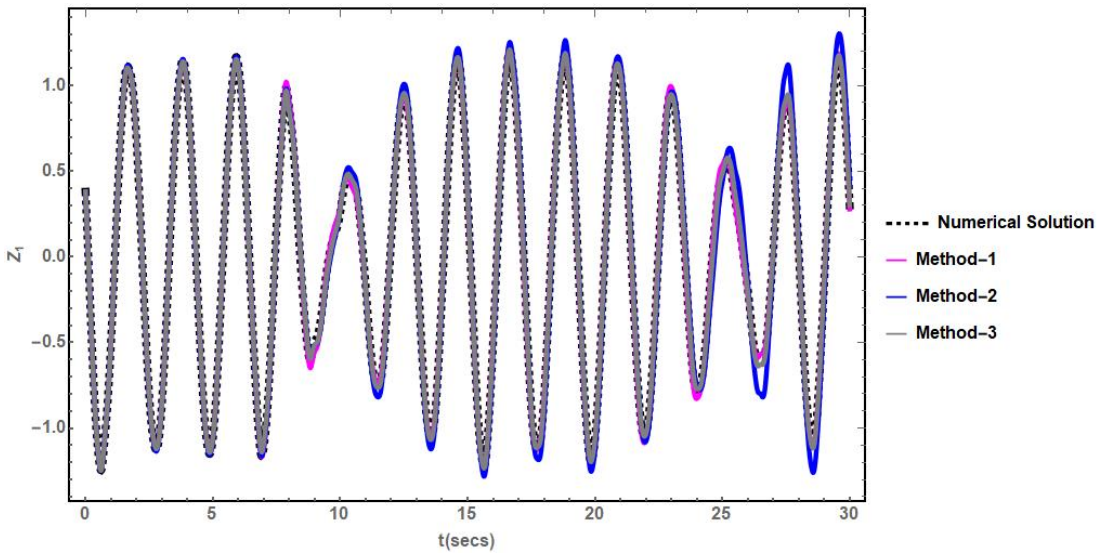

(**a**)

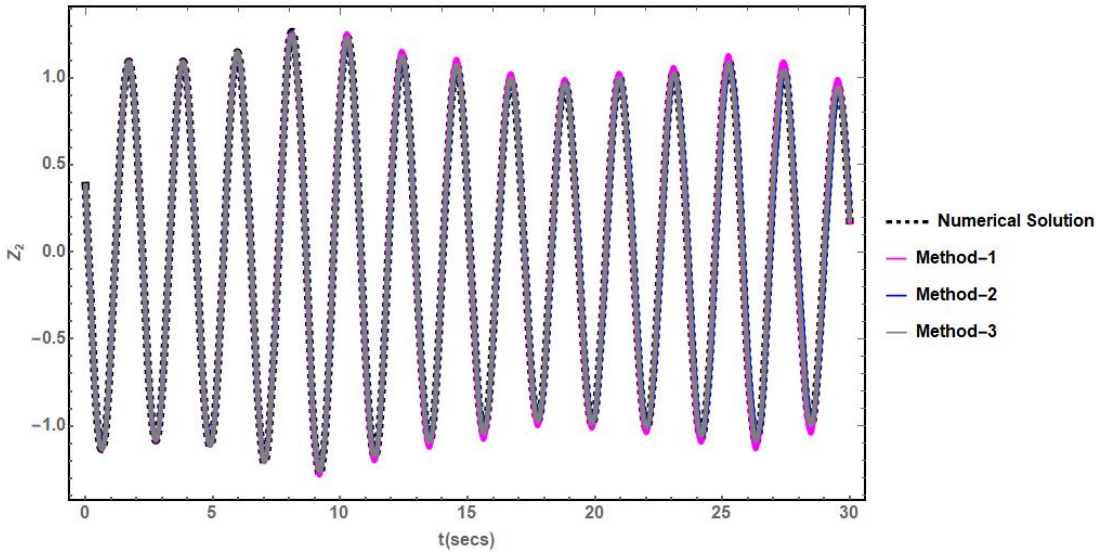

(**b**)

Figure 6.6: Comparison of System State Variation Non-commutative Hills Quasi-periodic System with Coupled Nonlinear Terms, Where (**a**) Shows z_1 State and (**b**) Shows z_2 State Variations

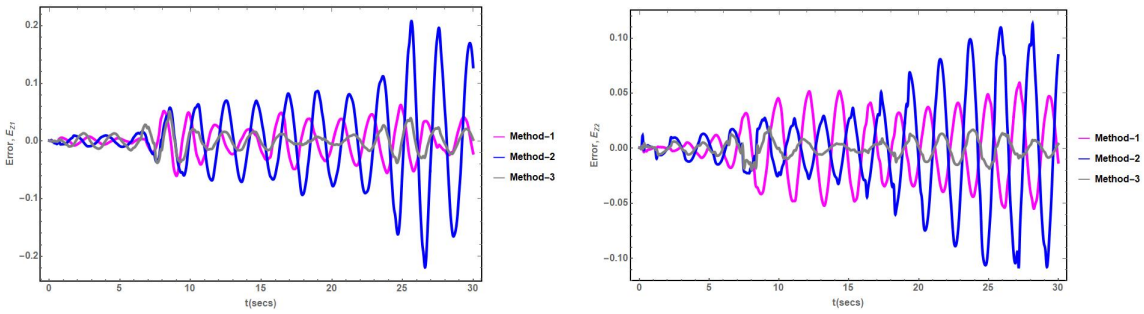

(**a**) (**b**)

Figure 6.7: Error in the System State Variation Comparison of Non-commutative Hills Quasi-periodic System with Coupled Nonlinear Terms, Where (**a**) E_{z1} Is That of z_1 State, (**b**) E_{z2} Is That of z_2 State

original nonlinear system.

The error plots with respect to the numerical solution aided in understanding the performance of each method. In the case of commutative quasi-periodic system, from Figures 6.5 a,b, it is observed that the nonlinear method's error plot is better than that of the linear method and later (approximately after 20 seconds) error in nonlinear projection method goes higher than other two methods. However, in both figures, the error plot of the invariant manifold method consistently remained the lowest. Also, for the case of Hills (non-commutative) quasi-periodic system, from Figures 6.7 a,b, the invariant manifold method performs much better than the other two reduction methods for both the system states. From Figures 6.7 a,b, it is also observed that the nonlinear projection method started to sway away from the numerical solution towards the end of the simulation. Though the nonlinear projection method was expected to behave better than the linear method, the long term dynamics of the system indicate that it may not be the case throughout. As long as a nonlinear relationship is identified between the dominant states and the non-dominant states, using the center manifold theory, this method preserves the significant dynamics of the original nonlinear quasi-periodic system.

6.3.7 Conclusion

In this section, the application of the L-P transformation and its inverse towards the analysis of a highly nonlinear quasi-periodic system is demonstrated for both commutative and non-commutative systems. Furthermore, the dominant system states were identified for both classes of nonlinear quasi-periodic systems, and multiple order reduction techniques were applied.

Initially, the contribution of the non-dominant states was neglected in the behavior of dominant states. Later, a nonlinear projection of the non-dominant states was considered in the behavior of dominant states, using a singular perturbation method. Finally, the relationship between the non-dominant states and dominant states was identified using the invariant manifold theory. Among the three methods, the order reduction using the invariant manifold theory was observed to imitate the numerical solution of the system behavior closely for both commutative and non-commutative nonlinear quasi-periodic systems. The extension of this approach towards the stability analysis is detailed in the next chapter.

Chapter 7

STABILITY ROBUSTNESS ANALYSIS OF QUASI-PERIODIC SYSTEM

The earliest studies of the stability of linear systems with random excitations, by Rosenbloom (1954); Bertram and Sarachik (1959); Kats and Krasovskii (1960); Samuels (1959), were concentrated on the solution and not on the system. From the works of Infante (1968) emerged stability theorems for linear time invariant systems. Using a Lyapunov function and the theory of pencils of quadratic forms, subsequent researchers (Wiens and Sinha (1984); Ariaratnam and Ly (1989)) extended the theorem and related corollaries towards time varying systems. Using the approach of Integral Quadratic Constraint (IQC), a time periodic system with parametric uncertainties was analyzed for stability characteristics Megretski and Rantzer (1997); Pfifer and Seiler (2015). Recently, multiple Lyapunov function based techniques have been developed towards stability analysis of matrix second-order systems by Bernstein and Bhat (1995), axially moving material systems by Zhao and Rahn (2006), control of vibrating non-classical microscale beam by Vatankhah *et al.* (2015), and multidegrees of freedom fractional oscillators by Zhang *et al.* (2016).

In the frequency domain, the Circle or Luré criterion and the Popov criterion guaranteed the stability of a system with nonlinearity that met a sector type bounding condition. The Popov criteria for Luré system were recently analyzed using complex scaling stability analysis by Zhou (2018). The sufficient conditions were identified for asymptotic stability of systems with deterministic and structured perturbations by Patel and Toda (1980); Yedavalli (1985); Zhou and Khargonekar (1987); Keel *et al.* (1988). A comprehensive review of these techniques and their applications is detailed by Kozin (1969); Bhattacharyya *et al.* (1995). Vrabel (2020) used the logarithmic

norm and constant variation formula based approach to evaluate the local and global asymptotic stability property at the origin of a nonlinearly perturbed system. Additionally applying the proposed approach without computing the fundamental solution matrix for a linear system is also demonstrated. A stochastic Lyapunov function based approach was employed by Quevedo and Nešić (2012) to derive the stability conditions for the control of nonlinear systems with Markovian packet losses. Recently, the robustness and boundedness of nonlinearities were analyzed using Markovian switching in hybrid stochastic differential delay equations Hu *et al.* (2013).

In this chapter, the stability and robustness of linear quasi-periodic systems under multiple perturbations are analyzed and asymptotic stability conditions are derived. The Infante's approach and Lyapunov direct method aids in performing this analysis. The construction of Lyapunov functions is detailed in section 4.5.1.

7.1 Stability and Robustness of Quasi-periodic System Subjected to Random Excitations

Similar to the case of periodic system, consider a quasi-periodic linear differential equation with parametric stochastic perturbation given by

$$\dot{\mathbf{x}} = [\mathbf{A}(t) + \mathbf{F}(t)]\mathbf{x} \tag{7.1}$$

where $\mathbf{x}$ and quasi-periodic $\mathbf{A}(t)$ are as defined before in Chapter 5. $\mathbf{F}(t)$ is $n \times n$ matrix whose nonzero elements $f_{ij}(t)$ are stochastic process, measurable, strictly stationary, and that they satisfy an ergodic property by Kushner (1967). The quasi-periodic part of the equation (7.1) is assumed to be asymptotically stable, and the stability bounds on $\mathbf{F}(t)$ need to be determined. As discussed in section 5.3, using the L-P transformation $\mathbf{x} = \bar{\mathbf{P}}(t)\mathbf{z}$, the equation (7.1) can be reduced as

$$\dot{\mathbf{z}} = [\bar{\mathbf{J}} + \mathbf{G}(t)]\mathbf{z} \tag{7.2}$$

where $\mathbf{G}(t) = \bar{\mathbf{P}}^{-1}(t)\mathbf{F}(t)\bar{\mathbf{P}}(t)$ and the properties of $\mathbf{G}(t)$ is the same as that of $\mathbf{F}(t)$. In the case of the non-commutative system, the $\bar{\mathbf{J}}$ matrix is a diagonal matrix with semi-simple eigenvalues having negative real parts. For brevity, the rest of the theory is explained considering the case of a non-commutative linear quasi-periodic system. The stability bounds on $\mathbf{F}(t)$ are identified using the approach presented by Infante (1968) and detailed in section 4.5. The theorem-2 and corollary are extended towards the linear quasi-periodic system except for using an L-P transformation instead of L-F transformation to reduce the system equations corresponding to equation (4.30) and (4.34). Also, in the case of the commutative system, the $\bar{\mathbf{J}}$ matrix is replaced with a constant real matrix $\mathbf{C}$ (analytically derived), and the L-P transformation matrix ($\bar{\mathbf{P}}(t)$) is replaced with the analytically derived $\mathbf{P}(t)$ matrix expressions. The theorem and corollary, explained in section 4.5, on the stability and robustness of the randomly excited systems are applied on multiple examples of quasi-periodic systems in the following subsections.

7.1.1 Example-10: Non-commutative Quasi-periodic System with Stochastic Excitations

Initially, a damped linear Hills quasi-periodic system is considered of the form

$$\ddot{x} + \zeta\dot{x} + [a + b(\cos(\omega_1 t) + \cos(\omega_2 t)) + f(t)]\, x = 0 \tag{7.3}$$

where ω_1 and ω_2 are incommensurate frequencies, a and b are constants representing the system parameters, ζ is the damping coefficient, and the $f(t)$ is a stochastic process, measurable, strictly stationary, and it satisfies an ergodic property Kushner

(1967). It is assumed that $E\{f(t)\} = 0$. Considering $\mathbf{x} = [x_1, x_2]^T = [x, \dot{x}]^T$ equation (7.3) can be expressed in the matrix form as

$$\begin{bmatrix} \dot{x}_1 \\ \dot{x}_2 \end{bmatrix} = \begin{bmatrix} 0 & 1 \\ -(a + b(\cos\omega_1 t + \cos\omega_2 t)) & -\zeta \end{bmatrix} \begin{bmatrix} x_1 \\ x_2 \end{bmatrix} + \begin{bmatrix} 0 & 0 \\ -f(t) & 0 \end{bmatrix} \begin{bmatrix} x_1 \\ x_2 \end{bmatrix} \tag{7.4}$$

For this example, the system parameters considered are a=3, b=2.5, ω_1 =2π, and ω_2 =7. The stability conditions are derived in terms of $f(t)$ as a function of the damping parameter ζ. For multiple values of ζ, the corresponding L-P transformation matrix ($\bar{\mathbf{P}}(t)$) is computed, and the system in equation (7.4) is transformed (using $\mathbf{x} = \bar{\mathbf{P}}(t)\mathbf{z}$) to the form similar to equation (7.2). For ζ=0.4, as mentioned earlier, the $\bar{\mathbf{J}}$ matrix has a negative real part, and it is computed to be $\bar{\mathbf{J}} = \begin{bmatrix} -0.2 & 0 \\ 0 & -0.2 \end{bmatrix}$

A symmetric, positive definite matrix ($\bar{\mathbf{B}}$) is required to apply the theorem and corollary. Considering a quadratic Lyapunov function $V(\mathbf{z}) = \mathbf{z}^T\bar{\mathbf{B}}\mathbf{z}$, then

$$\dot{V} = \dot{\mathbf{z}}^T\bar{\mathbf{B}}\mathbf{z} + \mathbf{z}^T\bar{\mathbf{B}}\dot{\mathbf{z}} = \mathbf{z}^T\left[\bar{\mathbf{J}}^T\bar{\mathbf{B}} + \bar{\mathbf{B}}\bar{\mathbf{J}}\right]\mathbf{z} \equiv -\mathbf{z}^T\bar{\mathbf{D}}\mathbf{z} \tag{7.5}$$

By considering

$$\bar{\mathbf{B}} = \begin{bmatrix} B_{11} & B_{12} \\ B_{12} & B_{22} \end{bmatrix}, \quad \bar{\mathbf{D}} = \mathbf{I}_2 = \begin{bmatrix} 1 & 0 \\ 0 & 1 \end{bmatrix} \tag{7.6}$$

and substituting equation (7.6) into equation (7.5) and using symbolic software like MATHEMATICA, the expression for $\bar{\mathbf{B}}$ matrix is computed to be $\bar{\mathbf{B}} = \begin{bmatrix} 2.5 & 0 \\ 0 & 2.5 \end{bmatrix}$

By applying theorem-2 and corollary-2 the expressions for $\lambda_{max}\left[\bar{\mathbf{J}}^T + \mathbf{G}(t)^T + \bar{\mathbf{B}}\left[\bar{\mathbf{J}} + \mathbf{G}(t)\right]\bar{\mathbf{B}}^{-1}\right]$, $\lambda_{max}\left[\mathbf{G}(t)^T + \bar{\mathbf{B}}\mathbf{G}(t)\bar{\mathbf{B}}^{-1}\right]$ and $\lambda_{max}\left[\bar{\mathbf{J}}^T + \bar{\mathbf{B}}\bar{\mathbf{J}}\bar{\mathbf{B}}^{-1}\right]$ are computed. The expression obtained, using MATHEMATICA, for these terms are long and are omitted for brevity.

Using theorem-2 and Schwarz's Inequality along with considering $E\{sin(nt)\} = 0$, $E\{cos(nt)\} = 0$ and $E\{f(t)\} = 0$ yields the stability condition as

$$(-3.39 \times 10^{-6} - i2.78 \times 10^{-6})[(70403.9 - i57728.9) - \{(1.62 \times 10^{9} - i8.13 \times 10^{9}) + (352019 - i288645)((-14080.8 + i11545.8) + (90651.2 - i74331.1)E\{f^2(t)\})\}^{1/2}] \leq 0 \tag{7.7}$$

Solving the equation (7.7) for the $E\{f^2(t)\}$ results in

$$E\{f^2(t)\} \leq 0.155329 \tag{7.8}$$

Following similar procedure with the expressions of corollary-2, using Schwarz's Inequality and considering $E\{sin(nt)\} = 0$, $E\{cos(nt)\} = 0$ and $E\{f(t)\} = 0$, results in the stability condition for the case of $\zeta = 0.4$

$$E\{f^2(t)\} \leq 0.155330 \tag{7.9}$$

The almost sure asymptotic stability conditions obtained by theorem and the corollary for varying damping coefficient values (ζ), are shown in Figure 7.1. The trend indicated in the dashed blue line corresponds to the condition derived from theorem-2, and the one indicated in solid black lines represents the condition derived from corollary-2 for the given non-commutative quasi-periodic system. The stability conditions obtained via the corollary-2 are observed to be comparable to the results generated from theorem-2 for the case of a non-commutative quasi-periodic system.

7.1.2 Example-11: Commutative Quasi-periodic System with Stochastic Parametric Excitations

In this example, a commutative quasi-periodic with a parametric excitation term is considered, given by

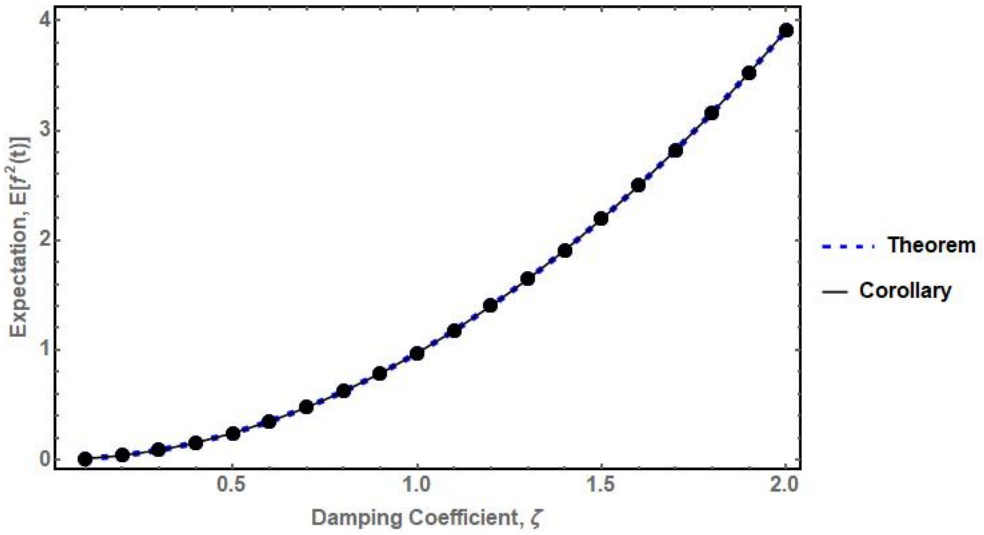

Figure 7.1: Results for the Non-commutative Quasi-periodic System with Stochastic Parametric Excitations.

$$\begin{aligned}\ddot{x} - 2b(\cos(\omega_1 t) + \cos(\omega_2 t))\dot{x} - d\dot{x} + [a + b\omega_1 \sin(\omega_1 t) \\ + b\omega_2 \sin(\omega_2 t) + (b\cos(\omega_1 t) + b\cos(\omega_2 t) - d)^2 + f(t)]x = 0\end{aligned} \tag{7.10}$$

where ω_1, ω_2, a, b and $f(t)$ same as defined for the case of non-commutative system in section 7.1.1. The constants d corresponds to the damping coefficient. By considering $x_1 = x$ and $x_2 = \dot{x}_1 - (b\cos(\omega_1 t) + b\cos(\omega_2 t))x_1$ as the systems states, the equation (7.10) can be expressed in the state space form as equation (7.11) where

$$\mathbf{A}(t) = \begin{bmatrix} b(\cos(\omega_1 t) + \cos(\omega_2 t)) - d & 1 \\ -a & b(\cos(\omega_1 t) + \cos(\omega_2 t)) - d \end{bmatrix}, \quad \mathbf{F}(t) = \begin{bmatrix} 0 & 0 \\ -f(t) & 0 \end{bmatrix} \tag{7.11}$$

As detailed in section 5.1, the commutative property of the system can be verified, and the STM for the linear part of the given system can be given by equation (5.13), where

$$\mathbf{P}(t) = \begin{bmatrix} e^{(\frac{b(\sin(\omega_1 t))}{\omega_1} + \frac{b(\sin(\omega_2 t))}{\omega_2})} & 0 \\ 0 & e^{(\frac{b(\sin(\omega_1 t))}{\omega_1} + \frac{b(\sin(\omega_2 t))}{\omega_2})} \end{bmatrix}, \mathbf{C} = \begin{bmatrix} -d & 1 \\ -a & -d \end{bmatrix} \tag{7.12}$$

Thus applying the L-P transformation, $\mathbf{x}(t) = \mathbf{P}(t)\mathbf{z}(t)$, to equation (7.10) yields

$$\dot{\mathbf{z}} = \mathbf{C}\mathbf{z} \tag{7.13}$$

The expression for the L-P transformation matrix is also verified using the condition indicated in equation (5.16). For the given system in equation (7.3), the system parameters considered are $b = 1, d = 0.25, \omega_1 = 2\pi$ and $\omega_2 = 7$. Similar to the case of non-commutative system, the condition from the Lyapunov function ($\mathbf{C}^T\bar{\mathbf{B}} + \bar{\mathbf{B}}\mathbf{C} + \mathbf{I}_2 = 0$) is used to compute a symmetric, positive definite matrix ($\bar{\mathbf{B}}$) in terms of the linear constant a

$$\bar{\mathbf{B}} = \begin{bmatrix} \frac{0.125+a+a^2}{0.0625+a} & \frac{1-a}{4(0.0625+a)} \\ \frac{1-a}{4(0.0625+a)} & \frac{0.125+a}{0.0625+a} \end{bmatrix} \tag{7.14}$$

For values of $a > 1$, the $\bar{\mathbf{B}}$ matrix is observed to be a positive definite symmetric matrix, and the conditions of Lyapunov stability are fulfilled. After the computation of the $\bar{\mathbf{B}}$ matrix, the stability conditions for the commutative system are derived using theorem-2 and its corollary. As mentioned earlier, the $\bar{\mathbf{J}}$ matrix is replaced with the $\mathbf{C}$ matrix for the case of a commutative quasi-periodic system. Consider

$$\mathbf{K} = \mathbf{C}^T + \mathbf{G}(t)^T + \bar{\mathbf{B}}\left[\mathbf{C} + \mathbf{G}(t)\right]\bar{\mathbf{B}}^{-1} \tag{7.15}$$

The eigenvalues ($\lambda_{1,2}$) of $\mathbf{K}$ matrix are utilized towards the application of theorem-2 ($E\{\lambda_{max}\left[\mathbf{K}\right]\} \leq \varepsilon$). Again, using the Schwarz's Inequality ($(E\{f(t)\})^2 \leq E\{f^2(t)\}$) and setting $E\{f(t)\} = 0$ results in

$$E\{f^2(t)\} \leq \frac{(0.0625+a)^3(1.25+2a+a^2)}{0.098877+1.91602a+5.78223a^2+7.28125a^3+4.3125a^4+a^5} \quad (7.16)$$

The results obtained from equation (7.16) for values of parameter a varying from 0 to 1 are shown in Figure 7.2, using solid blue dots. In order to obtain the conditions for robust stability from corollary-2, the following matrices are evaluated to be

$$\begin{aligned}
\mathbf{G}(t)^T + \bar{\mathbf{B}}\mathbf{G}(t)\bar{\mathbf{B}}^{-1} &= \begin{bmatrix} \frac{0.25(-1+a)(1.125+a)f(t)}{(0.0625+a)(1.25+2a+a^2)} & -\frac{(0.015625+1.5a+2a^2+a^3)f(t)}{(0.0625+a)(1.25+2a+a^2)} \\ -\frac{(1.125+a)^2 f(t)}{(0.0625+a)(1.25+2a+a^2)} & -\frac{0.25(-1+a)(1.125+a)f(t))}{(0.0625+a)(1.25+2a+a^2)} \end{bmatrix}, \\
\mathbf{C}^T + \bar{\mathbf{B}}\mathbf{C}\bar{\mathbf{B}}^{-1} &= \begin{bmatrix} -\frac{(1.125+a)}{1.25+2a+a^2} & -\frac{0.25(-1+a)}{1.25+2a+a^2} \\ -\frac{0.25(-1+a)}{1.25+2a+a^2} & -\frac{(0.125+a+a^2)}{1.25+2a+a^2} \end{bmatrix}
\end{aligned} \quad (7.17)$$

The maximum eigenvalues of the above matrices are evaluated to be

$$\begin{aligned}
\lambda_{max}\left[\mathbf{G}(t)^T + \bar{\mathbf{B}}\mathbf{G}(t)\bar{\mathbf{B}}^{-1}\right] &= -\frac{(1.125+a)f(t)\sqrt{0.078125+1.375a+2.0625a^2+a^3}}{(0.0625+a)(1.25+2a+a^2)}, \\
\lambda_{max}\left[\mathbf{C}^T + \bar{\mathbf{B}}\mathbf{C}\bar{\mathbf{B}}^{-1}\right] &= \frac{0.5(-1.25-2a-a^2-(-1+a)\sqrt{1.25+2a+a^2})}{1.25+2a+a^2}
\end{aligned} \quad (7.18)$$

By applying the corollary-2 as per equation (4.34) and then using Schwarz's Inequality results in the condition for the expectation function as

$$E\{f^2(t)\} \leq \frac{0.25(0.0625+a)^2(1.25+2a+a^2+(-1+a)\sqrt{1.25+2a+a^2})^2}{(1.125+a)^2(0.078125+1.375a+2.0625a^2+a^3)} \quad (7.19)$$

Figure 7.2 displays the result obtained from equation (7.19) for a in the range of 0 to 1, using solid black dots. A comparison of the trend of the stability conditions yielding from the theorem-2 (in dashed blue line) and corollary-2 (in solid black line) for the case of a commutative quasi-periodic system is also shown in Figure 7.2.

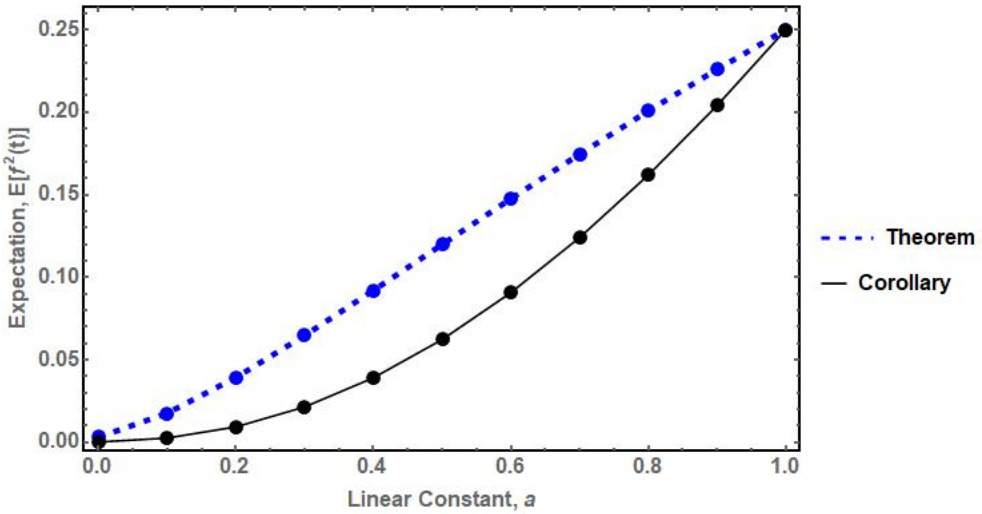

Figure 7.2: Results for the Commutative Quasi-periodic System with Stochastic Parametric Excitations.

7.2 Stability and Robustness of Quasi-periodic System Subjected to Nonlinear Perturbation

Here, the robustness of linear time periodic systems subjected to nonlinear perturbations is investigated. Consider a linear quasi-periodic differential equation with nonlinear perturbation, $\mathbf{f}(\mathbf{x}, t)$, given by

$$\dot{\mathbf{x}} = \mathbf{A}(t)\mathbf{x} + \mathbf{f}(\mathbf{x}, t) \tag{7.20}$$

Using the L-P transformation $\mathbf{x} = \bar{\mathbf{P}}(t)\mathbf{z}$ on equation (7.20) results in

$$\dot{\mathbf{z}} = \bar{\mathbf{J}}\mathbf{z} + \bar{\mathbf{P}}^{-1}(t)\mathbf{f}(\bar{\mathbf{P}}(t)\mathbf{z}, t) \tag{7.21}$$

It is to be noted that the original unperturbed system in equation (7.20) is stable, and the eigenvalues of matrix $\bar{\mathbf{J}}$ have negative real parts. The following is a theorem guaranteeing the stability of the system described by equation (7.20).

Theorem-3: The system described in equation (7.20) is asymptotically stable if the following bounding condition is met.

$$||\bar{\mathbf{P}}^{-1}(t)\mathbf{f}(\mathbf{x},t)|| \leq \mu||\mathbf{x}|| \qquad \mu \geq 0, \quad \forall t \geq 0 \tag{7.22}$$

where

$$\mu = \frac{\lambda_{max}^2[(\bar{\mathbf{J}}^T\bar{\mathbf{B}} + \bar{\mathbf{B}}\bar{\mathbf{J}})\bar{\mathbf{B}}^{-1}]}{4||\bar{\mathbf{P}}^{-1}(t)||} \tag{7.23}$$

$\lambda_{max}[.]$ is defined as the largest eigenvalue of the argument, and $\bar{\mathbf{B}}$ is a positive definite, symmetric matrix that satisfies the condition $\bar{\mathbf{J}}^T\bar{\mathbf{B}} + \bar{\mathbf{B}}\bar{\mathbf{J}} = -\bar{\mathbf{D}}$

Proof: Consider the transformed nonlinear system described by equation (7.22). Define a Lyapunov function and $||\mathbf{z}||$ by

$$V(\mathbf{z}) = \mathbf{z}^T\bar{\mathbf{B}}\mathbf{z} \equiv ||\mathbf{z}||, \qquad \bar{\mathbf{B}} = \bar{\mathbf{B}}^T \tag{7.24}$$

Similar to equation (7.5), the Lyapunov function in equation (7.24) is differentiated, equation (7.21) is substituted and rearranged to obtain

$$\dot{V}(\mathbf{z}) = \mathbf{z}^T[\bar{\mathbf{J}}^T\bar{\mathbf{B}} + \bar{\mathbf{B}}\bar{\mathbf{J}}]\mathbf{z} + 2\mathbf{z}^T\bar{\mathbf{B}}\bar{\mathbf{P}}^{-1}(t)\mathbf{f}(\bar{\mathbf{P}}(t)\mathbf{z},t) \tag{7.25}$$

By using the Schwarz's inequality, the second term in equation (7.25) satisfies

$$\mathbf{z}^T\bar{\mathbf{B}}\bar{\mathbf{P}}^{-1}(t)\mathbf{f}(\bar{\mathbf{P}}(t)\mathbf{z},t) \leq [\mathbf{z}^T\bar{\mathbf{B}}\mathbf{z}]^{1/2}[\{\bar{\mathbf{P}}^{-1}(t)\mathbf{f}(\bar{\mathbf{P}}(t)\mathbf{z},t)\}^T\bar{\mathbf{B}}\{\bar{\mathbf{P}}^{-1}(t)\mathbf{f}(\bar{\mathbf{P}}(t)\mathbf{z},t)\}]^{1/2} \tag{7.26}$$

At this point the nonlinearity needs to satisfy a bounding condition

$$||\bar{\mathbf{P}}^{-1}(t)\mathbf{f}(\bar{\mathbf{P}}(t)\mathbf{z},t)|| \leq \mu'||\mathbf{z}||, \qquad \mu' \geq 0, \quad \forall t \geq 0 \tag{7.27}$$

The quantity μ' is to be determined by substituting the bounding condition into equation (7.26) and determining what values of μ' that make $\dot{V}$ negative definite. Ob-

serving that $\bar{\mathbf{P}}^{-1}(t)\mathbf{f}(\bar{\mathbf{P}}(t)\mathbf{z},t)\}^T\bar{\mathbf{B}}\{\bar{\mathbf{P}}^{-1}(t)\mathbf{f}(\bar{\mathbf{P}}(t)\mathbf{z},t)\}$ is equal to $||\bar{\mathbf{P}}^{-1}(t)\mathbf{f}(\bar{\mathbf{P}}(t)\mathbf{z},t)||$, equation (7.27) can be substituted into equation (7.26) to obtain

$$\mathbf{z}^T\bar{\mathbf{B}}\bar{\mathbf{P}}^{-1}(t)\mathbf{f}(\bar{\mathbf{P}}(t)\mathbf{z},t) \leq [\mathbf{z}^T\bar{\mathbf{B}}\mathbf{z}]^{1/2}\mu'[\mathbf{z}^T\bar{\mathbf{B}}\mathbf{z}]^{1/2} \tag{7.28}$$

Now substituting equation (7.28) into equation (7.25) and dividing both sides by $V(\mathbf{z})$ yields

$$\frac{\dot{V}(\mathbf{z})}{V(\mathbf{z})} \leq \frac{\mathbf{z}^T[\bar{\mathbf{J}}^T\bar{\mathbf{B}} + \bar{\mathbf{B}}\bar{\mathbf{J}}]\mathbf{z} + 2\sqrt{\mu'}V(\mathbf{z})}{V(\mathbf{z})} \tag{7.29}$$

By applying the eigenvalues of pencils of quadratic form

$$\dot{V}(\mathbf{z}) \leq [\lambda_{max} + 2\sqrt{\mu'}]V(\mathbf{z}) \tag{7.30}$$

where λ_{max} is the largest eigenvalue of $[(\bar{\mathbf{J}}^T\bar{\mathbf{B}} + \bar{\mathbf{B}}\bar{\mathbf{J}})\bar{\mathbf{B}}^{-1}]$. From equation (7.29)

$$V(\mathbf{z}) \leq V(0)e^{(\lambda_{max}+2\sqrt{\mu'})t} \tag{7.31}$$

or

$$||\mathbf{z}(t)|| \leq ||\mathbf{z}(0)||e^{(\lambda_{max}+2\sqrt{\mu'})t} \tag{7.32}$$

with $(\lambda_{max} + 2\sqrt{\mu'}) < 0$, the norm of $||\mathbf{z}|| \to 0$ as $t \to \infty$. Since the stability of $\mathbf{z}$ and $\mathbf{x}$ are linked if it is guaranteed that $\mathbf{z}$ is stable, the same can be said for $\mathbf{x}$. Noting that λ_{max} is real and less than zero, μ' must be less than $\frac{\lambda_{max}^2}{4}$. Thus making our smallest bound $\mu' = \frac{\lambda_{max}^2}{4}$.

With the bounding condition described in equation (7.27) in the transformed domain $||\mathbf{z}||$, it is limited in its usefulness. In order to arrange it in terms of $||\mathbf{x}||$, a more useful form, equation (7.27) is multiplied by $\bar{\mathbf{P}}(t)$

$$||\bar{\mathbf{P}}(t)||\,||\bar{\mathbf{P}}^{-1}(t)\mathbf{f}(\bar{\mathbf{P}}(t)\mathbf{z},t)|| \leq \mu'||\bar{\mathbf{P}}(t)||\,||\mathbf{z}|| \tag{7.33}$$

Now, consider the norms of the L-P transformation

$$||\mathbf{x}|| \leq ||\bar{\mathbf{P}}(t)||\,||\mathbf{z}|| \tag{7.34}$$

The norm $||\bar{\mathbf{P}}(t)||\,||\mathbf{z}||$ in equation (7.32) can be replaced with $||\mathbf{x}||$ without increasing the allowable bound on the nonlinearity $||\bar{\mathbf{P}}^{-1}(t)\mathbf{f}(\bar{\mathbf{P}}(t)\mathbf{z},t)||$. This substitution decreases the bound on the nonlinearity making it more conservative. Performing this operation and dividing through by $||\bar{\mathbf{P}}(t)||$ yields

$$||\bar{\mathbf{P}}^{-1}(t)\mathbf{f}(\mathbf{x},t)|| \leq \mu||\mathbf{x}||, \qquad \mu = \frac{\mu'}{||\bar{\mathbf{P}}(t)||} \tag{7.35}$$

The above discussed theorem on the stability of a nonlinearly perturbed quasi-periodic system is also verified with multiple examples of linear quasi-periodic systems and is detailed in the following sections.

7.2.1 Example-12: Non-commutative Quasi-periodic System with Nonlinear Perturbations

Consider a damped Hills quasi-periodic equation with cubic nonlinearity and a quasi-periodic coefficient.

$$\ddot{x} + \zeta\dot{x} + \left[a + b(\cos(\omega_1 t) + \cos(\omega_2 t))\right] x - \epsilon(\cos(\pi t) + \cos(t))x^3 = 0 \tag{7.36}$$

where a, b are constants, ω_1, ω_2 are the incommensurate frequencies, and ζ is the damping coefficient. Considering $x_1 = x$ and $x_2 = \dot{x}$ as the system states, equation (7.36) can be expressed in the state space form as equation (7.20) where

$$\mathbf{A}(t) = \begin{bmatrix} 0 & 1 \\ -(a + b(\cos(\omega_1 t) + \cos(\omega_2 t))) & -\zeta \end{bmatrix}, \quad \mathbf{f}(\mathbf{x},t) = \begin{Bmatrix} 0 \\ \epsilon(\cos(\pi t) + \cos(t))x_1^3 \end{Bmatrix} \tag{7.37}$$

For this example, the bounds for the nonlinearity are found as a function of ζ with the values of system parameters a, b, ω_1 and ω_2 fixed at $5, 4, 2\pi$ and 7 respectively. As discussed in section 7.2, the L-P transformation $\mathbf{x} = \bar{\mathbf{P}}(t)\mathbf{z}$ reduces the system to a form similar to equation (7.21). When $\zeta = 0.2$, the $\bar{\mathbf{J}}$ matrix is computed to be

$$\bar{\mathbf{J}} = \begin{bmatrix} -0.1 - i2.387 & 0 \\ 0 & -0.1 + i2.387 \end{bmatrix} \tag{7.38}$$

Considering only the real part of the $\bar{\mathbf{J}}$ matrix, the Lyapunov equation $\bar{\mathbf{J}}^T\bar{\mathbf{B}} + \bar{\mathbf{B}}\bar{\mathbf{J}} + \mathbf{I} = \mathbf{0}$ is used to compute the symmetric positive definite matrix $\bar{\mathbf{B}}$ as

$$\bar{\mathbf{B}} = \begin{bmatrix} 5 & 0 \\ 0 & 5 \end{bmatrix} \tag{7.39}$$

For the case when $\zeta = 0.2$, the maximum eigenvalue and norm for $\bar{\mathbf{P}}(t)$ are computed to be

$$\lambda^2_{max}[(\bar{\mathbf{J}}^T\bar{\mathbf{B}} + \bar{\mathbf{B}}\bar{\mathbf{J}})\bar{\mathbf{B}}^{-1}] = 0.04, \qquad ||\bar{\mathbf{P}}(t)|| = 1.14013 \tag{7.40}$$

With these values known, the value of μ for the case of $\zeta = 0.2$ is computed to be $\mu = 0.00877$. For varying values of ζ, the values for μ is computed and indicated in Figure 7.3 in solid blue dots. The trend for bounding constant is indicated in the dashed blue line and is observed to increase with more significant amounts of damping in the system. However, this is the boundary for the norm of the product between the nonlinearity and $\bar{\mathbf{P}}(t)$.

For this particular problem, a greater simplification is possible on the bounding condition as there is only one entry in the perturbation matrix. The bounding condition, equation (7.22), takes the form

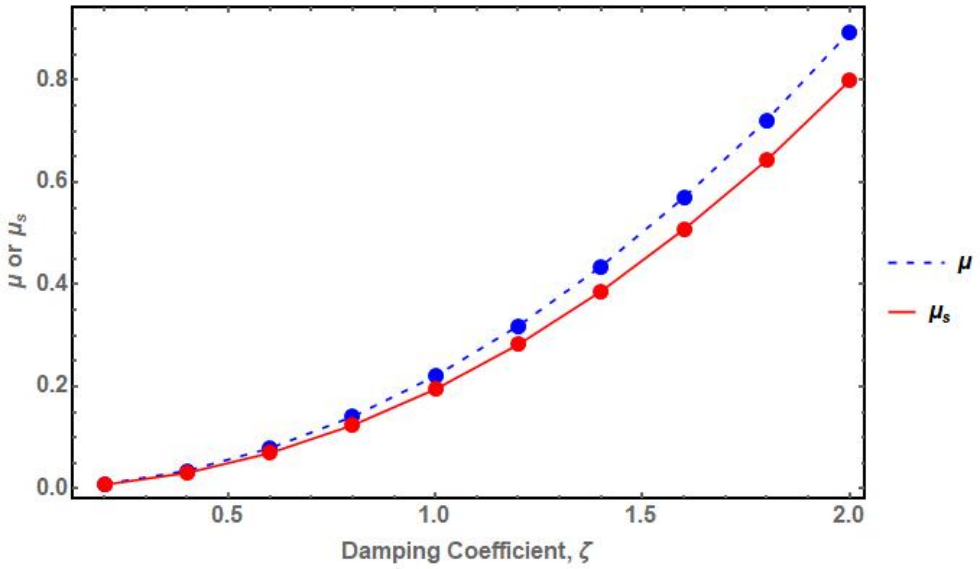

Figure 7.3: Results for the Commutative Quasi-periodic System with Nonlinear Perturbations.

$$\left\| \bar{\mathbf{P}}^{-1}(t) \begin{Bmatrix} 0 \\ \epsilon(\cos(\pi t) + \cos(t))x_1^3 \end{Bmatrix} \right\| \leq \mu ||\mathbf{x}|| \tag{7.41}$$

After expanding the left hand term, recognizing $\epsilon(\cos(\pi t) + \cos(t))x_1^3$ to be scalar, the following is obtained

$$|\epsilon(\cos(\pi t) + \cos(t))x_1^3|^2 \leq \frac{\mu ||\mathbf{x}||}{\left\| \begin{Bmatrix} \bar{\mathbf{P}}_{12}^{-1}(t) \\ \bar{\mathbf{P}}_{22}^{-1}(t) \end{Bmatrix} \right\|} \tag{7.42}$$

Defining $\mu_s = \dfrac{\mu}{\left\| \begin{Bmatrix} \bar{\mathbf{P}}_{12}^{-1}(t) \\ \bar{\mathbf{P}}_{22}^{-1}(t) \end{Bmatrix} \right\|}$, the expression $\mu_s ||\mathbf{x}||$ yields the upper bound for the nonlinearity. A plot of this ratio (μ_s) versus ζ is also given in Figure 7.3 in a solid red line. As in the plot of μ, the boundary increases with more significant amounts of damping in the system.

Figure 7.4 shows the response of the system states versus time for the system

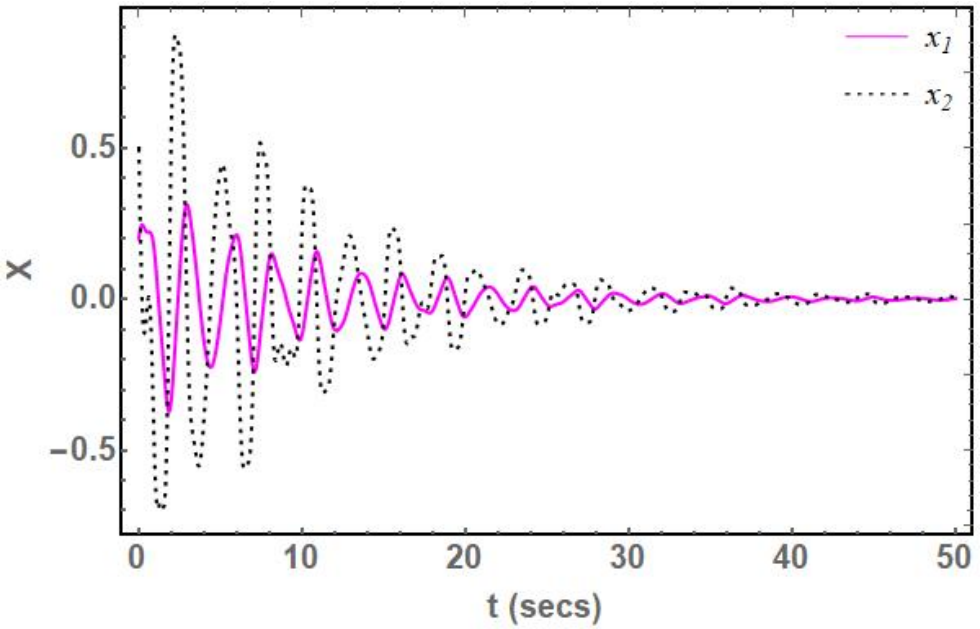

Figure 7.4: Temporal Variations of the System States of the Non-commutative Quasi-periodic System with $\zeta = 0.2$ and Nonlinear Perturbations

equation (7.36), with $\zeta = 0.2, \epsilon = 0.8$ and an initial condition of $x_{10} = 0.2, x_{20} = 0.5$. A graphical illustration of the bounding condition is shown in Figure 7.5. Here, the dynamical system was numerically integrated using MATHEMATICA to generate a plot of $\mu_s||\mathbf{x}||$ and $|\mathbf{f}(\mathbf{x},t)|^2 = |\epsilon(\cos(\pi t) + \cos(t))x_1^3|^2$ versus $||\mathbf{x}||$ for the same set of initial conditions and system parameters. It is shown that for this initial condition, the system is stable, and thus the nonlinearity never exceeds the bounding condition.

However, the theorem only provides sufficient conditions for stability. Therefore, another initial condition could have been chosen to cause the nonlinearity to exceed the bounding condition, yet the system would remain stable.

Example-13: Commutative Quasi-periodic System with Nonlinear Perturbations

Similar to the example in section 7.1.2, initially consider a commutative quasi-periodic with a nonlinear perturbation of the form indicated as

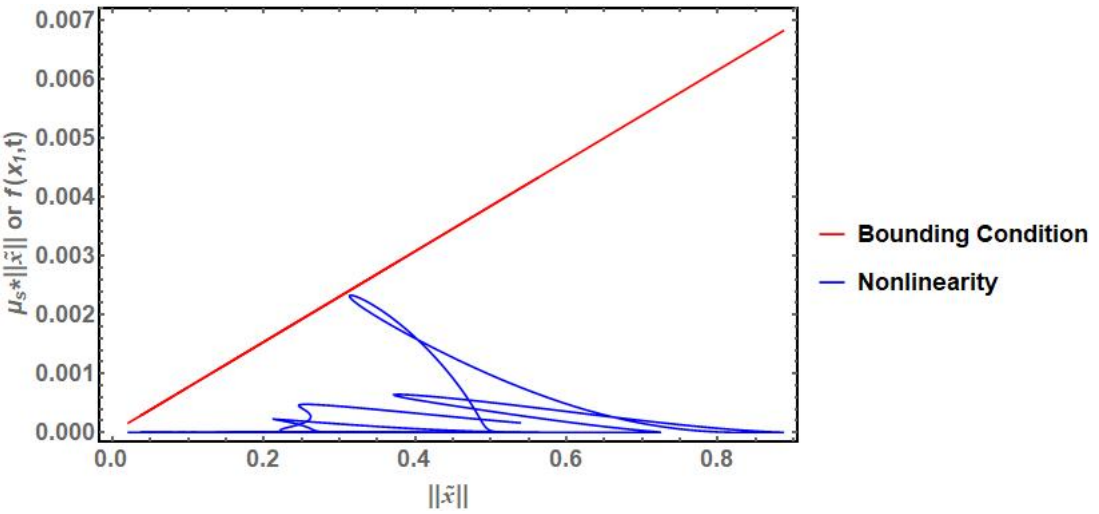

Figure 7.5: Results for the Non-commutative Quasi-periodic System with Nonlinear Perturbations Indicating the Bounding Condition and Nonlinear Behavior.

$$\begin{aligned}\ddot{x} - 2b(\cos(\omega_1 t) + \cos(\omega_2 t))\dot{x} - d\dot{x} + [a + b\omega_1 \sin(\omega_1 t) + b\omega_2 \sin(\omega_2 t) \\ + (b\cos(\omega_1 t) + b\cos(\omega_2 t) - d)^2]x + \epsilon x^3 = 0\end{aligned} \tag{7.43}$$

where ω_1 and ω_2 are incommensurate frequencies, constants a, b are real positive integers. Again, by considering $x_1 = x$ and $x_2 = \dot{x}_1 - (b\cos(\omega_1 t) + b\cos(\omega_2 t))x_1$ as the system states, the equation (7.43) can be expressed in the state space form as equation (7.20) where

$$\mathbf{A}(t) = \begin{bmatrix} b(\cos(\omega_1 t) + \cos(\omega_2 t)) - d & 1 \\ -a & b(\cos(\omega_1 t) + \cos(\omega_2 t)) - d \end{bmatrix}, \quad \mathbf{f}(\mathbf{x}, t) = \begin{Bmatrix} 0 \\ -\epsilon x_1^3 \end{Bmatrix} \tag{7.44}$$

As detailed in section 7.1.2, the closed form expressions for the L-P transformation matrix ($\mathbf{P}(t)$) and exponent matrix ($\mathbf{C}$) are computed for the linear part. For this example, the system parameters considered are $a = 3, b = 1, \omega_1 = 2\pi$ and $\omega_2 = 7$, resulting in

$$\mathbf{C} = \begin{bmatrix} -d & 1 \\ -3 & -d \end{bmatrix} \tag{7.45}$$

Similar to the case of non-commutative system, equation (7.45) is used for solving the Lyapunov equation $\mathbf{C}^T\bar{\mathbf{B}}+\bar{\mathbf{B}}\mathbf{C}+\mathbf{I} = \mathbf{0}$, considering the $\bar{\mathbf{B}}$ matrix to be symmetric, the following is obtained

$$\bar{\mathbf{B}} = \begin{bmatrix} \frac{6+d^2}{6d+2d^3} & -\frac{0.5}{3+d^2} \\ -\frac{0.5}{3+d^2} & \frac{2+d^2}{6d+2d^3} \end{bmatrix} \tag{7.46}$$

Following the procedure described before in the case of non-commutative system, the maximum eigenvalue and norm for $\mathbf{P}(t)$ can be computed as

$$\lambda_{max}[(\mathbf{C}^T\bar{\mathbf{B}}+\bar{\mathbf{B}}\mathbf{C})\bar{\mathbf{B}}^{-1}] = -\frac{2d(4+d^2+0.5\sqrt{16+4d^2})}{4+d^2}, \qquad ||\mathbf{P}(t)|| = 1.3395 \tag{7.47}$$

A plot of μ versus d is given in Figure 7.6, indicated in the dashed blue line. As expected, the bounding constant boundary increases with an increase in system damping. In this example too, since the perturbation matrix consists of only one element, the bounding condition in equation (7.22) takes the form

$$\left\| \mathbf{P}^{-1}(t) \begin{Bmatrix} 0 \\ \epsilon x_1^3 \end{Bmatrix} \right\| \leq \mu||\mathbf{x}|| \tag{7.48}$$

After expanding the left hand term, recognizing $\mathbf{P}_{12}^{-1}(t) = 0$ and ϵx_1^3 to be scalar, the following is obtained

$$|\epsilon x_1^3|^2 \leq \frac{\mu||\mathbf{x}||}{||\mathbf{P}_{22}^{-1}(t)||} \tag{7.49}$$

By defining $\mu_s = \frac{\mu}{||\mathbf{P}_{22}^{-1}(t)||}$, the expression $\mu_s||\mathbf{x}||$ yields the upper bound for the nonlinearity. A plot of this ratio (μ_s) versus d is also given in Figure 7.6 in the solid

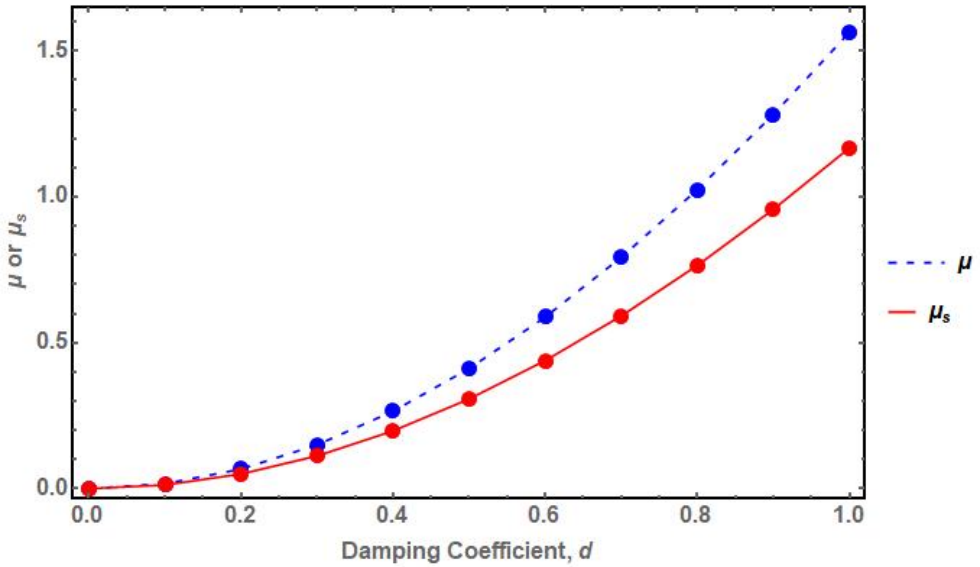

Figure 7.6: Results for the Commutative Quasi-periodic System with Nonlinear Perturbations.

red line. As in the plot of μ, the boundary increases with the increase in system damping.

Figure 7.7 shows the response of the system states versus time for the system equation (7.43), with $d = 0.2, \epsilon = 0.2$ and an initial condition of $x_{10} = 1, x_{20} = 0$. It is observed that both the system states dampen out in less than 30 seconds. A graphical illustration of the bounding condition is shown in Figure 7.8. Again, the dynamical system is numerically integrated to generate a plot of $\mu_s||\mathbf{x}||$ and $|\mathbf{f}(\mathbf{x}, t)|^2 = |\epsilon x_1^3|^2$ versus $||\mathbf{x}||$.

However, the theorem only provides sufficient conditions for stability. Therefore, another initial condition could have been chosen to cause the nonlinearity to exceed the bounding condition, yet the system would remain stable.

7.3 Discussion and Conclusion

In this work, the sufficient conditions for robust stability of the linear quasi-periodic system with stochastic excitation and nonlinear perturbations are showcased.

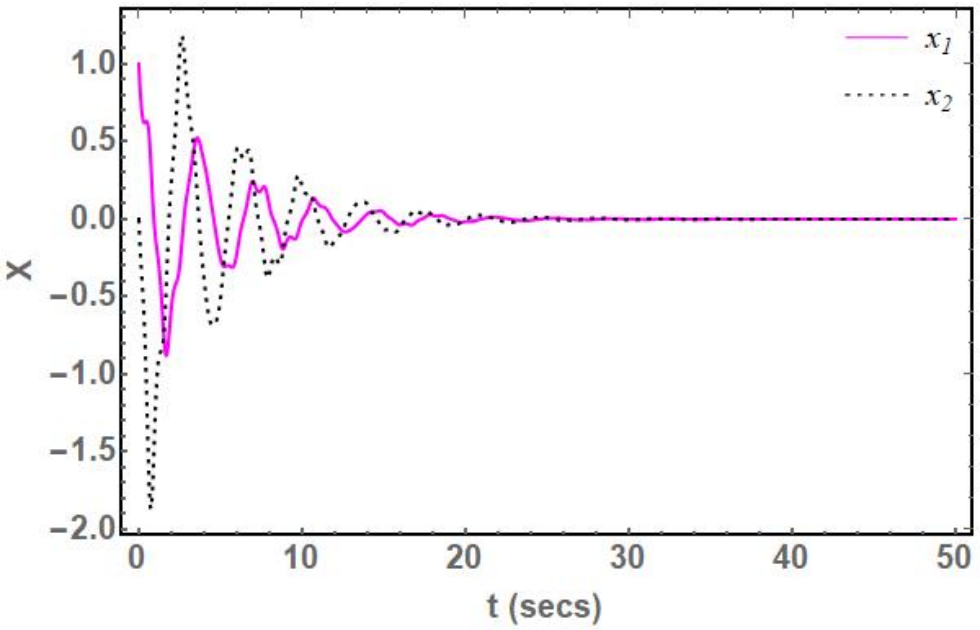

Figure 7.7: Temporal Variations of the System States of the Commutative Quasi-periodic System with $d = 0.2$ and Nonlinear Perturbations

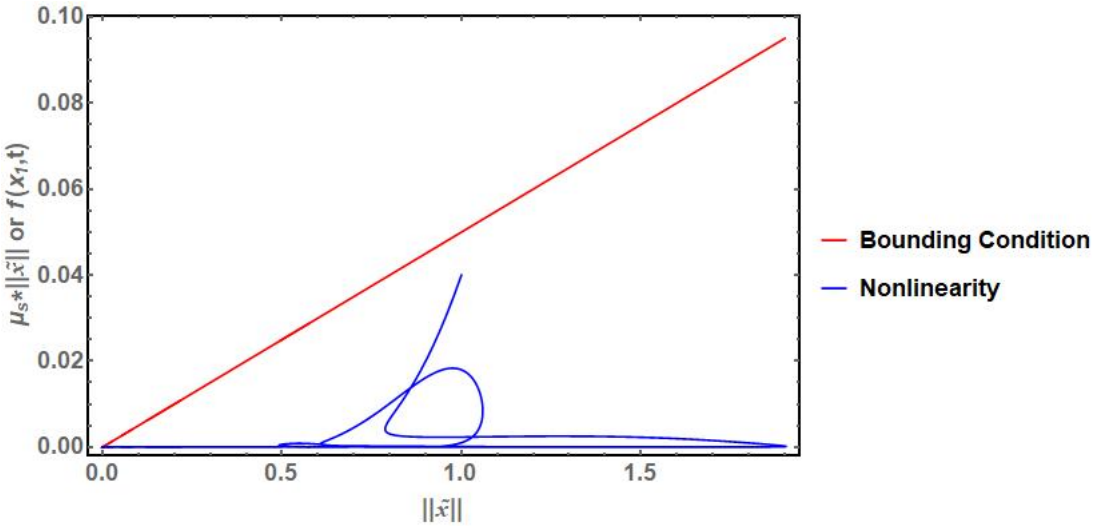

Figure 7.8: Results for the Commutative Quasi-periodic System with Nonlinear Perturbations Indicating the Bounding Condition and Nonlinear Behavior.

Initially, the system with stochastic parametric excitation is considered, and an L-P transformation converts the time-varying linear matrix to its time-invariant form. In the case of a non-commutative system, the Jordan form of the time-invariant matrix is obtained, and for the commutative system, the closed form expression of the same is computed analytically. Using the Infante approach and Lyapunov function, a theorem and related corollary proposed for time periodic system are also extended towards the linear quasi-periodic system with stochastic parametric excitation. The linear matrix ($\bar{\mathbf{J}}$) requirements needing to have negative real parts and $\bar{\mathbf{B}}$ matrix to be positive definite may limit the application of this technique. However, this approach is feasible to extend towards systems with deterministic variation in parameters too.

Later, the quasi-periodic system with external nonlinear perturbations is considered for the asymptotic stability analysis. In this system too, an L-P transformation is performed to the linear time varying part. Subsequently, a Lyapunov function is constructed, and using Schwarz's inequality, and pencils of quadratic form, the bounding condition on the nonlinear perturbations are derived. Finally, a theorem with the bounding condition of nonlinearities guaranteeing the stability of a nonlinearly perturbed quasi-periodic system is suggested with proof.

Additionally, in this chapter, the application of both theorems of robust stability is demonstrated with the examples of commutative and non-commutative quasi-periodic systems subjected to uncertain parametric excitations and nonlinear perturbations. In all cases, the bounds of stability were observed to increase as the damping in the corresponding system increased. However, these bounds only define the sufficient condition for asymptotic stability, and the system may continue to remain stable beyond these bounds. The implementation of these bounding conditions in controller design will be presented in future work.

Chapter 8

LIMITATIONS AND FUTURE WORK

The novel unified approach discussed in this work aided in analyzing both periodically and quasi-periodically time varying systems. It was also applicable towards the analysis of these systems with multiple perturbations. However, this approach also has some limitations and is discussed in the following sections.

8.1 Convergence

In this work, the unified theory is based on the method of Normal Forms and intuitive state augmentation. The method of Normal Forms could be viewed as a higher-order averaging technique Kahn and Zarmi (2014). Unfortunately, in general cases, the near identity transformation may not be convergent. If the eigenvalues are in the Poincare Domain, a finite number of resonances are possible, and the near identity transformation generally convergences. However, when the eigenvalues are on the Seigel domain, the convergence is not guaranteed even if they do not resonate (as the case discussed in this work) Kahn and Zarmi (2014). However, Seigel's theorem Siegel (1961) provides the condition when the near identity transformation is convergent. The near identity transformation is convergent for sufficiently small $|\epsilon|$ and for some initial conditions if eigenvalues obey the condition $|\lambda_i - (\boldsymbol{\lambda}, \mathbf{m})| \geq \frac{C}{|\mathbf{m}|^\nu}$ where C and ν are positive real numbers. Intuitively, it means that for all possible $(\boldsymbol{\lambda}, \mathbf{m})$ products are separated from all λ_i by a strip, then the near identity transformation converges Kahn and Zarmi (2014); Siegel (1961). In this work, the examples discussed are verified to satisfy these conditions. If the values are selected such that the system is on the stability boundary or very close to it, then the near identity

transformation in the quasi-periodic system does not converge.

8.2 Reducibility

The reducibility of quasi-periodic systems via the L-P transformation presented in this work can be viewed as "almost reducibility" where the reduced system is close to a constant system. In general, complete reducibility for a quasi-periodic system cannot be achieved because Floquet type theory does not exist for general quasi-periodic system by Arnold (2012). In very special cases, if a quasi-periodic system satisfies special conditions expressed in terms of the solution operator of the associated partial differential equation, then perfect reducibility may be achieved, as discussed by Murdock (1978). However, for practical purposes, "almost reducibility" may be sufficient. In this section, the approach presented by Jorba and Simó (1992) and the similarities between their approach and the approach presented here are drawn.

Jorba and Simó (1992) discussed the reducibility of a quasi-periodic system of the form

$$\dot{\mathbf{x}} = (\mathbf{A} + \epsilon \mathbf{K}(t))\mathbf{x} \tag{8.1}$$

where $\mathbf{x}$ is a d dimensional vector. The eigenvalues of $\mathbf{A}$ matrix are denoted by λ_i and $\lambda^T = [\lambda_1, \lambda_2, ..., \lambda_d]$, the frequencies in $\mathbf{K}(t)$ are denoted by $\omega = [\omega_1, \omega_2, ..., \omega_r]^T$. They presented a theorem when a non-resonant condition for the vector, $\mathbf{v}^T = \left[\lambda^T, \omega^T\right]$, is satisfied by a set of big relative measures in the space of parameter $\mathbf{v}$, under some non-degeneracy condition. If ϵ_0 is small enough, there exists a Cantorian subset $\boldsymbol{\epsilon}$ of $[0, \epsilon_0]$ of a positive measure such that, if $\epsilon \in \boldsymbol{\epsilon}$ then system given by the equation 8.1 is *almost* reducible. It is noted that the result is valid when the eigenvalues of $\mathbf{A}$ are purely imaginary. They show the convergence using the ideas similar to those presented by Bogoljubov *et al.* (1976) and KAM theory by Arnol'd (1963). They

perform averaging at each step and use the change of variables $\mathbf{x} = (\mathbf{I}+\epsilon\mathbf{P})\mathbf{y}$ to solve matrix differential equations at each order of ϵ. Thus, they perform averaging at each order of ϵ and finally obtain

$$\dot{\mathbf{x}}_n = (\mathbf{A}_n + \epsilon^{2n}\tilde{\mathbf{K}}_n(t))\mathbf{x}_n \tag{8.2}$$

It can be noted that the process discussed in this work to compute the L-P transformation is similar to the successive averaging approach presented by Jorba and Simo.

8.3 Higher Excitation

In this work, the Normal Forms technique is applied when the eigenvalues of the Jordan form are semi-simple, but the technique can be extended to non semi-simple eigenvalues, as discussed by Bi and Yu (1998). Though the Normal Forms technique is considered local in nature, the techniques are tested for high or strongly excited systems in this section.

The comparisons of the temporal variations of the linear quasi-periodic system with a higher coefficient of the quasi-periodic system are indicated in the following figures. The equation (5.23) is modified slightly as indicated below to remove the damping terms and to vary each periodic term individually.

$$\ddot{x} + (a + b_1\cos(\omega_1 t) + b_2\cos(\omega_2 t))x = 0 \tag{8.3}$$

The incommensurate frequencies considered in all the cases remain the same as $\omega_1 = 2\pi$ rads and $\omega_2 = 7$ rads. The temporal variation comparisons of system states of Hills quasi-periodic systems with significant parametric excitation are indicated in Figures 8.1a,b, and 8.2a,b.

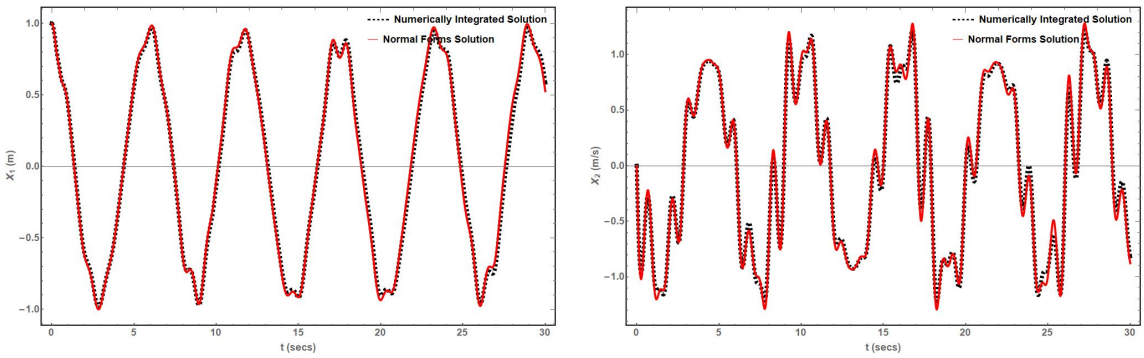

(**a**) (**b**)

Figure 8.1: The System State Variation Comparisons for the Quasi-periodic System with System Parameters ($a = 1, b_1 = b_2 = 2.5$ in Equation (8.3)), Where (**a**) Is That of x_1 State, (**b**) Is That of x_2 State

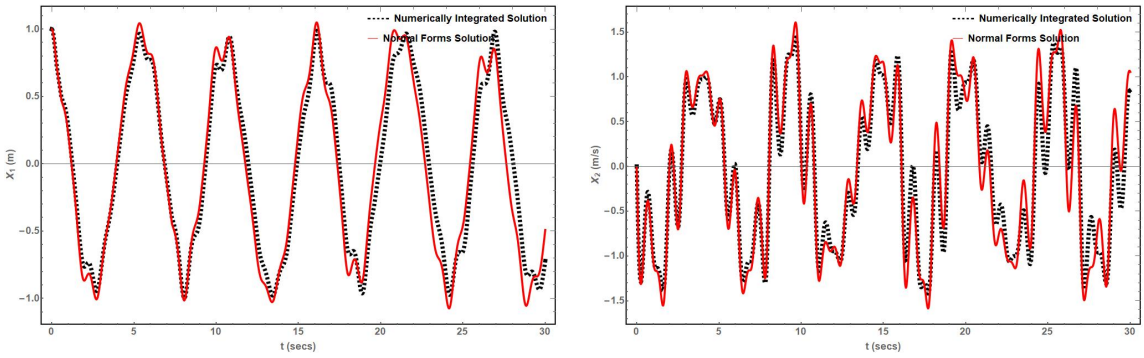

(**a**) (**b**)

Figure 8.2: The System State Variation Comparisons for the Quasi-periodic System with System Parameters ($a = 1.0, b_1 = 2.5, b_2 = 5.0$ in Equation (8.3)), Where (**a**) Is That of x_1 State, (**b**) Is That of x_2 State

It is observed that as the quasi-periodic system tends to have stronger excitations or higher coefficients, the proposed unified approach fails to converge with the numerical simulations. In such a case an alternate approach to apply L-F transformation successively twice is suggested. A brief overview of the formulation is provided in the subsequent section.

8.4 Double L-F Method

Consider a linear quasi-periodic system expressed as

$$\ddot{x} + (a_1 + b_1\cos(\omega_1 t) + c_1\cos(\omega_2 t))x + (a_2 + b_2\cos(\omega_1 t) + c_2\cos(\omega_2 t))\dot{x} = 0 \quad (8.4)$$

where the frequencies ω_1 and ω_2 are incommensurate. The system in equation (8.4), can be expressed in its generic form as indicated below

$$\dot{\mathbf{x}} = \mathbf{A}_0\mathbf{x} + \mathbf{A}_1(\omega_1 t)\mathbf{x} + \mathbf{A}_2(\omega_2 t)\mathbf{x} \quad (8.5)$$

where $\mathbf{A}_0$ is the constant matrix, $\mathbf{A}_1(\omega_1 t)$ is the matrix containing all the terms of or multiples of frequency ω_1. Similarly, $\mathbf{A}_2(\omega_1 t)$ matrix contains all the terms of or multiples of frequency ω_2. By grouping the first two terms and applying an L-F transformation of the form $\mathbf{x} = \mathbf{Q}(t)\mathbf{z}$, updates the system equation as follows

$$\dot{\mathbf{z}} = \mathbf{R}\mathbf{z} + \mathbf{Q}^{-1}(t)\mathbf{A}_2(\omega_2 t)\mathbf{Q}(t)\mathbf{z} \quad (8.6)$$

where $\mathbf{Q}^{-1}(t)$ and $\mathbf{Q}(t)$ matrix elements contain truncated Fourier series of the form indicated below

$$\sum_{n=1}^{\infty} k_0 + k_n\cos(n\omega_1 t) + k_n\sin(n\omega_1 t) \quad (8.7)$$

The state augmentation of the form indicated below is applied

$$\begin{aligned} p &= \cos(\omega_1 t) \\ \dot{p} &= -\omega_1\sin(\omega_1 t) = q \\ \ddot{p} &= -{\omega_1}^2\cos(\omega_1 t) = -{\omega_1}^2 p = \dot{q} \end{aligned} \quad (8.8)$$

Since the augmented states are with frequency ω_1, the terms with multiples of this frequency (in both $\mathbf{Q}^{-1}(t)$ and $\mathbf{Q}(t)$ matrices) are expanded/redefined using Ptolemy's and double-angle formulae trigonometric identities and replaced using 'p's and 'q's.

The system states are updated as follows

$$\tilde{\mathbf{z}} = [\mathbf{z}, p, q] \tag{8.9}$$

The updated system equation after the state augmentation is represented as

$$\dot{\tilde{\mathbf{z}}} = \tilde{\mathbf{R}}\tilde{\mathbf{z}} + (\mathbf{B}_1(\tilde{\mathbf{z}})\mathbf{A}_2(\omega_2 t)\mathbf{B}_2(\tilde{\mathbf{z}}))\tilde{\mathbf{z}} \tag{8.10}$$

where $\mathbf{B}_1(\tilde{\mathbf{z}})$ and $\mathbf{B}_2(\tilde{\mathbf{z}})$ represent the state augmented $\mathbf{Q}^{-1}(t)$ and $\mathbf{Q}(t)$ matrices respectively. The updated system equation is further rearranged as shown below

$$\dot{\tilde{\mathbf{z}}} = \tilde{\mathbf{R}}\tilde{\mathbf{z}} + \mathbf{A}_3(\omega_2 t)\tilde{\mathbf{z}} + \breve{\mathbf{B}}(\tilde{\mathbf{z}}, \omega_2 t) \tag{8.11}$$

where $\mathbf{A}_3(\omega_2 t)$ matrix contains only the linear terms of frequency ω_2, and the $\breve{\mathbf{B}}(\tilde{\mathbf{z}}, \omega_2 t)$ vector contains the nonlinear monomials in $\tilde{\mathbf{z}}$ and nonlinear time varying terms. By rearranging the terms and dropping ω_2 for brevity, the system equation can be updated as follows

$$\dot{\tilde{\mathbf{z}}} = (\tilde{\mathbf{R}} + \mathbf{A}_3(t))\tilde{\mathbf{z}} + \breve{\mathbf{B}}(\tilde{\mathbf{z}}, t) \tag{8.12}$$

Since the linear part is periodic with frequency ω_2, the updated equation is now amenable to a second L-F transformation of the form $\tilde{\mathbf{z}} = \mathbf{P}(t)\mathbf{y}$, resulting in the following expression

$$\dot{\mathbf{y}} = \mathbf{C}\mathbf{y} + \mathbf{P}^{-1}(t)\breve{\mathbf{B}}(\mathbf{P}(t)\mathbf{y}, t) \tag{8.13}$$

The application of a modal transformation of the form $\mathbf{y} = \mathbf{M}\mathbf{v}$, updates the system equation as follows

$$\dot{\mathbf{v}} = \mathbf{J}\mathbf{v} + \mathbf{M}^{-1}\mathbf{P}^{-1}(t)\breve{\mathbf{B}}(\mathbf{P}(t)\mathbf{M}\mathbf{v}, t) \tag{8.14}$$

The updated system in equation (8.14) is in its Jordan canonical form and is eligible to apply near identity transformation and Time Dependent Normal Forms technique as detailed in section 2.3.2. In this formulation, the amplitude of periodicity and quasi-periodicity is not assumed to be small, extending its application to resonant conditions.

Amaechi, C. V., F. Wang, X. Hou and J. Ye, "Strength of submarine hoses in chinese-lantern configuration from hydrodynamic loads on calm buoy", Ocean Engineering **171**, 429–442 (2019).

Apiwattanalunggarn, P., S. W. Shaw and C. Pierre, "Component mode synthesis using nonlinear normal modes", Nonlinear Dynamics **41**, 1-3, 17–46 (2005).

Ariaratnam, S. and B. Ly, "Almost-sure stability of some linear stochastic systems", Journal of Applied Mechanics (1989).

Arnold, V., "Mathematical methods of classical mechanics", Ann Arbor **1001**, 48109 (1978).

Arnol'd, V. I., "Small denominators and problems of stability of motion in classical and celestial mechanics", Russian Mathematical Surveys **18**, 6, 85 (1963).

Arnold, V. I., *Geometrical methods in the theory of ordinary differential equations*, vol. 250 (Springer Science & Business Media, 2012).

Belhaq, M., K. Guennoun and M. Houssni, "Asymptotic solutions for a damped non-linear quasi-periodic mathieu equation", International Journal of Non-Linear Mechanics **37**, 3, 445–460 (2002).

Belhaq, M. and M. Houssni, "Quasi-periodic oscillations, chaos and suppression of chaos in a nonlinear oscillator driven by parametric and external excitations", Nonlinear Dynamics **18**, 1, 1–24 (1999).

Bernstein, D. S. and S. P. Bhat, "Lyapunov Stability, Semistability, and Asymptotic Stability of Matrix Second-Order Systems", Journal of Vibration and Acoustics **117**, B, 145–153, URL `https://doi.org/10.1115/1.2838656` (1995).

Bertram, J. and P. Sarachik, "Stability of circuits with randomly time-varying parameters", IRE Transactions on Circuit Theory **6**, 5, 260–270 (1959).

Bhattacharyya, S., H. Chapellat and L. Keel, *Robust Control: The Parametric Approach*, Prentice-Hall information and system sciences series (Prentice Hall PTR, 1995), URL `https://books.google.com/books?id=jKMeAQAAIAAJ`.

Bi, Q. and P. Yu, "Computation of normal forms of differential equations associated with non-semisimple zero eigenvalues", International Journal of Bifurcation and Chaos **8**, 12, 2279–2319 (1998).

Biran, A. and R. L. Pulido, *Ship hydrostatics and stability* (Butterworth-Heinemann, 2013).

Birkhoff, G. D., *Dynamical systems*, vol. 9 (American Mathematical Soc., 1927).

Bittanti, S., P. Bolzern and P. Colaneri, "Stability analysis of linear periodic systems via the lyapunov equation", IFAC Proceedings Volumes **17**, 2, 213–216 (1984).

Bogoljubov, N., J. A. Mitropoliskij and A. Samoilenko, *Methods of accelerated convergence in nonlinear mechanics* (Berlin, 1976).

Broer, H. W., G. B. Huitema and M. B. Sevryuk, *Quasi-periodic motions in families of dynamical systems: order amidst chaos* (Springer, 2009).

Brogan, W., *Modern Control Theory*, QPI series (Prentice-Hall, 1985), URL `https://books.google.com/books?id=PPBQAAAAMAAJ`.

Broomhead, D. and M. Kirby, "Dimensionality reduction using secant-based projection methods: The induced dynamics in projected systems", Nonlinear Dynamics **41**, 1-3, 47–67 (2005).

Butcher, E. A. and S. Sinha, "Symbolic computation of local stability and bifurcation surfaces for nonlinear time-periodic systems", Nonlinear Dynamics **17**, 1, 1–21 (1998).

Castro-Santos, L., A. R. Bento, D. Silva, N. Salvação and C. Guedes Soares, "Economic feasibility of floating offshore wind farms in the north of spain", Journal of Marine Science and Engineering **8**, 1, 58 (2020).

Chen, C.-W., C.-w. Shen, C.-Y. Chen and M.-J. Cheng, "Stability analysis of an oceanic structure using the lyapunov method", Engineering Computations (2010).

Cheung, K., A. Phadke, D. Smith, S. Lee and L. Seidl, "Hydrodynamic response of a pneumatic floating platform", Ocean engineering **27**, 12, 1407–1440 (2000).

Chua, L. O. and H. Kokubu, "Normal forms for nonlinear vector fields. i. theory and algorithm", IEEE transactions on circuits and systems **35**, 7, 863–880 (1988).

Corvaro, S., A. Crivellini, F. Marini, A. Cimarelli, L. Capitanelli and A. Mancinelli, "Experimental and numerical analysis of the hydrodynamics around a vertical cylinder in waves", Journal of Marine Science and Engineering **7**, 12, 453 (2019).

Dabiri, A. and E. A. Butcher, "Optimal observer-based feedback control for linear fractional-order systems with periodic coefficients", Journal of Vibration and Control **25**, 7, 1379–1392 (2019).

Dai, L. and C. Chen, "Dynamic stability analysis of a cracked nonlinear rotor system subjected to periodic excitations in machining", Journal of Vibration and Control **13**, 5, 537–556 (2007).

Davidson, J. and R. Costello, "Efficient nonlinear hydrodynamic models for wave energy converter design—a scoping study", Journal of Marine Science and Engineering **8**, 1, 35 (2020).

Davis, S. H. and S. Rosenblat, "A quasiperiodic mathieu–hill equation", SIAM Journal on Applied Mathematics **38**, 1, 139–155 (1980).

De La Fuente, J., S. C. Subramanian, T. G. Sugar and S. Redkar, "A robust phase oscillator design for wearable robotic systems", Robotics and Autonomous Systems p. 103514 (2020).

Deshmukh, V. and S. Sinha, "Control of dynamic systems with time-periodic coefficients via the lyapunov-floquet transformation and backstepping technique", Journal of Vibration and Control **10**, 10, 1517–1533 (2004).

Deshmukh, V., S. Sinha and P. Joseph, "Order reduction and control of parametrically excited dynamical systems", Journal of Vibration and Control **6**, 7, 1017–1028 (2000).

Ding, Q. and K. Zhang, "Order reduction and nonlinear behaviors of a continuous rotor system", Nonlinear Dynamics **67**, 1, 251–262 (2012).

Driscoll, T. A., N. Hale and L. N. Trefethen, "Chebfun guide", (2014).

Ellermann, K., E. Kreuzer and M. Markiewicz, "Nonlinear dynamics of floating cranes", Nonlinear Dynamics **27**, 2, 107–183 (2002).

Faltinsen, O. M., *Hydrodynamics of high-speed marine vehicles* (Cambridge University Press, New York, USA, 2005).

Floquet, G., "Sur les équations différentielles linéaires à coefficients périodiques", in "Annales scientifiques de l'École normale supérieure", vol. 12, pp. 47–88 (1883).

Follinger, O. *et al.*, "Design of time-varying system by pole assignment", Regelungstechnik **6**, 189–196 (1978).

Gabale, A. and S. Sinha, "Construction of reduced order controllers for nonlinear systems with periodic coefficients", Journal of Vibration and Control **17**, 3, 391–406 (2011).

Gabale, A. P. and S. Sinha, "A direct analysis of nonlinear systems with external periodic excitations via normal forms", Nonlinear Dynamics **55**, 1-2, 79–93 (2009).

Gantmakher, F., *The Theory of Matrices: Volume one*, The Theory of Matrices (Chelsea Publishing Company, 1990), URL `https://books.google.com/books?id=oxHvAAAAMAAJ`.

Giorgi, G., J. Davidson, G. Habib, G. Bracco, G. Mattiazzo and T. Kalmár-Nagy, "Nonlinear dynamic and kinematic model of a spar-buoy: Parametric resonance and yaw numerical instability", Journal of Marine Science and Engineering **8**, 7, 504 (2020).

Glass, L., "Cardiac arrhythmias and circle maps- a classical problem", Chaos: An Interdisciplinary Journal of Nonlinear Science **1**, 1, 13–19 (1991).

Guennoun, K., M. Houssni and M. Belhaq, "Quasi-periodic solutions and stability for a weakly damped nonlinear quasi-periodic mathieu equation", Nonlinear Dynamics **27**, 3, 211–236 (2002).

Guo, D., Z. Nie and L. Yan, "Novel discrete-time zhang neural network for time-varying matrix inversion", IEEE Transactions on Systems, Man, and Cybernetics: Systems **47**, 8, 2301–2310 (2017).

Guo, D. and Y. Zhang, "Zhang neural network for online solution of time-varying linear matrix inequality aided with an equality conversion", IEEE transactions on neural networks and learning systems **25**, 2, 370–382 (2013).

Haller, G. and S. Ponsioen, "Exact model reduction by a slow–fast decomposition of nonlinear mechanical systems", Nonlinear Dynamics **90**, 1, 617–647 (2017).

Harrington, H. A. and R. A. Van Gorder, "Reduction of dimension for nonlinear dynamical systems", Nonlinear Dynamics **88**, 1, 715–734 (2017).

Harris, J. W. and H. Stöcker, *Handbook of mathematics and computational science* (Springer Verlag New York Inc., New York, USA, 1998).

Hu, L., X. Mao and L. Zhang, "Robust stability and boundedness of nonlinear hybrid stochastic differential delay equations", IEEE Transactions on Automatic Control **58**, 9, 2319–2332 (2013).

Huang, J., L. Xiao and W. Zhu, "Investigation of quasi-periodic response of a buckled beam under harmonic base excitation with an "unexplained" sideband structure", Nonlinear Dynamics (2020).

Iakubovich, V. A. and V. M. Starzhinskiĭ, *Linear differential equations with periodic coefficients*, vol. 2 (Wiley, 1975).

Ibrahim, R. and I. Grace, "Modeling of ship roll dynamics and its coupling with heave and pitch", Mathematical Problems in Engineering **2010** (2010).

Infante, E. F., "On the Stability of Some Linear Nonautonomous Random Systems", Journal of Applied Mechanics **35**, 1, 7–12, URL `https://doi.org/10.1115/1.3601177` (1968).

Jezequel, L. and C.-H. Lamarque, "Analysis of non-linear dynamical systems by the normal form theory", Journal of sound and vibration **149**, 3, 429–459 (1991).

Johnson, R. and J. Moser, "The rotation number for almost periodic potentials", Communications in Mathematical Physics **84**, 3, 403–438 (1982).

Jorba, À. and C. Simó, "On the reducibility of linear differential equations with quasiperiodic coefficients", Journal of Differential Equations **98**, 1, 111–124 (1992).

Kacem, N., S. Hentz, S. Baguet and R. Dufour, "Forced large amplitude periodic vibrations of non-linear mathieu resonators for microgyroscope applications", International Journal of Non-Linear Mechanics **46**, 10, 1347–1355 (2011).

Kahn, P. B. and Y. Zarmi, *Nonlinear dynamics: exploration through normal forms* (Courier Corporation, 2014).

Kats, I. I. and N. Krasovskii, "On the stability of systems with random parameters", Journal of Applied Mathematics and Mechanics **24**, 5, 1225–1246 (1960).

Keel, L. H., S. Bhattacharyya and J. W. Howze, "Robust control with structure perturbations", IEEE Transactions on Automatic Control **33**, 1, 68–78 (1988).

Kerschen, G., J.-c. Golinval, A. F. Vakakis and L. A. Bergman, "The method of proper orthogonal decomposition for dynamical characterization and order reduction of mechanical systems: an overview", Nonlinear dynamics **41**, 1-3, 147–169 (2005).

Konovessis, D., K. H. Chua and D. Vassalos, "Stability of floating offshore structures", Ships and Offshore Structures **9**, 2, 125–133 (2014).

Kovacic, I., R. Rand and S. Mohamed Sah, "Mathieu's equation and its generalizations: Overview of stability charts and their features", Applied Mechanics Reviews **70**, 2 (2018).

Kozin, F., "A survey of stability of stochastic systems", Automatica **5**, 1, 95–112 (1969).

Kushner, H. J., "Stochastic stability and control", Tech. rep., Brown Univ Providence RI (1967).

Kwakernaak, H. and R. Sivan, *Linear optimal control systems*, vol. 1 (Wiley-interscience New York, 1972).

Li, Y., C. Le, H. Ding, P. Zhang and J. Zhang, "Dynamic response for a submerged floating offshore wind turbine with different mooring configurations", Journal of Marine Science and Engineering **7**, 4, 115 (2019).

Liao, H., Q. Zhao and D. Fang, "The continuation and stability analysis methods for quasi-periodic solutions of nonlinear systems", Nonlinear Dynamics **100**, 2, 1469–1496 (2020).

Lukes, D. L., *Differential Equations: Classical to Controlled: Mathematics in science and engineering v.162*, vol. 162 of *Mathematics in science and engineering ; 1* (Academic Press, 1982).

Luongo, A. and A. Di Egidio, "Bifurcation equations through multiple-scales analysis for a continuous model of a planar beam", Nonlinear Dynamics **41**, 1-3, 171–190 (2005).

Lyapunov, A., "Sur une série relative a la théorie des équations différentielles linéaires avec coeficient périodiques", Compte Rendu Acad. Sci. Paris **123**, 26, 1248–1252 (1896).

McLachlan, N., *Theory and Application of Mathieu Functions* (Clarendon Press, 1947), URL `https://books.google.com/books?id=ZGC4AAAAIAAJ`.

Megretski, A. and A. Rantzer, "System analysis via integral quadratic constraints", IEEE Transactions on Automatic Control **42**, 6, 819–830 (1997).

Modi, P. and S. Seth, *Hydraulics and Fluid Mechanics (Including Hydraulic Machines)(in Metric Units).* (Standard Book House, New Delhi, India, 1980).

Mond, M., G. Cederbaum, P. Khan and Y. Zarmi, "Stability analysis of the non-linear mathieu equation", Journal of Sound and Vibration **167**, 1, 77–89 (1993).

Moreno-Ahedo, L. and S. Diarte-Acosta, "Stability analysis of linear systems with switchable stiffness using the floquet theory", Journal of Vibration and Control **25**, 5, 963–976 (2019).

Moser, J. and D. Saari, "Stable and random motions in dynamical systems", Physics Today **28**, 47 (1975).

Murdock, J., "On the floquet problem for quasiperiodic systems", Proceedings of the American Mathematical Society **68**, 2, 179–184 (1978).

Murdock, J., *Normal forms and unfoldings for local dynamical systems* (Springer Science & Business Media, 2006).

Nabergoj, R., A. Tondl and Z. Virag, "Autoparametric resonance in an externally excited system", Chaos, Solitons & Fractals **4**, 2, 263–273 (1994).

Nayfeh, A. H., "Order reduction of retarded nonlinear systems–the method of multiple scales versus center-manifold reduction", Nonlinear Dynamics **51**, 4, 483–500 (2008).

Nayfeh, A. H., *Introduction to Perturbation techniques* (John Wiley & Sons, 2011a).

Nayfeh, A. H., *The method of normal forms* (John Wiley & Sons, 2011b).

Nayfeh, A. H., D. T. Mook and L. R. Marshall, "Nonlinear coupling of pitch and roll modes in ship motions", Journal of Hydronautics **7**, 4, 145–152 (1973).

Nayfeh, A. H., M. I. Younis and E. M. Abdel-Rahman, "Reduced-order models for mems applications", Nonlinear dynamics **41**, 1-3, 211–236 (2005).

Oh, I., A. Nayfeh and D. Mook, "Theoretical and experimental study of the nonlinearity coupled heave, pitch, and roll motions of a ship in longitudinal waves", in "19th Symposium on Naval Hydrodynamics, Seoul, Korea", pp. 93–111 (1994).

Oh, I. G., A. H. Nayfeh and D. T. Mook, "A theoretical and experimental investigation of indirectly excited roll motion in ships", Philosophical Transactions of the Royal Society A: Mathematical, Physical and Engineering Sciences **358**, 1771, 1853–1881 (2000).

Pandiyan, R. and S. Sinha, "Time-varying controller synthesis for nonlinear systems subjected to periodic parametric loadings", Journal of Vibration and Control **7**, 1, 73–90 (2001).

Patel, R. and M. Toda, "Quantitative measures of robustness for multivariable systems", in "Joint Automatic Control Conference", vol. 17, p. 35 (1980).

Paulling, J. R., "On unstable ship motions resulting from nonlinear coupling", J. Ship Res. **3**, 36–46 (1959).

Peruzzi, N., F. R. Chavarette, J. M. Balthazar, A. M. Tusset, A. L. P. M. Perticarrari and R. Brasil, "The dynamic behavior of a parametrically excited time-periodic mems taking into account parametric errors", Journal of Vibration and Control **22**, 20, 4101–4110 (2016).

Pfifer, H. and P. Seiler, "Robustness analysis of linear parameter varying systems using integral quadratic constraints", International Journal of Robust and Nonlinear Control **25**, 15, 2843–2864 (2015).

Poincaré, H., *Les méthodes nouvelles de la mécanique céleste*, vol. 3 (Gauthier-Villars et fils, 1899).

Puig, J., "Reducibility of linear equations with quasi-periodic coefficients. a survey", Mathematical Physics Preprint Archive Preprint pp. 02–246 (2002).

Puig, J. and C. Simó, "Analytic families of reducible linear quasi-periodic differential equations", Ergodic Theory and Dynamical Systems **26**, 2, 481–524 (2006).

Quevedo, D. E. and D. Nešić, "Robust stability of packetized predictive control of nonlinear systems with disturbances and markovian packet losses", Automatica **48**, 8, 1803–1811, URL `https://www.sciencedirect.com/science/article/pii/S0005109812002191` (2012).

Ramakrishnan, V. and B. F. Feeny, "Resonances of a forced mathieu equation with reference to wind turbine blades", Journal of vibration and acoustics **134**, 6 (2012).

Rao, B. R. and S. Ganapathy, "Linear time-varying systems—state transition matrix", in "Proceedings of the Institution of Electrical Engineers", vol. 126, pp. 1331–1335 (IET, 1979).

Redkar, S., "Lyapunov stability of quasiperiodic systems", Mathematical Problems in Engineering **2012** (2012).

Redkar, S., S. Sinha and E. A. Butcher, "Some techniques for order reduction of nonlinear time periodic systems", in "ASME International Mechanical Engineering Congress and Exposition", vol. 37122, pp. 649–658 (2003).

Rega, G., "Nonlinear dynamics in mechanics and engineering: 40 years of developments and ali h. nayfeh's legacy", Nonlinear Dynamics URL `https://doi.org/10.1007/s11071-019-04833-w` (2019).

Rega, G. and H. Troger, "Dimension reduction of dynamical systems: methods, models, applications", Nonlinear Dynamics **41**, 1-3, 1–15 (2005).

Rosenbloom, A., "Analysis of linear systems with randomly time-varying parameters", in "Proc. Symp. Inf. Nets", vol. 3, p. 145 (Poly. Inst. Brooklyn, 1954).

Samuels, J., "On the mean square stability of random linear systems", IRE Transactions on Circuit Theory **6**, 5, 248–259 (1959).

Sanders, J. A., F. Verhulst and J. A. Murdock, *Averaging methods in nonlinear dynamical systems*, vol. 59 (Springer, 2007).

Sharma, A. and S. Sinha, "Control of nonlinear systems exhibiting chaos to desired periodic or quasi-periodic motions", Nonlinear Dynamics **99**, 1, 559–574 (2020).

Sharma, A. and S. C. Sinha, "An approximate analysis of quasi-periodic systems via floquét theory", Journal of Computational and Nonlinear Dynamics **13**, 2, 021008 (2018).

Siegel, C. L., "Uber die normalform analytischer differentialgleichungen in der nahe einer gleichgewichtslosung", Matematika **5**, 2, 119–128 (1961).

Sinha, S. and E. Butcher, "Symbolic computation of fundamental solution matrices for linear time-periodic dynamical systems", Journal of Sound and Vibration **206**, 1, 61 – 85, URL `http://www.sciencedirect.com/science/article/pii/S0022460X97910798` (1997).

Sinha, S., E. Butcher and A. Dávid, "Construction of dynamically equivalent time-invariant forms for time-periodic systems", Nonlinear Dynamics **16**, 3, 203–221 (1998).

Sinha, S., E. Gourdon and Y. Zhang, "Control of time-periodic systems via symbolic computation with application to chaos control", Communications in Nonlinear Science and Numerical Simulation **10**, 8, 835 – 854, URL `http://www.sciencedirect.com/science/article/pii/S1007570404001170` (2005a).

Sinha, S. and P. Joseph, "Control of general dynamic systems with periodically varying parameters via liapunov-floquet transformation", Journal of Dynamic Systems, Measurement and Control **116**, 4, 650–658 (1994).

Sinha, S. and V. Juneja, "An approximate analytical solution for systems with periodic coefficients via symbolic computation", in "32nd Structures, Structural Dynamics, and Materials Conference", p. 1020 (1991).

Sinha, S. and R. Pandiyan, "Analysis of quasilinear dynamical systems with periodic coefficients via Liapunov-Floquet transformation", International Journal of Non-Linear Mechanics **29**, 5, 687 – 702 (1994).

Sinha, S., S. Redkar, E. A. Butcher and V. Deshmukh, "Order reduction of nonlinear time periodic systems using invariant manifolds", in "International Design Engineering Technical Conferences and Computers and Information in Engineering Conference", vol. 37033, pp. 1197–1207 (2003).

Sinha, S., S. Redkar, V. Deshmukh and E. A. Butcher, "Order reduction of parametrically excited nonlinear systems: techniques and applications", Nonlinear Dynamics **41**, 1-3, 237–273 (2005b).

Sinha, S., D.-H. Wu, V. Juneja and P. Joseph, "Analysis of dynamic systems with periodically varying parameters via chebyshev polynomials", Journal of Vibration and Acoustics (1993).

Sinha, S. C., R. Pandiyan and J. Bibb, "Liapunov-floquet transformation: computation and applications to periodic systems", Journal of Vibration and Acoustics (1996).

Smith, H. L., "Normal forms for periodic systems", Journal of mathematical analysis and applications **113**, 2, 578–600 (1986).

Sultania, A. and L. Manuel, "Extreme loads on a spar buoy-supported floating offshore wind turbine", in "51st AIAA/ASME/ASCE/AHS/ASC Structures, Structural Dynamics, and Materials Conference 18th AIAA/ASME/AHS Adaptive Structures Conference 12th", p. 2738 (2010).

Susheelkumar, C., S. Redkar and T. Sugar, "Parametric resonance and energy transfer in suction stabilized floating platforms: a brief survey", International Journal of Dynamics and Control **5**, 3, 931–945 (2017).

Tondl, A., A. Tondl, M. Ruijgrok, T. Ruijgrok, R. Nabergoj and F. Verhulst, *Autoparametric resonance in mechanical systems* (Cambridge University Press,New York, USA, 2000).

Utsunomiya, T., H. Matsukuma, S. Minoura, K. Ko, H. Hamamura, O. Kobayashi, I. Sato, Y. Nomoto and K. Yasui, "At sea experiment of a hybrid spar for floating offshore wind turbine using 1/10-scale model", Journal of offshore mechanics and Arctic engineering **135**, 3 (2013).

Vatankhah, R., A. Najafi, H. Salarieh and A. Alasty, "Lyapunov-Based Boundary Control of Strain Gradient Microscale Beams With Exponential Decay Rate", Journal of Vibration and Acoustics **137**, 3, URL `https://doi.org/10.1115/1.4028964`, 031003 (2015).

Verhulst, F., "Nonlinear differential equations and dynamical systems", (1990).

Vidic-Perunovic, J., "Influence of the gz calculation method on parametric roll prediction", Ocean Engineering **38**, 2-3, 295–303 (2011).

Vrabel, R., "Logarithmic norm-based analysis of robust asymptotic stability of nonlinear dynamical systems", Communications in Nonlinear Science and Numerical Simulation **80**, 104957 (2020).

Wang, H., A. Somayajula, J. Falzarano and Z. Xie, "Development of a blended time-domain program for predicting the motions of a wave energy structure", Journal of Marine Science and Engineering **8**, 1, 1 (2020).

Waswa, P. M. and S. Redkar, "Lucid analysis of periodically forced nonlinear systems via normal forms", in "International Design Engineering Technical Conferences and Computers and Information in Engineering Conference", vol. 59261, p. V006T09A044 (American Society of Mechanical Engineers, 2019).

Waswa, P. M. and S. Redkar, "Analysis and control of nonlinear attitude motion of gravity-gradient stabilized spacecraft via lyapunov-floquet transformation and normal forms", in "Advances in Spacecraft Attitude Control", (IntechOpen, 2020a).

Waswa, P. M. and S. Redkar, "A direct approach for simplifying nonlinear systems with external periodic excitation using normal forms", Nonlinear Dynamics **99**, 2, 1065–1088 (2020b).

Waswa, P. M., S. Redkar and S. C. Subramanian, "A plain approach for center manifold reduction of nonlinear systems with external periodic excitations", Journal of Vibration and Control **26**, 11-12, 929–940 (2020).

Waters, T. J., "Stability of a 2-dimensional mathieu-type system with quasiperiodic coefficients", Nonlinear dynamics **60**, 3, 341–356 (2010).

Wayman, E. N., P. Sclavounos, S. Butterfield, J. Jonkman and W. Musial, "Coupled dynamic modeling of floating wind turbine systems", Tech. rep., National Renewable Energy Lab.(NREL), Golden, CO (United States) (2006).

Wiens, G. and S. Sinha, "On the application of liapunov's direct method to discrete dynamic systems with stochastic parameters", Journal of Sound and Vibration **94**, 1, 19–31 (1984).

Wooden, S. M. and S. Sinha, "Analysis of periodic-quasiperiodic nonlinear systems via lyapunov-floquet transformation and normal forms", Nonlinear Dynamics **47**, 1-3, 263–273 (2007).

Wu, M.-Y., "Transformation of a linear time-varying system into a linear time-invariant system", International Journal of Control **27**, 4, 589–602 (1978).

Wu, M.-Y. and A. Sherif, "On the commutative class of linear time-varying systems", International Journal of Control **23**, 3, 433–444 (1976).

Xiao, L., B. Liao, S. Li and K. Chen, "Nonlinear recurrent neural networks for finite-time solution of general time-varying linear matrix equations", Neural Networks **98**, 102–113 (2018).

Yedavalli, R., "Improved measures of stability robustness for linear state space models", IEEE Transactions on Automatic Control **30**, 6, 577–579 (1985).

Zhang, H., D. Xu, S. Xia and Y. Wu, "A new concept for the stability design of floating airport with multiple modules", Procedia IUTAM **22**, 221–228 (2017).

Zhang, Y., K. Chen and H.-Z. Tan, "Performance analysis of gradient neural network exploited for online time-varying matrix inversion", IEEE Transactions on Automatic Control **54**, 8, 1940–1945 (2009a).

Zhang, Y., C. Yi and W. Ma, "Simulation and verification of Zhang neural network for online time-varying matrix inversion", Simulation Modelling Practice and Theory **17**, 10, 1603–1617 (2009b).

Zhang, Y., J. Yuan, J. Liu and B. Shi, "Lyapunov Functions and Sliding Mode Control for Two Degrees-of-Freedom and Multidegrees-of-Freedom Fractional Oscillators", Journal of Vibration and Acoustics **139**, 1, URL `https://doi.org/10.1115/1.4034843`, 011014 (2016).

Zhao, H. and C. D. Rahn, "On the Control of Axially Moving Material Systems", Journal of Vibration and Acoustics **128**, 4, 527–531, URL `https://doi.org/10.1115/1.2202170` (2006).

Zhou, J., "Interpreting popov criteria in luré systems with complex scaling stability analysis", Communications in Nonlinear Science and Numerical Simulation **59**, 306–318 (2018).

Zhou, K. and P. Khargonekar, "Stability robustness bounds for linear state-space models with structured uncertainty", IEEE Transactions on Automatic Control **32**, 7, 621–623 (1987).

Zounes, R. S. and R. H. Rand, "Transition curves for the quasi-periodic mathieu equation", SIAM Journal on Applied Mathematics **58**, 4, 1094–1115 (1998).

APPENDIX A

EQUATIONS OF MOTION FOR SSF

The equations of motion for the heave-roll model for SSF platform is derived using the Lagrangian approach detailed in Tondl *et al.* (2000). The position vector, velocity vector and acceleration vector of mass m_1, in the vertical direction is given by

$$\begin{aligned} r_{m1} &= \begin{bmatrix} \breve{z} \\ 0 \end{bmatrix} = \begin{bmatrix} z + \alpha\cos(\omega t) \\ 0 \end{bmatrix}; \dot{r}_{m1} = \begin{bmatrix} \dot{\breve{z}} \\ 0 \end{bmatrix} = \begin{bmatrix} \dot{z} - \alpha\omega\sin(\omega t) \\ 0 \end{bmatrix}; \\ \ddot{r}_{m1} &= \begin{bmatrix} \ddot{\breve{z}} \\ 0 \end{bmatrix} = \begin{bmatrix} \ddot{z} - \alpha\omega^2\cos(\omega t) \\ 0 \end{bmatrix} \end{aligned} \tag{A.1}$$

The position vector and velocity vector of mass m_2 is expressed as

$$r_{m2} = \begin{bmatrix} \breve{z} - l\cos\phi \\ l\sin\phi \end{bmatrix}; \dot{r}_{m2} = \begin{bmatrix} \dot{\breve{z}} + l\dot{\phi}\sin\phi \\ l\dot{\phi}\cos\phi \end{bmatrix} \tag{A.2}$$

The total kinetic energy of the system can be expressed as

$$T = \frac{1}{2}m_1\dot{\breve{z}}^2 + \frac{1}{2}m_2\{\dot{\breve{z}} + l\dot{\phi}\sin\phi\}^2 + \frac{1}{2}m_2\{l\dot{\phi}\cos\phi\}^2 \tag{A.3}$$

The total potential energy of the system can be expressed as

$$V = m_2gl(1-\cos\phi) + \frac{1}{2}k\breve{z}^2 + \frac{1}{2}k_t\phi^2 \tag{A.4}$$

For the given system of SSF, the Lagrangian equation of motion is expressed as

$$(m_1+m_2)\{\ddot{z} - \alpha\omega^2\cos(\omega t)\} + b\dot{z} + kz + m_2l\{\ddot{\phi}\sin\phi + \dot{\phi}^2\cos\phi\} = 0 \tag{A.5}$$

$$m_2l^2\ddot{\phi} + c\dot{\phi} + k_t\phi + m_2gl\sin\phi + m_2l\{\ddot{z} - \alpha\omega^2\cos(\omega t)\}\sin\phi = 0 \tag{A.6}$$

The Equations (A.5) and (A.6) can be converted to a dimensionless form, by introducing a new variable, called time constant given as $\tau = (\sqrt{\frac{g}{l}})t$. The equations are updated as follows

$$\ddot{x} + \overline{B}\dot{x} + q^2x + \mu\{\ddot{\phi}\sin\phi + \dot{\phi}^2\cos\phi\} = a\eta^2\cos(\eta\tau) \tag{A.7}$$

$$\ddot{\phi} + \overline{C}\dot{\phi} + \sin\phi + q_t^2\phi + \{\ddot{x} - a\eta^2\cos(\eta\tau)\}\sin\phi = 0 \tag{A.8}$$

where $x = \frac{z}{l}, \omega_0 = \sqrt{\frac{g}{l}}, \overline{B} = \frac{b}{\omega_0(m_1+m_2)}, q^2 = \frac{k}{\omega_0^2(m_1+m_2)}, \mu = \frac{m_2}{(m_1+m_2)}, \overline{C} = \frac{c}{\omega_0 m_2 l^2}, \eta = \frac{\omega}{\omega_0}, q_t^2 = \frac{k_t}{\omega_0^2 m_2 l^2}$ and $a = \frac{\alpha}{l}$

APPENDIX B

ELEMENTS OF L-P TRANSFORMATION MATRIX

The following are the elements of the near-identity transformation matrix, obtained for the quasi-periodic system without damping.

$$
\begin{aligned}
P(1,1) =& 1.00 + (0.0441156 + 0.i)2.71828^{(0.-0.716815i)t} - \\
& (0.0356973 + 0.i)2.71828^{(0.+0.716815i)t} + \\
& (0.0574301 + 0.i)2.71828^{(0.-6.28319i)t} - (0.0574301 + 0.i)2.71828^{(0.+6.28319i)t} + \\
& (0.0515491 + 0.i)2.71828^{(0.-7.i)t} - (0.0515491 + 0.i)2.71828^{(0.+7.i)t} + \\
& (0.000586079 + 0.i)2.71828^{(0.-12.5664i)t} - \\
& (0.00202643 + 0.i)2.71828^{(0.+12.5664i)t} + \\
& (0.00101803 + 0.i)2.71828^{(0.-13.2832i)t} - (0.003289 + 0.i)2.71828^{(0.+13.2832i)t} + \\
& (0.000439847 + 0.i)2.71828^{(0.-14.i)t} - (0.00130168 + 0.i)2.71828^{(0.+14.i)t}, \\
P(1,2) =& (0.0165154 + 0.i) + (0.00931405 + 0.i)2.71828^{(0.-0.716815i)t} + \\
& (0.00756359 + 0.i)2.71828^{(0.+0.716815i)t} - (0.128 + 0.i)2.71828^{(0.-6.28319i)t} + \\
& (0.0370199 + 0.i)2.71828^{(0.+6.28319i)t} - (0.102052 + 0.i)2.71828^{(0.-7.i)t} + \\
& (0.034484 + 0.i)2.71828^{(0.+7.i)t} - (0.00279764 + 0.i)2.71828^{(0.-12.5664i)t} + \\
& (0.00045943 + 0.i)2.71828^{(0.+12.5664i)t} - \\
& (0.00444933 + 0.i)2.71828^{(0.-13.2832i)t} + \\
& (0.000807458 + 0.i)2.71828^{(0.+13.2832i)t} - (0.00172966 + 0.i)2.71828^{(0.-14.i)t} + \\
& (0.000352601 + 0.i)2.71828^{(0.+14.i)t}, \\
P(2,1) =& (0.0165154 + 0.i) + (0.00756359 + 0.i)2.71828^{(0.-0.716815i)t} + \\
& (0.00931405 + 0.i)2.71828^{(0.+0.716815i)t} + (0.0370199 + 0.i)2.71828^{(0.-6.28319i)t} - \\
& (0.128 + 0.i)2.71828^{(0.+6.28319i)t} + (0.034484 + 0.i)2.71828^{(0.-7.i)t} - \\
& (0.102052 + 0.i)2.71828^{(0.+7.i)t} + (0.00045943 + 0.i)2.71828^{(0.-12.5664i)t} - \\
& (0.00279764 + 0.i)2.71828^{(0.+12.5664i)t} + (0.000807458 + 0.i)2.71828^{(0.-13.2832i)t} - \\
& (0.00444933 + 0.i)2.71828^{(0.+13.2832i)t} + (0.000352601 + 0.i)2.71828^{(0.-14.i)t} - \\
& (0.00172966 + 0.i)2.71828^{(0.+14.i)t}, \\
P(2,2) =& 1.00 - (0.0356973 + 0.i)2.71828^{(0.-0.716815i)t} + \\
& (0.0441156 + 0.i)2.71828^{(0.+0.716815i)t} - (0.0574301 + 0.i)2.71828^{(0.-6.28319i)t} + \\
& (0.0574301 + 0.i)2.71828^{(0.+6.28319i)t} - (0.0515491 + 0.i)2.71828^{(0.-7.i)t} + \\
& (0.0515491 + 0.i)2.71828^{(0.+7.i)t} - (0.00202643 + 0.i)2.71828^{(0.-12.5664i)t} + \\
& (0.000586079 + 0.i)2.71828^{(0.+12.5664i)t} - (0.003289 + 0.i)2.71828^{(0.-13.2832i)t} + \\
& (0.00101803 + 0.i)2.71828^{(0.+13.2832i)t} - (0.00130168 + 0.i)2.71828^{(0.-14.i)t} + \\
& (0.000439847 + 0.i)2.71828^{(0.+14.i)t}
\end{aligned}
\tag{B.1}
$$